N71-20732

NASA CR-117402

CASE FILE
COPY

RE-ORDER NO. 70-430

N71-20732

NASA CR-117402

INVESTIGATION OF
INTEGRATING SPHERE MEASUREMENT PARAMETERS

Jet Propulsion Laboratories Contract 952304

TRW Sales Number 12085

31 December 1970

Signed: _____
B. E. Newnam
Member of the Technical Staff

_____
G. L. Brown
Member of the Technical Staff

Approved: _____
E. E. Luedke
Head, Thermophysics Section

13

SUMMARY

- Two important parameters affecting integrating sphere reflectometer
efficiency and accuracy are the sphere wall reflectance characteristics
and the detector directional response. The directional and bidirectional
reflectance properties of MgO sphere wall coatings (smoke and pressed pow-
der) were measured as a function of age and angle and polarization of inci-
dent radiation at wavelengths between 400 and 2500 nm. The directional
reflectance increased slightly with angle of incidence. For large angles
of incidence, the bidirectional reflectance was very non-diffuse both in
and out of the plane of incidence. Degradation of the reflectance with age
is almost entirely due to atmospheric moisture and progresses slowly after
the first two weeks. Pressed MgO powder, in comparison to smoked MgO, is
easier to prepare, more uniform optically, and more durable. Thick coat-
ings of the smoked surface, however, have higher reflectance, degrade less
with age, are more depolarizing and more diffuse. For maximum measurement ac-
curacy, a thick smoked MgO wall coating is superior. The directional charac-
teristics of a photomultiplier tube were also measured for incident energy
of two polarizations and for three tube envelope conditions. The detector
was found to be very directionally sensitive unless coated with MgO smoke.
With this treatment, the detector was essentially cosine in response. Recom-
mendations for significant improvements in equipment and operational techniques
are presented.

INTRODUCTION

For over a dozen years, integrating sphere reflectometers have provided a relatively accurate method of determining the solar absorptance of opaque solid materials. These values have been used in predicting and optimizing the thermal performance of hundreds of spacecraft. The sophisticated missions of the present generation of spacecraft require even more accurate knowledge of the thermal properties of the component surfaces.

The relative importance and magnitudes of the many small uncertainties in integrating sphere measurements have been evaluated by TRW Systems in an error analysis report to the Jet Propulsion Laboratories (JPL Purchase Order Number ES-453477)[15]. From that analysis, it became apparent that careful measurements of certain integrating sphere parameters were needed to accurately determine the total errors.

This report describes the investigation of the two main areas which needed further study; the sphere wall reflectance characteristics, and the radiation detector directional response. The directional and bidirectional reflectance properties of MgO sphere wall coatings (smoke and pressed powder) were measured as a function of age and angle and polarization of incident radiation at wavelengths between 400 and 2500 nm. The directional characteristics of a photomultiplier tube were also measured for incident energy of two polarizations and for three tube envelope conditions. Based on the results of this work, a number of recommendations for significant improvements in equipment and operational techniques can be made.

TABLE OF CONTENTS

Page

LIST OF ILLUSTRATIONS

Page

Page

Page

LIST OF TABLES

1.0 SPHERE WALL COATING

1.1 SUMMARY

Several smoked and pressed powder MgO samples were prepared and measured for directional reflectance at several ages up to one month. The smoked and pressed powder samples degraded similarly with age, the degradation of the powder being more severe. The worst degradation occurred at wavelengths below and above the 0.6 to 0.8 micron region. The degradation began almost immediately after sample preparation and continued for approximately two weeks. A control sample stored in a dry nitrogen gas filled dessicator degraded only slightly after one month. One pressed powder sample was prepared using MgO powder and was measured before and after baking at 350°C for one hour. Although the reflectance did rise slightly due to this treatment, the aging of this sample was even more rapid than the unbaked samples. There seems to be no good method of prevention of this aging. A continuous dry gas purge or lowering of the relative humidity will only slow down the degradation.

The consequences of this type of degradation are:

    a. There is a decrease in reflectometer efficiency and signal-to-noise ratio due to lower sphere wall reflectance.

    b. There is a greater significance of the "first-bounce" energy, which is incident on the detector after only one bounce off the sphere wall (this makes many of the possible errors larger).

    c. It is necessary that both hemispheres and all ports be coated at the same time to help assure a uniform sphere wall reflectance at any particular time thereafter.

After measuring the directional reflectance of MgO samples of various thicknesses, it was found that a smoked coating two millimeters or greater in thickness has the highest reflectance, is most diffuse and depolarizing, and, therefore, will provide the most accurate data when used as a sphere wall coating.

A significant result of this study was the in-depth study and elimination of certain major integrating sphere measurement errors. In the attempt to provide the most accurate values obtainable for the directional reflectance of the MgO surfaces, several relatively large errors were analyzed and either eliminated by more sophisticated measurement techniques or calculated out of the data. These errors include:

a. Substitution error

b. Errors resulting from the azimuthal and polar angular dependence of the lead sulfide cell and photomultiplier tube detectors.

c. Errors due to the selective polarization response of the detectors.

d. Port loss errors.

e. Reference signal measurements errors resulting from non-normal beam incidence.

f. Errors due to direct irradiation of the detectors and/or detector/sphere geometry.

Incorporation of the techniques and calculations which were used in this study has resulted in highly accurate values of spectral directional reflectance for various MgO surfaces. This data may now be used to quantify many of the reflectance measurement errors which must, until better wall coatings are developed or discovered, remain fundamental limitations on measurement accuracy.

The bidirectional reflectance (BDR) of smoked and pressed powder MgO samples was measured as a function of a number of parameters. It was found that smoked MgO is more diffuse than pressed MgO powder. For polar angles of incidence, θ_1, less than 40°, the samples appeared to be quite diffuse. At larger values of θ_1, forward and backward scattering increased. Polarized energy, when incident on a MgO surface, is greatly depolarized. The degree of depolarization is dependent upon the various parameters concerning the incident beam such as wavelength and angle of incidence.

In general, the importance of the bidirectional reflectance characteristics of sphere wall coatings only pertains to that portion of the

energy inside the sphere which has experienced only one reflection off the walls. (This is referred to as the "first-bounce energy".) A number of integrating sphere measurement errors may result from this "first bounce" energy.

1.2 INTRODUCTION

An investigation has been completed to evaluate the characteristics of magnesium-oxide (MgO) coatings which are commonly used in integrating sphere reflectometers. The following are the properties of an ideal sphere coating:

a. Its directional reflectance is nearly 100% for all incident energy within the spectral region of interest.

b. It reflects energy as a perfect diffusor, which means that

● The directional reflectance is invariant with angle of incidence, and

● The bidirectional reflectance is invariant with angle of incidence and reflection.

c. It reflects energy of all states of polarization equally well for any angle of incidence.

d. All reflected rays are unpolarized regardless of the state of polarization of the incident rays.

e. Its reflectance properties are not significantly degraded by a typical optical laboratory environment.

The properties of all real materials, of course, deviate from these ideals. The extent to which the real properties of MgO coatings deviate from the ideals largely determines the limiting accuracy with which the integrating sphere can be used to measure the directional reflectance of materials. This report presents the results of reflectance measurements which were performed to accurately determine the actual properties of MgO coatings.

1.3 MgO PREPARATION

Samples of representative sphere coatings of several thicknesses were prepared by three methods. The methods were combustion of magnesium

ribbon, with and without an electrostatic potential difference between ribbon and sample, and compression of MgO powder. All samples were deposited or compressed upon 1-3/4" diameter aluminum alloy (7075) discs. The discs were fabricated to have a 1/32-inch thick rim to contain the coatings. The rim heights were sized to each thickness of coating prepared (See Figure 1-1).

1.3.1 Smoked MgO Samples

The smoked MgO samples were prepared by burning twisted magnesium ribbon (Baker and Adamson A240, Code 1901) in a special box enclosure which was free of lateral drafts. The ribbon was twisted by use of a hand drill and then cut into convenient sections approximately four inches long. These sections were successively set upon an iron screen of heavy gauge, directly below the suspended aluminum substrate discs, and ignited by use of an oxygen-rich acetylene torch. According to Priest and Riley (Ref. 1), no contamination of the MgO coatings occurs from the use of an iron screen. The distances between the iron screen and the aluminum discs were 5 to 6 inches. Four of the five samples were prepared by applying an electrostatic potential difference (of suitable polarity) between the iron screen and the sample discs. The potential varied from 3500 to 5000 volts. These four electrostatically-deposited samples had thicknesses of 1, 2, 3, and 4 mm (See Table 1). The one sample smoked without an applied potential was 2 mm thick.

1.3.2 Compressed MgO Powder Samples

A bottle of Reagent Grade (A.C.S.) code 1917 MgO powder was obtained from Baker and Adamson (A205). A generous portion of the powder was heaped onto an aluminum disc, and by use of a cylindrical nylon rod with roughened flat surface and lead weights, the powder was compressed for five-minutes at 565 gm/cm^2. The time period and pressure were determined so as to yield a coating with maximum reflectance and adequate mechanical strength. Comparative measurements of the reflectance were made with the Beckman DK2A Spectrophotometer to determine the optimum time and pressure. Samples of 2, 3, and 4 mm thicknesses were prepared (See Table 1). It was observed that these samples were quite rugged, increasingly so with time. Extra samples survived intentional drops onto the floor and did not crumble when purposely gouged with a rod.

-4-

Smoked MgO Sample - 3 mm Thick

Pressed MgO Powder Sample - 4 mm Thick
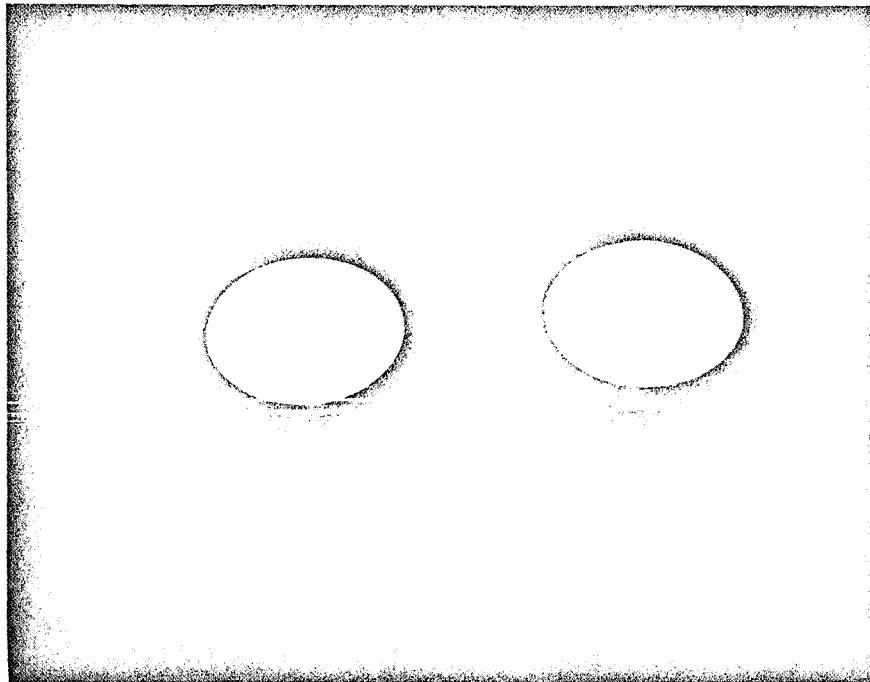
FIGURE 1-1:   PHOTOGRAPH OF PREPARED SAMPLES
OF SMOKED AND PRESSED MgO POWDER

TABLE 1

DESCRIPTION OF SAMPLES

TRW NO.	PREPARATION TECHNIQUE	THICKNESS (mm)
570-68	Smoked with Electro-static Field	1
571-68	Smoked with Electro-static Field	2
572-68	Smoked with Electro-static Field	3
576-68	Smoked with Electro-static Field	4
577-68	Smoked without Elec-trostatic Field	2
578-68	Pressed Powder	2
579-68	Pressed Powder	3
580-68	Pressed Powder	4
581-68	Pressed Powder	4

1.4 STORAGE AND AGING

1.4.1 Summary

- Several smoked and pressed powder MgO samples were prepared and measured for directional reflectance at zero hours age and subsequent ages up to one month. The smoked and pressed powder samples degraded similarly with age, the degradation of the powder being more severe. The worst degradation occurred at wavelengths below and above the 0.6 to 0.8 micron region. The degradation began almost immediately after sample preparation and continued for approximately two weeks. A control sample stored in a dry nitrogen gas filled dessicator degraded only slightly after one month. One pressed powder sample was prepared using MgO powder and was measured before and after baking at 350°C for one hour. Although the reflectance did rise slightly due to this treatment, the aging of this sample was even more rapid than the unbaked samples. There seems to be no good method of prevention of this aging. A continuous dry gas purge or lowering of the relative humidity will only slow down the degradation.

The consequences of this type of degradation are:

a. There is a decrease in reflectometer efficiency and signal-to-noise ratio due to lower sphere wall reflectance.

b. There is a greater significance of the "first-bounce" energy, which is incident on the detector after only one bounce off the sphere wall (this makes many of the possible errors larger).

c. It is necessary that both hemispheres and all ports be coated at the same time to help assure a uniform sphere wall reflectance at any particular time thereafter.

1.4.2 Storage Conditions

In order to simulate the environment of actual integrating sphere coatings, the samples were stored in a closed dark cabinet in a laboratory room used for optical measurements. Each sample was kept in an individual plastic box with the lid raised enough to allow air circulation but still providing a shield to prevent dust from settling directly on the coatings. The room was air conditioned, and the relative humidity was measured daily and found to vary between 50 and 55%.

1.4.3 Control Samples

In order to determine the effect of moisture upon the reflectance, one pressed powder sample (781-68) was kept within a nitrogen gas purged dessicator in the same cabinet.

1.4.4 Reflectance Measurements

The directional reflectance tests were measured in a Gier Dunkle Integrating Sphere at an angle of 10° and with the incident beam having the normal polarization produced by the Perkin-Elmer Model 99 Monochromator with a fused quartz prism. The reflectance of each sample was measured within one hour after preparation at seven wavelengths (.4, .6, .8, 1.0, 1.5, 2.0, and 2.5 microns) in the solar region. The samples were re-measured 2 hours, 24 hours, 72 hours, one week, and one month after preparation. Two samples were also remeasured after two and three weeks, and the control sample was remeasured only after one month. Care was taken to orient the samples in the same relative position in the integrating sphere for each test.

1.4.5 Results

Since a measure of degradation with time was the quantity desired, the directional reflectance measurements were not corrected for port losses, and a dual detector mount (PbS cell mounted on photomultiplier tube) was used. The representative data is shown graphed in Figure 1 - 2 as reflectance versus wavelength, with time as a parameter. Complete data for all samples are presented in the Appendix, Figures A1 - A9.

1.4.6 Discussion of Results

It can be seen that the smoked and pressed powder samples degraded similarly, the degradation for the powder being more severe. After two hours, a small degradation had occurred beyond 2 microns only. After one day, this drop in the infrared had increased. At the end of the three-day test, a decrease was also measured at .4 microns in the ultraviolet. This general degradation continued for about one to two weeks after which time further decreases were slight. For the purpose of direct comparison, the spectral reflectance of fresh (0 hours) and aged (672 hours) samples of smoked and pressed powder MgO samples are shown in Figure 1-2. In addition,
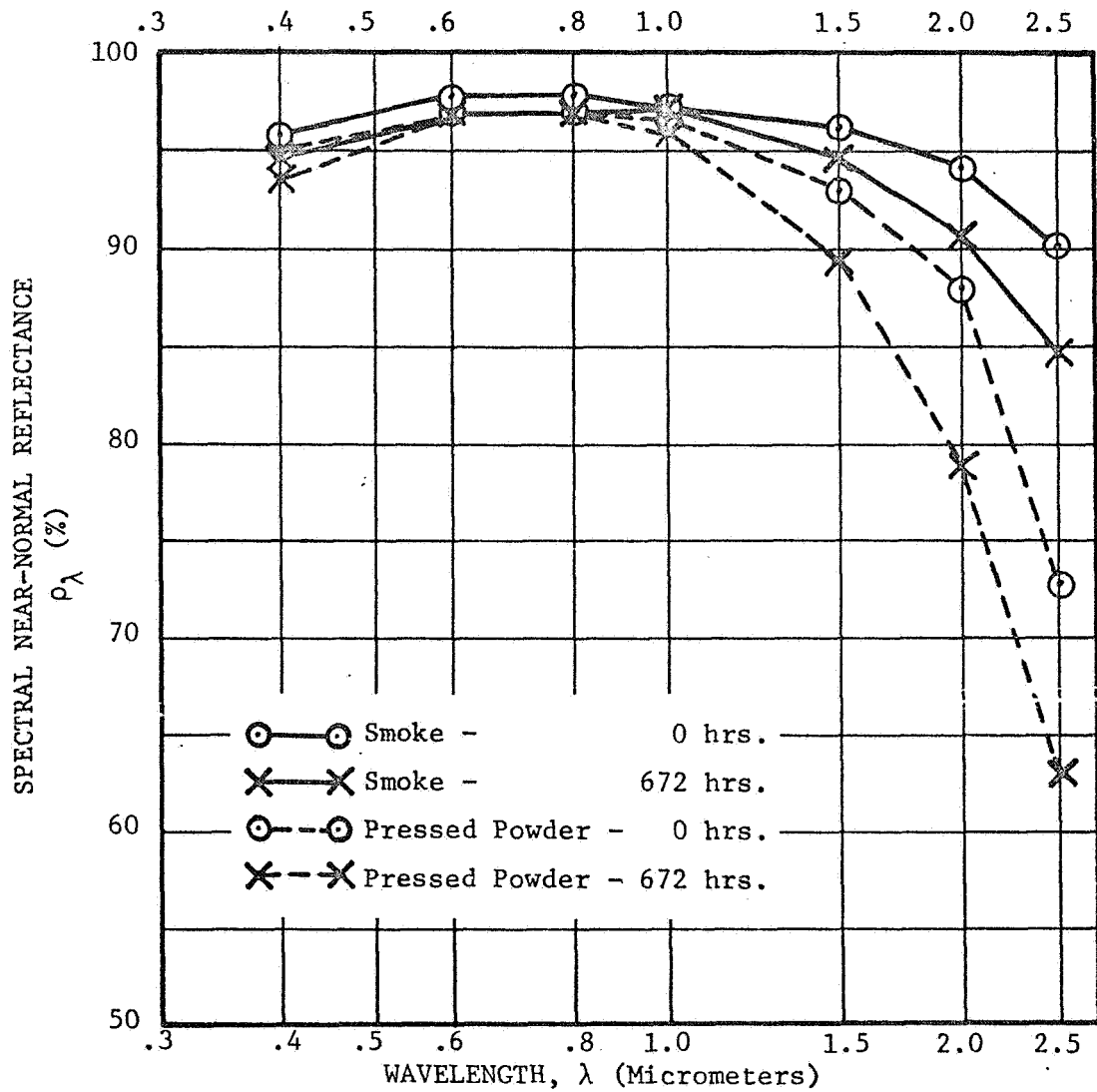
FIGURE 1-2: SPECTRAL DIRECTIONAL REFLECTANCE OF MgO COATINGS
AS A FUNCTION OF AGE

Smoke — 3mm Thick (572-68)

Powder — 4mm Thick (580-68)

the rate of degradation of these two samples is shown in Figure 1-3. No detectable difference between electrostatically smoked and normally smoked coatings was discernible in terms of aging. The control sample (581-68) after one month in the dry nitrogen gas filled dessicator degraded a very slight amount, equivalent to about one day in air (See Appendix, Figure A-9). (The actual exposure of the control sample to the atmosphere after the initial measurement was one hour.)

1.4.7 Baking of MgO Powder

Since it was not known how long the commercially prepared MgO powder might have been exposed to the atmosphere during manufacture, baking experiments were tried. The result of moisture on MgO is the formation of magnesium hydroxide (Brucite). It was believed (correctly so) that formation of $Mg(OH)_2$ in MgO depresses the reflectance. Therefore, a sample was placed in an oven at a temperature above 350°C, the dissociation temperature of Brucite, for 24 hours in order to drive off the OH-radical, and thus raise the reflectance level. Indeed, the reflectance did rise but by approximately 1% only. The aging process on this sample was even more rapid than unbaked samples, so no advantage was achieved.

1.4.8 Conclusions

These tests indicate that the atmospheric water moisture content of a typical air-conditioned optics laboratory degrades the reflectance of MgO powder and smoke significantly over a period of a few weeks. By reducing the relative humidity to 30 to 40% instead of the 50 to 55% measured at this laboratory, the rate of degradation would decrease, but the long-term reflectance values would probably be similar. A continuous purge of dry gas will also slow the aging process considerably, but frequent exposure to air during sample insertion and removal will ultimately cause the same decrease in ultraviolet and infrared reflectance.
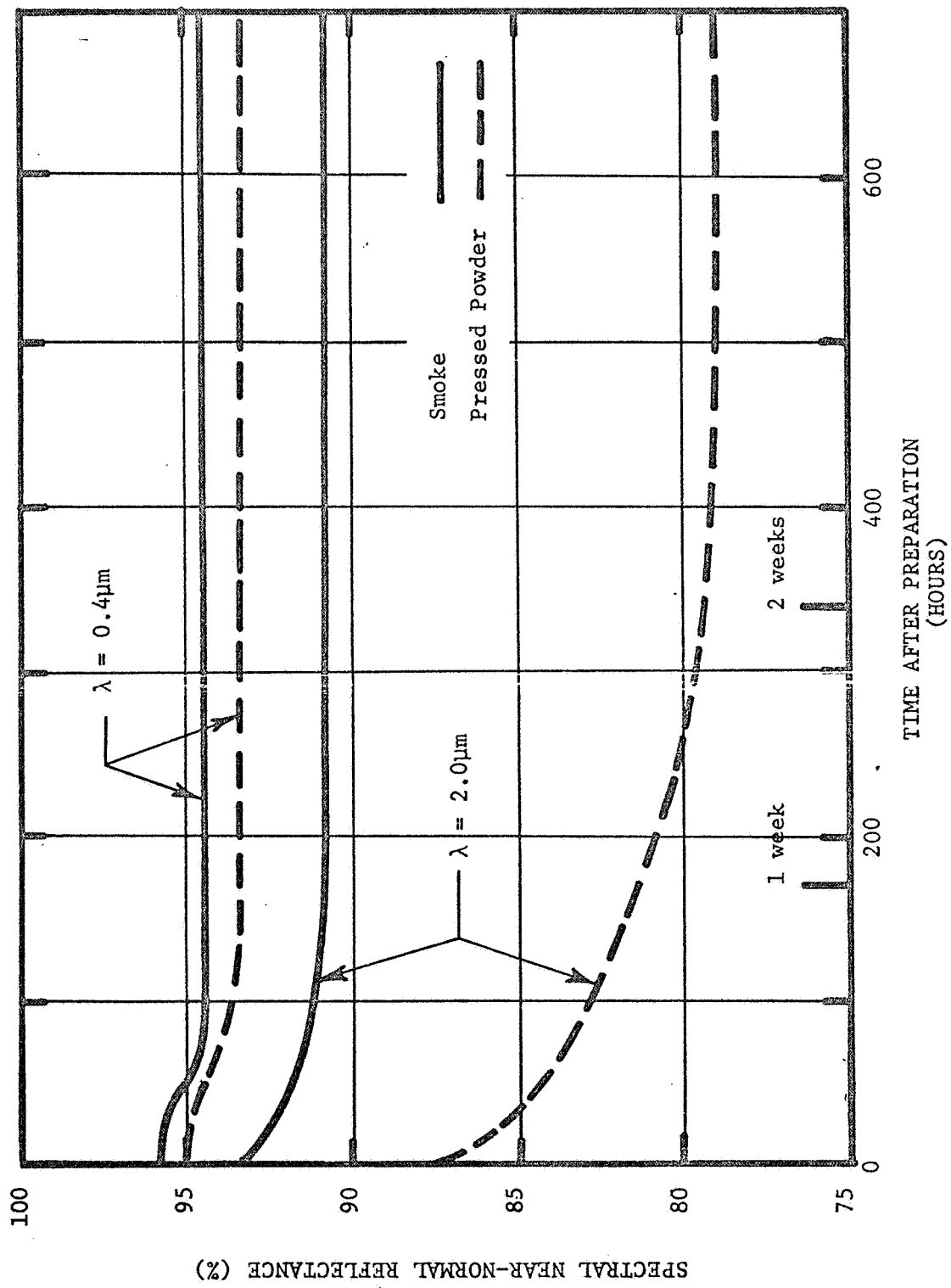
FIGURE 1-3: DEGRADATION OF REFLECTANCE WITH TIME FOR MgO COATINGS

Smoke -- 3mm Thick (572-68)

Powder -- 4mm Thick (580-68)

1.5 DIRECTIONAL REFLECTANCE

1.5.1 Summary

Integrating sphere reflectometer theory prescribes that the internal sphere wall coating be highly reflecting, diffuse and depolarizing for maximum measurement accuracy. This section describes the experimental study performed to determine these characteristics for MgO surfaces as a function of method of application, thickness and wavelength. The results permit a quantitative determination of the optimum MgO surface.

It was found that a smoked MgO coating, two millimeters or greater in thickness, has the highest reflectance, is most diffuse and depolarizing and, therefore, will provide the most accurate data when used as a sphere wall coating.

A more significant result of this portion of the study, however, was the in-depth study and elimination of certain major integrating sphere measurement errors. In the attempt to provide the most accurate values obtainable for the directional reflectance of the MgO surfaces, several relatively large errors were analyzed and either eliminated by more sophisticated measurement techniques or calculated out of the data. These errors include:

      a. Substitution error.

      b. Errors resulting from the azimuthal and polar angular dependence of the lead sulfide cell and photomultiplier tube detectors.

      c. Errors due to the selective polarization response of the detectors.

      d. Port loss errors.

      e. Reference signal measurements errors resulting from non-normal beam incidence.

      f. Errors due to direct irradiation of the detectors and/or detector/sphere geometry.

Incorporation of the techniques and calculations which were used in this study has resulted in highly accurate values of spectral directional reflectance for various MgO srufaces. This data may now be used to quantify many of the reflectance measurement errors which must, until better

wall coatings are developed or discovered, remain fundamental limitations on measurement accuracy.

1.5.2 Introduction

In the course of the directional reflectance measurements, several modifications of the standard integrating sphere reflectometer and measurement techniques were used to increase accuracy. Errors which were calculable were computed and removed from the directional reflectance values. The limitations included:

     a.   Substitution error.

     b.   Direct irradiation of detectors/detector geometry.

     c.   Azimuthal angle dependent detector response.

     d.   Polar angle dependent detector response.

     e.   Polarization dependent detector response.

     f.   Entrance port losses

The following sections describe the measurement apparatus and procedures and the methods used to compensate for the errors mentioned above. The directional reflectance measurement results are also presented and discussed.

1.5.3 Measurement Parameters

Using the Gier Dunkle Integrating Sphere Reflectometer, the directional reflectance of four electrostatically smoked MgO samples (1, 2, 3, and 4 mm thick), one non-electrostatically smoked MgO sample (2 mm thick) and two pressed MgO powder samples (3 and 4 mm thick) were measured at the following wavelengths and angles of incidence and incident beam polarization characteristics:

$$\lambda = 0.4, \ 0.6, \ 0.8, \ 1.0, \ 1.5, \ 2.0 \text{ and } 2.5 \text{ microns,}$$

$$\theta_i = 0°, \ 10°, \ 30°, \ 40°, \ 50°, \ 75° \text{ from normal,}$$

Incident beam polarized parallel and perpendicular to the plane of incidence.

1.5.4 Description of Measurement Apparatus

Measurements of directional reflectance were performed with an integrating sphere reflectometer (Model DIS-4A), designed by Edwards, *et al.*, (Figure 1-4) and manufactured by Gier Dunkle Instruments, Santa Monica, California. In this instrument, a hydrogen lamp is used in the ultraviolet and short visible region ($\lambda < .5\mu$), and a tungsten strip lamp is used for the longer wavelengths. The dispersion system is a Model 99 Perkin Elmer Monochromator (double pass). The integrating sphere (8 inches I.D.) walls are coated with a three millimeter thick diffusing MgO smoke layer. Test specimens are mounted at the center of the sphere on a rotatable sample holder. PbS cell and photomultiplier detectors are mounted in the bottom of the sphere directly below the sample. The 13 cps chopped output signal is amplified by a Brower Laboratories Model 129A Lock-In Amplifier, and the resultant signal is displayed on a Non-Linear Systems Model 2900 digital voltmeter.

During early reflectance measurements under this program, it was found that the energy source housing introduced a large heat load into the monochromator which, in combination with the monochromator heaters, produced a temperature cycling of the prism. This, in turn, caused variations in the monochromator output wavelengths, and reproducible results were not obtained.

This problem was eliminated by inserting a water-cooled heat sink between the source housing and the monochromator.

1.5.5 Measurement Procedure

After allowing a sufficient time for the electronic system to warm up and alignment of the optics, the directional reflectance measurements were performed with the following procedures:

    a.   The prescribed wavelength and slit width were set.

    b.   The Glan-Thomson polarizer was rotated to the position which corresponded to the incident energy polarized either parallel or perpendicular to the plane of incidence of the sample.

-14-
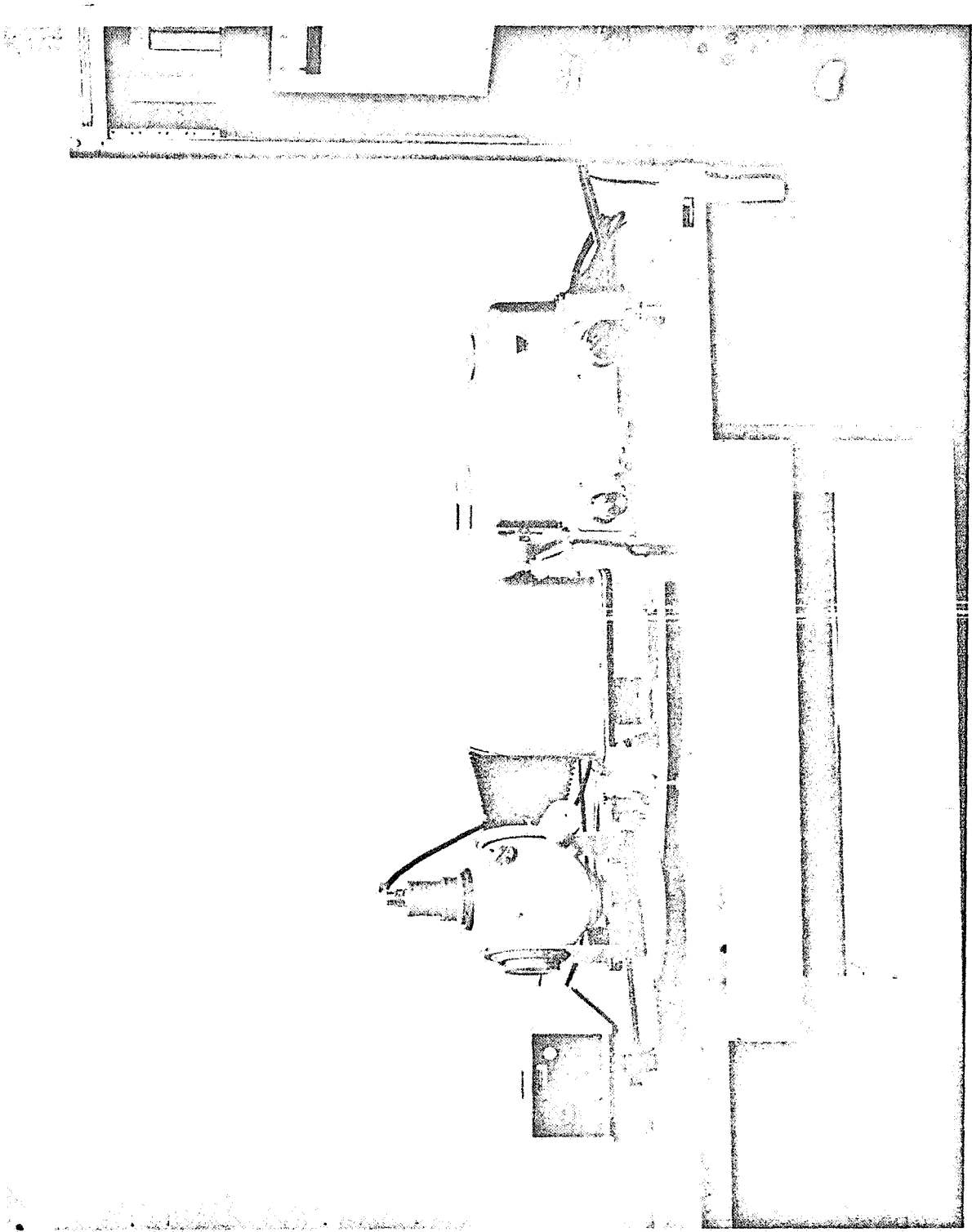
FIGURE 1-4: GIER DUNKLE DIRECTIONAL INTEGRATING SPHERE REFLECTOMETER

c. The null signal setting was confirmed.

d. The 100% reference was obtained, using the sphere in the absolute mode of operation, by directing the incident energy onto the sphere wall at an angle of 40° from the normal to the wall (See Figure 1-5). In order to reduce the "substitution" error, the sample was rotated to face the reference spot during the reference setting.

e. The incident beam was directed onto the sample.

f. The sample was rotated to each polar angle of interest, and the reflectance was read on a digital voltmeter.

g. These readings were recorded on the data sheet as shown in Figure 1-6 (These data were later corrected for known errors).

1.5.6 Elimination of Typical Errors from Reflectance Data

During the directional reflectance measurement program, it was found that special measurement techniques could be employed to reduce or eliminate some of the known errors. In addition, some of the errors were calculable, and the reflectance data was therefore corrected to eliminate these known errors.

1.5.6.1 Special Techniques to Eliminate Certain Errors

The Substitution Error arises in normal operation because a different fraction of the total energy is absorbed by the sample and sample holder during the 100% reference measurement than is absorbed during the sample measurement. This occurs because a fraction of the energy initially reflected from the wall in the 100% reference mode is partially absorbed by the low reflectance back and side of the sample, whereas the corresponding energy reflected from the wall after being reflected from the sample in the sample mode is incident on the sample face.

This error was largely eliminated by turning the sample to face the reference "spot" during the 100% measurement. This technique increased the measurement time by one third. This error is illustrated in Figure 1-7. A minor and apparently easy modification of the reflectometer would be to electrically connect the sample holder rotation

29

FIGURE 1-5: TOP VIEW OF CROSS SECTION OF INTEGRATING SPHERE
SHOWING STANDARD DUAL DETECTOR MOUNTING
AND SPOT IRRADIATED BY REFERENCE BEAM

FIGURE 1-6: DIRECTIONAL REFLECTANCE DATA SHEET

GIER-DUNKLE INTEGRATING SPHERE
SOURCE - TUNGSTEN AND HYDROGEN LAMP
DETECTOR - PHOTOMULTIPLIER AND LEAD SULFIDE CELL
PRISM - QUARTZ
SAMPLE DESCRIPTION Pressed MgO Powder - 4MM Thick 171λₘ

SAMPLE NO. 580-68
SOLAR ABSORPTANCE, α_s
OPERATOR P.E.F
DATE 8-1-68

Det	Drum	LAMP, Slit mm	λ ρL=	θ = 0° ρ0°	90°	10° ρ0°	90°	30° ρ0°	90°	40° ρ0°	90°	50° ρ0°	90°	75° ρ0°	90
PM(700)	7.75	HYD 2.00	.40	.939	.931	.941	.925	.948	.936	.957	.940	.965	.850	.982	.865
PbS	5.615	W .90	.60	.975	.960	.972	.960	.975	.944	.978	.967	.980	.868	.985	.975
	4.780	.80	.80	.983	.963	.978	.962	.977	.969	.980	.970	.981	.968	.991	.975
	4.24	1.00	1.00	.969	.963	.968	.963	.970	.969	.970	.968	.980	.973	.988	.980
	3.26	2.00	1.50	.916	.915	.914	.915	.920	.920	.927	.928	.923	.930	.951	.950
	2.349	2.00	2.00	.823	.822	.817	.825	.832	.836	.840	.845	.852	.855	.880	.885
	0.655	2.00	2.50	.672	.683	.666	.680	.687	.698	.696	.707	.710	.729	.756	.780

-18-

31

FIGURE 1-7

Illustration of Substitution Error
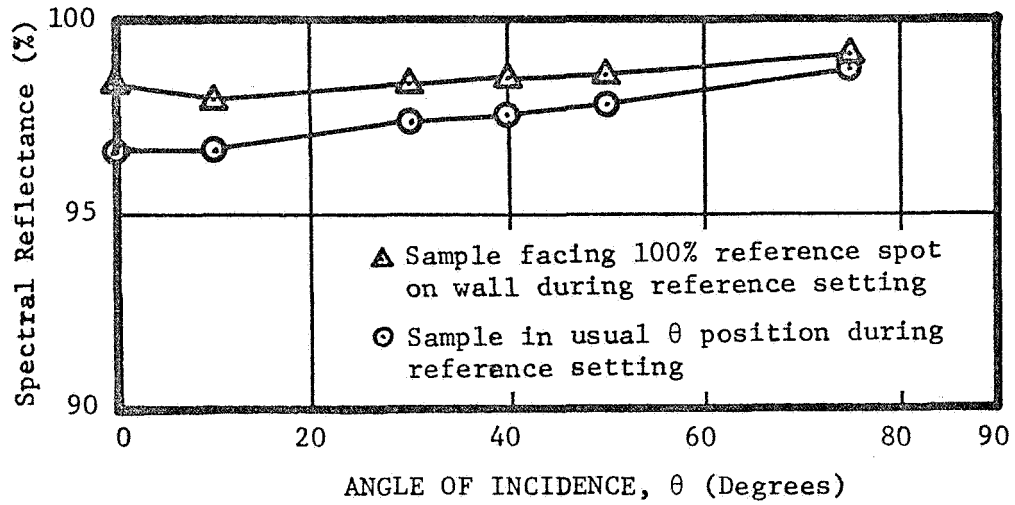
Spectral Reflectance of Smoked MgO, S/N 576-68,
for Incident Energy of 0.8 microns Wavelength
(Polarization Parallel to Plane of Incidence)

3-2

mechanism with the rotating mirror in the transfer optics. With a proper stop, the sample would automatically rotate to face the reference spot in the reference mode and then rotate back to the proper angle of incidence in the sample mode.

The azimuthal angular dependence of the PbS cell detector was eliminated by covering it with an insulated piece of aluminum foil with a centered one-centimeter diameter hole (See Figure 1-16).

The azimuthal angular dependence of the PM tube was essentially eliminated by the masking sandblast/MgO smoke treatment described in Section 2.3.4.

As discussed in that section, the PM tube with a light coat of MgO has an essentially cosine polar angle response.

Shaefer[3], Limperis[4], and Grover and Stoliar[5] have found the PbS cell detector polar angle response to vary considerably from a cosine curve.

There should be no polar response error for specular samples, since the first reflection to the detectors for both reference and sample beams occurs for the same polar angle (45°) relative to the detector surface. For imperfectly specular surfaces, however, this PbS cell characteristic may produce an error.

If reflected energy from the MgO wall coating has a net polarization and if the detectors are more sensitive to one type of polarization than the other, the measured value of reflectance for non-specular samples will be in error. Our measurements on a PM tube coated with a light coat of MgO have shown only a very small polarization dependence. For PbS detectors, however, Shaefer[3] has reported a large polarization dependent response, which at present is a fundamental limitation on integrating sphere measurement accuracy.

1.5.6.2 Computation of Correction Factors for Directional Reflectance

In addition to the special techniques described above for reducing or eliminating some of the error sources, the reflectance data may be corrected for the following three errors:

33

a. Energy lost through the entrance port for the first reflection from the sample.

b. Reference measurement errors due to non-normal beam incidence.

c. Direct irradiation of the detectors by the sample and detector/sphere geometry.

Port Losses - For diffuse samples, the amount of reflected energy escaping out the entrance port must be taken into account. In order to measure samples (of diameter $\sim$ 1 inch) at angles of incidence greater than 45°, the incident energy must be focussed on the sample. In this case, the incident beam nearly fills the cross section of the entrance port (1-inch diameter), so that a reduction of the port size is not possible. To obtain the most accurate values of reflectance, a port loss correction term must be applied to the data. Assuming that the MgO samples are perfect diffusors, the error is $e_{PL} = \frac{A_p}{\pi r^2} \cos \theta$. Where θ is the angle of incidence, r is the radius of the sphere, and A_p is the area of the port.

In addition, a near cosine port loss dependence was measured by suspending a small area (0.015 in^2) silicon solar cell in the center of the port. These data are shown graphically in Figure 1-8. To compensate for port losses, the correction factor $C_{PL} = 1 + e_{PL}$ was applied to each measurement. For the test geometry used in the present investigation (1" dia. port), $e_{PL} = 0.0156 \cos \theta$. The respective correction factors are illustrated in Figure 1-9.

Figure 1-10 illustrates the difference between the corrected reflectance values and values uncorrected for port-loss errors.

Several researchers (Meacock, *et al.*[6], Miller and Van Kannon[7], and Oetking[8]) have measured a retro-reflectance value for MgO larger than for a diffuse surface (See Figure 1-11). A large retroreflectance component would increase the energy lost out the entrance port and the associated correction term. Stockham and Love[9] have recently developed analytic expressions for integrating sphere reflectance errors which specifically include terms accounting for retroreflectance of MgO. Using the reported

FIGURE 1-8: DIRECT REFLECTION OUT ENTRANCE PORT
FROM A CENTER-MOUNTED MgO SAMPLE
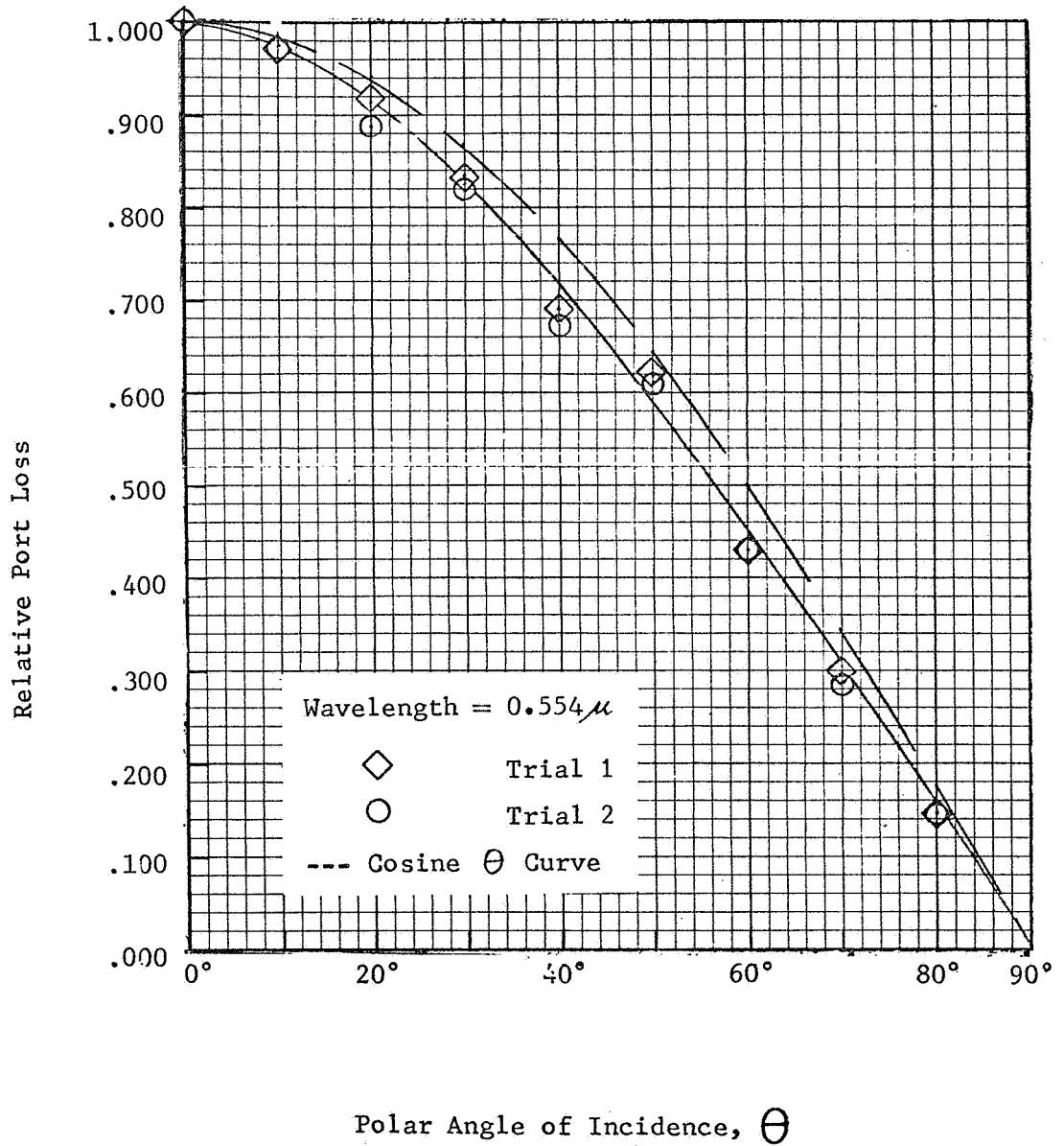
FIGURE 1-9
PORT LOSS ERROR CORRECTION FACTORS
FOR PERFECTLY DIFFUSE SPECIMEN.

Correction Factor – C_{PL}

Polar Angle of Energy Incidence – Θ (Degrees)
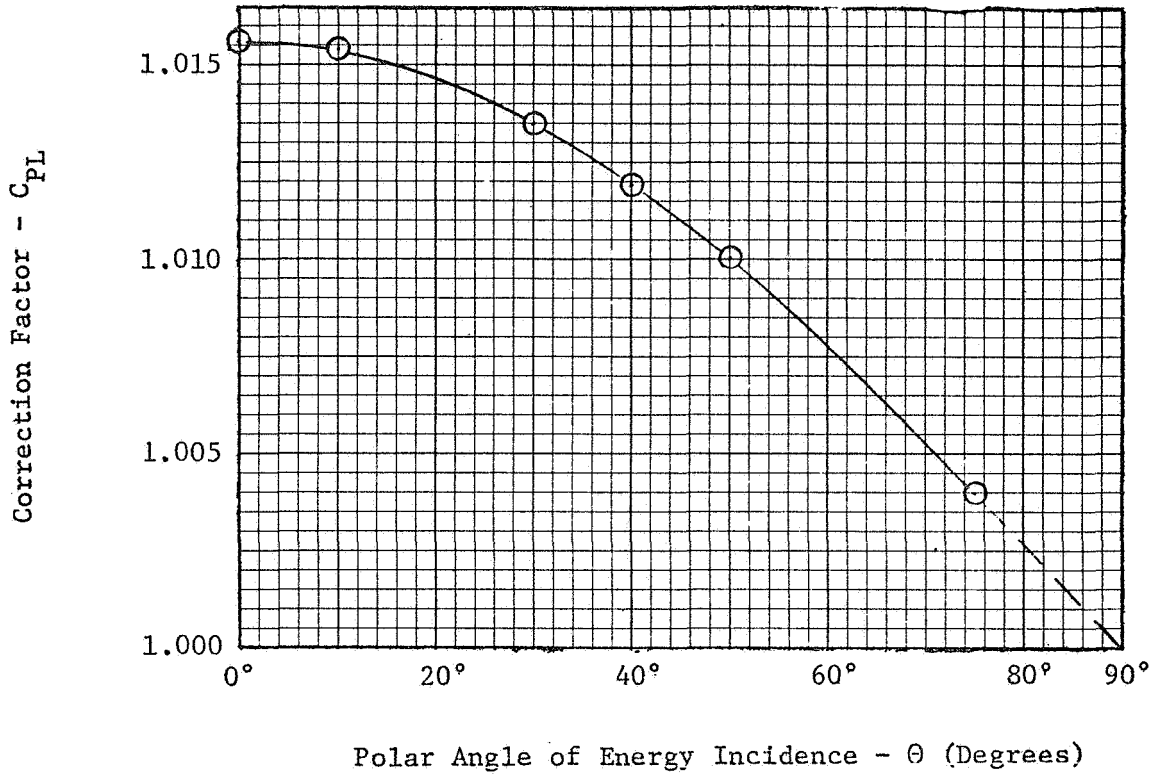
FIGURE 1-10

SPECTRAL REFLECTANCE OF S/N 572-68 (Smoked MgO, 3mm Thick,
ELECTROSTATICALLY APPLIED, (172 HOURS OLD) AT 1.0 MICRON
WITH AND WITHOUT PORT LOSS CORRECTION.

Spectral Reflectance at
1.0 Micron – $\rho_{1.0\mu}$ (Per Cent)

○ – Corrected for Port Loss

△ – Uncorrected for Port Loss

Polar Angle of Energy Incidence – Θ (Degrees)

Angle of View (Degrees)
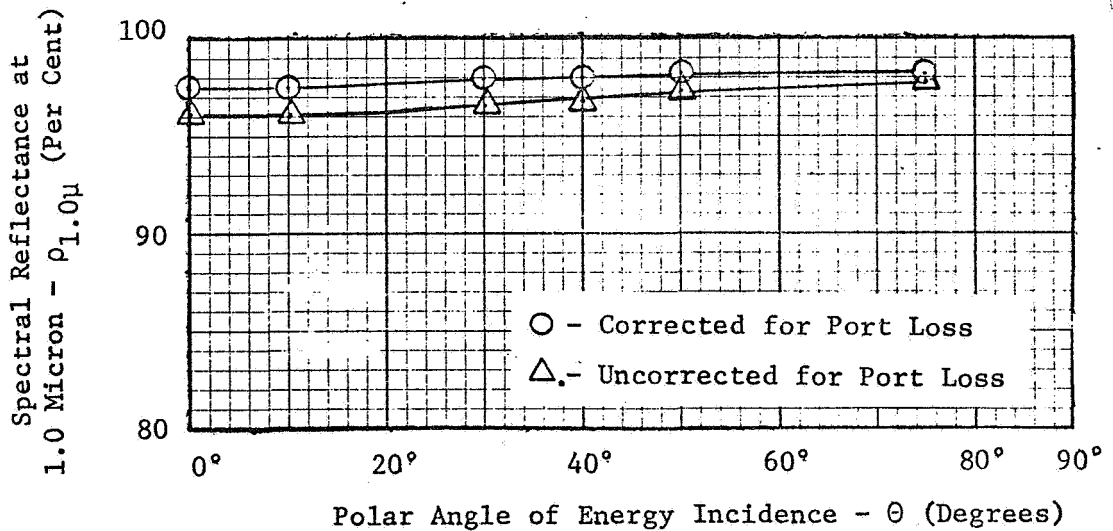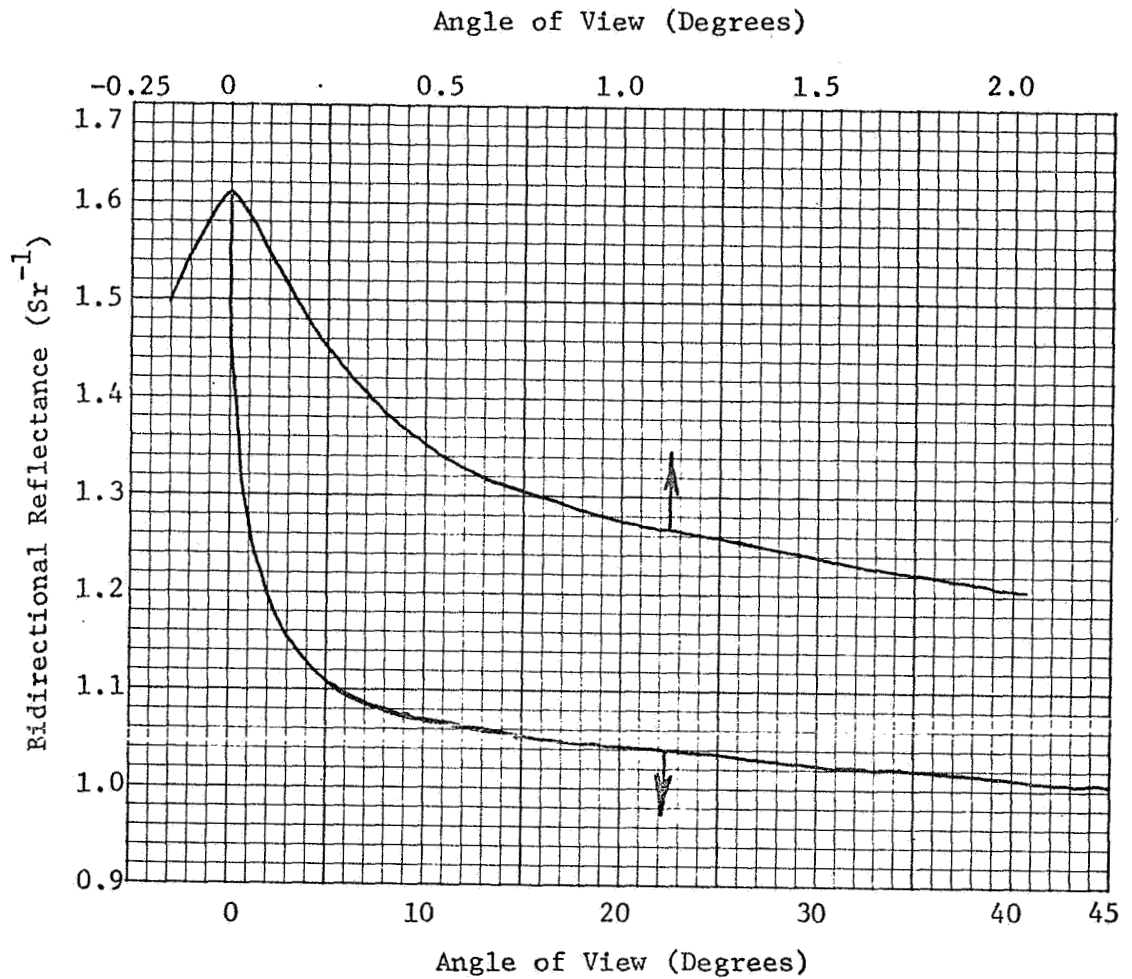
FIGURE 1-11:   BIDIRECTIONAL REFLECTANCE FOR NORMAL INCIDENCE
        FOR NON-ELECTRICALLY SMOKED MgO (1 mm THICK) ON SILVER
                WITH A TUNGSTEN STRIP LIGHT SOURCE
             (Measurements reported by Meacock, *et al.*[6])

data of Oetking[8], they concluded that the error should probably be negligible. Measurements of bidirectional reflectance of MgO during this study have not detected any significant retro-reflectance (See discussion of tests in Section 1.6.8).

Reference Measurement Errors Due to Non-Normal Incidence - As seen in Figure 1-12, the reflectance of smoked and pressed MgO coating is dependent on the polar angle of incidence. Figures 1-20 and 1-21 of Section 1.5.7 illustrate the dependence of spectral reflectance on the state of polarization of the incident energy. Since reflected energy from a central sample strikes the MgO-coated sphere wall at 0°, the 100% reference measurement should also be performed at normal incidence. However, before the present program to perform reflectance measurements of MgO was begun, the common practice in this laboratory and many others was to perform the 100% wall reference measurement at an angle of approximately 40° (as in Gier Dunkle Model DIS-4A Reflectometer). Considering the reflectance properties of MgO, this is a poor practice. Unfortunately, this fact became obvious during the analysis of the results after the completion of testing using a reference beam incidence angle of 37° to 40°. Figure 1-5 (Section 1.5.4) shows this typical position of the reference beam used during the measurements.

An additional test was performed to obtain relative reflectance values for 1) energy striking the back of the sphere wall at 0° incidence, and 2) energy striking the sphere wall at the location and angle typically used for the reference beam (40° incidence angle). These tests were performed at each of the eight wavelengths used and for each polarization state. The beam leaving the monochromator was polarized using a Glan Thomson polarizer and directed onto the back of the sphere wall by rotating the sphere about a vertical axis through the entrance port. In this position, the output was amplified to read 100%. The sphere was then rotated until the reference beam was in its typical operation location and the output was recorded. This same test was then performed at the other polarization state. The difference between the outputs at the two polarization states in the typical reference beam position was thereby determined. This
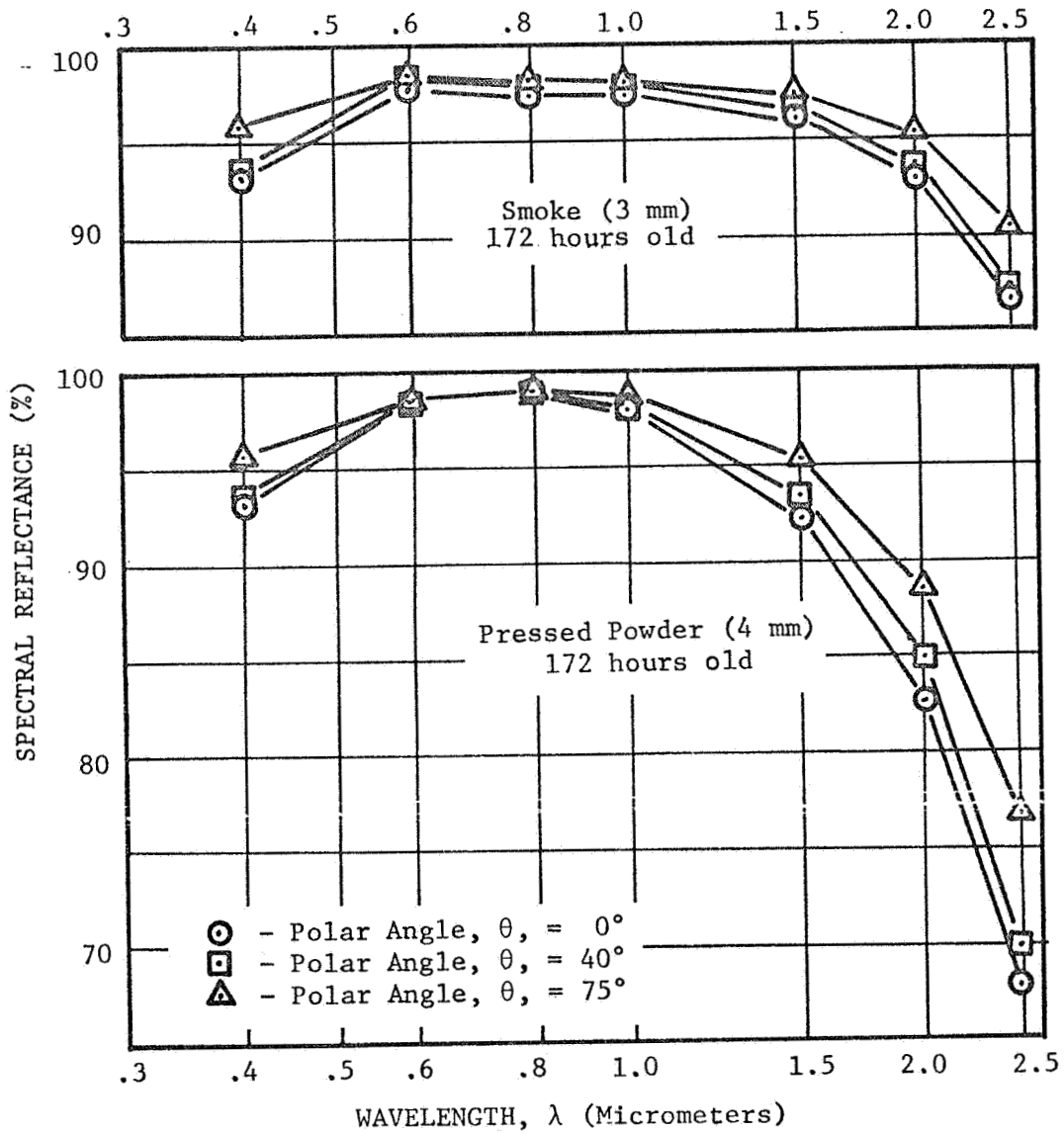
FIGURE 1-12:   SPECTRAL DIRECTIONAL REFLECTANCE OF MgO COATINGS
AS A FUNCTION OF WAVELENGTH

-26-

difference represents the degree of polarization of the reference beam intro-
duced by striking the sphere wall at an angle of incidence of approximately
40°. One half of this difference must be applied to all measurements using
completely polarized incident energy. The direction of the correction,
however, depends upon the polarization state at which the measurement was
performed.

The correction factors which were determined are illustrated in
Figure 1-13. Figure 1-14 illustrates corrected values and values uncorrected
for non-normal incidence of reference beam.

To avoid this reference beam correction procedure, a more desirable
reference beam position could be attained by modification of the transfer
optics. Such a geometry is shown in Figure 1-15.

Errors Due to Direct Irradiation of Detector/Detector Geometry - In Ref. 2,
describing the advantages of the center-mounted sample type of integrating
sphere, the authors reported no measureable signal attributable to direct
irradiation of the detectors which were singly mounted directly below the
sample. The Gier Dunkle Integrating Sphere is the commercial version of
the Edwards sphere, but both detectors are mounted on the same port to sim-
plify the operation of the reflectometer (See Figure 1-16). The present
investigation, however, has shown this simplification to produce signifi-
cant direct irradiation/detector geometry errors for highly diffuse samples.

When detectors are mounted off center, it is also probable that the
distance between the reference beam image area on the sphere wall and the
detector is different than the distance between the sample beam image area
on the sphere wall and the detector. These two areas on the sphere wall there-
fore have different shape factors to the detector. The "first bounce" por-
tion of the detector signal is proportional to these shape factors. There-
fore, an error may result. The combined direct irradiation/detector geometry
error is significant for detectors mounted off center on a dual detector
mount which is presently standard equipment in the commercially manufactured
Gier Dunkle Integrating Sphere Reflectometers. During the present measure-
ments of MgO surfaces, it was noticed that different results were obtained at
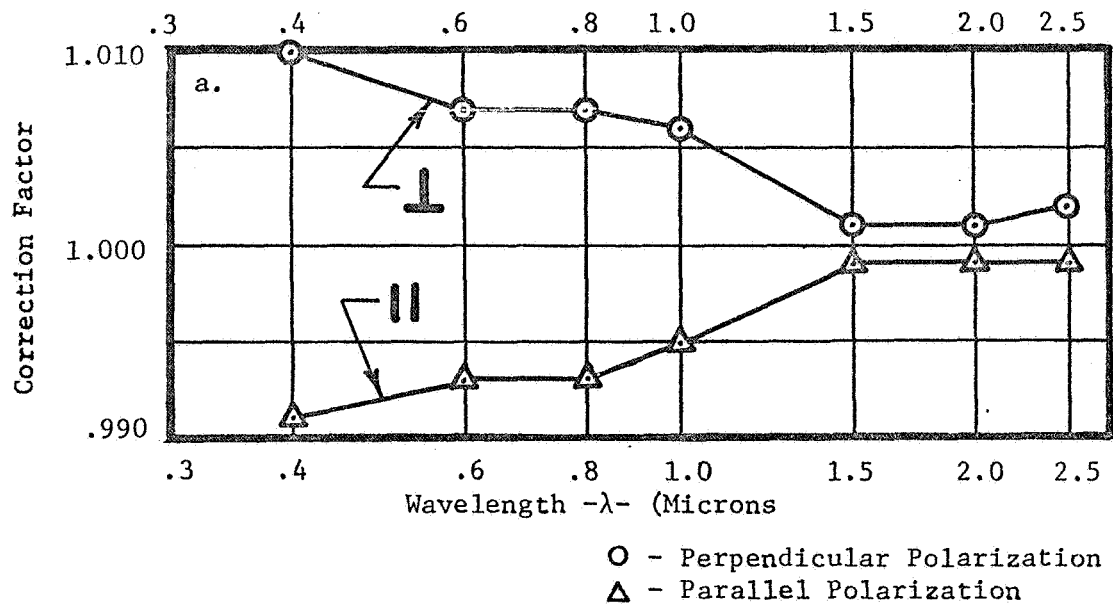
FIGURE 1-13: CORRECTION FACTORS FOR NON-NORMAL INCIDENCE OF REFERENCE BEAM
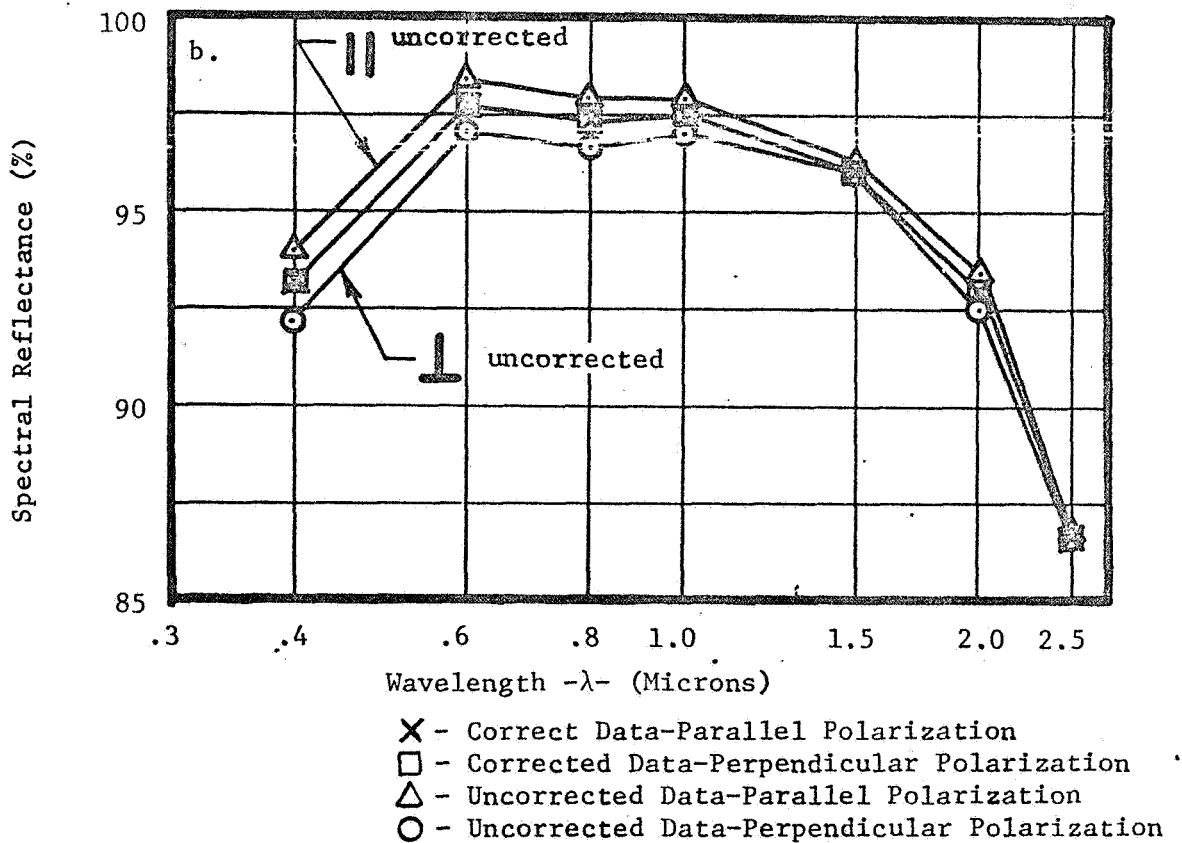
FIGURE 1-14: SPECTRAL REFLECTANCE OF S/N 572-68 AT 0° POLAR ANGLE
WITH AND WITHOUT NON-NORMAL REFERENCE BEAM INCIDENCE CORRECTION.

⊥ (‖) – Incident Beam Polarized Perpendicular (Parallel)
to Plane of Incidence

-28-

FIGURE 1-15: TOP VIEW OF CROSS SECTION OF INTEGRATING SPHERE
SHOWING RECOMMENDED SINGLE, CENTRAL DETECTOR MOUNTING
AND PRACTICAL REFERENCE BEAM GEOMETRY

Pbs Cell or
PM Tube Detector
1cm dia. Active Area

-8°

-16°

Sample Orientations
during 100% Reference
Measurement

MgO Smoke
Coating
(3mm thick)

2 inch and 1 inch dia.
Samples in Typical
Orientations

Inside
Sphere
Wall
(4 inch
radius)

Entrance Port
(1 inch diameter)
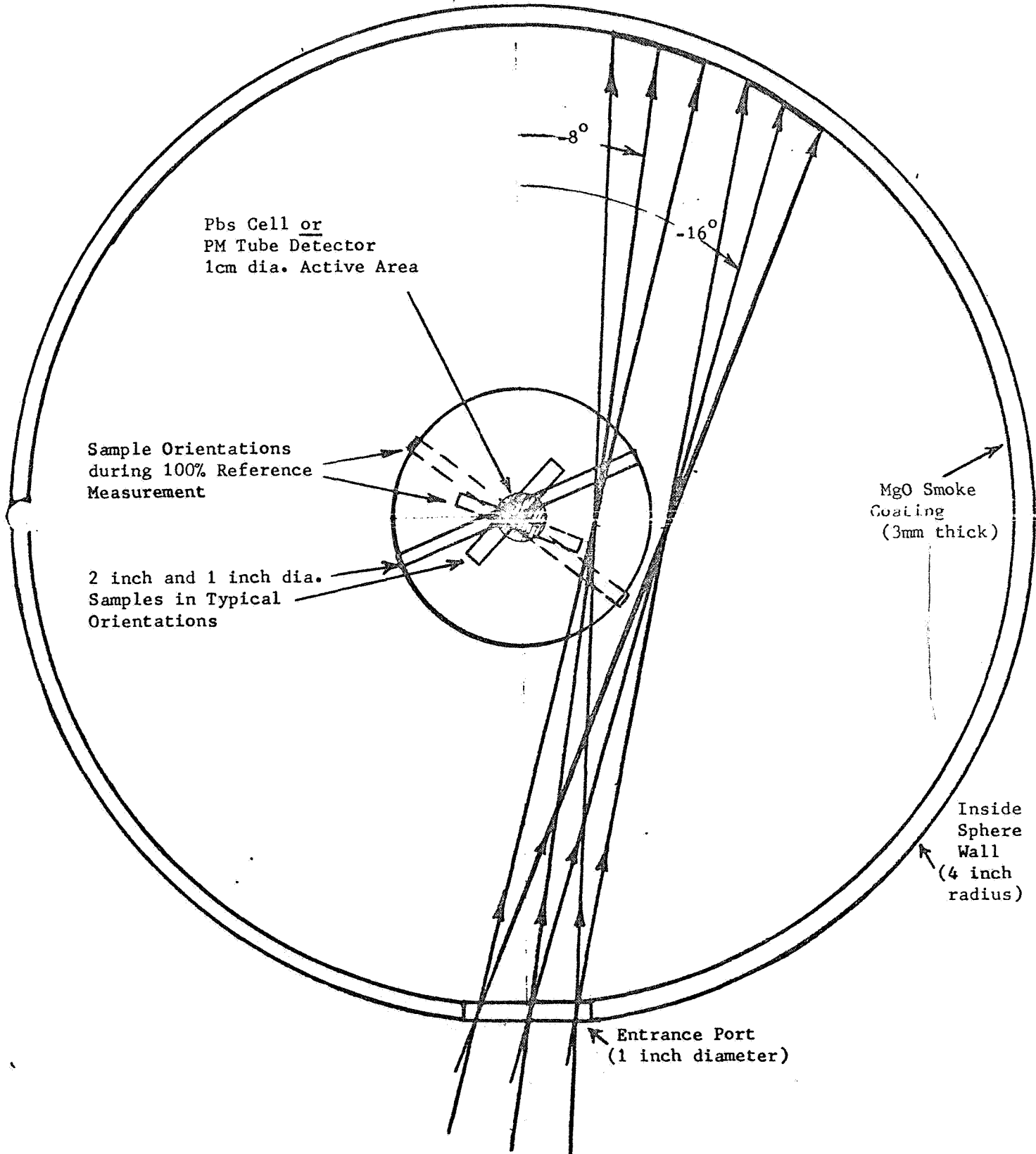
Port with dual detectors –
PM tube and PbS cell both mounted off-center
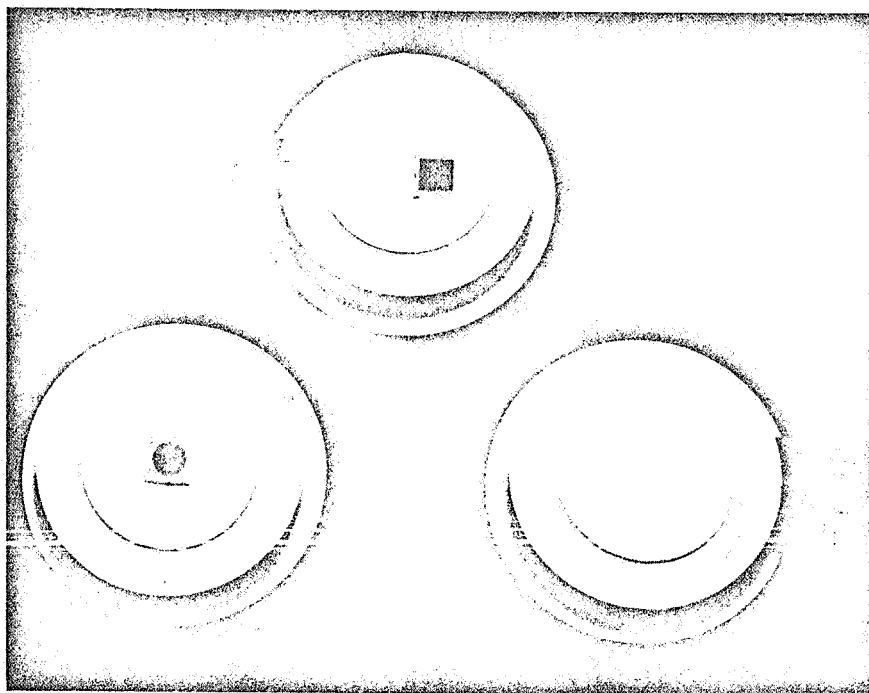
Port with single (PbS
Cell) detector mounted
on-center

Port with single (PM
Tube) detector mounted
on-center

FIGURE 1-16:   PHOTOGRAPH OF INTEGRATING SPHERE PORTS WITH
SINGLE AND DUAL DETECTOR MOUNTINGS

FIGURE 1-17a

Illustration of Errors in Directional
Reflectance of Diffusing Surfaces
(MgO Pressed Powder) Due to Detector
Geometry and Direct Irradiation of Detector

PbS Cell
$\lambda = 0.6\mu m$

REFLECTANCE

0.990
0.980
0.970
0.960

−80° −60° −40° −20° 0° 20° 40° 60° · 80°

Top View
of Sphere
Cross
Section

PM
−Θ

PbS
+Θ

ENTRANCE
PORT

——— Detector Mount in Normal Position

− − − − Detector Mount Rotated by 180°

FIGURE 1-17b

PM Tube
$\lambda = 0.6\mu m$

REFLECTANCE

0.990
0.980
0.970

−80° −60° −40° −20° 0° 20° 40° 60° 80°

ANGLE OF INCIDENCE, Θ

−31−
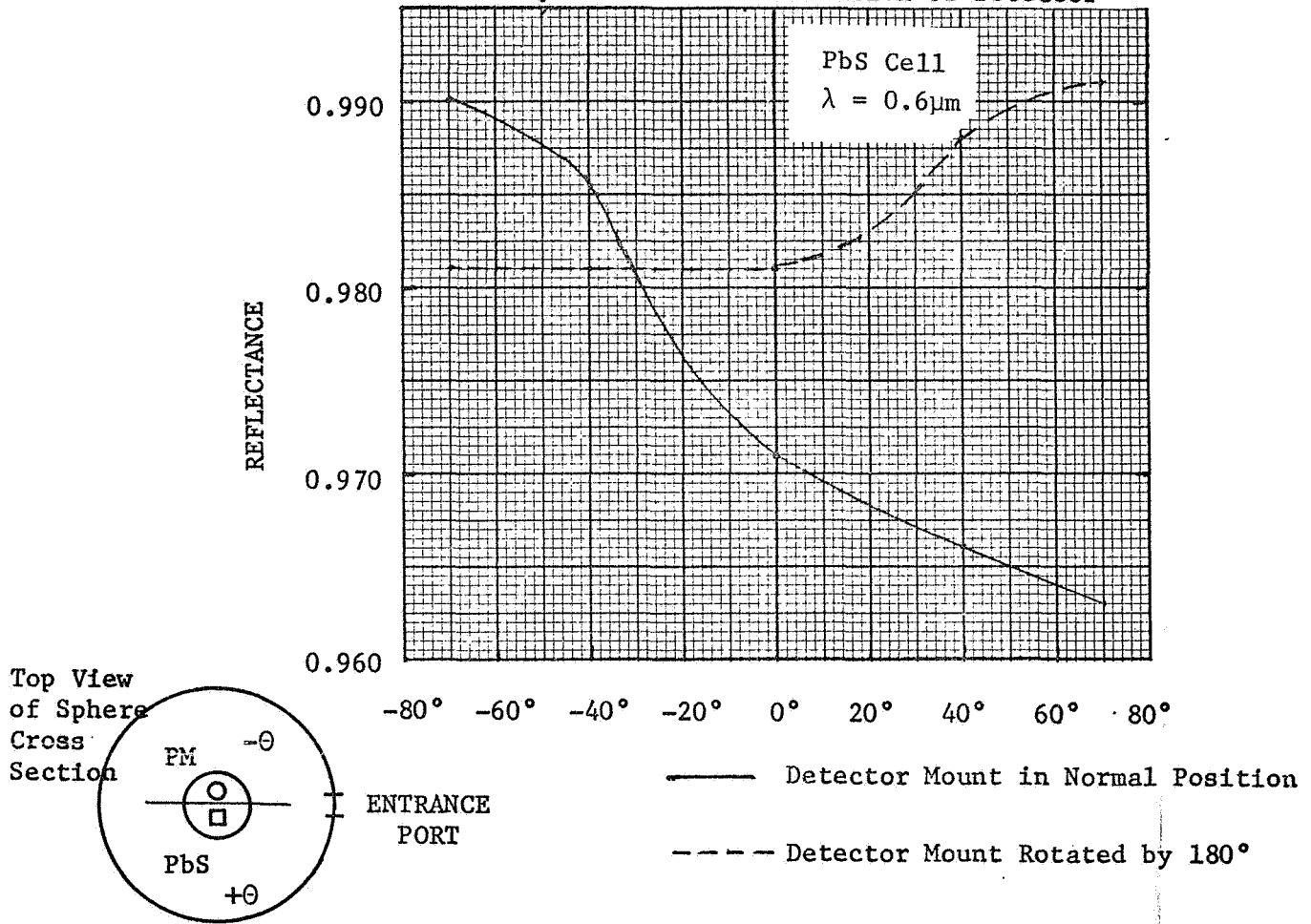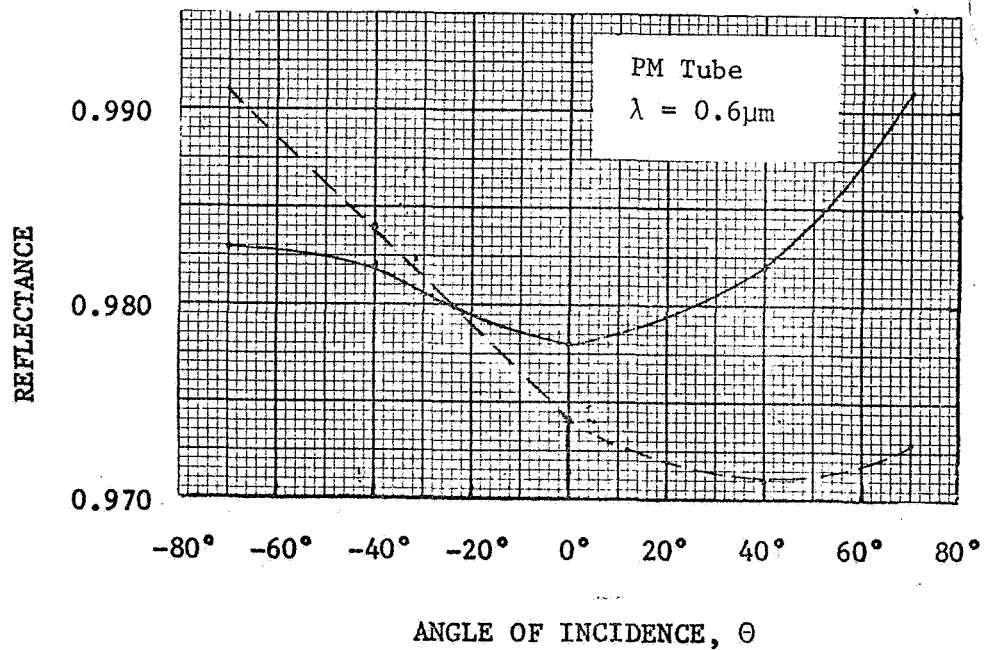
FIGURE 1-18a

PM TUBE

Illustration of Errors in Directional
Reflectance of Specular Surfaces
(Second Surface Silver on Quartz) Due to
Detector Geometry

PbS Cell

$\lambda = 0.6\mu m$

REFLECTANCE

0.980

0.970

0.960

0.950

-80° -60° -40° -20° 0° 20° 40° 60° 80°

—————— Detector Mount in Normal Position

— — — — Detector Mount Rotated by 180°

FIGURE 1-18b

PbS Cell

PM Tube

$\lambda = 0.6\mu m$

REFLECTANCE

0.990

0.980

0.970

0.960

-80° -60° -40° -20° 0° 20° 40° 60° 80°

ANGLE OF INCIDENCE, Θ

-32-
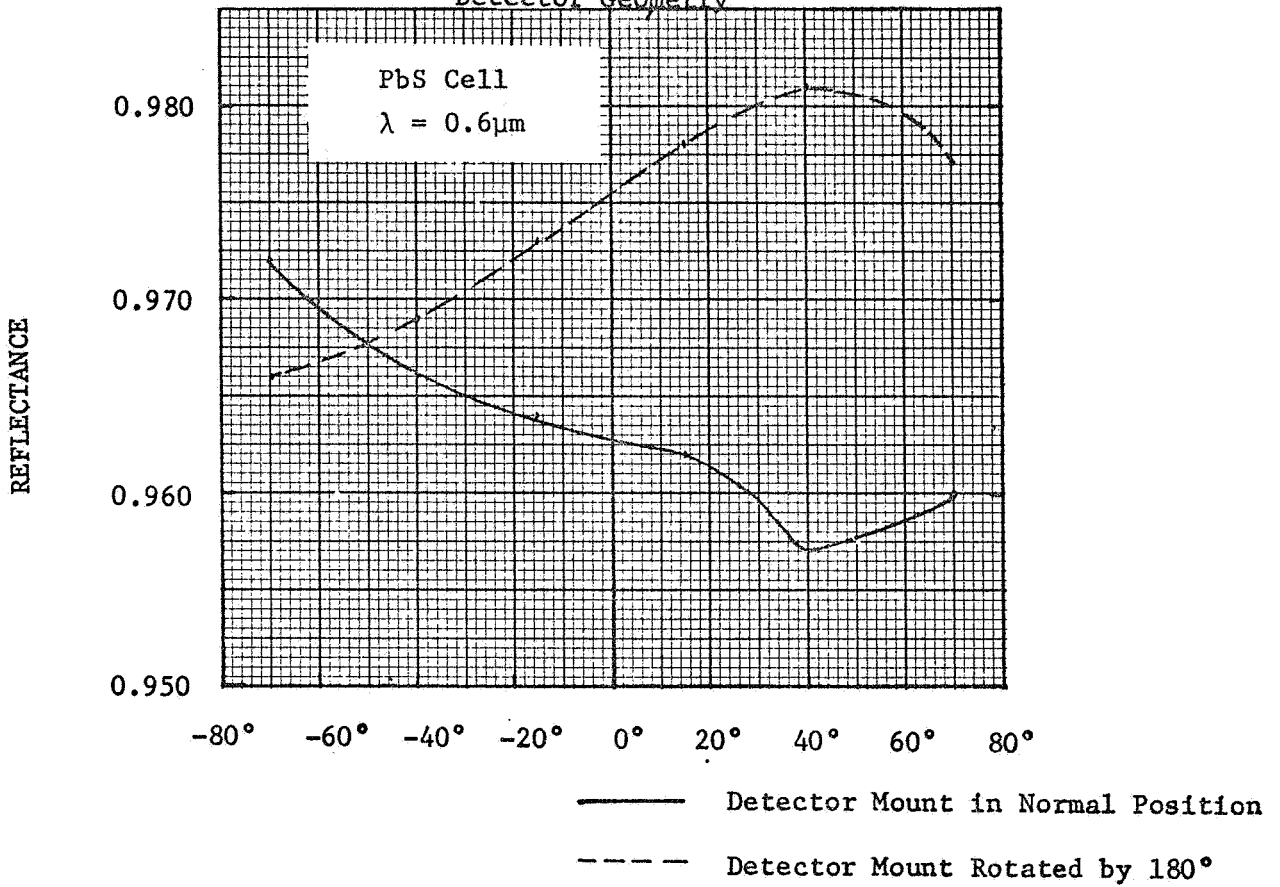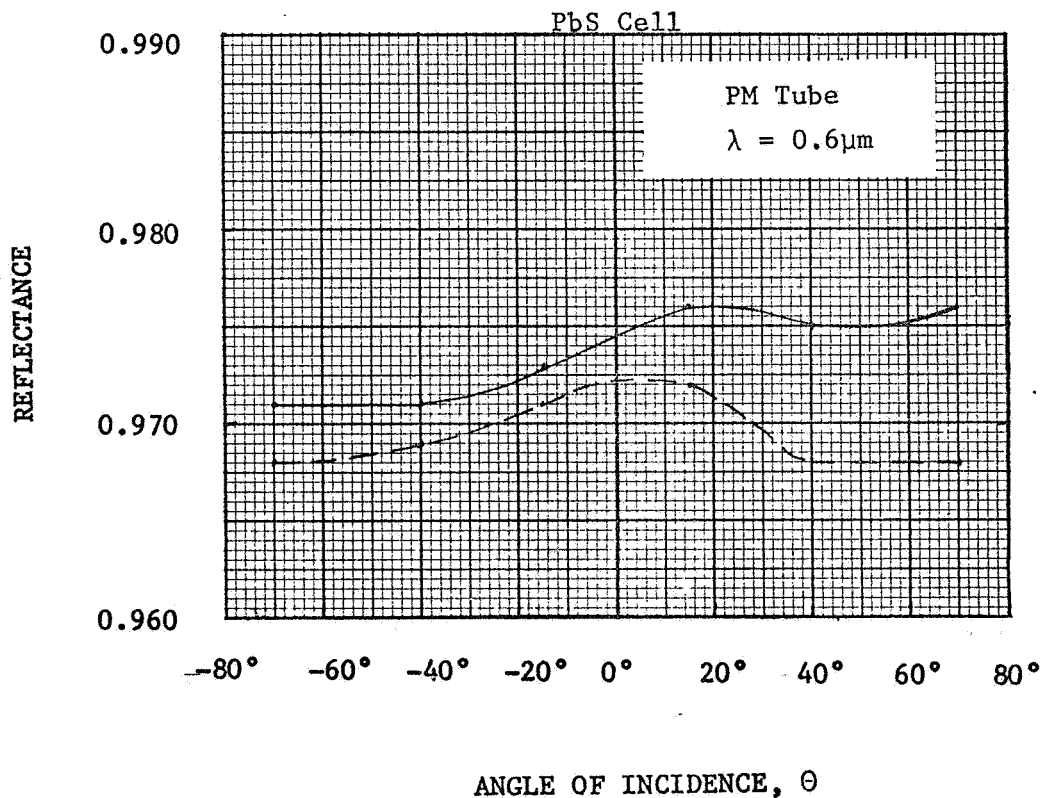
positive and negative polar angles of incidence for a given detector (See Figure 1-17 a and b). The reflectance apparently increased as the sample was turned toward the side on which the detector was mounted off center. Conclusive evidence that the measured reflectance of a diffuse test sample varies greatly with detector position was obtained by rotating the detector mount by 180°. As can be seen in Figure 1-17, the rapid increase of reflectance with angle of incidence changed sides. To determine the separate effect of detector geometry without direct irradiation contribution, the reflectance of a specular sample (second surface silver on quartz) was measured at the regular and the 180° rotated detector positions. These results are shown in Figure 1-18 a and b.

An additional test to eliminate possible variations in sphere wall reflectance from this detector geometry analysis is illustrated in Figure 1-19. Here energy was directed onto the sphere wall, and a signal was obtained for four detector mount orientations. The difference in the readings results from varied distances of the detector from the irradiated spot on the sphere wall.

The sandblast/smoked MgO coating treatment of the PM tube detector was shown to essentially eliminate asymmetric response (see Detector Measurements, Section 2.3). Further evidence of symmetric polar response is shown in Figure 1-19, in that the response in the regular and 180° rotation position is exactly equal to 1.000. As the sphere wall reflectance decreases at the shorter (0.4) and larger (1.5) wavelengths, the "first bounce" energy from the sphere wall to the detector becomes more important, and the effect of the detector position increases. The present series of measurements have been performed with the standard Gier Dunkle Detector Mount. In order to obtain a compensating correction factor, one smoked MgO sample (572-68, 3 mm thick) was completely remeasured using single central mounted detectors. By obtaining a ratio for each respective value, original and new, a set of correction factors was derived. These correction factors, C_D, listed below, were applied to each sample. Reflectance values for the single central mounted detector configuration were thus obtained.

Integrating Sphere
with Dual Detector Mount –
Sectional Plan View
Detector in Regular Measurement
Position

Beam Incident on
Sphere wall 180°
opposite entrance
port

PM Tube Detector

Entrance
Port

Energy Beam

PbS Cell Detector

1.000

1.007 .997

1.000

$\lambda = .6\mu$

PM TUBE

1.000

1.009 .992

1.000

$\lambda = .4\mu$

1.000

1.000 1.000

1.000

$\lambda = .6\mu$

PbS CELL

1.000

1.000 1.000

1.000

$\lambda = 2.0\mu$
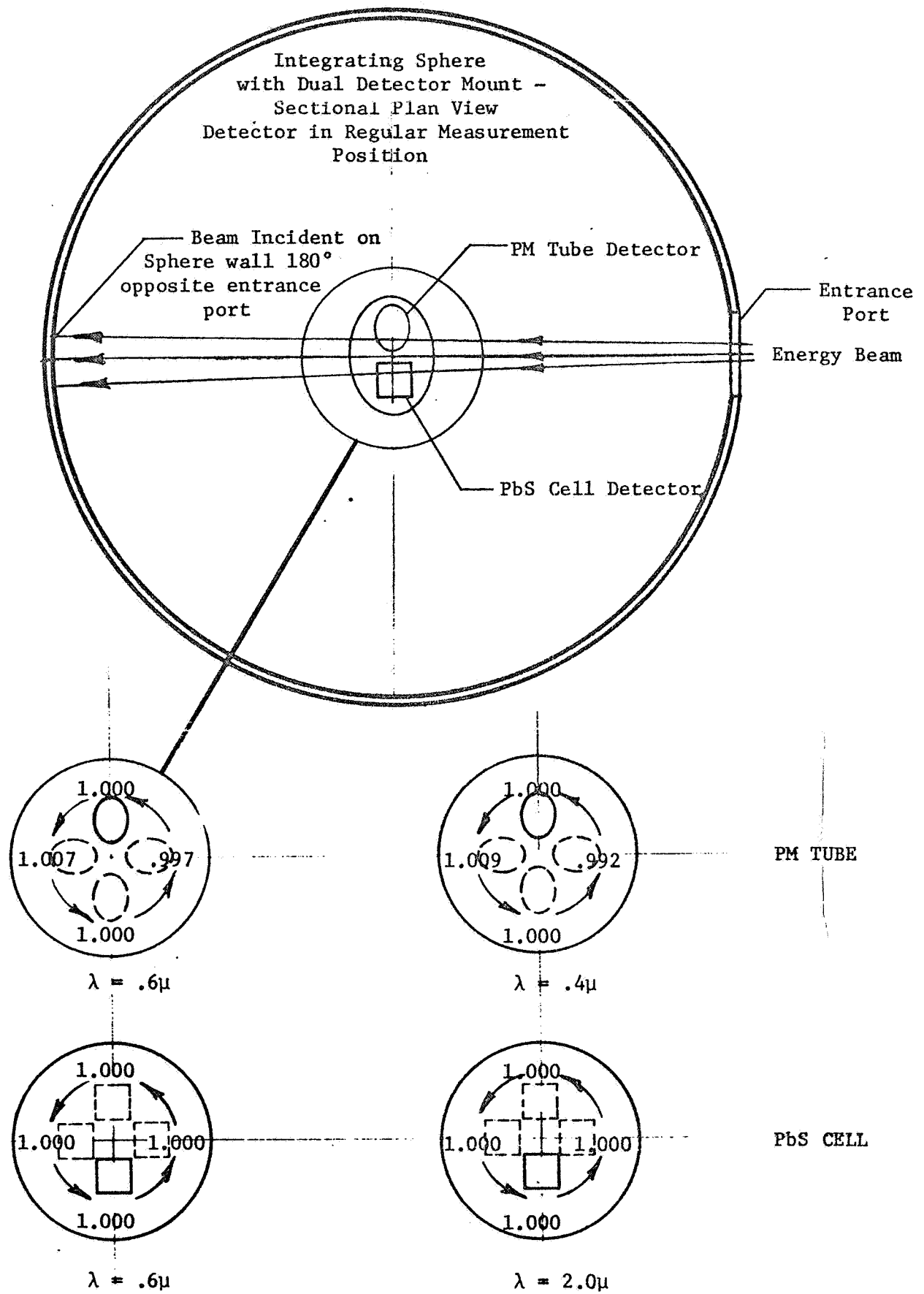
FIGURE 1-19: TEST TO DETERMINE RELATIVE DETECTOR RESPONSE
FOR SEVERAL DETECTOR POSITIONS
RELATIVE TO SPOT OF BEAM INCIDENCE ON SPHERE WALL.

TABLE 2: CORRECTION FACTORS USED TO CONVERT REFLECTANCE DATA
OBTAINED WITH THE GIER DUNKLE DUAL DETECTOR MOUNT
TO REFLECTANCE FOR SINGLE DETECTOR MOUNTING

λ	$\theta =$ 0°	10°	30°	40°	50°	75°
.40	.984	.982	.977	.973	.975	.978
.60	.999	.998	1.000	.999	1.000	1.000
.80	.999	.998	1.000	.999	1.000	1.000
1.00	.997	.996	.999	.998	.999	.999
1.50	.992	.991	.994	.994	.995	.998
2.00	.989	.991	.993	.995	.995	.998
2.50	.991	.991	.989	.989	.997	.998

The net correction factor to compensate for port losses, reference beam reflectance anomalies and direct irradiation of detectors was the product of the three:

$$C = (C_{PL}) \ (C_R) \ (C_D)$$

These values, listed in Table 3, were applied to each sample.

1.5.7 Directional Reflectance Measurement Results

Tables A-1 through A-7 of the Appendix present the directional reflectance data for MgO corrected for the errors described in the preceding section. These data are also shown plotted in Figures A-10 through A-16 of the Appendix for $\theta = 0°$, 40°, and 75°. Figures 1-20 and 1-21 show the spectral reflectance of smoked MgO and pressed MgO powder at various angles of incidence irradiance with completely polarized energy. Figures 1-22 and 1-23 are for unpolarized energy.

1.5.8 Discussion of Directional Reflectance Measurement Results

From a study of Tables A-1 to A-7 and Figures A-10 to A-16, some general observations can be made. The criteria for a perfectly diffuse reflector, that ρ_D is a constant as the angle of incidence is varied, was used in the portions of the discussion concerning diffuseness.

-35-

TABLE 3

COMPOSITE CORRECTION FACTORS FOR PORT LOSSES,
REFERENCE BEAM ANOMALIES, DIRECT IRRADIATION OF DETECTORS,
DETECTOR GEOMETRY

Wavelength (Microns)	0°		10°		30°		40°		50°		75°	
	$\parallel^1$	$\perp^2$	$\parallel$	$\perp$	$\parallel$	$\perp$	$\parallel$	$\perp$	$\parallel$	$\perp$	$\parallel$	$\perp$
PM (700) Hydrogen Lamp .40	.991	1.010	.988	1.007	.982	1.001	.976	.995	.976	.995	.973	.992
.60	1.008	1.022	1.006	1.020	1.007	1.021	1.004	1.018	1.003	1.017	.997	1.011
.80	1.008	1.022	1.006	1.020	1.007	1.021	1.004	1.018	1.003	1.017	.997	1.011
Tungsten Lamp 1.00	1.008	1.019	1.006	1.017	1.008	1.019	1.005	1.016	1.004	1.015	.998	1.009
1.50	1.007	1.009	0.005	1.007	1.007	1.009	1.005	1.007	1.004	1.006	1.001	1.003
2.00	1.004	1.006	1.005	1.007	1.006	1.008	1.006	1.008	1.004	1.006	1.002	1.003
PbS 2.50	1.006	1.009	1.005	1.008	1.002	1.005	1.000	1.003	1.006	1.009	1.001	1.004

(1) $\parallel$ → incident energy polarized parallel to plane of incidence.

(2) $\perp$ → incident energy polarized perpendicular to plane of incidence.
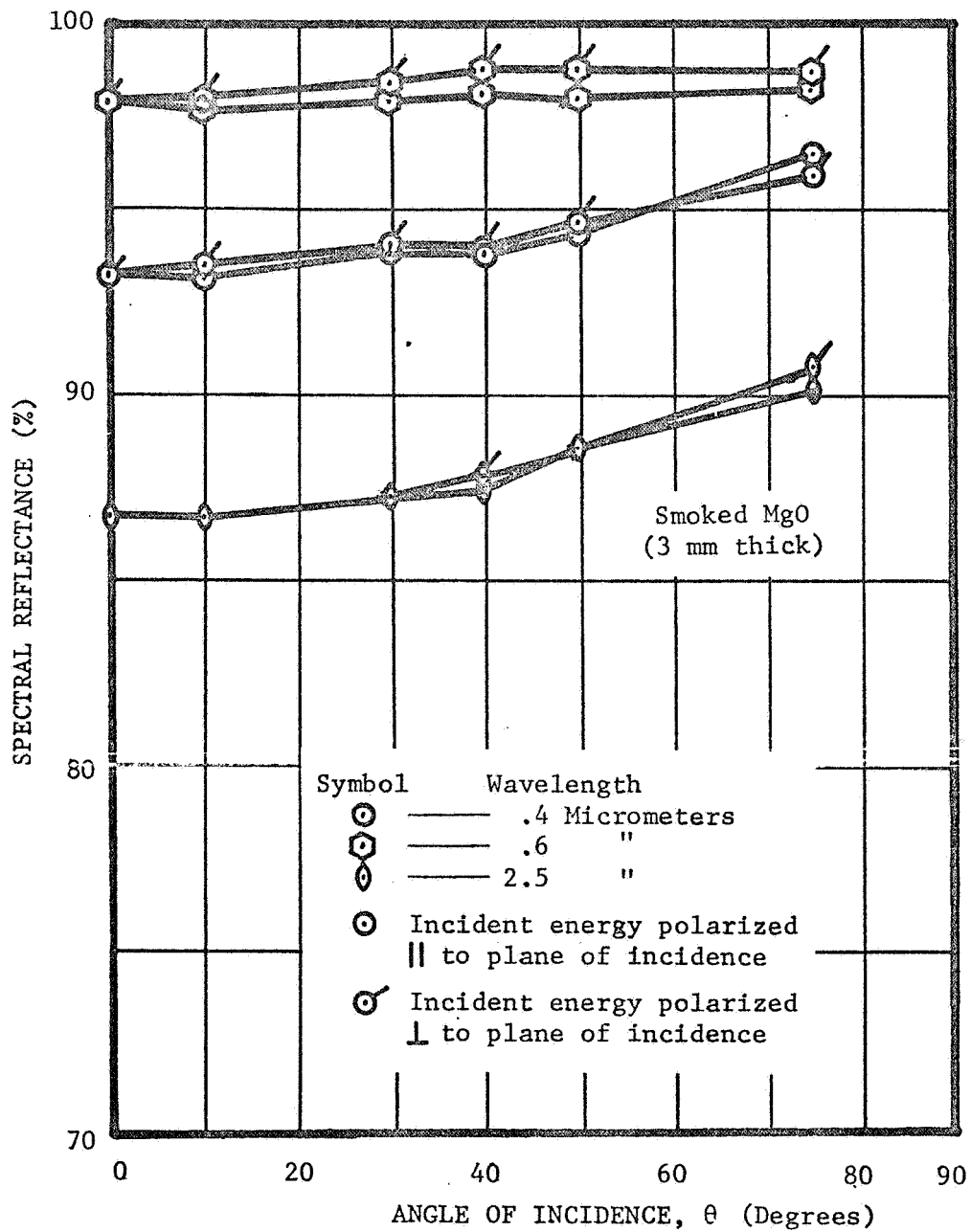
Spectral Directional Reflectance of Smoked MgO
as a Function of Polarization
(Sample 572-68)

FIGURE 1-20
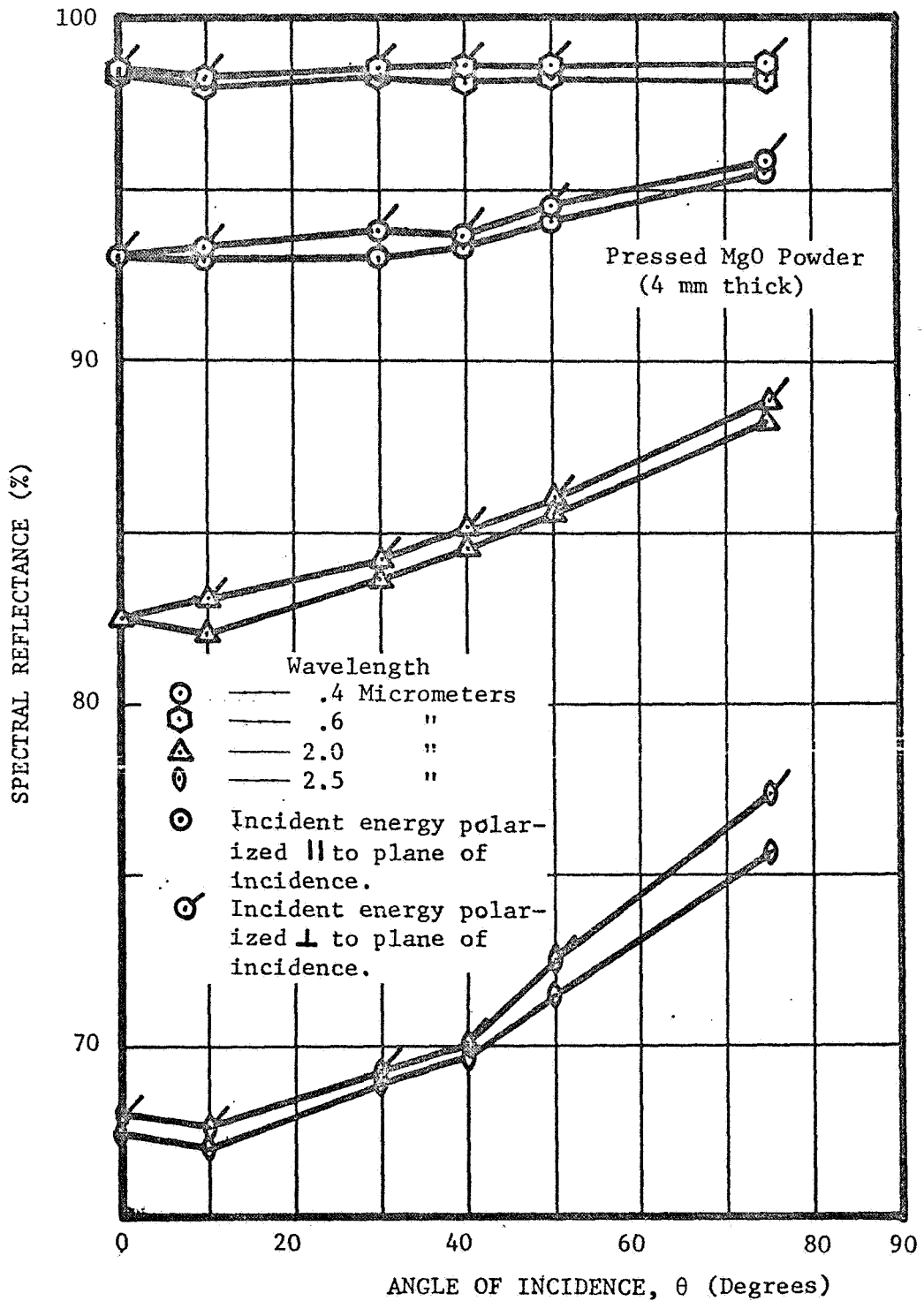
Spectral Directional Reflectance of Pressed MgO Powder
as a Function of Polarization
(Sample 580-68)

FIGURE 1-21
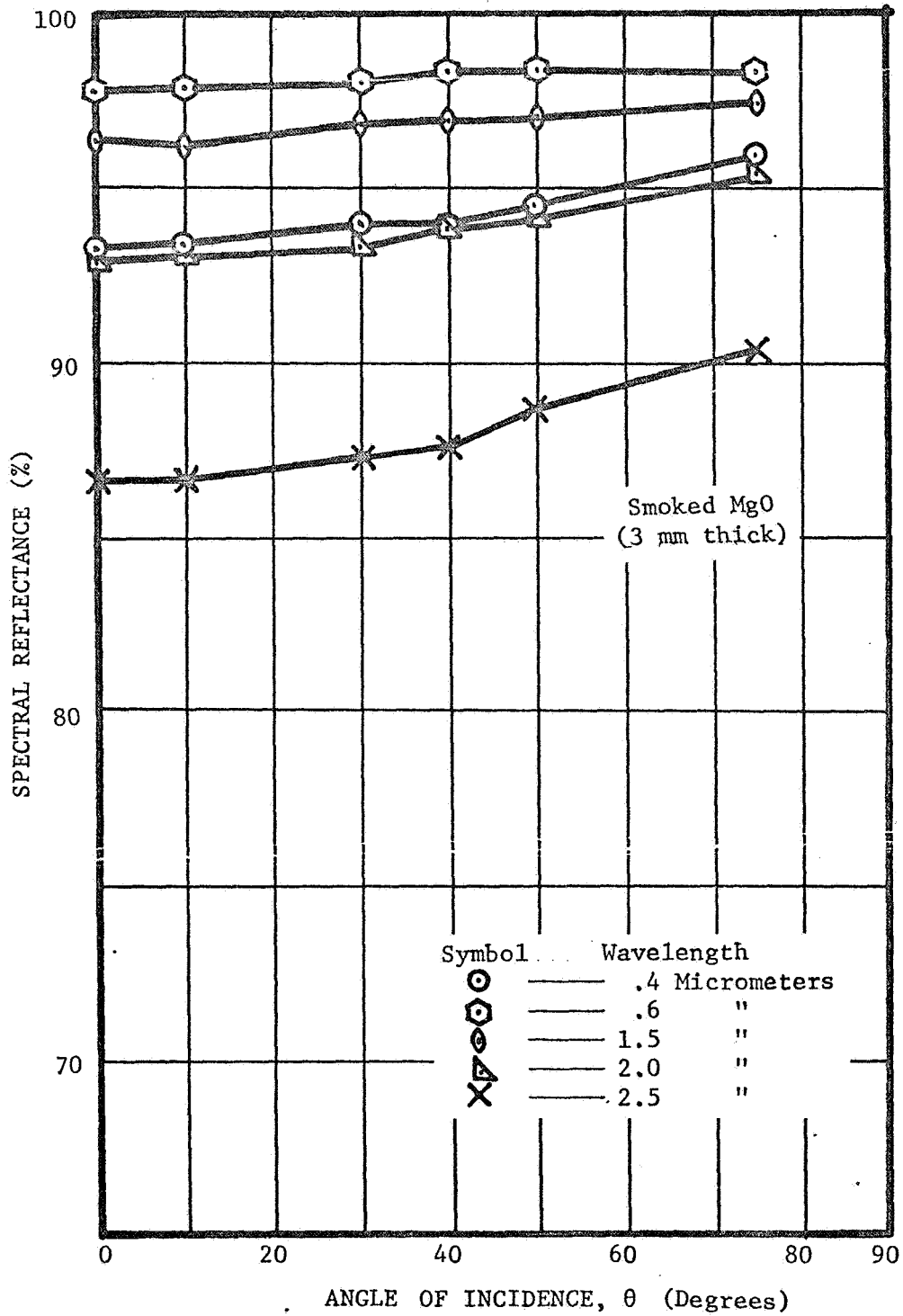
Spectral Directional Reflectance of
Smoked MgO for Unpolarized Incident Energy
(Sample 572-68)

FIGURE 1-22
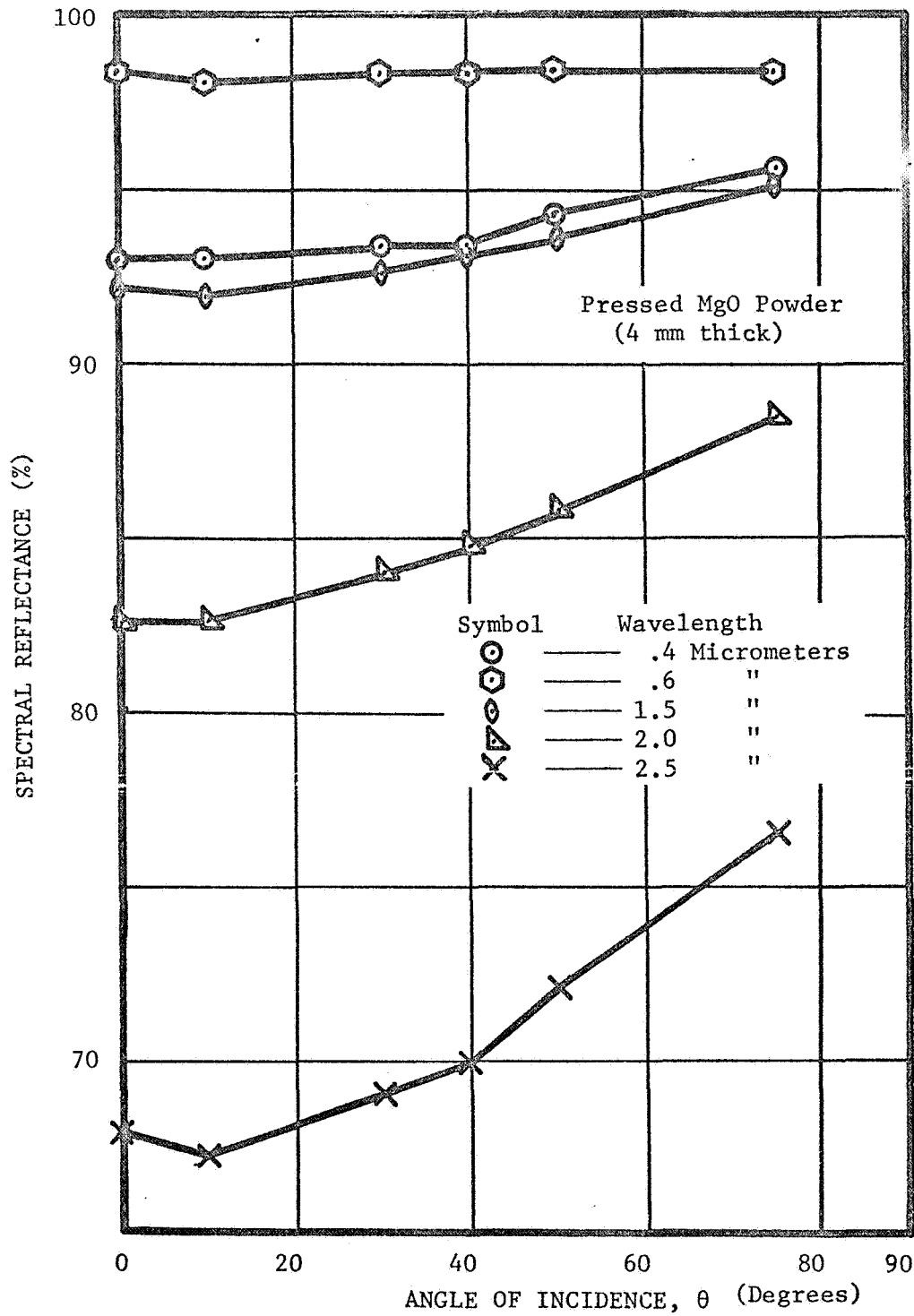
Spectral Directional Reflectance of Pressed MgO Powder
for Unpolarized Incident Energy
(Sample 580-68)

FIGURE 1-23

1.5.8.1 Smoked MgO Surfaces

a. Unpolarized incident energy

- The reflectance is slowly increasing as θ increases.

- There is essentially no difference between $\rho_D(0°)$ and $\rho_D(10°)$.

- For $\lambda = 0.4$, 1.5, 2.0, and 2.5μ, $\rho_D(40°)$ is less than 1% larger than $\rho_D(0°)$; $i.e.$, the reflectance in the ultraviolet and infrared is diffuse to about 40° angle of incidence. The deviation from diffuseness increases for $\theta > 40°$.

- The coatings are most nearly diffuse for wavelengths which have the greatest reflectance.

- To the extent that the reflectance level drops from 100%, for $\lambda = 0.4$ to 0.6μ and 1.0 to 2.5μ, the deviation from $\rho_D(\theta) =$ constant grows larger.

b. Polarized Incident Energy

- There are slight indications the $\rho_D(\perp) > \rho_D(\parallel)$.

- In general, $\left| \rho_D(\perp) - \rho_D(\parallel) \right| < 0.005$ for all θ's and λ's.

  NOTE: Differences of $\left| \rho_D(\perp) - \rho_D(\parallel) \right| < 0.005$ are not considered significant due to random errors in measurement and the correction factors applied to account for systematic errors. Theoretically, $\rho_D(\perp)$ must equal $\rho_D(\parallel)$ for $\theta = 0°$. The difference between the average value of ρ_D and $\rho_D(\parallel)$ and $\rho_D(\perp)$ at $\theta = 0°$ is a measure of the uncompensated errors in the measurement and data analysis techniques.

c. Reflectance as a Function of Thickness

- For the <u>electrostatically</u> smoked MgO surfaces, few definite trends are seen. As expected, $\rho_D(2$ mm thick coating) $> \rho_D(1$ mm thick coating), but no additional increase in ρ_D is seen for $t = 3$ mm and 4 mm.

- The reflectance for <u>non-electrostatically</u> smoked MgO surface (2 mm), compares well with the 2 and 3 mm thick electrostatically smoked samples in magnitudes, but in the visible region it appears to be increasing faster as θ increases ($i.e.$, less diffuse).

1.5.8.2 Pressed MgO Powder Surfaces

    a. Unpolarized incident energy

- The reflectance is of the same magnitude as for the smoked samples for $\lambda < 1\mu$, but is very much lower for $\lambda > 1\mu$.

- For $\lambda > 1\mu$, ρ_D changes rapidly with θ (*i.e.*, quite non-diffuse).

    b. Polarized Incident Energy

- Same as for smoked samples.

    c. Reflectance as a function of thickness

- The overall reflectance of the 4 mm thick sample is greater than that of the 3 mm sample.

1.5.8.3 General Conclusions on Directional Reflectance

    a. Electrostatically smoked MgO, 2 mm thick or more, most nearly follows the diffuse criterion, $\rho_D(\theta)$ = constant.

    b. The directional reflectance is <u>not</u> a very strong function of the polarization of the incident energy; *i.e.*, $\rho_D(\perp) \approx \rho_D(||)$ with $\rho_D(\perp)$ only slightly larger than $\rho_D(||)$ for both smoked and powder samples.

    c. MgO pressed powder is <u>not</u> very diffuse, relative to smoked MgO, and ρ_D decreases rapidly for $\lambda > 1.0\mu$.

    d. Some errors in integrating sphere measurements are proportional to $\left[\dfrac{1 - \rho_D}{\rho_D}\right]$ of the sphere coating. For $\lambda > 1\mu$, this factor is very much larger for pressed powder than for smoked coatings. Therefore, we recommend the use of smoked rather than pressed powder for integrating sphere wall coatings.

1.5.9 Recommendations for Measurements of Directional Reflectances

In the course of performing the measurements on MgO samples, it becomes very obvious that several improvements over the standard measurement techniques and modifications to the Gier Dunkle Integrating Sphere Reflectometer (GDISR) were needed in order to obtain accurate data.

These are described briefly and are recommended to those investigators desiring improved ease and/or accuracy in performing reflectance measurements.

1.5.9.1 Thermal Isolation of the Source Lamps from the Monochromator

In the standard arrangement of the optics of this reflectometer, the hydrogen and tungsten lamp sources are mounted to the side of the Perkin-Elmer monochromator. When a polarizer is used to filter the output of the monochromator, the source intensities required for adequately large output signals are about double those needed when not using a polarizer. As a result, there is a considerable quantity of heat conducted from the source housing into the monochromator. Additionally, a large quantity of underlined source radiation is dispersed by the monochromator before being directed into the integrating sphere. This quantity of heat causes temperature oscillations of the monochromator which are beyond the capabilities of the monochromator's temperature regulating heaters. This instability has been observed to cause the wavelength calibration of the monochromator to oscillate with time, and as a result, it was heretofore difficult to obtain valid measurements. After tracking down the cause of this problem, the solution was easy and effective. A water-cooled aluminum plate was installed as the light baffle for the source housing to eliminate the source to monochromator heat conduction. This modification eliminated the temperature cycling.

1.5.9.2 Improved Amplification and Display Systems

Until the last several years, the amplification system specified by Gier Dunkle Inc. was the Perkin Elmer Model 107. Recently developed solid state lock-in amplifiers have far surpassed the PE107 in noise-rejection ability, easy phase matching to one set of chopper points, linearity, and absence of zero drift. During the measurements performed for this contract, a Brower Model 129 Lock-in Amplifier was used very successfully to obtain high signal-to-noise ratios. Combined with an integrating digital voltmeter readout, reflectance values were read with very little noise problems. Use of a DVM also avoids the mechanical hysteresis problems inherent with chart recorders.

1.5.9.3 Change from Dual Mount to Single Mount Detectors

In order to eliminate direct irradiation from sample to detector,

the standard dual detector mount was replaced by two separate detector mounts. The detectors were oriented directly below the sample. The PbS cell detectors azimuthally dependent response was eliminated by enclosing it in an aluminized Mylar mask with a circular opening for detection.

1.5.9.4 Complete Elimination of Direct Irradiation Error

Since even a single detector mounted just below the sample will present a small, but finite, area which may detect direct irradiation from diffuse or extraordinary reflecting samples, a direct irradiation error may arise. This can be totally eliminated by mounting the samples on a metal disc which has a 2-1/2 degree wedge in its thickness. Adequate compensation of the polar angle settings of the sample would be required for near-normal angles of incidence.

1.5.9.5 Sample Angular Orientation during 100% Setting

To save the operator time required in manually turning the sample to face the reference on the sphere wall, an electronic switching circuit should be incorporated into the sample motor mount for this purpose.

1.5.9.6 Modification of Transfer Optics

As shown in Figure 1-15, and discussed earlier in Section 1.5.6.2 (b), the reflectometer translation optics should be changed to provide near-normal incidence of the reference beam on the sphere wall. This would eliminate the small but constant error in the reference measurement which occurs with the present arrangement for 40° incidence.

1.6 BIDIRECTIONAL REFLECTANCE

1.6.1 Summary

 In general, the importance of the bidirectional reflectance character-
istics of diffuse sphere wall coatings pertains primarily to that portion
of the energy inside the sphere which has experienced only one reflection
off the walls. (This is referred to as the "first-bounce energy".) One
reason for this is that a number of integrating sphere measurement errors
may result from this energy.

In the reference signal measurement mode, the energy enters the sphere
through the entrance port, is incident upon the sphere wall, and a majority
is reflected. In the sample measurement mode, the energy enters the sphere,
is incident upon the sample, and partially reflected to the sphere wall
where, again, the majority is reflected. The energies striking the wall in
these two modes, however, are not of the same polarization state and do not
strike the sphere walls at the same location or incidence angle. When the
sphere wall coating reflectance is a function of these parameters, errors
may result.

The bidirectional reflectance (BDR) of smoked and pressed powder MgO
samples was measured as a function of a number of parameters. It was found
that smoked MgO is more diffuse than pressed MgO powder. For polar angles
of incidence, θ_1, less than 40°, the samples appeared to be quite diffuse.
At larger values of θ_1, forward and backward scattering increased. The BDR
at a wavelength of 0.5 microns is generally similar to that at 1.5 microns.
The exceptions to this statement are discussed in Section 1.6.8.3. Polarized
energy, when incident on a MgO surface, is greatly depolarized. The degree
of depolarization is dependent upon the various parameters concerning the
incident beam such as wavelength and angle of incidence.

1.6.2 Measured Quantity

The quantity measured by the test apparatus is the relative reflectance
distribution, V/V_o, which is a function of the wavelength of incident energy,
the angles of incidence and reflection, the polarization of the incident and

reflected energy, and the solid angle of detection. It is a measure of the fraction of the energy, incident from direction (θ_1,ϕ_1) in the solid angle Ω_1, which is reflected in a direction (θ_2,ϕ_2) into the solid angle of detection (Ω_2) of the reflectometer (See Figure 1-24).

For flat extended surfaces such as the present MgO samples, another quantity, the spectral bidirectional reflectance (ρ_B), may be derived which is theoretically independent of the measurement apparatus. The relation-ship between the relative reflectance and the spectral bidirectional reflectance is presented below.

1.6.3 Definitions

The spectral bidirectional reflectance can be defined as π times the power reflected in direction (θ_2,ϕ_2) per unit area normal to that direction, per unit wavelength, and per unit solid angle divided by the power incident from direction (θ_1,ϕ_1) in the solid angle $d\Omega_1$ (Ref 1). In equation form, we have

$$\rho_B(\theta_1,\phi_1,\theta_2,\phi_2,\lambda) = \frac{\pi I_2(\theta_2,\phi_2,\lambda)}{I_1(\theta_1,\phi_1,\lambda)\ \cos\ \theta_1\ d\Omega_1} \qquad [1]$$

where I_1 and I_2 are the incident and reflected spatial intensities, respec-tively, with units of watts/cm^2-steradian-micron.

The more commonly used quantity, the spectral directional reflectance (ρ_D) may be found by integrating ρ_B over the hemisphere with respect to $1/\pi(\cos\ \theta_2\ d\Omega_2)$; i.e.,

$$\rho_D(\theta_1,\phi_1,\lambda) = \frac{1}{\pi} \int_\Omega \rho_B\ \cos\ \theta_2 d\Omega_2$$

The quantity measured by the instrumentation was the relative bidirectional reflectance;

$$\frac{V}{V_o} = \frac{\rho_B(\theta_1,\phi_1,\theta_2,\phi_2;\lambda;X_i,Y_r)\ \cos\ \theta_1}{\rho_B\left(\theta_1=0°,\phi_1=0°,\theta_2=45°,\phi_2=180;\ ;X_i=\|,Y_r=\|\right)}$$
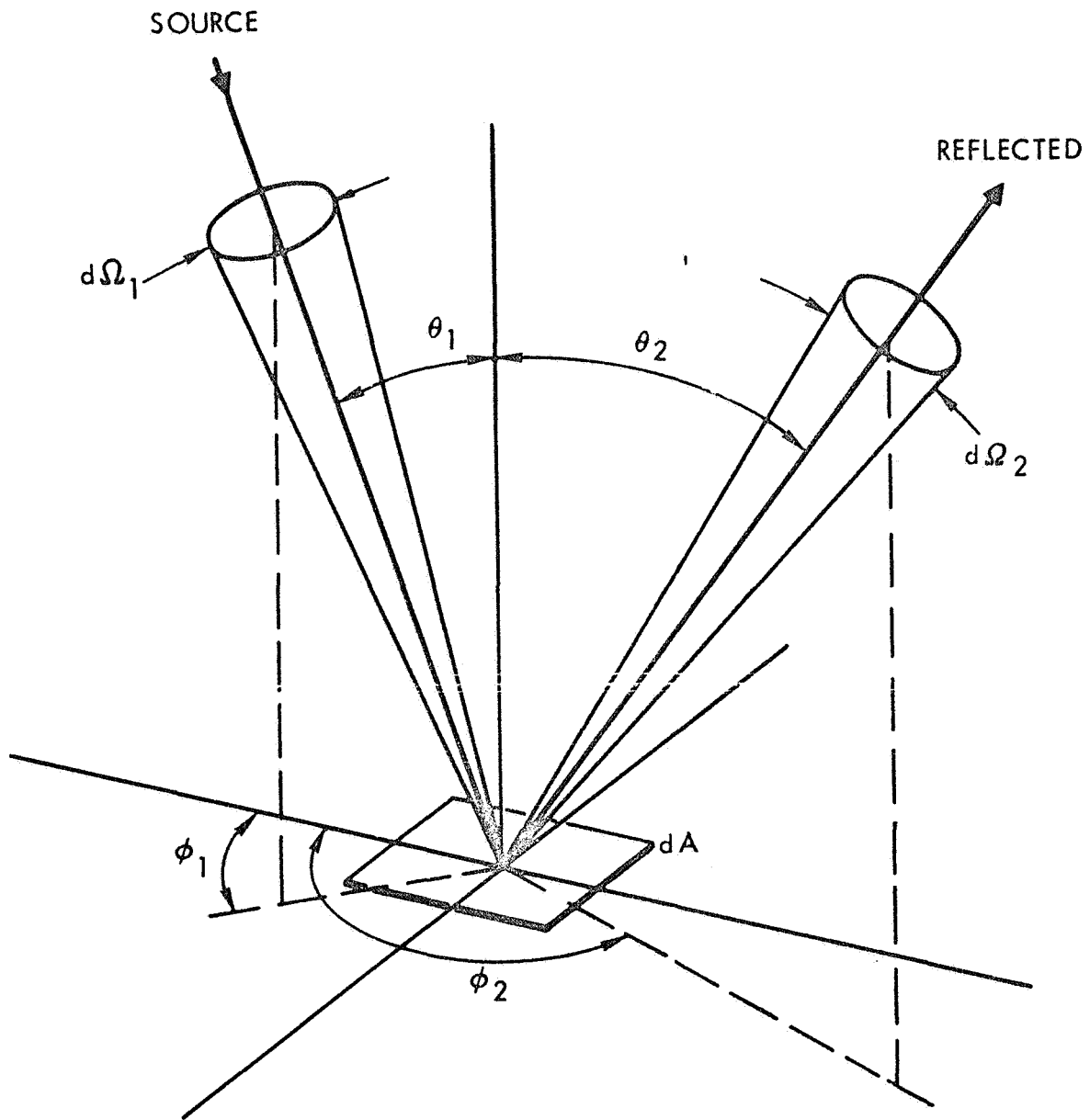
GEOMETRY OF RADIATION INCIDENT AND LEAVING A DIFFERENTIAL AREA

FIGURE 1-24

That is, the bidirectional reflectance for the conditions specified in the denominator was set to read 1.000 on the digital voltmeter as a reference for all other readings.

X_i and Y_r are the polarizations of the energy incident and reflected from the sample respectively, relative to the plane of incidence of the sample. (The plane of incidence is defined as the plane containing both the normal vector to the sample surface and the ray vector representing the incident energy.)

1.6.4 Parameters Investigated

Using the TRW bidirectional reflectometer, the bidirectional reflectance of two MgO samples was measured with the following parameters:

Samples:

        a. Electrostatically smoked MgO (Sample 572-68), 3 mm thick.

        b. Pressed MgO powder (Sample 580-68), 4 mm thick.

Wavelengths:

        a. 0.5 microns

        b. 1.5 microns

Angles of Incidence:

        a. Polar Angles, θ_1 = 0°, 40°, 60°, 70°, 75°.

        b. Azimuthal Angle, ϕ_1 = 0°

Angles of Reflectance:

        a. Polar angles, θ_2 = 0°, 20°, 40°, 60°, 75°

        b. Azimuthal Angles, ϕ_2 = 0°, 180°, also 45°, 90°, 135° for ϕ_1 = 40° and 70°

Polarization: · The incident energy was polarized both parallel and perpendicular to the plane of incidence. The reflected energy was analyzed for components parallel and perpendicular to the plane of incidence.

1.6.5 Test Apparatus

The measurements were performed with the TRW Systems-constructed bidirectional reflectometer as illustrated in Figures 1-25 and 1-26, and
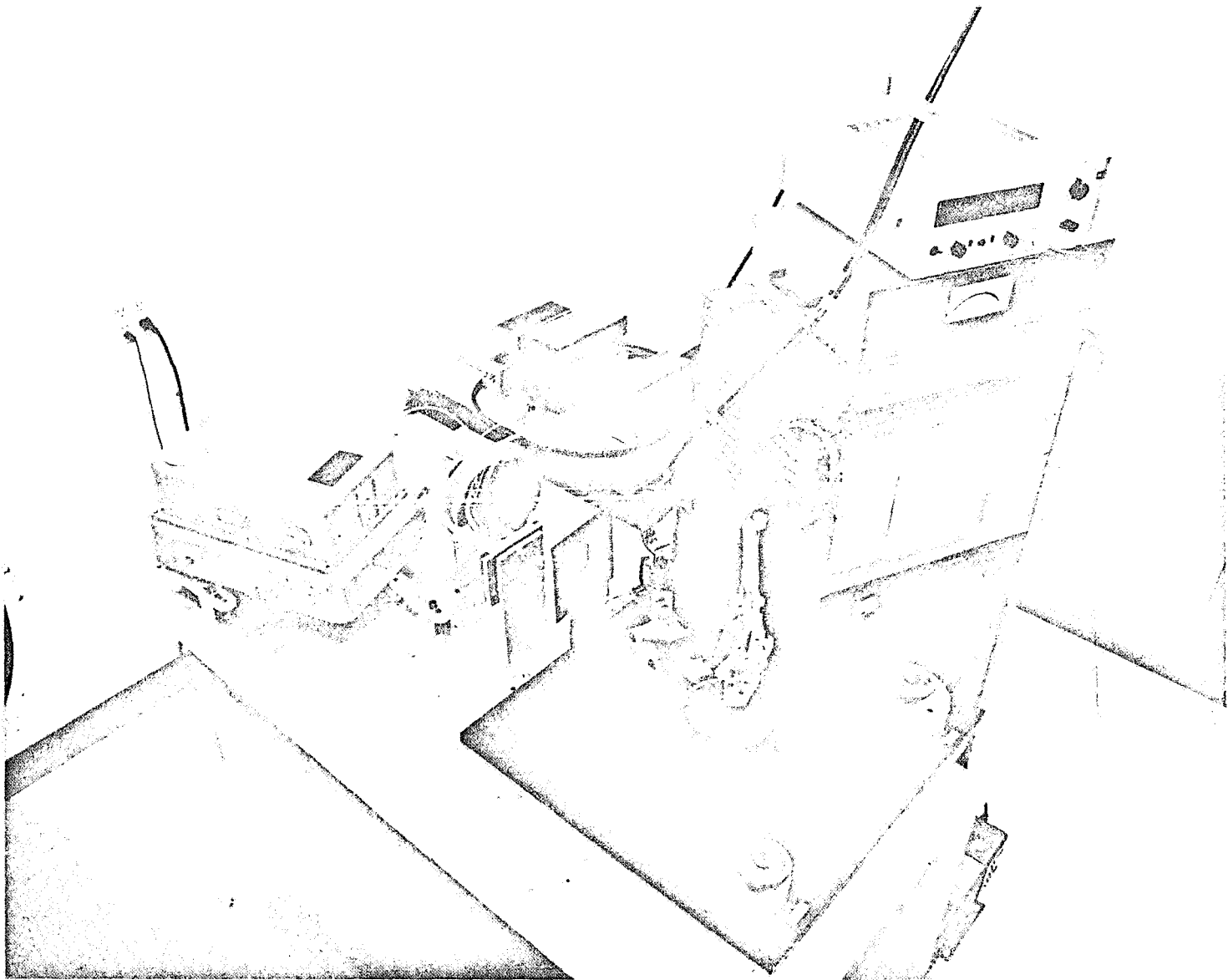
FIGURE 1-25. TRW BIDIRECTIONAL REFLECTOMETER
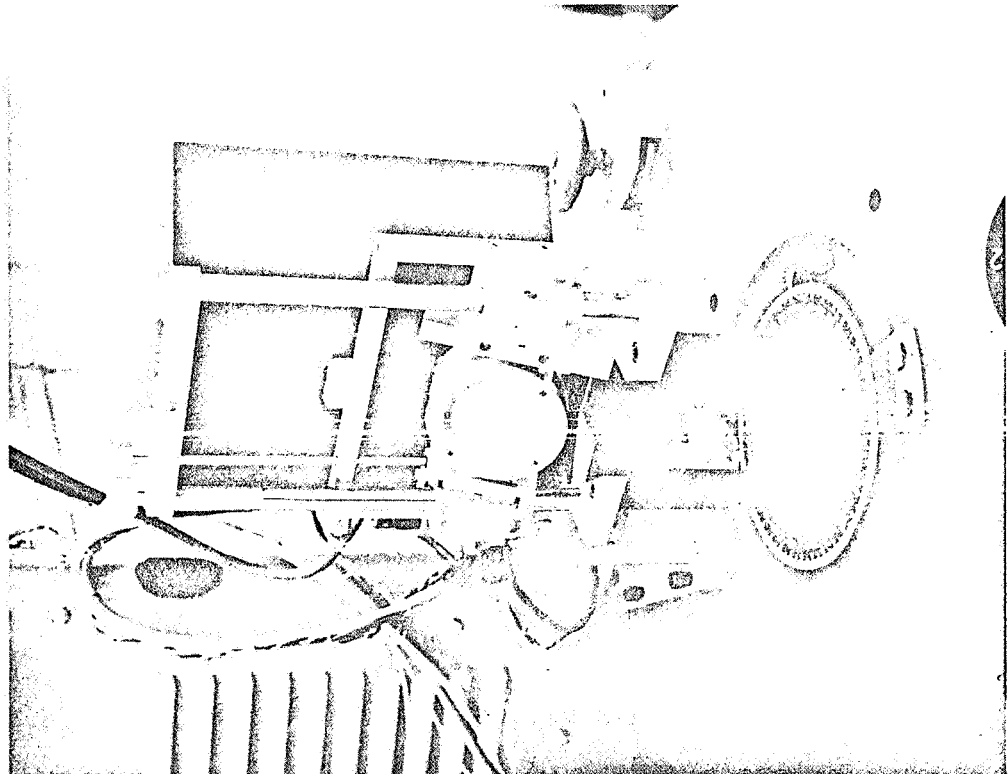
FIGURE 1-26. FRONT AND REAR VIEWS OF THE SAMPLE HOLDER –
TRW BIDIRECTIONAL REFLECTOMETER

schematically shown in Figure 1-27. The arrangement of the incident energy beam, the sample, and the detector is such that by systematically changing θ_2 and ϕ_2 it is possible to map the directional distribution of the reflected radiation over the hemispherical space above the test surface for a given direction of incidence (θ_1, ϕ_1) and wavelength λ. The source of radiant energy was a tungsten strip lamp contained in a water-cooled housing, and the detection system was a Perkin-Elmer Model 98 monochromator. For the present test series, the reflected energy was chopped at 13 cps before entering the monochromator. This arrangement produces no significant sample emission error for the short wavelengths of interest. The detected signal was amplified by a Brower Laboratories Model 129 Lock-In Amplifier, and the resultant signal was displayed on a Non-Linear Systems digital voltmeter (Model 2900).

The mechanical slit width of the monochromator was set at 0.435 mm for the 0.5 micron wavelength and at 2.137 mm for 1.5 microns. These mechanical slit widths correspond to spectral slit widths of 0.002μ and 0.046μ , respectively. The detectors were a 1P28 RCA photomultiplier tube (S-5 response, operated at 500v) for 0.5μ and a Reeder Model RP-3Q thermocouple detector with a KBr window for 1.5μ. To prevent stray radiation other than 0.5μ and 1.5μ from being detected, Corning filters were placed in front of the tugnsten lamp source. These were Corning's filter numbers 3-74 and 4-71 for $.5\mu$ and 3-74 and 7-57 for 1.5μ. Furthermore, because the photomultiplier detector is sensitive to external visible light, the monochromator and detector were shielded by a black felt cover for 0.5μ, and the tests were performed in a darkened room.

For polarizing the incident energy and for analyzing the reflected energy, Polaroid linear sheet polarizers were used: HN32 for 0.5μ and HR for 1.5μ.

1.6.6 Test Procedures

    a. The test specimen was installed in the sample holder, and the reflectometer was optically aligned.

    b. The detection electronics and the tungsten source were turned on and allowed to reach equilibrium.
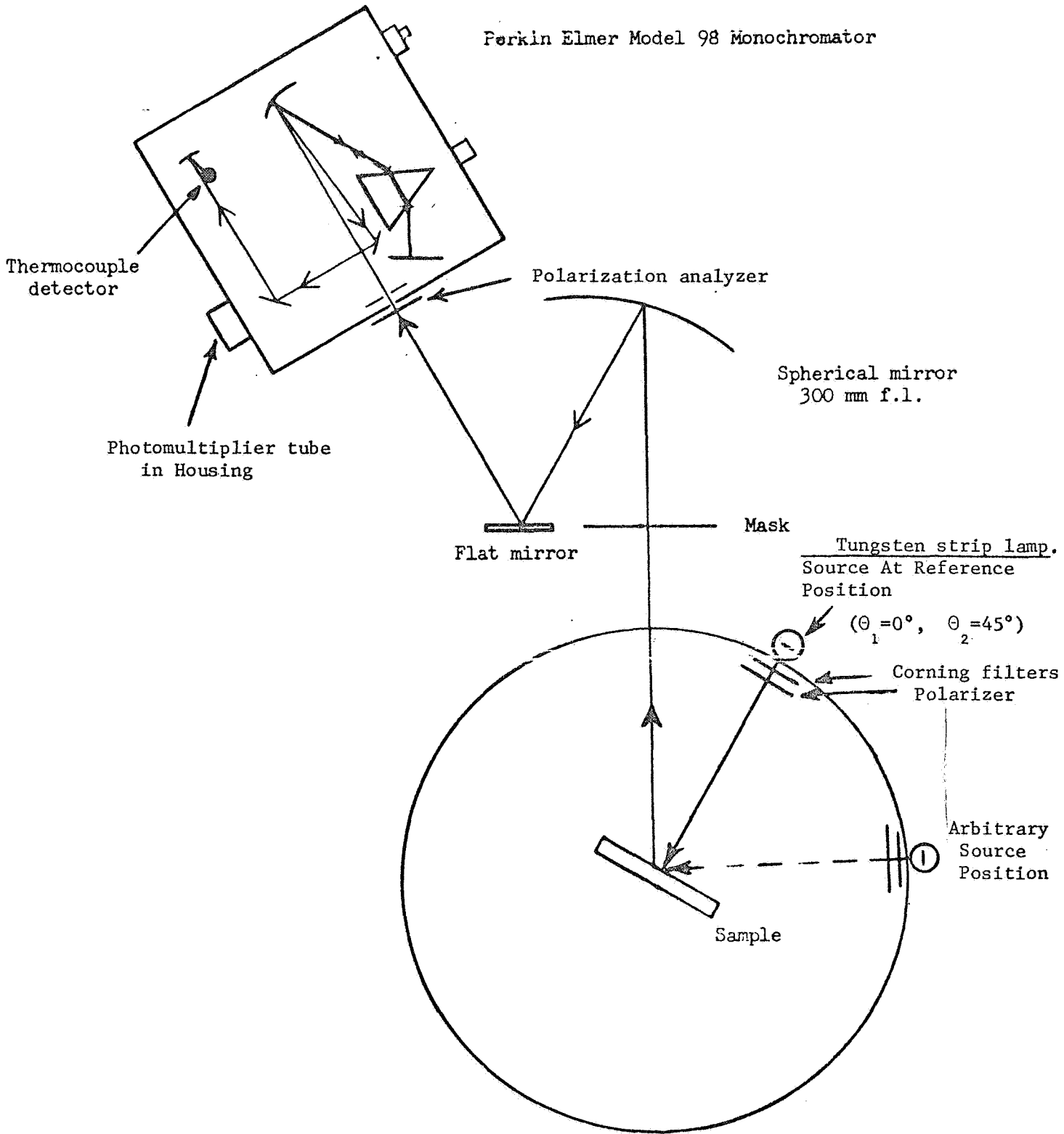
FIGURE 1-27. SCHEMATIC REPRESENTATION OF THE TRW BIDIRECTIONAL REFLECTOMETER
FOR VISIBLE AND NEAR INFRARED WAVELENGTHS

c. The source and sample were set at the reference position specified in the preceding section, and the amplifier was adjusted to provide a reference reading of 1.000.

d. The test specimen and source were oriented to the prescribed angles of incidence and reflection. The polarizer and analyzer were independently oriented, and the relative reflectance was read from the digital voltmeter.

1.6.7 Test Results

The test results have been tabulated in Tables 1-11 and 1-12 and graphed in Figures 1-28 to 1-35 and A-17 to A-37 (See Appendix). The quantities tabulated and graphed are the relative bidirectional reflectance,

$$\rho_{RB} = \frac{\rho_B(\theta_1,\phi_1,\theta_2,\phi_2;\lambda;X_i,Y_r)}{\rho_B(\theta_1=0°,\phi_1=0°,\theta_2=45°,\phi_2=180°;\lambda;||,||)} = \frac{1}{\cos\theta_1}\frac{V}{V_o}$$

The accuracy of the data is largely determined by five considerations:

1. Alignment of the reflectometer optics and the individual angle settings of source and detector.

2. Accuracy of polarizer and analyzer settings.

3. The practical least count of the voltmeter.

4. Signal-to-noise ratio of the system.

5. Non-linearities in detection and amplification.

A good test of the relative instrument accuracy is to compare measurements of $\rho_{RB}(\theta_1,\phi_1,\theta_2,\phi_2;\lambda;X_i,Y_r)$ with those of $\rho_{RB}(\theta_2,\phi_2,\theta_1,\phi_1;\lambda;Y_i,X_r)$ which should be equal by the law of reciprocity. Any discrepancies between two such measurements can only be due to the limits of the instrumentation. Table 1-13 contains an ample number of comparisons of ρ_{RB} for reciprocal angle and polarization settings. Except for the very large polar angles of reflection, the comparison indicates discrepancies within 15%. The comparison at large angles of incidence is not quite as good, since the rate of change of ρ_{RB}, $(\frac{d\rho}{d\theta})$, is very large there. At these angles, small inaccuracies in angle settings become noticeable.

TABLE 1-11
RELATIVE BIDIRECTIONAL REFLECTANCE OF MgO SMOKE
ELECTROSTATICALLY DEPOSITED 3mm THICK, SAMPLE NO. 572-68

Angles of Incidence ϕ_1	θ_1	Angles of Reflection θ_2	ϕ_2	$\lambda=0.5\mu$ ρ^1_{RB} (a) $\|_r$	$\perp_r$	ρ^2_{RB} (b) $\perp_r$	$\|_r$	$\lambda=1.5\mu$ ρ^1_{RB} (a) $\|_r$	$\perp_r$	ρ^2_{RB} (b) $\perp_r$	$\|_r$
0°	0°	20°	0°	1.08	.87	1.06	.97	1.08	.79	1.02	.91
		40	0	1.02	.85	1.0.	.95	1.02	.76	1.00	.89
		60	0	.94	.79	.97	.88	.92	.72	.97	.85
		75	0	.86	.72	.92	.81	.82	.66	.94	.78
	40	0	---	.96	.79	.95	.88	.97	.74	.97	.87
		20	0	1.03	.81	1.00	.90	1.05	.73	.99	.87
			180	.90	.78	.92	.84	.91	.72	.98	.85
		40	45	1.02	.84	.97	.93	1.04	.91	.85	.90
			90	.91	.82	.85	.94	.97	.91	.77	.95
			135	.88	.84	.90	.88	.88	.77	.93	.88
			180	.88	.73	.94	.80	.87	.69	1.01	.83
		60	0	1.13	.84	1.08	.94	1.12	.70	1.02	.85
			180	.88	.65	.95	.72	.89	.64	1.07	.77
		70	45	.95	.82	.89	.94	1.00	.90	.79	.89
			90	.93	.87	.88	.95	.89	.89	.75	.88
			135	.88	.71	.93	.80	.91	.76	.93	.74
		75	0	1.10	.85	1.07	.95	1.07	.69	1.02	.83
			180	.88	.57	.97	.63	.95	.57	1.12	.68
	60	0	---	.81	.69	.83	.75	.86	.68	.94	.80
		20	0	.91	.73	.87	.79	.96	.68	.94	.81
			180	.77	.65	.82	.71	.82	.64	.97	.79
		40	0	1.06	.79	1.00	.86	1.09	.69	1.00	.82
			180	.81	.61	.87	.66	.86	.62	1.03	.74
		60	180	.93	.54	.98	.58	1.04	.55	1.22	.69
		75	0	1.44	1.08	1.37	1.21	1.31	.77	1.19	.93
			180	1.11	.48	1.19	.53	1.29	.49	1.44	.61
	70	0	---	.70	.59	.73	.66	.83	.64	.93	.78
		40	45	.81	.72	.84	.84	1.00	.83	.91	.95
			90	.73	.65	.71	.81	.87	.78	.83	.96
			135	.74	.55	.78	.67	.85	.64	.97	.84
		70	45	1.53	1.34	1.54	1.56	1.44	1.27	1.64	1.46
			90	1.34	.97	1.21	1.15	1.43	1.02	1.17	1.11
			135	1.22	.69	1.35	.80	1.41	.72	1.35	.78
	75	0	---	.63	.53	.65	.57	.73	.60	.86	.73
		20	0	.71	.59	.71	.64	.83	.60	.88	.73
			180	.60	.48	.64	.52	.73	.55	.90	.69
		40	0	.90	.69	.86	.75	1.00	.64	.94	.76
			180	.65	.44	.68	.46	.83	.48	1.00	.64
		60	0	1.22	.86	1.15	.95	1.24	.66	1.11	.81
			180	.89	.41	.90	.44	1.18	.46	1.33	.58
		75	180	1.32	.40	1.38	.44	1.78	.44	1.88	.54

$$(a) \quad \rho^1_{RB} = \frac{\rho_B(\theta_1,\phi_1,\theta_2,\phi_2,\lambda,\|_i,X_r)}{\rho_B(0°,0°,45°,180°,\lambda,\|_i,\|_r)} \qquad (b) \quad \rho^2_{RB} = \frac{\rho_B(\theta_1,\phi_1,\theta_2,\phi_2,\lambda,\perp_i,X_r)}{\rho_B(0°,0°,45°,180°,\lambda,\|_i,\|_r)}$$

$$\text{where } X_r = \perp_r \text{ or } \|_r$$

TABLE 1-12
RELATIVE BIDIRECTIONAL REFLECTANCE OF MgO PRESSED POWDER
(4mm THICK) SAMPLE NO. 580-68

Angles of Incidence ϕ_1	θ_1	Angles of Reflection θ_2	ϕ_2	$\rho^1_{RB}(a)$ $\|\|_r$	$\perp_r$	$\rho^2_{RB}(b)$ $\perp_r$	$\|\|_r$	$\rho^1_{RB}(a)$ $\|\|_r$	$\perp_r$	$\rho^2_{RB}(b)$ $\perp_r$	$\|\|_r$
				$\lambda=0.5\mu$				$\lambda=1.5\mu$			
0°	0°	20°	0°	1.10	.86	1.05	.91	1.08	.80	1.06	.95
		40	0	1.02	.83	1.02	.89	1.02	.78	1.05	.92
		60	0	.93	.79	.99	.84	.92	.73	1.03	.88
		75	0	.83	.72	.95	.78	.82	.66	1.01	.81
	40	0	---	.99	.82	.98	.85	.97	.75	.99	.87
		20	0	1.09	.83	1.03	.86	1.06	.74	.98	.87
			180	.92	.81	1.00	.85	.92	.75	1.04	.87
		40	45	1.07	.86	1.08	.96	1.02	.93	.89	.92
			90	.93	.86	.92	.96	.97	.95	.82	.99
			135	.90	.81	1.00	.93	.88	.80	1.00	.92
			180	.88	.79	1.02	.84	.89	.75	1.12	.88
		60	0	1.15	.81	1.07	.87	1.08	.68	.97	.81
			180	.87	.75	1.05	.80	.95	.73	1.26	.85
		70	45	.97	.86	.95	.94	.99	.94	.83	.93
			90	.91	.91	.94	.95	.95	1.04	.84	.97
			135	.86	.78	.99	.85	.94	.85	1.10	.86
		75	0	1.07	.77	1.04	.84	1.02	.63	.93	.77
			180	.90	.69	1.11	.74	1.00	.67	1.39	.79
	70	0	---	.78	.68	.88	.71	.72	.61	.88	.74
		40	45	.88	.77	.94	.84	.87	.75	.79	.81
			90	.80	.78	.87	.91	.80	.74	.82	.94
			135	.82	.71	.96	.81	.79	.68	1.05	.85
		70	45	1.55	1.39	1.66	1.55	1.38	1.29	1.72	1.50
			90	1.34	1.12	1.38	1.28	1.43	1.12	1.34	1.23
			135	1.20	.87	1.49	.96	1.53	.88	1.77	.97
	75	0	---	.70	.61	.82	.79	.66	.55	.79	.65
		20	0	.76	.62	.85	.68	.79	.55	.77	.65
			180	.68	.60	.86	.65	.66	.55	.90	.67
		40	0	.93	.65	.91	.72	.85	.51	.77	.61
			180	.77	.59	.97	.64	.79	.53	1.14	.67
		60	0	1.17	.71	1.09	.79	.96	.46	.81	.55
			180	1.15	.60	1.34	.65	1.41	.58	1.81	.66
		75	180	2.05	.68	2.23	.68	3.07	.55	3.65	.65

$$(a)\ \rho^1_{RB} = \frac{\rho_B(\theta_1,\phi_1,\theta_2,\phi_2,\lambda,\|\|_i,X_r)}{\rho_B(0°,0°,45°,180°,\lambda,\|\|_i,\|\|_r)}$$

$$(b)\ \rho^2_{RB} = \frac{\rho_B(\theta_1,\phi_1,\theta_2,\phi_2,\lambda,\perp_i,X_r)}{\rho_B(0°,0°,45°,180°,\lambda,\|\|_i,\|\|_r)}$$

$$\text{where } X_r = \perp_r \text{ or } \|\|_r$$

TABLE 1-13

Evaluation of the Accuracy of Relative Bidirectional Reflectance Measurements on MgO Smoke, Sample 572-68, by use of the Reciprocity Condition:

$$\rho_B(\theta_1=\alpha,\phi_1=\gamma;\theta_2=\beta,\phi_2=\psi;\lambda;X_i,Y_r)=\rho_B(\theta_1=\beta,\phi_1=\psi;\theta_2=\alpha,\phi_2=\gamma;\lambda;Y_i,X_r)$$

α	β	$\rho^1_{RB}(\theta_1=\alpha,\theta_2=\beta, \|_i, \|_r)$		$\rho^1_{RB}(\theta_1=\beta,\theta_2=\alpha, \|_i, \|_r)$		$\rho^2_{RB}(\theta_1=\alpha,\theta_2=\beta, \perp_i, \|_r)$		$\rho^1_{RB}(\theta_1=\beta,\theta_2=\alpha, \|_i, \perp_r)$	
		0.5μ	1.5μ	0.5μ	1.5μ	0.5μ	1.5μ	0.5μ	1.5μ
0°	40°	1.02	1.02	0.96	0.97	0.81	0.75	0.79	0.74
0	60	0.94	0.92	0.81	0.86	0.75	0.71	0.69	0.69
0	75	0.86	0.82	0.63	0.73	0.69	0.65	0.53	0.60
40	60	0.88	0.89	0.81	0.86	0.61	0.65	0.61	0.62
40	75	0.88	0.95	0.65	0.83	0.54	0.57	0.57	0.57
60	75	1.11	1.29	0.89	1.18	0.45	0.66	0.41	0.46

NOTES:

1) ρ^1_{RB} and ρ^2_{RB} are defined in Table 1-12.

2) For the cases considered above, $\phi_1=0$; $\phi_2=180°$.

3) Compare columns 1 with 3, 2 with 4, 5 with 7, and 6 with 8.

FIGURE 1-28   RELATIVE BIDIRECTIONAL REFLECTANCE OF MgO SMOKE, ELECTROSTATICALLY DEPOSITED, 3mm THICK, SAMPLE 572-68

FIGURE 1-29   RELATIVE BIDIRECTIONAL REFLECTANCE OF MgO SMOKE, ELECTROSTATICALLY DEPOSITED, 3mm THICK, SAMPLE 572-68
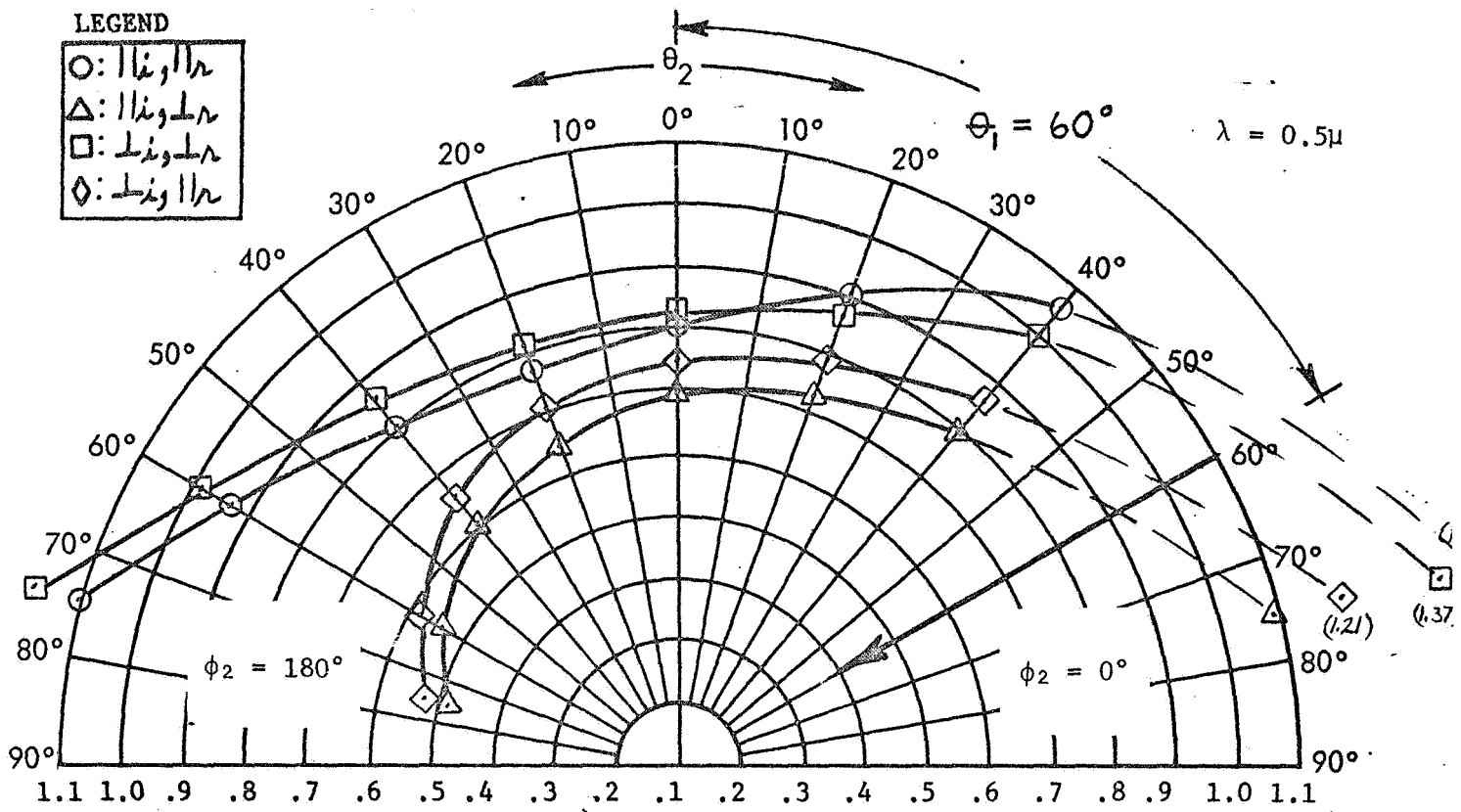
FIGURE 1-30 RELATIVE BIDIRECTIONAL REFLECTANCE OF MgO SMOKE, ELECTROSTATICALLY DEPOSITED, 3mm THICK, SAMPLE 572-68

FIGURE 1-31 RELATIVE BIDIRECTIONAL REFLECTANCE OF MgO SMOKE, ELECTROSTATICALLY DEPOSITED, 3mm THICK, SAMPLE 572-68

FIGURE 1-32 RELATIVE BIDIRECTIONAL REFLECTANCE OF MgO SMOKE, ELECTROSTATICALLY DEPOSITED, 3mm THICK, SAMPLE 572-68
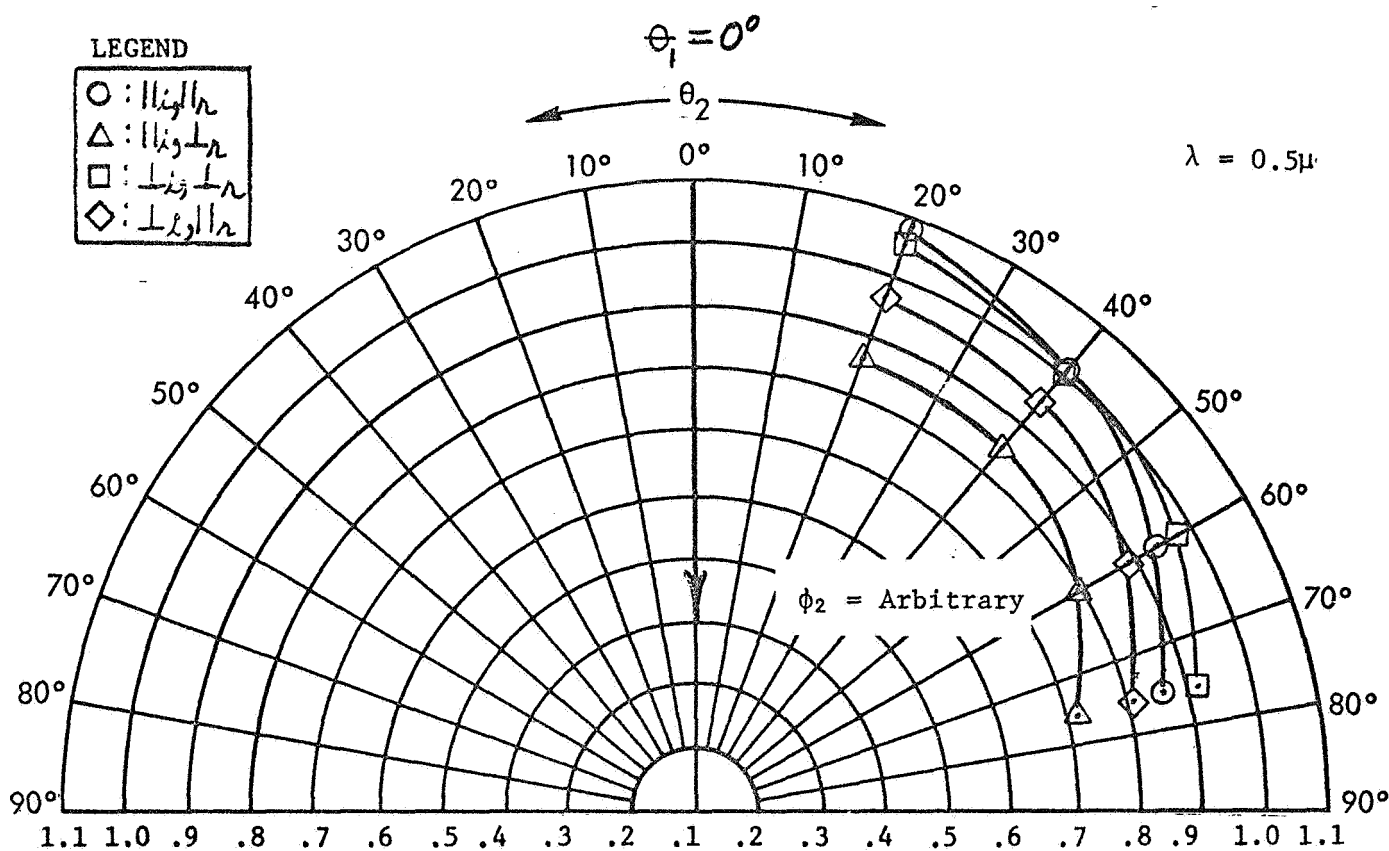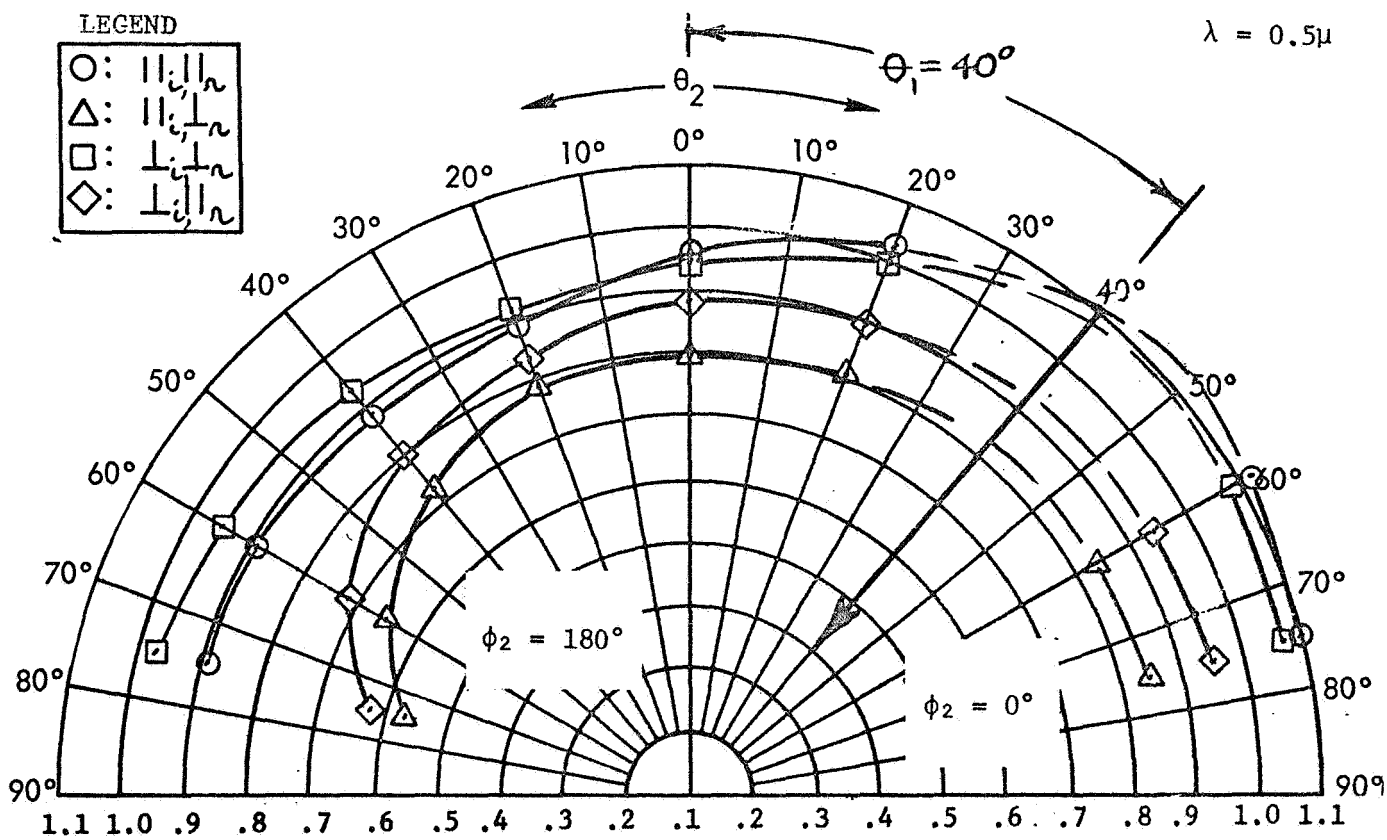

FIGURE 1-33 RELATIVE BIDIRECTIONAL REFLECTANCE OF MgO SMOKE, ELECTROSTATICALLY DEPOSITED, 3mm THICK, SAMPLE 572-68

FIGURE 1-34 RELATIVE BIDIRECTIONAL REFLECTANCE OF MgO SMOKE, ELECTROSTATICALLY DEPOSITED, 3mm THICK, SAMPLE 572-68
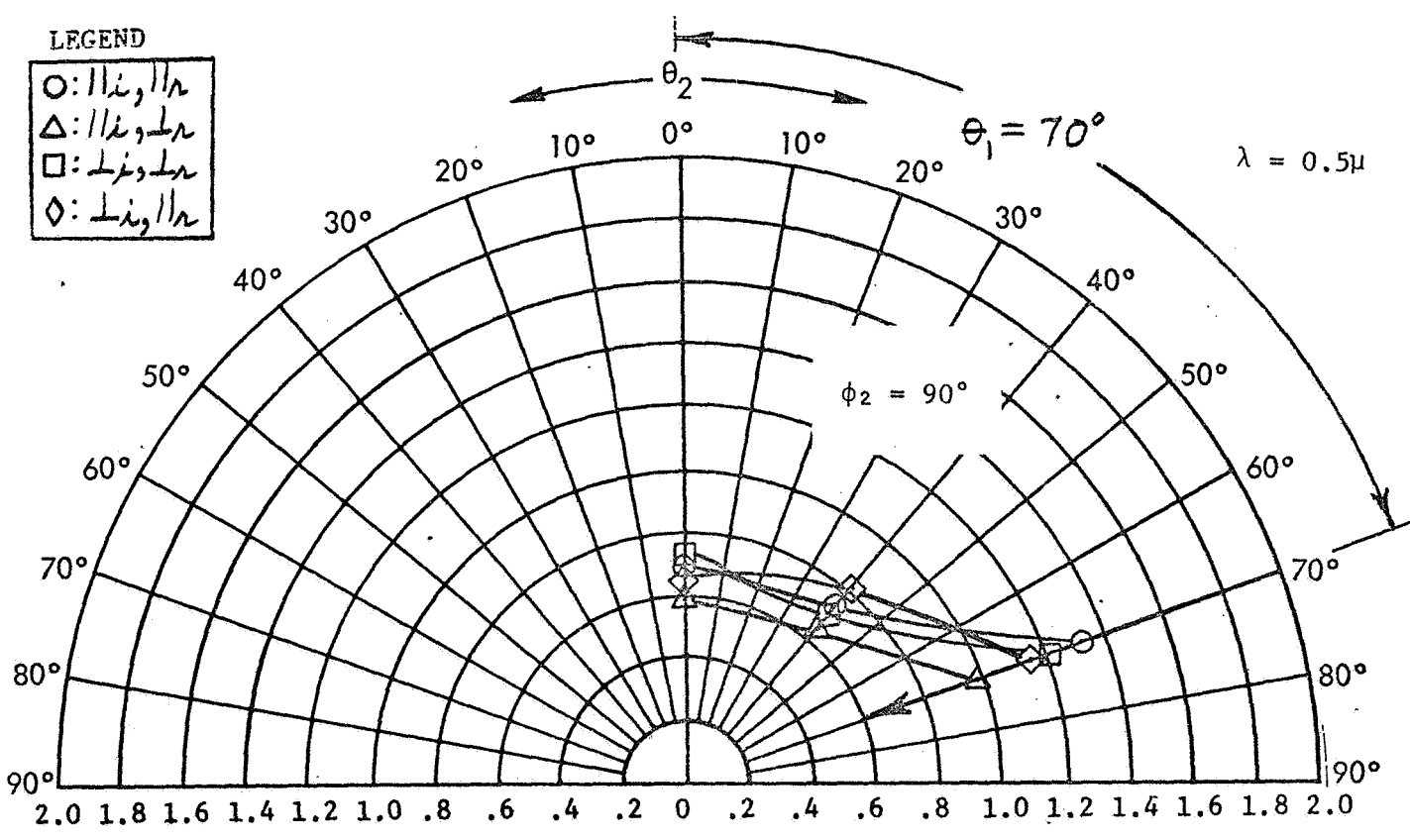
FIGURE 1-35 RELATIVE BIDIRECTIONAL REFLECTANCE OF MgO SMOKE, ELECTROSTATICALLY DEPOSITED, 3mm THICK, SAMPLE 572-68
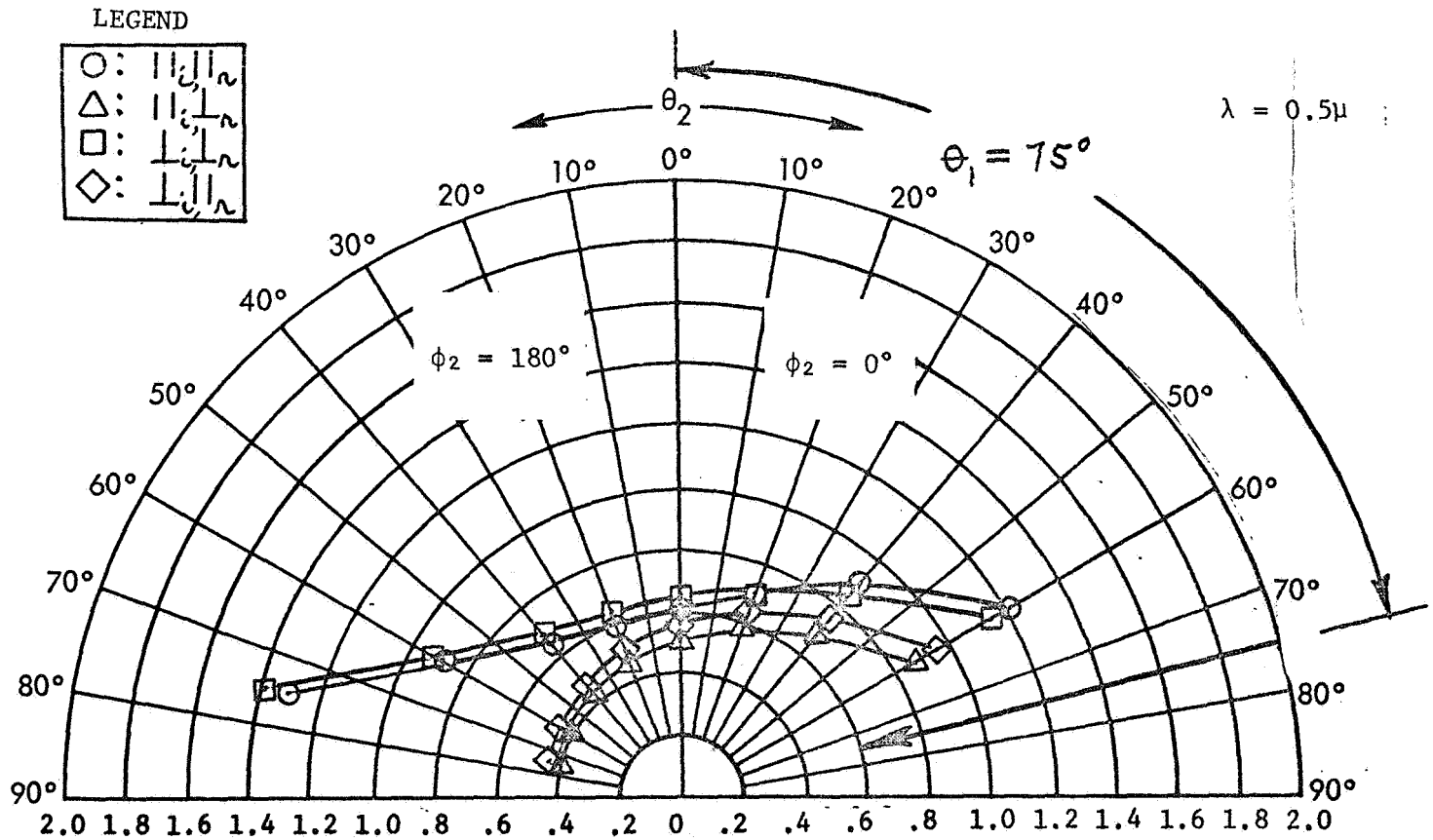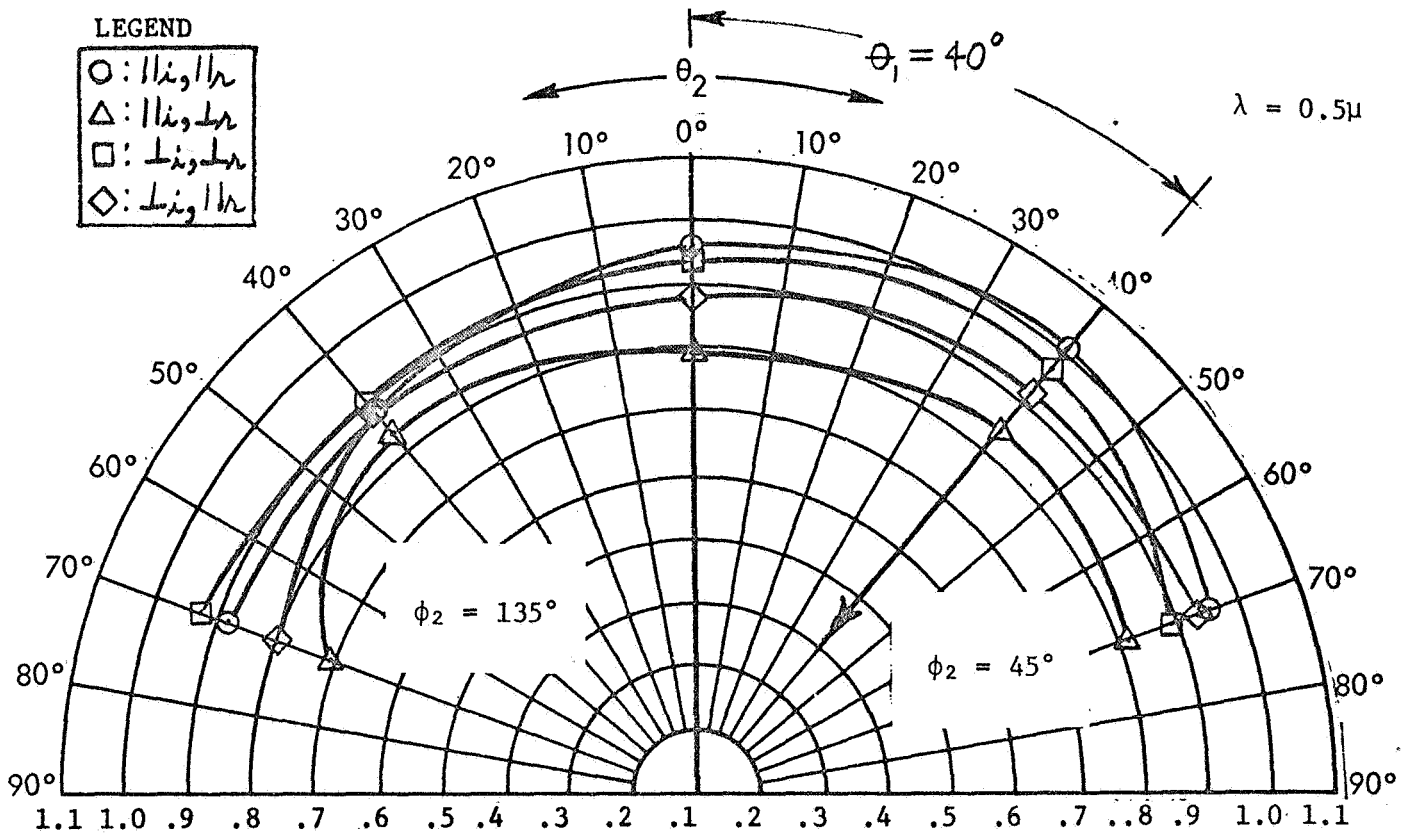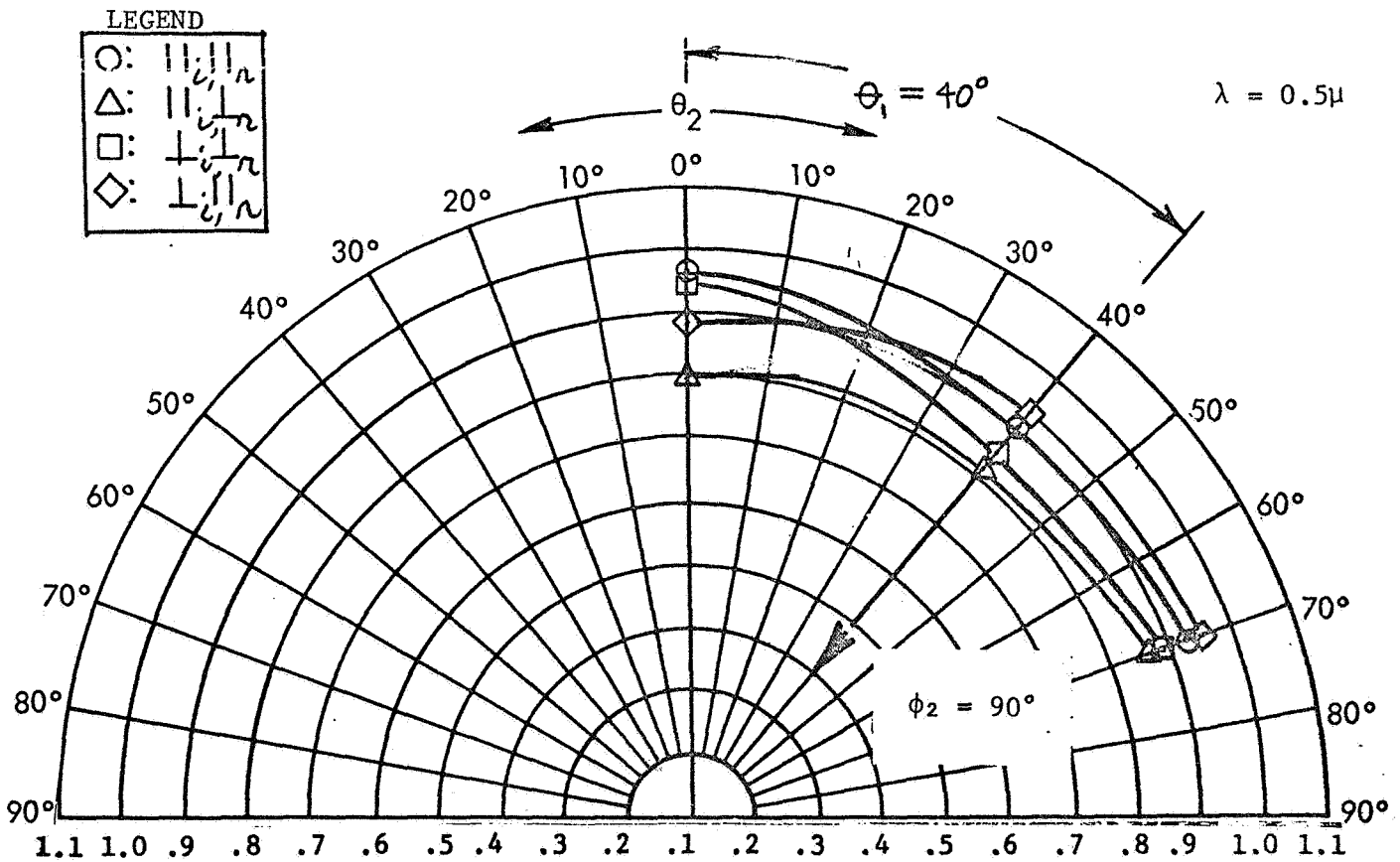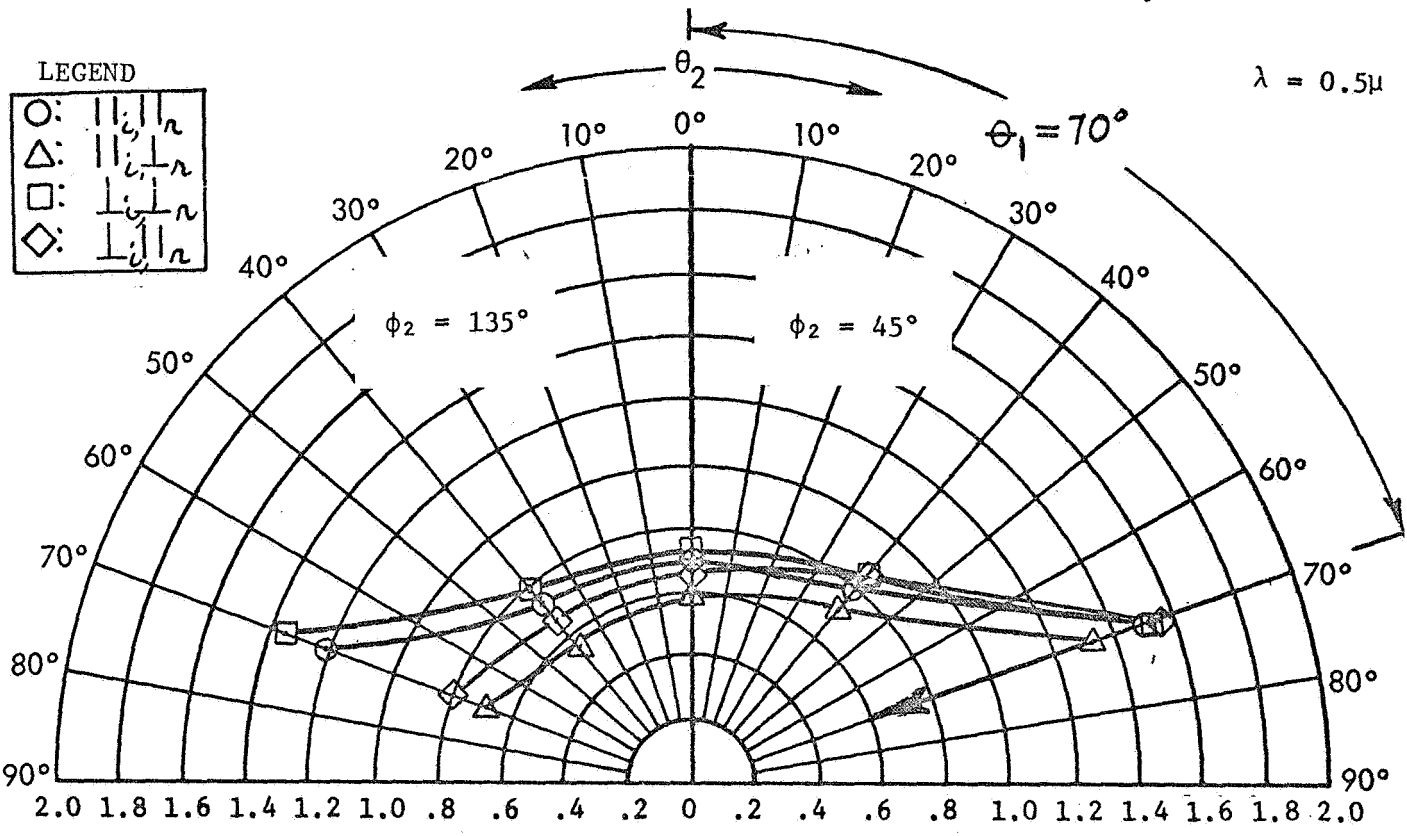
1.6.8 Conclusions Regarding the Bidirectional Reflectance of Magnesium Oxide Surfaces

In discussing the bidirectional reflectance, it is beneficial to define a few expressions which represent the states of polarization of the incident and reflected energy. These are shown below:

- o POI — Plane of incidence (plane containing both the normal vector to the sample surface and the ray vector representing the incident energy).

- o $\rho_B(\perp,\perp)$ — That portion of the bidirectionally reflected energy which is polarized perpendicular to the POI when the incident energy is polarized perpendicular to the POI.

- o $\rho_B(||,||)$ — That portion of the bidirectionally reflected energy which is polarized parallel to the POI when the incident energy is polarized parallel to the POI.

That is, the first symbol in the parentheses represents the polarization state of the incident energy; the second symbol, the polarization state of the reflected energy which was measured. $\rho_B(\perp,||)$ and $\rho_B(||,\perp)$, therefore, represent reflectance values in which the measured reflected energy was of opposite polarization to the incident energy.

- o λ — Wavelength

- o μ — Microns

1.6.8.1 Smoked versus Pressed MgO

Smoked MgO is more diffuse than pressed MgO powder. The largest differences occur for $\rho_B(\perp,\perp)$ and $\rho_B(||,||)$ in the forward direction.

1.6.8.2 Diffuseness

For polar angles of incidence, $\theta_1 \leq 40°$, the samples appeared to be quite diffuse. At large values of θ_1, forward scattering and backward scattering increased.

The portion of reflected energy opposite in polarization to that incident upon the sample [*i.e.*, $\rho_B(\perp,||)$ and $\rho_B(||,\perp)$] was reflected rather diffusely. The portion of reflected energy of the same polarization to that incident upon the sample [*i.e.*, $\rho_B(\perp,\perp)$ and $\rho_B(||,||)$] exhibited wide deviations from diffuseness as a function of θ_1.

1.6.8.3 Wavelength

ρ_B at $\lambda = 1.5\mu$ is generally similar to that at $\lambda = .5\mu$ for $\theta_1 \leq 40°$ with the following distinctions:

1. There is less depolarization in POI, although out of the POI "over-depolarization" occurs to a greater extent at $\lambda = 1.5\mu$ than at $\lambda = .5\mu$.

2. At high θ_1's ($\theta_1 > 40°$), forward scattering is greater.

3. As at $\lambda = .5$, $\rho_B(\perp,||)$ is always $> \rho_B(||,\perp)$. The difference between the two is greater at $\lambda = 1.5$ than at $\lambda = .5$.

4. As at $\lambda = .5$, $\rho_B(\perp,\perp) > \rho_B(||,||)$ in the forward direction. The difference between $\rho_B(\perp,\perp)$ and $\rho_B(||,||)$ is greater than at $\lambda = .5$.

5. As at $\lambda = .5$, $\rho_B(||,||)$ is $> \rho_B(\perp,\perp)$ in the back direction. The difference between $\rho_B(||,||)$ and $\rho_B(\perp,\perp)$ is greater than $\lambda = .5$.

At $\theta_2 \geq 40°$ in POI, both samples were much more diffusing for 0.5μ energy than for 1.5μ energy in the forward direction. In the back direction, however, both samples were less diffusing for 0.5μ energy than for 1.5μ energy.

1.6.8.4 Polarization

1. $\rho_B(\perp,\perp)$ is generally greater than $\rho_B(||,||)$ in the forward direction, i.e., for $\phi_2 > 90°$. Conversely, $\rho_B(||,||)$ is generally slightly greater than $\rho_B(\perp,\perp)$ in the backward direction ($\phi_2 \leq 90°$).

2. $\rho_B(\perp,||)$ is greater than $\rho_B(||,\perp)$ for nearly all coordinates investigated.

3. See other comment in Item number 1.6.8.2 Diffuseness.

A tabulation of the percentage of excess polarized energy is shown in Table 1-14. Refer to the equations below the table for the definition of this quantity. These values represent the ability of a surface to depolarize incident energy which is completely polarized. The lower the value, the better the surface depolarizes. These values are shown graphically in Figures 1-36 through 1-43. Data taken in the plane of incidence is shown in Figures 1-36 through 1-39; that taken out of the plane of incidence in Figures 1-40 through 1-43.

TABLE 1-14
PER CENT POLARIZATION OF BIDIRECTIONALLY REFLECTED ENERGY FOR MgO SMOKE (ELECTROSTATICALLY DEPOSITED, 3mm THICK) AND MgO PRESSED POWDER (4mm THICK) COATINGS

Angles of Incidence ϕ_1	θ_1	Angles of Reflection θ_2	ϕ_2	MgO Smoke S/N 572-68 $\lambda=0.5$ microns $\rho_{||}$	$\rho_{\perp}$	$\lambda=1.5$ microns $\rho_{||}$	$\rho_{\perp}$	MgO Pressed Powder S/N 580-68 $\lambda=0.5$ microns $\rho_{||}$	$\rho_{\perp}$	$\lambda=1.5$ microns $\rho_{||}$	$\rho_{\perp}$
0°	0°	20°	*	11	4.5	15.5	5.5	12	7	15	5.5
		40	*	9	3	14.5	6	10.5	7	13.5	6.5
		60	*	8.5	5	12	6.5	7.5	8	11.5	8
		75	*	9	6.5	11	9.5	7	10	11	11
	40	0	+	9.5	4	13.5	5.5	9.5	7	13	6.5
		20	0	12	5.5	18	6.5	13.5	9	18	6
			180	7	4.5	11.5	7	6.5	8	10	9
		40	45	9.5	2	6.5	- 3	11	6	4.5	- 1.5
			90	5	- 5	3	-10.5	4	- 2	1	- 9.5
			135	2.5	1	6.5	3	5.5	3.5	5	4
			180	9.5	8	11.5	10	5.5	9.5	8.5	12
		60	0	14.5	7	23	9	17.5	10.5	22.5	9
			180	15	14	16.5	16.5	7.5	13.5	13	19.5
		70	45	7.5	- 2.5	5.5	- 6	6	0.5	2.5	- 5.5
			90	3.5	- 4	0	- 8	0	- 0.5	- 4.5	- 7
			135	10.5	7.5	9	11.5	5	7.5	5	12
		75	0	13	6	21.5	10.5	16.5	10.5	23.5	9.5
			180	21.5	21	18.5	24.5	13	20	20	27.5
	60	0	+	8	5	11.5	8				
		20	0	11	5	17	7.5				
			180	8.5	7	12.5	10				
		40	0	14.5	7.5	22.5	10				
			180	14	13.5	16	16.5				
		60	180	26.5	25.5	31	27.5				
		75	0	23.5	6	26	12.5				
			180	39.5	38.5	45	40.5				
	70	0	+	8.5	5	13	9	7	10.5	8.5	8.5
		40	45	6	0	9.5	- 2	6.5	6	7.5	- 1.5
			90	6	- 6.5	5.5	- 7.5	1.5	- 2	4	- 7
			135	14.5	7.5	14	7	7	8.5	7.5	10.5
		70	45	6.5	- 0.5	6.5	6	5.5	3.5	3.5	7
			90	16	2.5	16.5	2.5	9	4	12	4.5
			135	27.5	25.5	32.5	27	16	21.5	27	29
	75	0	+	8.5	6	10	8	7	2	9	9.5
		20	0	9	5	16	9.5	10	11	18	8.5
			180	11	10.5	14	13	6	14	9	14.5
		40	0	13	7	18.5	10.5	17.5	11.5	25	11.5
			180	19.5	19.5	26.5	22	13	20.5	19.5	26
		60	0	17.5	9.5	30.5	15.5	25	16	35	19
			180	37	34.5	44	39.5	31.5	23	41.5	46.5
		75	180	53.5	51.5	60.5	55.5	50	53.5	69.5	70

*arbitrary ϕ_2

+undefined ϕ_2

$$\rho_{||} = \frac{\rho_{RB}(||,||) - \rho_{RB}(||,\perp)}{\rho_{RB}(||,||) + \rho_{RB}(||,\perp)} \times 100\% \qquad \rho_{\perp} = \frac{\rho_{RB}(\perp,\perp) - \rho_{RB}(\perp,||)}{\rho_{RB}(\perp,\perp) + \rho_{RB}(\perp,||)} \times 100\%$$

Per Cent Polarization of Reflected Energy
for Electrostatically Smoked MgO, 3mm Thick
Sample No. 572-68

Figure 1-36. $\theta_1 = 0°$
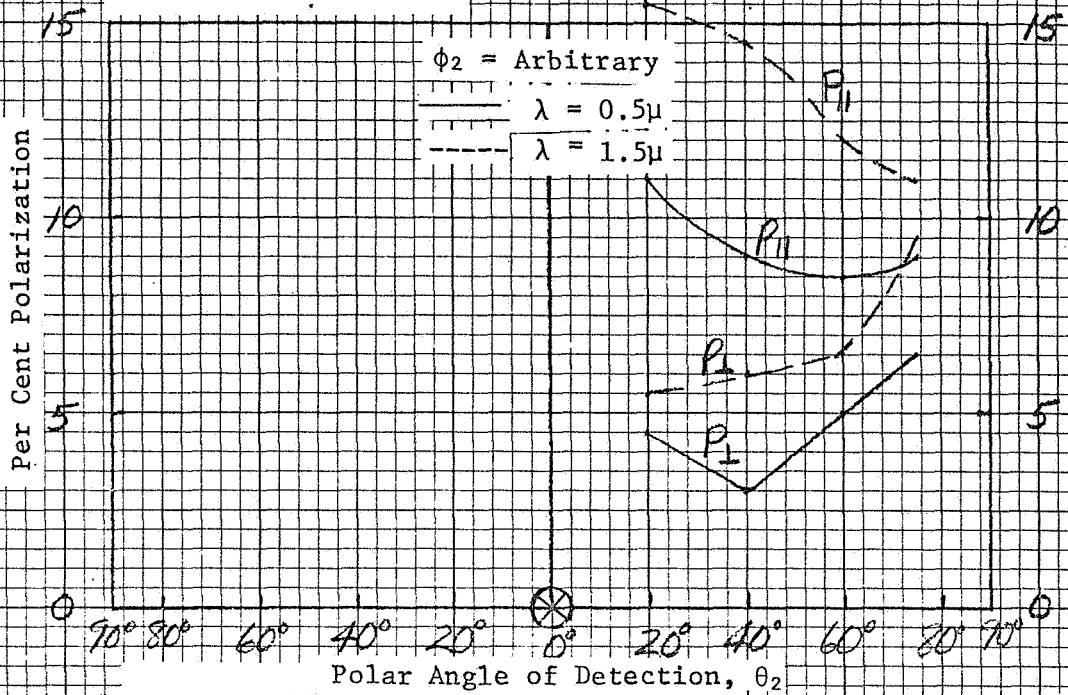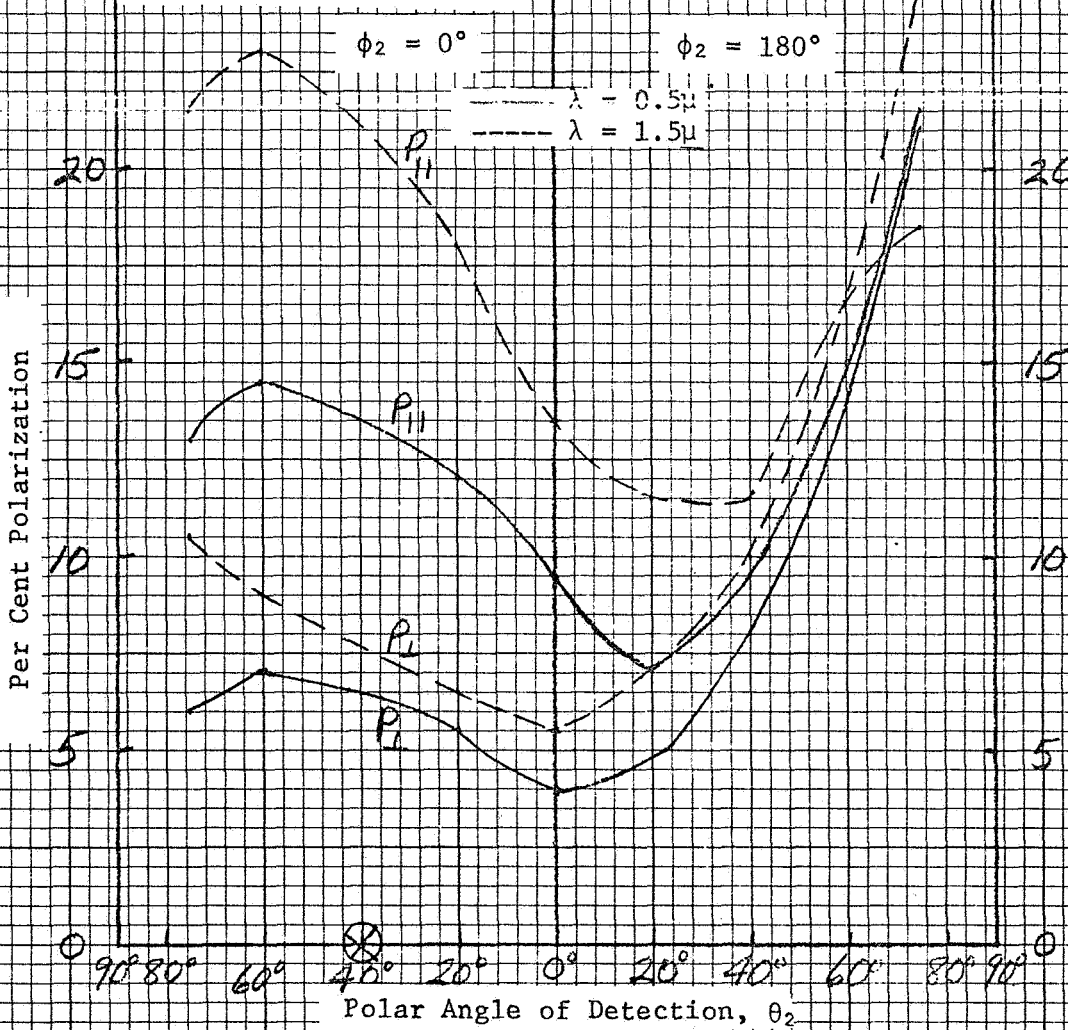
ϕ_2 = Arbitrary
—— $\lambda = 0.5\mu$
- - - $\lambda = 1.5\mu$

Per Cent Polarization

Polar Angle of Detection, θ_2

Figure 1-37. $\theta_1 = 40°$

$\phi_2 = 0°$ $\phi_2 = 180°$
—— $\lambda = 0.5\mu$
- - - $\lambda = 1.5\mu$

Per Cent Polarization

Polar Angle of Detection, θ_2

78

Per Cent Polarization of Reflected Energy
for Electrostatically Smoked MgO, 3mm Thick
Sample No. 572-68

-66-

Per Cent Polarization of Reflected Energy
for Electrostatically Smoked MgO, 3 mm Thick
Sample No. 572-68

Figure 1-39. $\theta_1 = 75°$

$\lambda = 0.5\mu$
$\lambda = 1.5\mu$

$\phi_2 = 0°$ $\phi_2 = 180°$

Per Cent Polarization

$P_{||}$
$P_{|||}$
$P_{\perp}$
$P_{\perp}$

90° 80°   60°   40°   20°   0°   20°   40°   60°   80° 90°

Polar Angle of Detection, θ_2

-67-
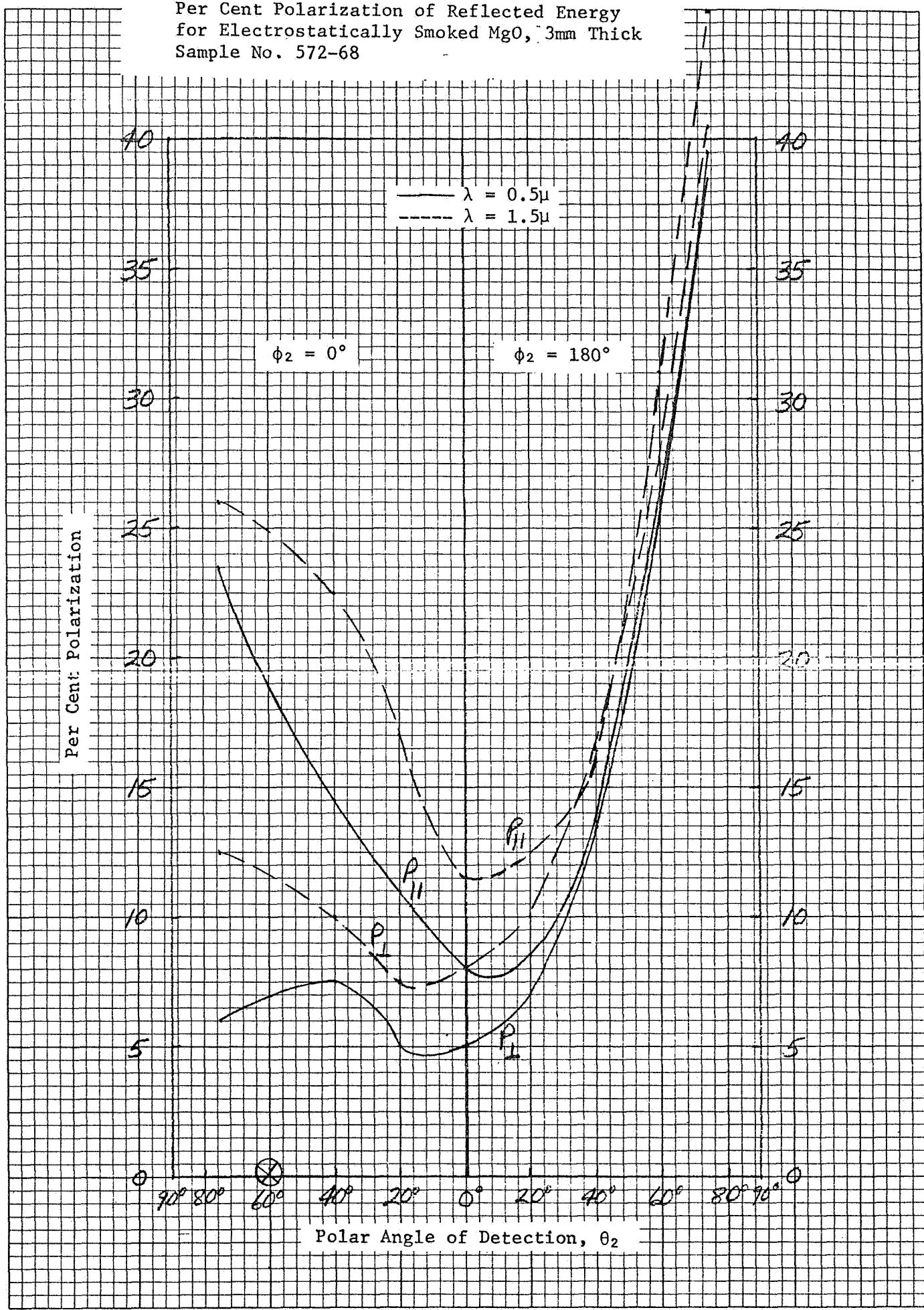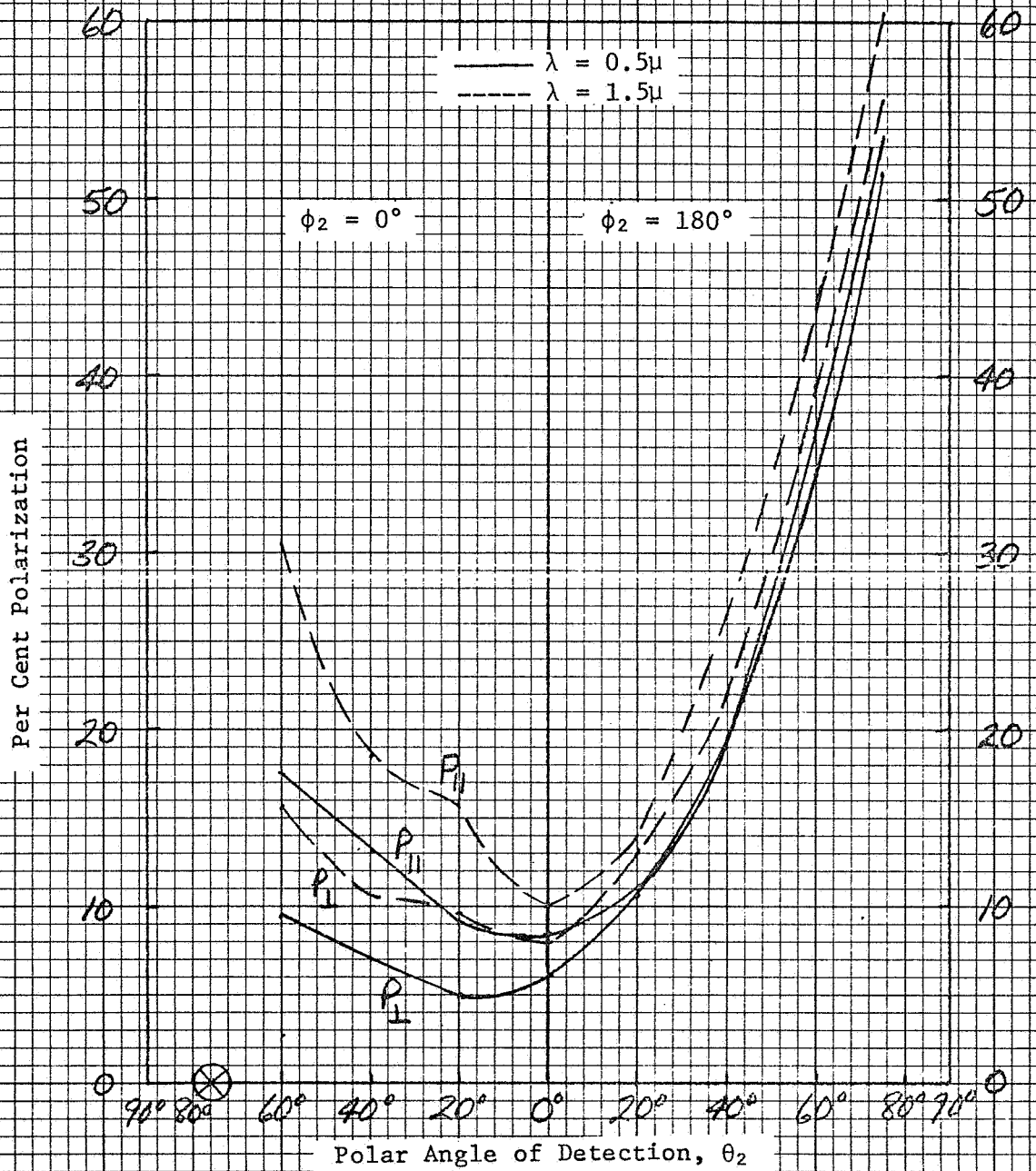
...tion of Reflected Energy
for Electrostatically Smoked MgO, 3mm Thick
Sample No. 572-68
Figure 1-40. $\theta_1 = 40°$

Figure 1-41. $\theta_1 = 40°$

Figure 1-42. $\theta_1 = 70°$

$\phi_2 = 135°$
$\phi_2 = 90°$
$\phi_2 = 45°$

$\lambda = 0.5\mu$

Per Cent Polarization

Polar Angle of Detection, θ_2

Figure 1-43 $\theta_1 = 70°$

$\phi_2 = 135°$
$\phi_2 = 90°$
$\phi_2 = 45°$

$\lambda = 1.5\mu$

Per Cent Polarization

Polar Angle of Detection, θ_2

-69-
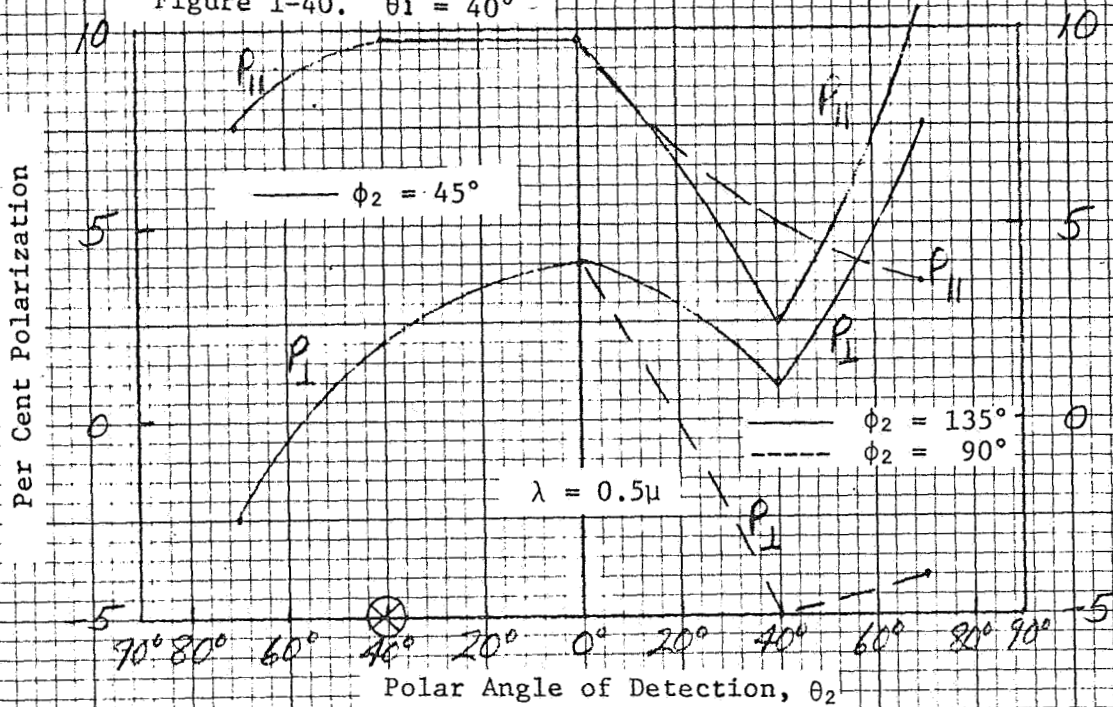
1.6.9 Discussion of Retro-Reflectance of Magnesium Oxide Surfaces

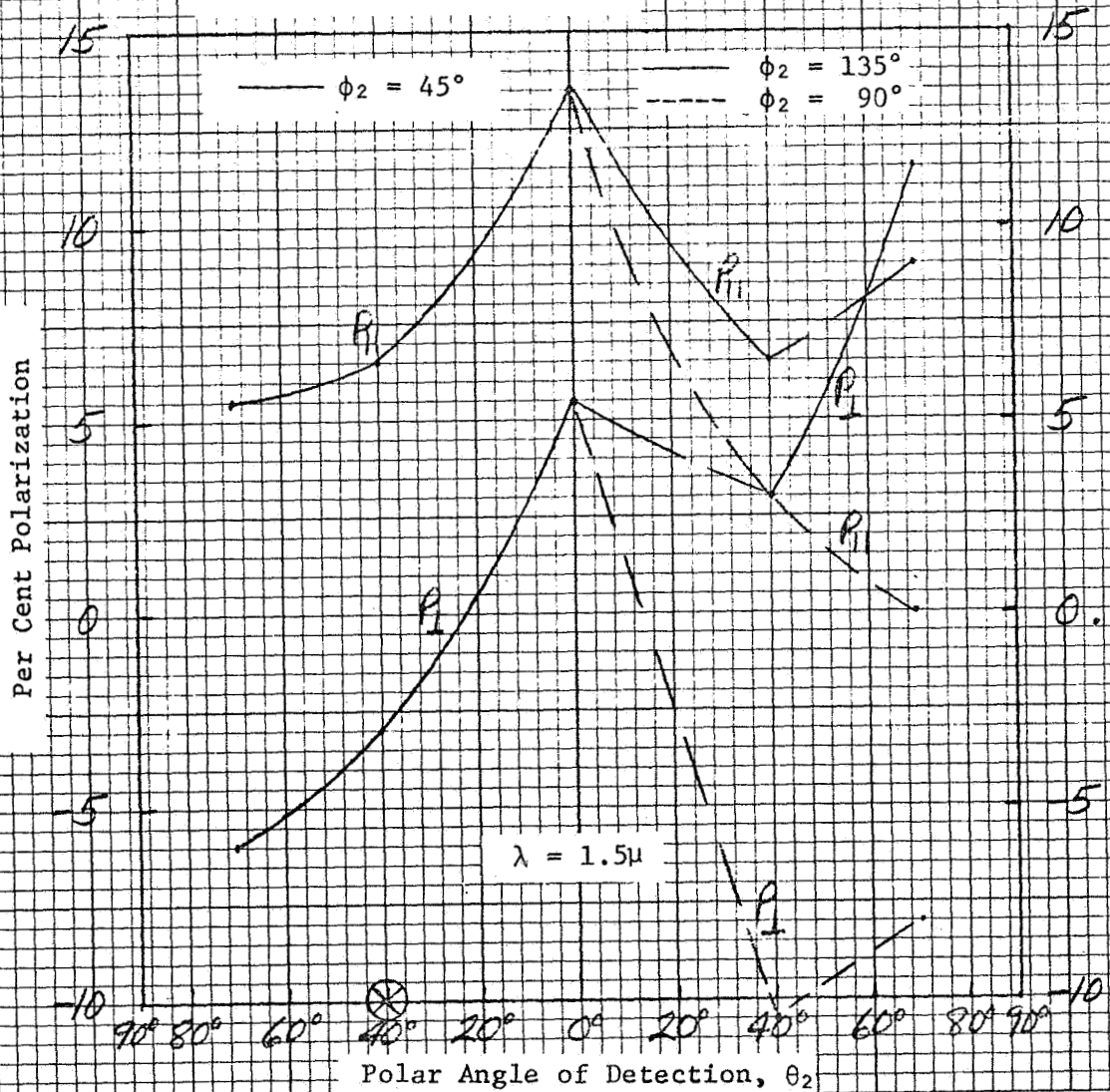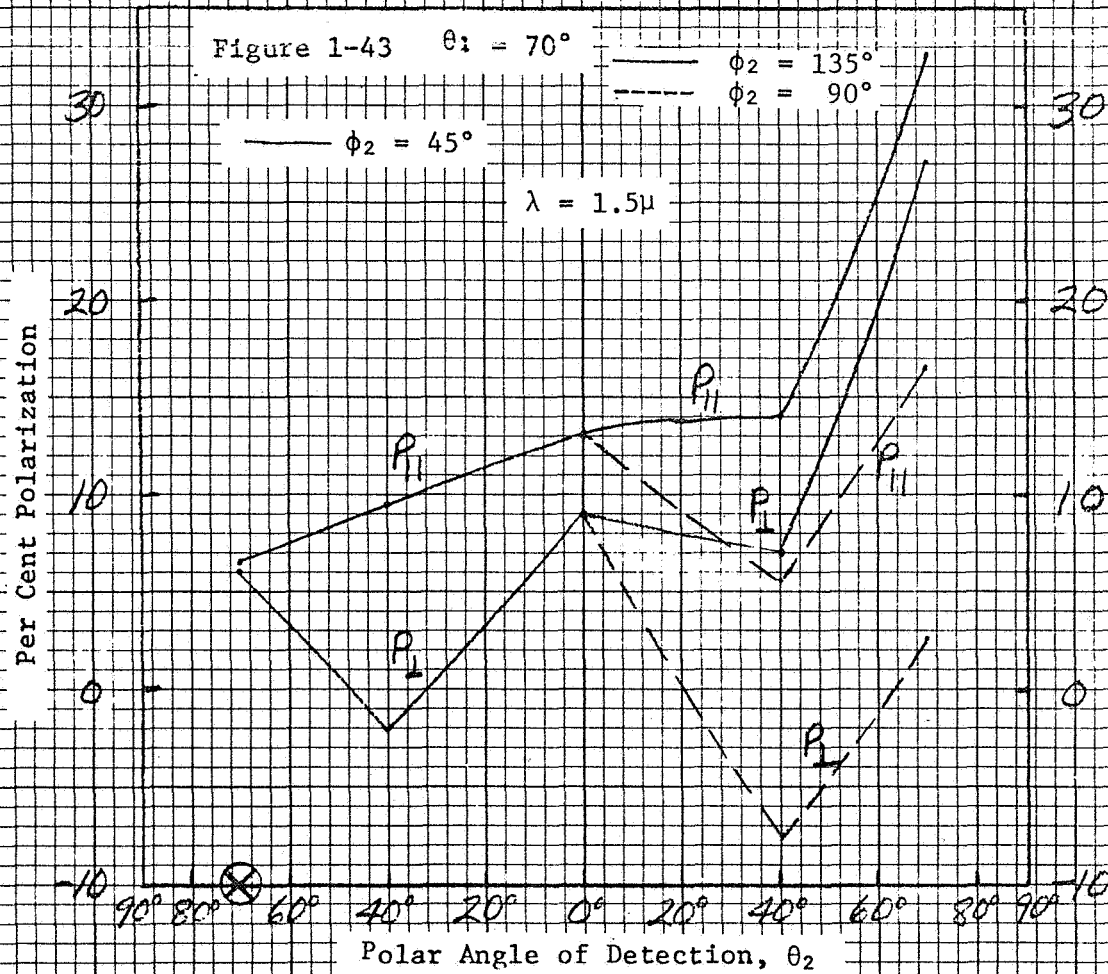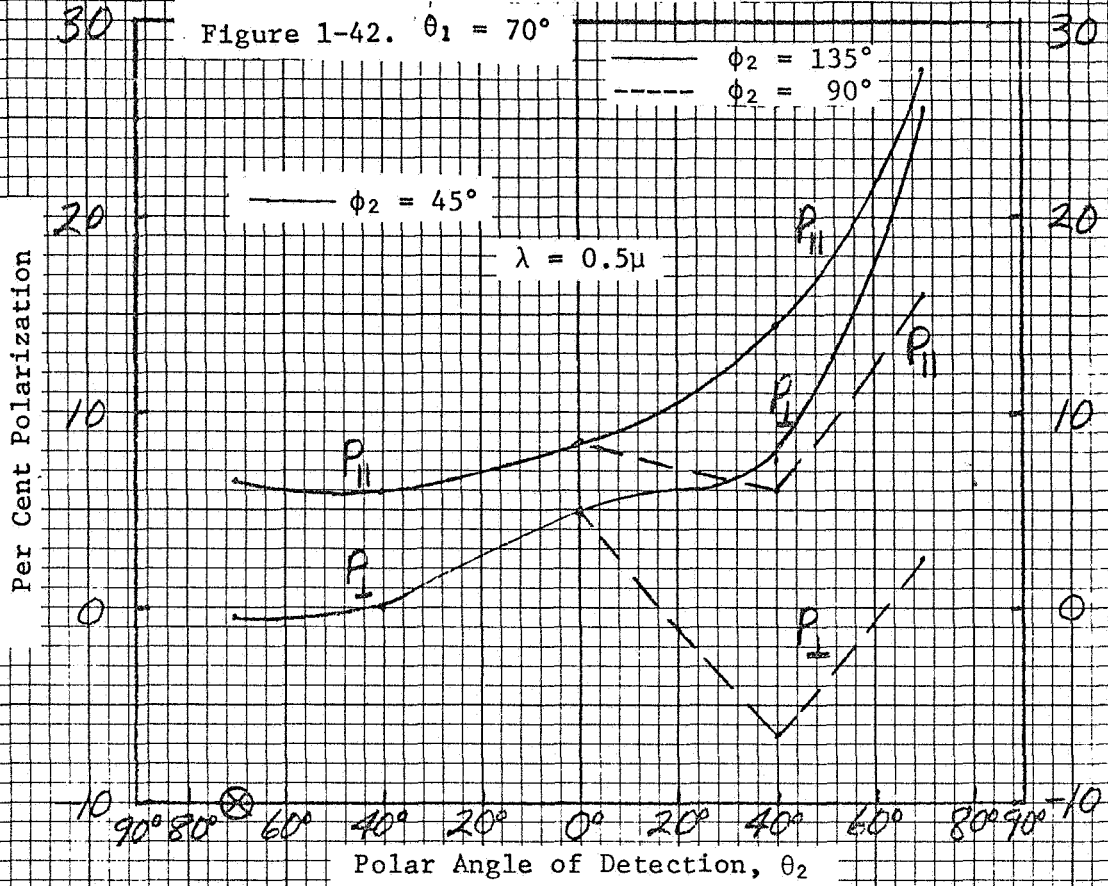Some investigators[6,7,8] have measured a large back-reflectance or retro-reflectance of smoked magnesium oxide which shows the coating to differ considerably from a Lambertian surface. Meacock's data is shown in Figure 1-36. This characteristic, if factual, could very likely cause significant errors in integrating sphere measurements made with MgO-coated sphere walls, since a sizable portion of the energy striking the walls could be reflected back out the entrance port.

From the BDR data presented earlier, one notes that at detection angles approaching the retro-reflective angle, a broad backscattering occurs. At angles of incidence which were near-normal, back scattering is small, and the reflectance distribution is essentially cosine. At higher angles of incidence, back-scattering as well as specular reflection becomes larger.

The standard TRW BDR test would not enable measurements of reflectance at detection angles less than 15° from the retro-reflectance angle; therefore, a special test set-up was constructed as shown in Figure 1-45. An actual retro-reflector was measured to verify that the apparatus was operating correctly. It was found that the apparatus had an inherent error which was evidenced by a change in reflectance and was approximately linear with the angle of detection. Still, a definite retro-reflectance "spike" was measured for the retro-reflector. Measurements of MgO, however, failed to show any detectable "spike" (See Figure 1.44). There was not time in this study to investigate this area further.
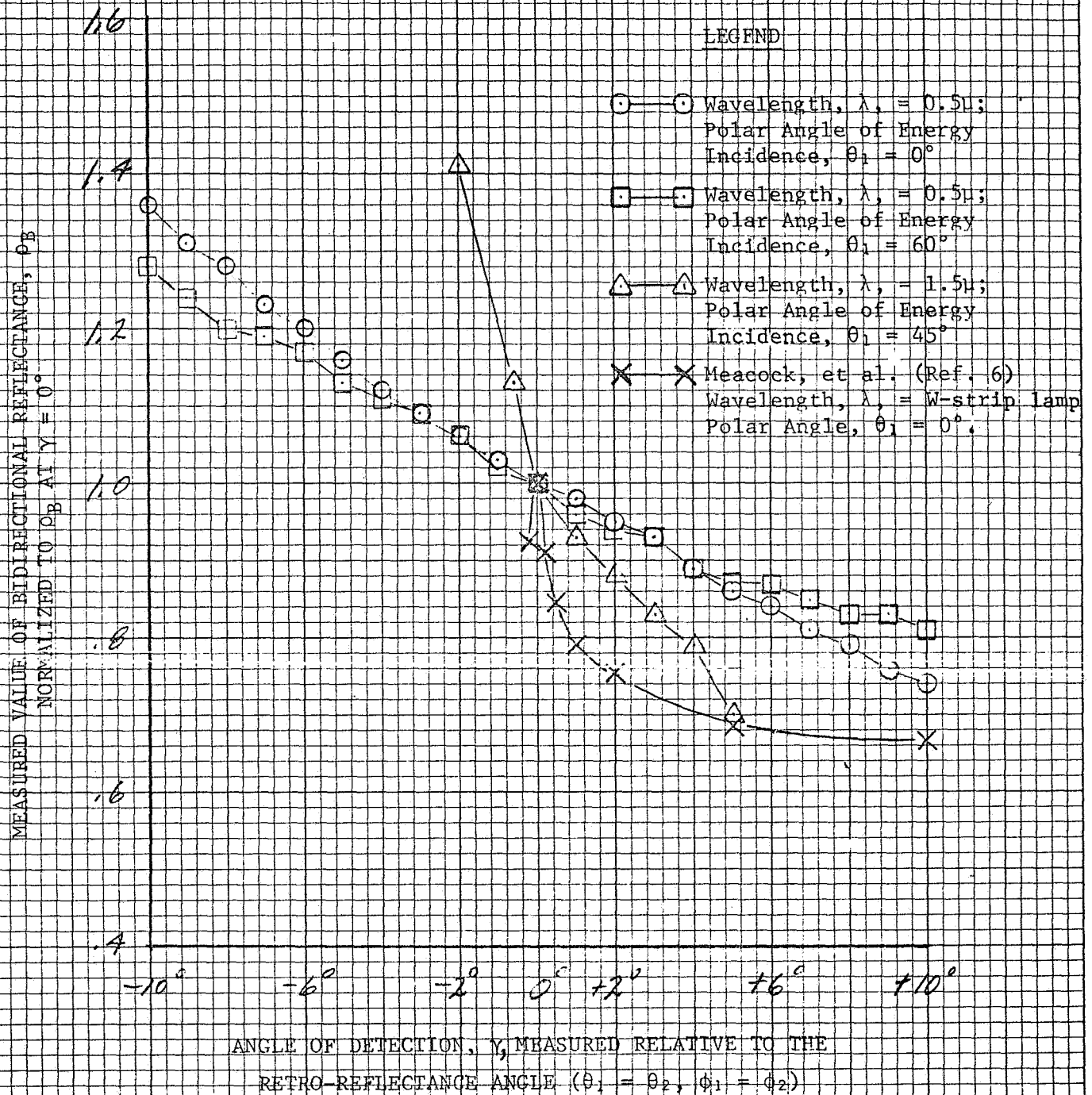
FIGURE 1-44. MEASURED VALUES OF BIDIRECTIONAL REFLECTANCE, ρ_B, NORMALIZED TO ρ_B AT $\gamma = 0°$ FOR SMOKED MgO (S/N 572-68) AT ANGLES NEAR THE RETRO-REFLECTANCE ANGLE (γ = DIFFERENCE BETWEEN POLAR ANGLE OF INCIDENCE AND POLAR ANGLE OF REFLECTANCE.)

Perkin Elmer Model 98 Monochromator

Thermocouple
Detector

Entrance
slit

Spherical Mirror
300 mm f.l.

Mask

Flat Mirror

Globar Source in
Typical Reflectance
Position

Reflective
Window

Mirror

Sample

FIGURE 1-45: RETRO-REFLECTANCE TEST SET-UP

2.0 DETECTOR CHARACTERISTICS

2.1 SUMMARY

Integrating sphere detector characteristics ideally would include uniform areal sensitivity, high sensitivity over a broad spectral range and perfectly cosine angular response. Real detectors deviate from these ideals to some extent and must therefore be studied if an attempt is to be made at quantifying the errors that result.

The lead sulfide cell and photomultiplier tube detectors have been used in integrating spheres for years due to their good spectral sensitivity and range. These detectors were therefore examined in detail to attempt to quantitatively characterize their response and reduce or eliminate some of their deficiencies.

After determining the characteristics of the two types of detectors in the "as received" condition by both literature search and various experimental techniques, methods of reducing or eliminating the undesirable features of the detectors were studied.
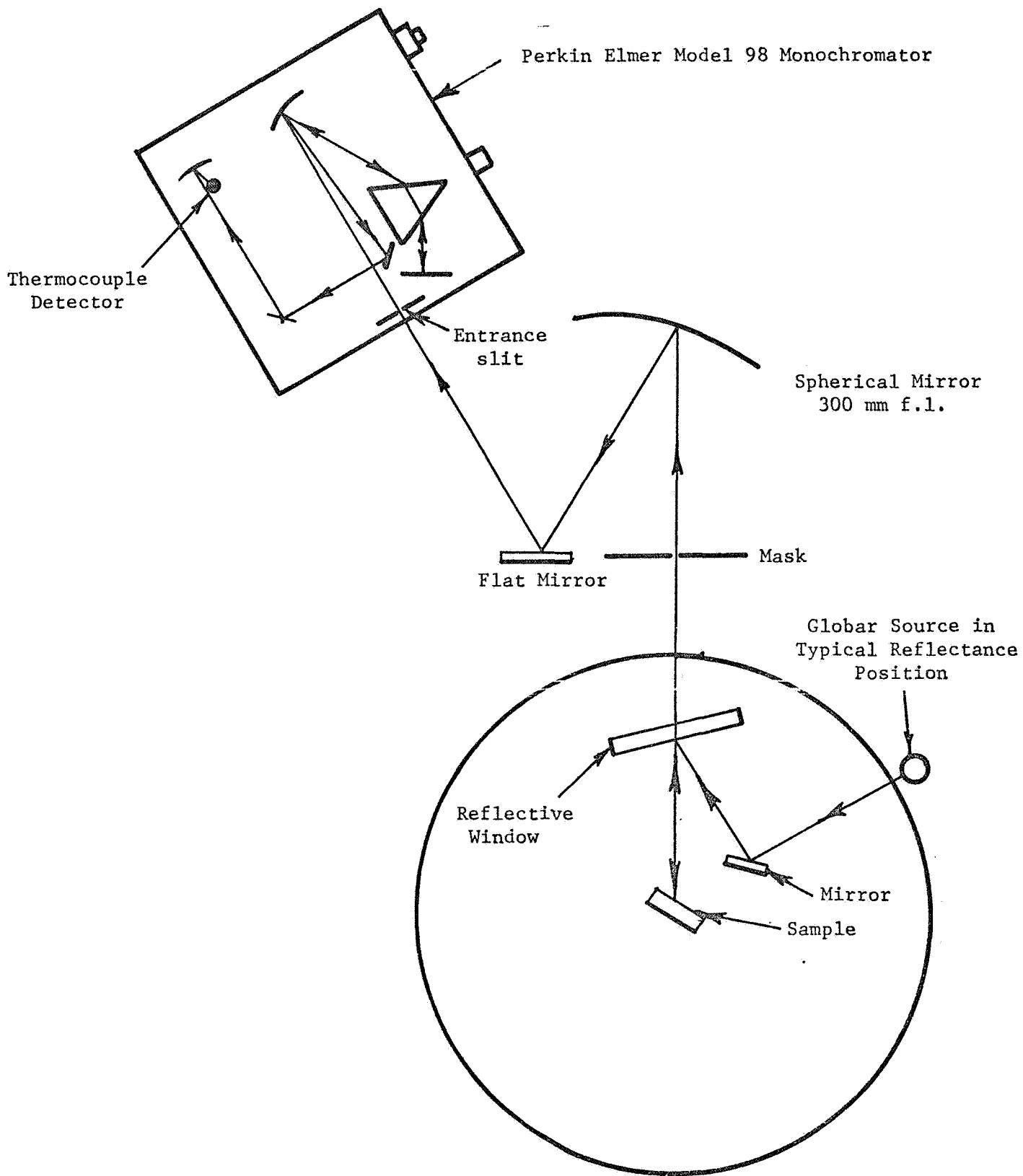
Improvements include:

a. Mounting the detectors on individual ports for insertion into the integrating sphere.

b. Masking the edges of the lead sulfide cell.

c. Masking, sandblasting, and smoking (MgO) the quartz envelope on the photomultiplier tube.

2.2 INTRODUCTION

Lead sulfide cell (PbS) and Photomultiplier (PM) tube detectors are the energy sensing elements normally associated with integrating sphere reflectometers. Earlier discussions (See Section 1.5.6.2) have shown that the geometrical arrangement of the detectors in the sphere relative to the sample surface, is of great importance in the consideration of errors associated with spectral reflectance measurements.

Other important detector characteristics which may influence the measurement errors include:

a. Areally dependent response

b. Spectral sensitivity and range

c. Short term stability

d. Directional response

e. Polarization sensitivity

The areal sensitivity of a detector may be a serious limitation for photometric work. The high areal sensitivity of both PM tube and PbS cell detectors has been demonstrated in the literature[11]. To reduce or eliminate the errors which may result from this situation, one must assure that the incident energy is essentially uniform over the detector sensitive area. Fortunately, the nature of the integrating sphere method of measurement is such that the energy which eventually reaches the detector is uniformly dispersed. The only portion of the energy reflected from the sample which is not uniformly dispersed is that which reflected directly from the sample onto the detector. Locating the detector in the sphere where it cannot "see" the samples eliminates this possibility.

Another method to provide uniformly dispersed energy on the detector is to place a diffusing surface or coating directly above the detector. This technique is discussed in the sections on PM tube directional sensitivity (Section 2.3.5).

For a particular detector, the spectral sensitivity and range are fundamental limitations. The effective spectral range can be broadened, however, by use of a fluorescent coating over the detector or on the sphere walls. (Energy frequencies outside the spectral range of the detector are absorbed by the coating which in turn fluoresces at frequencies within the detector spectral range). Sodium silicylate, in fact, is a coating frequently used to extend the effective spectral range of photomultiplier tube detectors. The short term stability is another basic limitation of a particular detector and is usually reflected as noise or drift of the output signal.

If a detector has undesirable directional response characteristics, steps may be taken to a.) improve these characteristics of the tube directly, b.) partially overcome these characteristics by special measurement techniques, or c.) partially account for these characteristics and modify the spectral data. Clearly, improvement of the directional characteristics directly is the most desirable approach. On the following pages are presented test data which demonstrate the dramatic improvements that can be made to the directional characteristics of a commercial photomultiplier tube detector.

A detector which is sensitive to the polarization of the incident energy may introduce errors in reflectance measurements. Only if one were perfectly assured that all of the energy incident on the detector was non-polarized could one assume this error to be negligible. Data on the polarization sensitivity of a PM tube with various surface treatments are presented on the subsequent pages.

The experimental work reported herein was primarily concerned with the PM tube detector (RCA 1P28), since the PbS cell detector characteristics have been analyzed and reported by several investigators[3,4,5,11,12].

2.3 PHOTOMULTIPLIER TUBE DETECTOR CHARACTERISTICS

2.3.1 Description of Parameters Investigated

Various optical characteristics of an RCA type 1P28 Photomultiplier tube (S-5 response) were investigated in detail. The response was measured as a function of the direction, wavelength and polarization of the incident energy. Each of these variables was investigated for each of three photomultiplier (PM) tube quartz envelope treatments. These were:

a. Envelope masked to 3/8 inch diameter opening by painting the quartz tube.

b. Envelope masked as above, opening sand-blasted to diffuse incident energy.

c. Envelope masked as above, opening sand-blasted and coated with approximately two (2) mils of smoked magnesium oxide to diffuse incident energy.

The PM tube masking and the angular conventions used are shown in Figure 2-1.
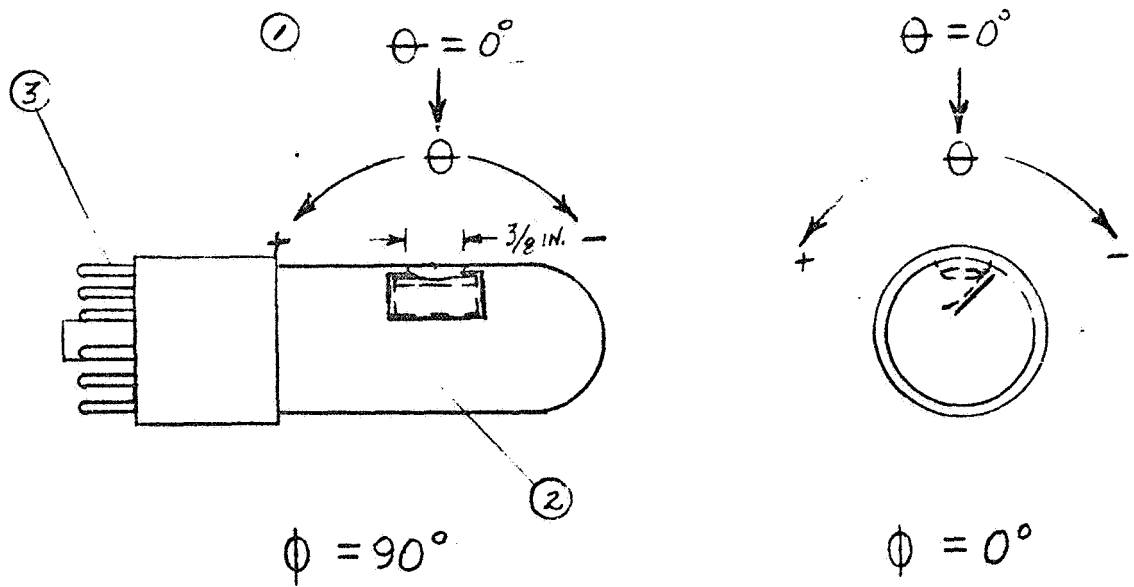
① — 3/8 inch diameter unmasked area on quartz envelope

② — This portion of quartz envelope painted with "Krylon" Zinc Chromate Primer and "Krylon" Flat white paint.

③ — P.M. tube electrical connector

Figure 2-1:   Illustration of Angular Conventions and Masking Used on RCA 1P28 Photomultiplier Tube.

Top View

Region of Best Collection

SHIELD

GRILL

INCIDENT LIGHT

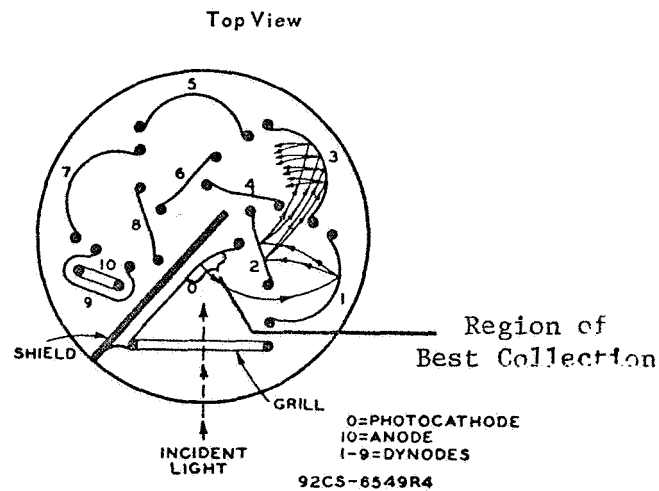0=PHOTOCATHODE
10=ANODE
1-9=DYNODES

92CS-6549R4

Figure 2-2. — Detailed Schematic Arrangement of RCA 1P28 Photomultiplier Tube Electrical Structure (from RCA 1P28 PM Tube Data Sheets[13])

2.3.2 Method of Measurement

The measurements were performed using the TRW Bidirectional Reflectometer (BDR) with the PM tube in the sample position. Variation of the azimuthal angle of energy incidence was obtained by rotating the detector about an axis normal to its quartz envelope at the center of the opening in the painted mask. The polar angle of energy incidence and polarization were varied as they normally are with the TRW BDR.

2.3.3 Results

The results of these measurements are shown in Figures 2-3, 2-4, and A-38 through A-43 in the Appendix.

2.3.4 Discussion of Results

Figure 2-3 is generally representative of the data taken at an azimuthal angle of $\phi = 0°$. One notes that the response of the masked but untreated tube is highly directional with the greatest sensitivity at polar angles of energy incidence between +25 and -40 degrees. The somewhat narrower angular response than that reported by RCA[13] can most likely be attributed to the masking. The RCA data did not specify a mask on the envelope, and it can probably be assumed that the values reported are for an unmasked tube. Both the TRW and RCA data show a displacement of the peak of the response to approximately eight degrees from the tube normal. This seems reasonable because of the tube photocathode geometry in the tube (See Figure 2-2).

Sandblasting the unmasked 3/8-inch diameter area on the quartz envelope resulted in only a slight broadening of the PM tube angular response (See Figure 2-3). The "bump" in the angular response curve of the untreated tube at $\theta = +45°$ was, however, eliminated by this operation. It should be pointed out that each curve shown in Figures 2-3 and 2-4 is normalized to the angular peak of the response for each particular PM tube condition. The response of the tube at its angular peak actually decreased to 12% of its initial value when sandblasted and coated with magnesium oxide.

Comparison of the curve representing the response of the PM tube after sandblasting and coating with MgO with the cosine curve in Figure 2-3 shows the treated tube to have a response which is very nearly cosine.
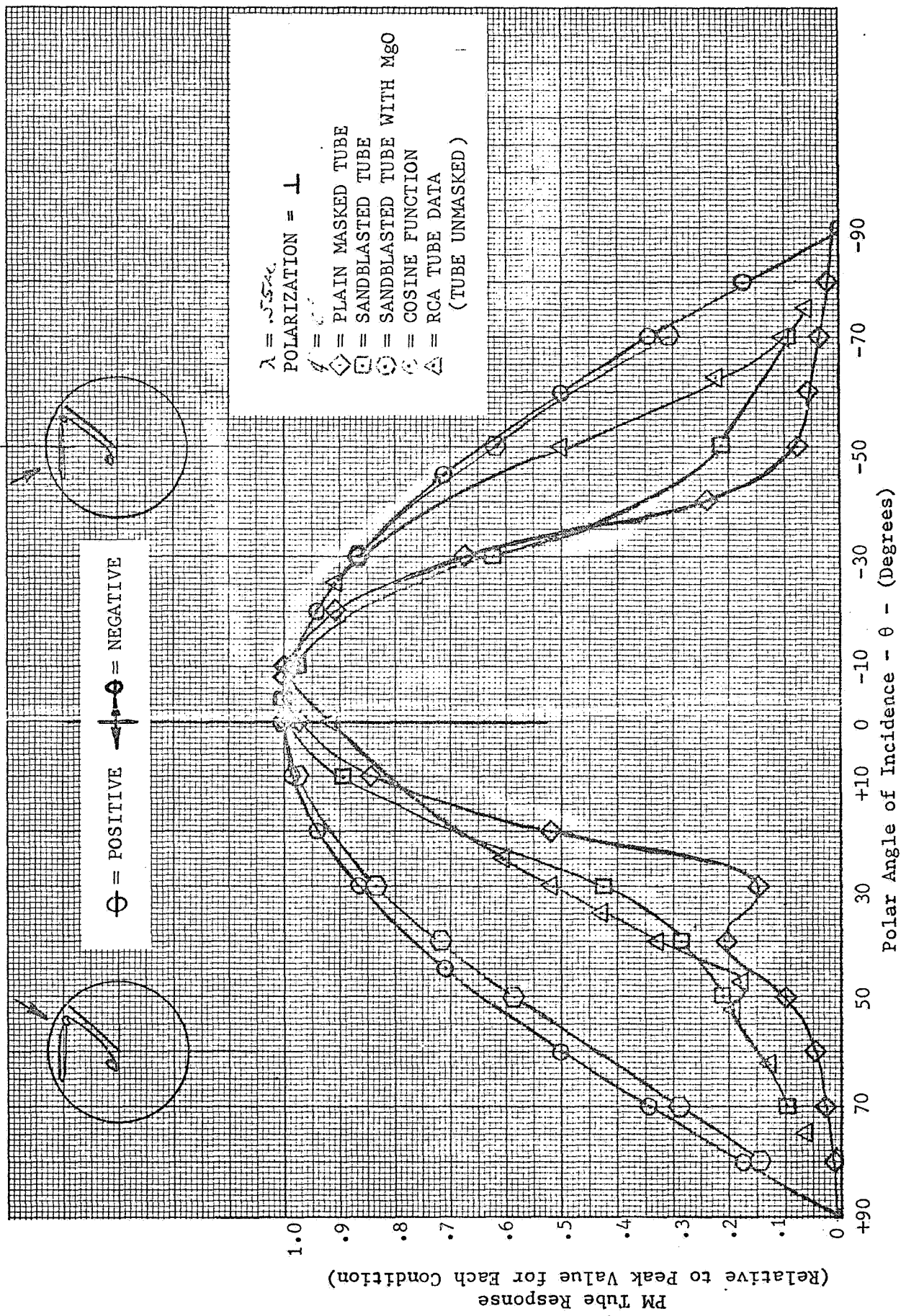
FIGURE 2-3: DIRECTIONAL RESPONSE CHARACTERISTICS OF RCA 1P-28 PHOTOMULTIPLIER TUBE DETECTOR
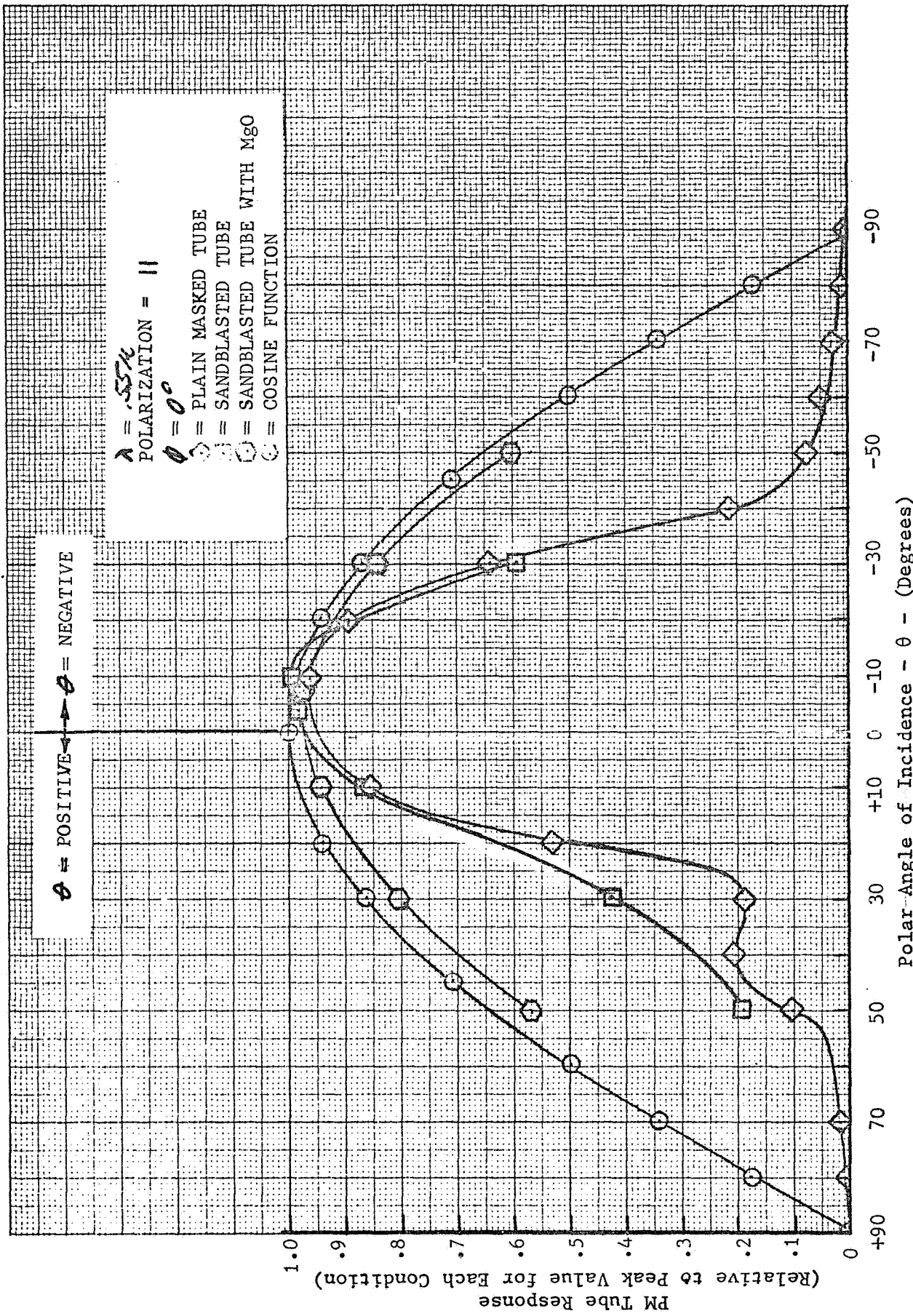
91

FIGURE 2-4: DIRECTIONAL RESPONSE CHARACTERISTICS OF RCA 1P-28 PHOTOMULTIPLIER TUBE DETECTOR

Figure 2-4 shows the detector response to have essentially the same angular dependency for the opposite polarization for each condition, although the response to energy at this polarization is approximately two to three per cent lower. Only enough data was taken at this polarization to assure that the tube angular response did not deviate from that for the opposite polarization.

Figures A-38 and A-39 in the Appendix present data for conditions similar to those in Figures 2-3 and 2-4, except for the other azimuthal angle investigated, $\phi = 90°$. For $\phi = 90°$, the untreated tube has a much broader angular response than for $\phi = 0°$, although it is still far from cosine. Again, sandblasting the unmasked area on the quartz envelope does not improve the directional characteristics significantly, but the combined treatment (sandblasting and coating with MgO) modified the tube angular response to the extent that it compares favorably with a perfectly cosine response. The tube angular responses at the two opposite polarizations once again compare closely with one another. Unlike the response at $\phi = 0°$, however, the response of the PM tube to incident energy of each polarization is essentially the same at $\phi = 90°$.

Figures A-40 through A-43 in the Appendix show data taken at the same conditions as the data in Figures 2-3, 2-4, A-38, and A-39 except for the wavelength and polarizer. These data were taken at 0.40 microns and another film polarizer (Polaroid KN36) was used. The results at this wavelength resemble that for 0.55 microns in that the angular response is not significantly improved by sandblasting, but compares favorably with the cosine response following sandblasting and coating with MgO. Errors in the measurement of directional reflectance in integrating spheres due to PM tube detector directional characteristics may be calculated from the data in Figures 2-3, 2-4 and A-38 through A-43 using the modification of Wildin's[14] analytical methods presented in Reference 15. The data may be used directly to calculate errors due to unequal detection of energy incident on the PM tube at the same polar angle but different azimuthal angles. To determine errors resulting from unequal detection of energy incident on the PM tube at different polar angles, the directional response curves must be normalized to the response at $\theta = 0°$ and compared to the cosine response curve.

It should be noted that although the sandblasting treatment did little to alter the directional response, it does provide a rough surface to which the smoked MgO can adhere. Without it, the layer of MgO smoke will slide off the tube.

2.3.5 Discussion of Related Literature on the PM Tube

2.3.5.1 Areal Sensitivity

The RCA literature on the 1P-28 PM tube[13] presents data on the areal sensitivity along the two major axes (Figures 2-5 and 2-6). Stair and Schneider[11] at the National Bureau of Standards expanded on the RCA data by completely mapping the areal sensitivity of this detector (Figure 2-7). This figure shows the approximate location of the circular area left uncoated on the PM tube analyzed in the present work. These data tend to further demonstrate the importance of diffusing the energy incident on the tube to reduce measurement errors. A diffuse coating tends to "smear" the incident energy over the sensitive area uniformly, regardless of its point of incidence on the tube.

2.3.5.2 Spectral Sensitivity

Figure 2-8, extracted from the RCA 1P-28 tube data sheets, shows the spectral sensitivity of the tube. As discussed earlier, the spectral range and sensitivity are fundamental limitations of detectors. The spectral range of a PM tube can be extended to slightly shorter wavelengths by the addition of a thin sodium silicylate coating.

The spectral data in Figure 2-8 are for tubes with no diffusing coating. The addition of a thin MgO coating probably reduces the spectral sensitivity and range, although this parameter was not investigated in the present study. It was found, as mentioned earlier, that the tube response was reduced by approximately 90% at the wavelengths investigated upon application of a MgO coating.

2.3.5.3 Directional Sensitivity

The RCA PM tube data sheets show the uncoated tube response as a function of polar angle of energy incidence. These data have been recopied and are shown in Figure 2-3. The uncoated tube is seen to be unsatisfactory for

**TYPICAL VARIATION OF PHOTOCATHODE
SENSITIVITY ALONG TUBE LENGTH. (Ref. 13)**

SPOT SIZE : 1MM DIA. APPROX.
VARIATIONS CAUSED BY INTERCEPTION OF LIGHT BY GRILL
AS WELL AS SURFACE IRREGULARITIES HAVE BEEN IGNORED.

RELATIVE ANODE CURRENT

DISTANCE ALONG CATHODE FROM END
OF CATHODE NEARER BASE — MILLIMETERS

92CS-7663R2
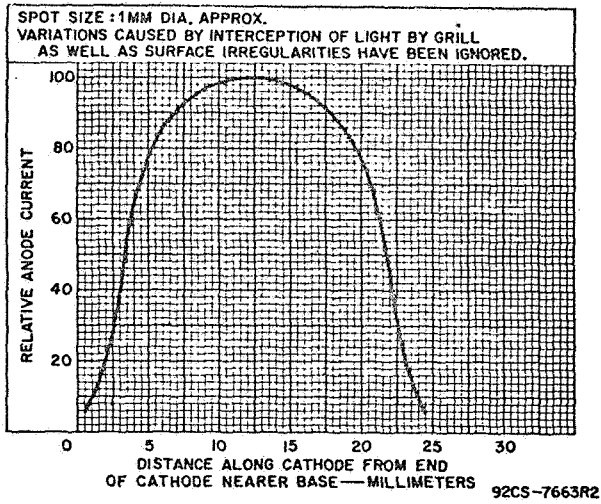
**TYPICAL VARIATION OF PHOTOCATHODE
SENSITIVITY ACROSS PROJECTED WIDTH
IN PLANE OF GRILL (Ref. 13)**

SPOT SIZE : 1MM DIA. APPROX.
GRILL TOWARD OBSERVER, BASE DOWN.
CATHODE WIDTH PROJECTED NORMAL TO PLANE OF GRILL.

VARIATIONS CAUSED
BY INTERCEPTION
OF LIGHT BY GRILL
AS WELL AS SUR-
FACE IRREGULAR-
ITIES HAVE BEEN
IGNORED.

RELATIVE ANODE CURRENT

DISTANCE ALONG PLANE OF GRILL
FROM LEFT TO RIGHT — MILLIMETERS

92CS-7667R2

VERTICAL POSITION, mm

HORIZONTAL POSITION, mm

FIGURE 2-7: VARIATION IN SENSITIVITY OVER THE SURFACE OF A
1P-28 PHOTOMULTIPLIER (After Stair and Schneider[11])

(Circle and cross-hatched areas shown one centimeter diameter
mask similar to that used on TRW PM tube detectors.)

SPECTRAL RESPONSE CHARACTERISTICS

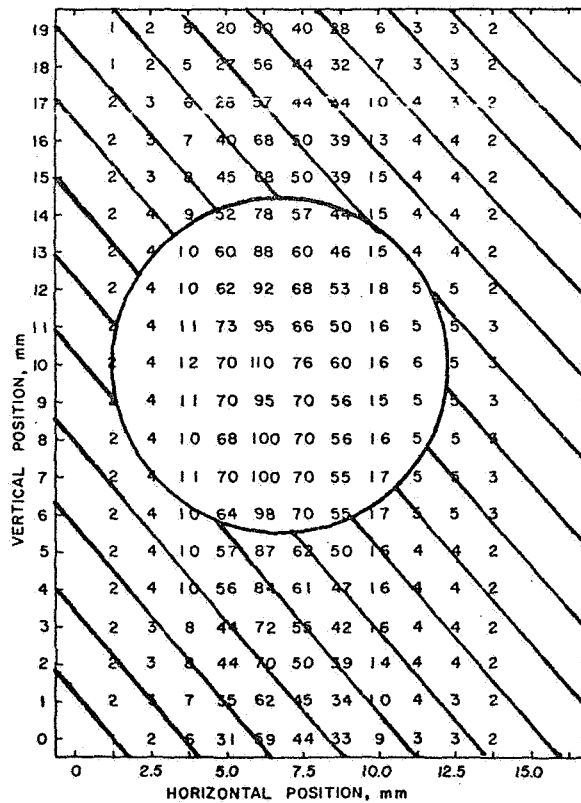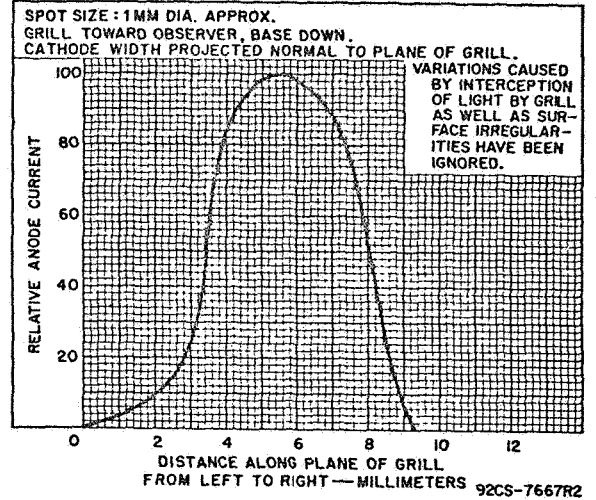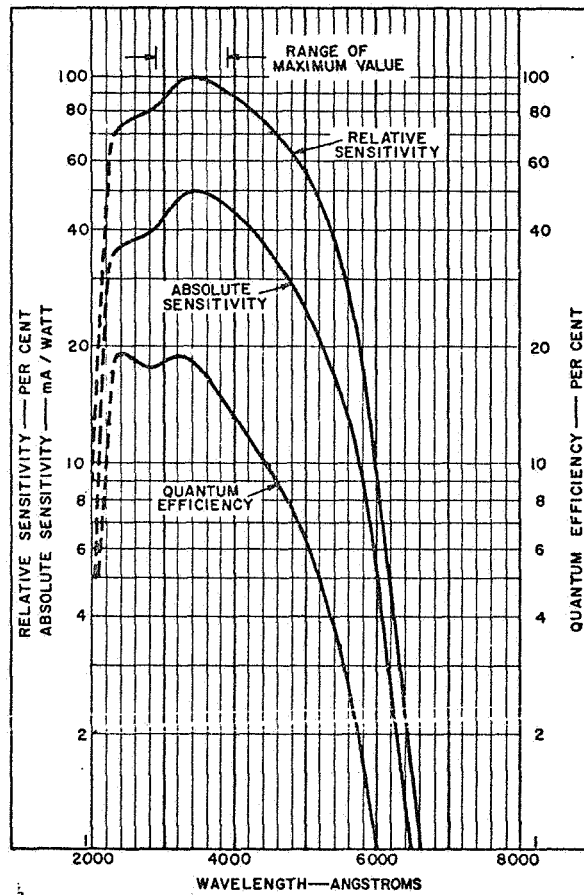FIGURE 2-8: SPECTRAL SENSITIVITY OF UNCOATED RCA 1P-28
PHOTOMULTIPLIER TUBE
(From RCA 1P-28 PM Tube Data Sheets[13])

integrating sphere measurements due to its high angular sensitivity.

Edwards, *et al.*[2], reported data taken on the directional sensitivity of a PM tube but did not mention the wavelength used in the experiment. The opal glass detector cover reported there appears to be effective in providing a detector response which is nearly cosine. The directional sensitivity as a function of polarization state of incident energy was not investigated in this early work.

2.3.6 Conclusions and Recommendations

An uncoated, uncovered RCA type 1P-28 PM tube is highly sensitive to polar and azimuthal angle of energy incidence, and has high areal non-uniformity. It does not, however, seem to be highly sensitive to the polarization state of incident energy.

The directional characteristics are only slightly improved by sand-blasting the PM tube. The combined treatment of sandblasting the tube and applying a light coat of MgO, however, results in significant improvements in the tube angular properties. It is believed that the diffuse overcoating also improves the areal sensitivity significantly, although no measurements were taken to confirm this.

The only disadvantageous effect of the over-coating appears to be a large ($\sim$90%) decrease in the detector response. This is due to the high coating reflectance and some coating absorptance of the incident flux. The detector output, however, is still sufficiently high to obtain reliable data.

2.4 LEAD SULFIDE CELL CHARACTERISTICS

In this section, we rely principally upon the published literature concerning PbS cell detectors.

Cells with sensitive area 1 cm square and a relatively long time constant (>300 microseconds), such as produced by Eastman Kodak, Infrared Industries, and Santa Barbara Research Center, are commonly used.

The spectral detectivity of an Infrared Industries Type T cell is shown in Figure 2-9 from Reference 12.

The relative areal sensitivity of an Eastman cell for normally incident tungsten lamp source radiation is shown in Figure 2-10 from Ref. 11.

The sensitivity is somewhat greater near the electrodes than near the side edges.
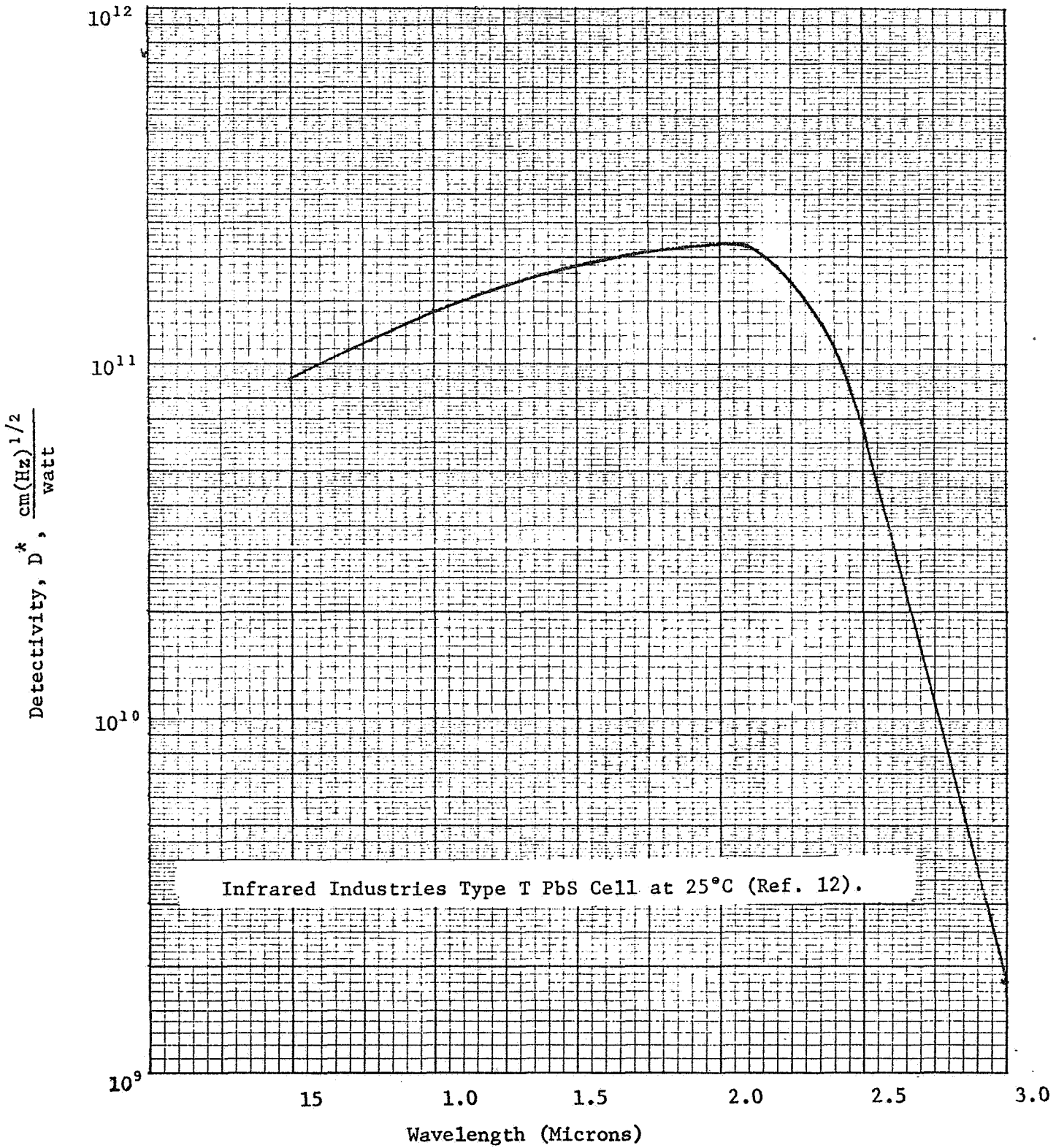
Covering the surface and edges with an opaque mask with a circular opening, as shown in Figure 1-16, Section 1.5.6.2, serves to eliminate cell areas of relatively low sensitivity.

In Figure 2-11, the polar angle response of an Eastman Ektron Type N Cell is drawn for two azimuthal orientations (Ref. 5). The incident light is assumed to be from an unpolarized tungsten lamp.

The large differences for azimuthal orientations 90° apart is greatly reduced by painting the side edges with black paint. This azimuthal dependence is completely eliminated by masking the cell as described above and shown in Figure 1-16. Since the PbS cell has a large index of refraction, the cell will reflect a large fraction (20 to 80%) of the light incident as a function of wavelength, angle of incidence and polarization. Therefore, deviations from a cosine polar angle response are expected (Shown in Figure 2-11).

A study of the polarization dependence of the response was reported by Schaefer (Ref. 3). Although the data reported therein is inadequate for characterizing a given detector, it does illustrate possible large polarization effects. Fortunately, in integrating spheres, all energy striking the detector has reflected at least one time from the MgO wall coating, and is therefore considerably depolarized (See Table 1-19).

FIGURE 2-9:   SPECTRAL DETECTIVITY OF A LEAD SULFIDE DETECTOR

Infrared Industries Type T PbS Cell at 25°C (Ref. 12).

Detectivity, D^*, $\dfrac{cm(Hz)^{1/2}}{watt}$
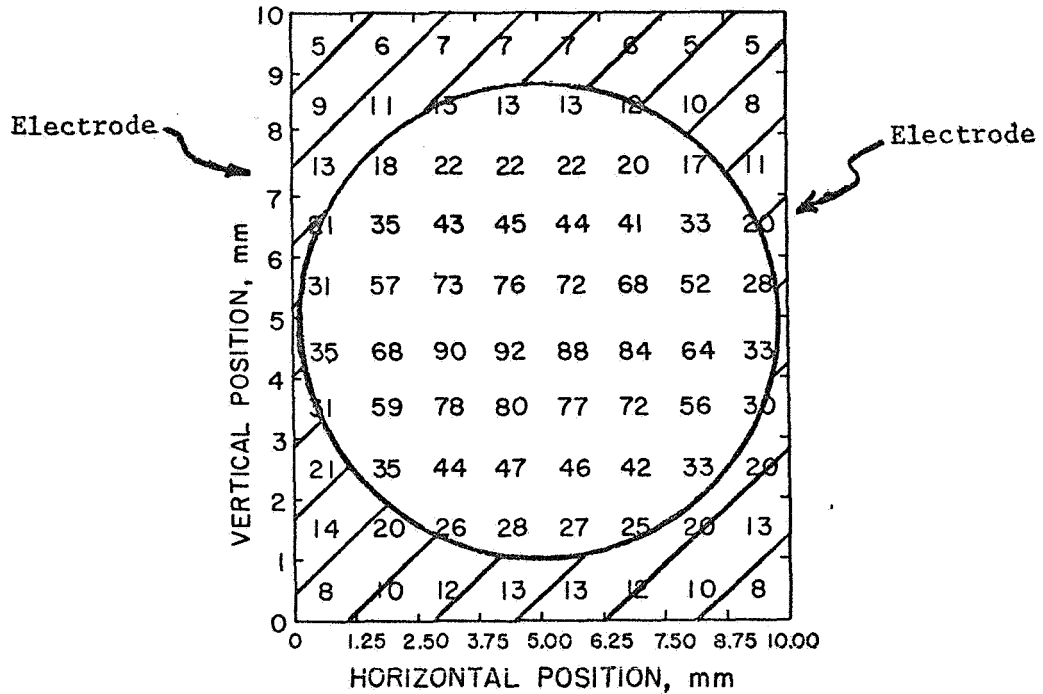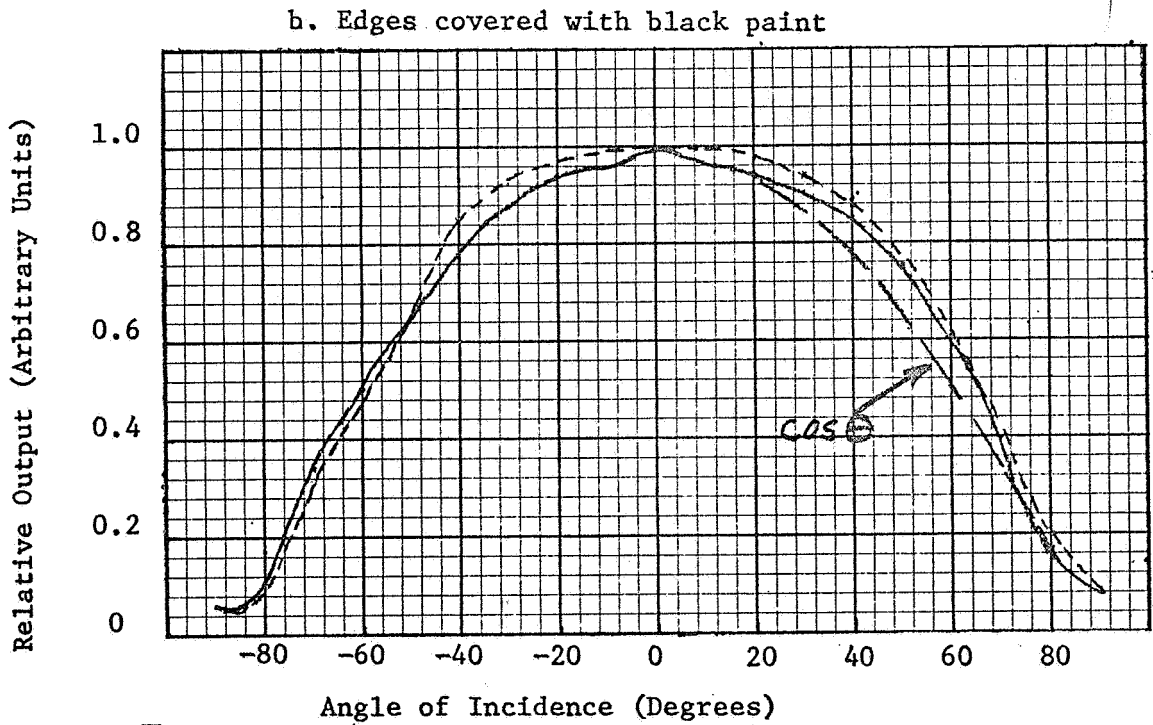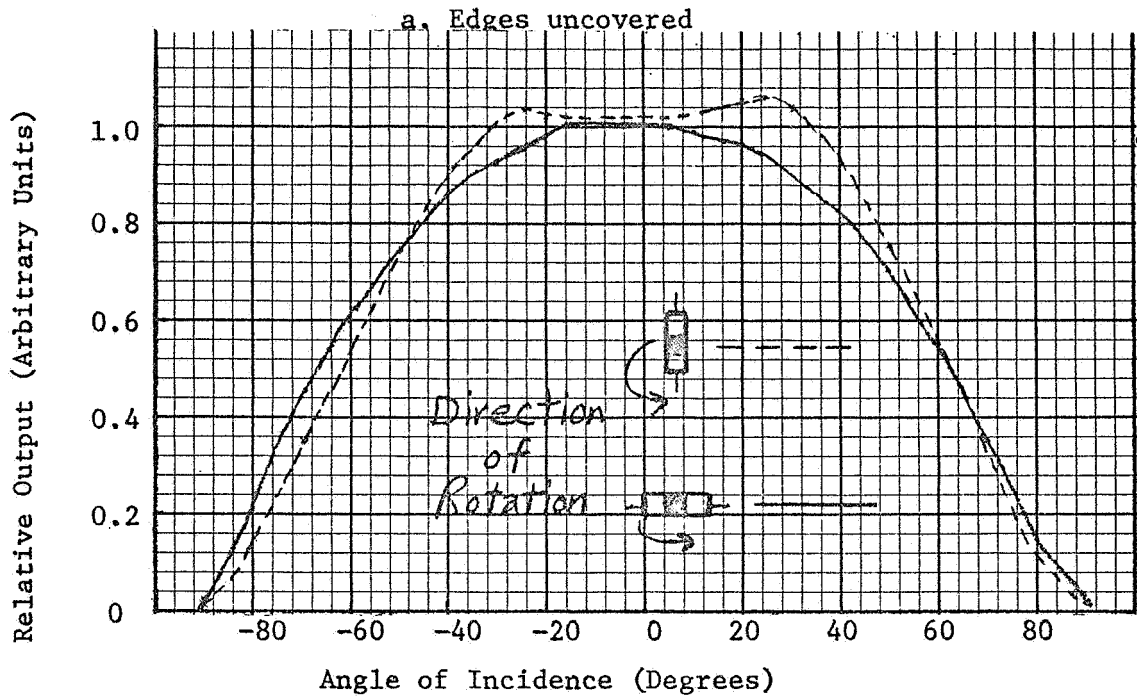
Wavelength (Microns)

FIGURE 2-10: VARIATION IN SENSITIVITY OVER THE SURFACE
OF AN EASTMAN PbS CELL (Ref. 11)

(Tungsten Lamp Source; Normal Incidence)

(Recommended mask is shown)

FIGURE 2-11: RELATIVE RESPONSE OF AN EASTMAN PbS DETECTOR FOR UNPOLARIZED RADIATION FROM A TUNGSTEN LAMP
(After Groner and Stoliar, Ref. 5)

a. Edges uncovered

b. Edges covered with black paint

3.0 REFERENCES

1. Priest I., and Riley, J., "The Selective Reflectance of Magnesium Oxide", J.O.S.A. 20:156-159 (1930).

2. Edwards, D.K., et al., "Integrating Sphere for Imperfectly Diffuse Samples", J.O.S.A. 51:1279-88 (1961).

3. Shaefer, G., "A Study of the Angular Response of Lead Sulfide Detectors", Applied Optics, 1:637-641 (1962).

4. Limperis, T.,"Polarization Response in Infrared Detectors", Private Communication to M. W. Wildin, JPL, September 13, 1967.

5. Groner, W., and Stoliar, A.P., "Variation of Lead Sulfide Response with Incident Angle and Orientation in Detector Plane", Applied Optics, 2:1204-1205 (1963).

6. Meacock, H.F.; Garforth, F.A.; and Shrubsall, R.G., "The Luminance Factor of Smoked Magnesium Oxide at Small Angles of View", J. Sci Inst 39:384-386 (1962).

7. Miller, E.R., and Vun Kannon, R.S., "Development and Use of a Bidirectional Spectroreflectometer", AIAA Paper No. 67-313 presented at the AIAA Thermophysics Specialist Conference, New Orleans, Lousiana, April 1967.

8. Oetking, R., Geophys. Rev. 71:2505 (1966).

9. Stockham, L.W., and Love, T.J., "Investigation of Opposition Effect in Integrating Spheres", J.O.S.A. 60:251-254 (1970).

10. Edwards, D.K., and Herold, L.M., "Experimental Investigation of the Infrared Spectral Reflection Distribution Function of Wire Meshes", Final Report No. 64-8, pp. 22, 3, UCLA Department of Engineering, (February 1964).

11. Stair, R., and Schneider, W.E., "Standards, Sources, and Detectors in Radiation Measurements", NASA SP-55, Symposium on Thermal Radiation of Solids, pp. 217 - 231, (1965).

12. Infrared Industries Infratron Handbook, p 1.3 (1970).

13. "Photomultiplier Tube, 9-Stage Side-On Type, S-5 Spectral Response", RCA-1CP28, RCA Technical Publication (1966).

14. Wildin, M.W., "Error Analysis of Integrating Spheres with Center Mounted Samples", Jet Propulsion Laboratories Space Program Summary 37-49, Vol. 3, pp. 153-159 (1968).

15. "An Error Analysis of the Gier Dunkle Integrating Sphere and Heated Cavity Reflectometers as Used in Measurements of Solar Absorptance and Emittance Properties", TRW Report No. 67-3346.11w-51 written by Brian Newnam, 1967; JPL Purchase Order ES-453477.

APPENDIX

103

APPENDIX

A.1 AGING CHARACTERISTICS OF SMOKED AND POWDER MgO SURFACES

A detailed discussion of the aging characteristics of smoked MgO and MgO powder surfaces is given in Section 1.2 of this report. This discussion is supplemented with Figures A1 through A9 of the following pages, which are graphs showing the degradation of several different MgO surfaces due to aging.

A.2 SPECTRAL DIRECTIONAL REFLECTANCE OF MgO

The discussion of the spectral directional reflectance of MgO is presented in Section 1.5 of this report. Tables A-1 through A-7 tabulate the corrected values of directional reflectance. Figures A-10 through A-16 supplement the graphs shown in Section 1.5.

A.3 SPECTRAL BIDIRECTIONAL REFLECTANCE OF MgO

The spectral bidirectional reflectance (BDR) of MgO is discussed in Section 1.6. This discussion includes the graphs of a portion of the data taken. Figures A-17 through A-38 are graphical presentations of the remainder of the data. Detailed comments on the BDR characteristics are given following Figure A-38.

A.4 DIRECTIONAL RESPONSE CHARACTERISTICS OF THE RCA 1P28 PHOTOMULTIPLIER TUBE DETECTOR

Figures A-39 through A-44, which show the directional response characteristics of the RCA 1P28 photomultiplier tube detector, supplement the discussion and figures presented in Section 2.3.

FIGURE A1

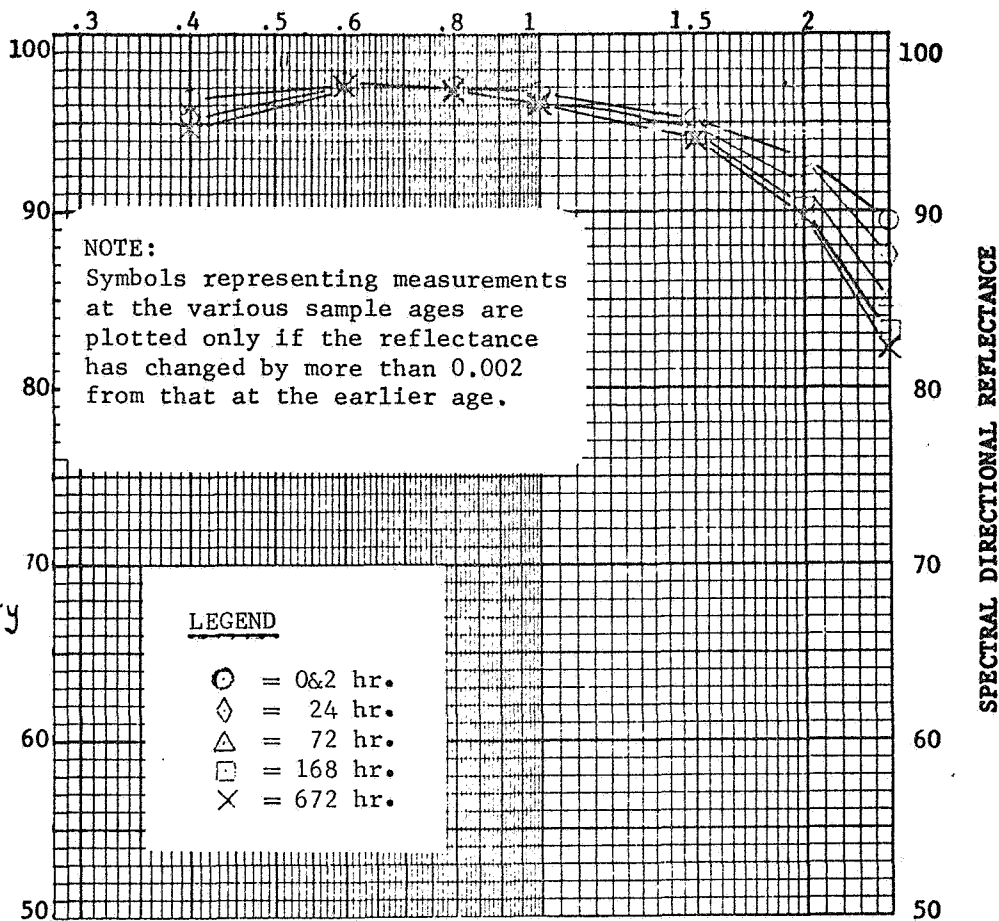CUSTOMER CODE NO.:

TRW DESIGNATION:
S/N 570-68

MATERIAL:
Smoked MgO, 1mm Thick

ANGLES:
POLAR, θ = 10°
AZIMUTHAL, φ = Arbitrary

MEASUREMENTS
INSTRUMENTS

FIGURE A1

WAVELENGTH (MICRONS)

SPECTRAL DIRECTIONAL REFLECTANCE

NOTE:
Symbols representing measurements at the various sample ages are plotted only if the reflectance has changed by more than 0.002 from that at the earlier age.

LEGEND

⊙ = 0&2 hr.
◊ = 24 hr.
△ = 72 hr.
▢ = 168 hr.
✕ = 672 hr.

FIGURE A2

CUSTOMER CODE NO.:

TRW DESIGNATION:
S/N 571-68

MATERIAL
Smoked MgO, 2mm Thick

ANGLES:
POLAR, θ = 10°
AZIMUTHAL, φ = Arbitrary

MEASUREMENT
INSTRUMENTS

FIGURE A2

WAVELENGTH (MICRONS)

SPECTRAL DIRECTIONAL REFLECTANCE

NOTE:
Symbols representing measurements at the various sample ages are plotted only if the reflectance has changed by more than 0.002 from that at the earlier age.

LEGEND

○ = 0 hr.
⊙ = 2 hr.
◊ = 24 hr.
△ = 72 hr.
▢ = 168 hr.
⊘ = 336 hr.
◁ = 504 hr.
✕ = 672 hr.

TRW DESIGNATION:

S/N 572-68

MATERIAL:

Smoked MgO, 3mm
Thick

ANGLES:

POLAR, θ = 10°

AZIMUTHAL, φ = Arbitrary

MEASUREMENTS

INSTRUMENTS

FIGURE A3

WAVELENGTH (MICRONS)

NOTE:
Symbols representing measurements
at the various sample ages are
plotted only if the reflectance
has changed by more than 0.002
from that at the earlier age.

LEGEND

⊙ = 0 hr.
⬡ = 2 hr.
◇ = 24 hr.
△ = 72 hr.
⊡ = 168 hr.
✕ = 672 hr.

SPECTRAL DIRECTIONAL REFLECTANCE

CUSTOMER CODE NO.:

TRW DESIGNATION:

S/N 576-68
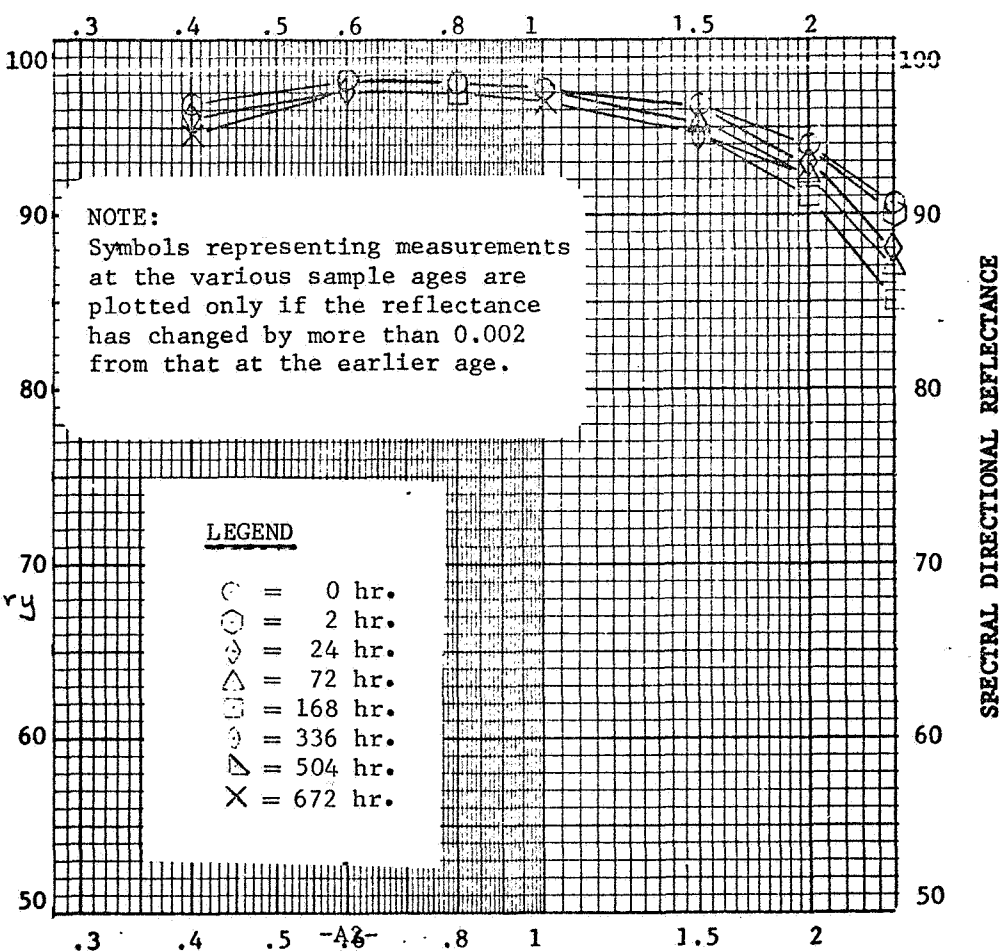
MATERIAL

Smoked MgO, 4mm
Thick

ANGLES:

POLAR, θ = 10°

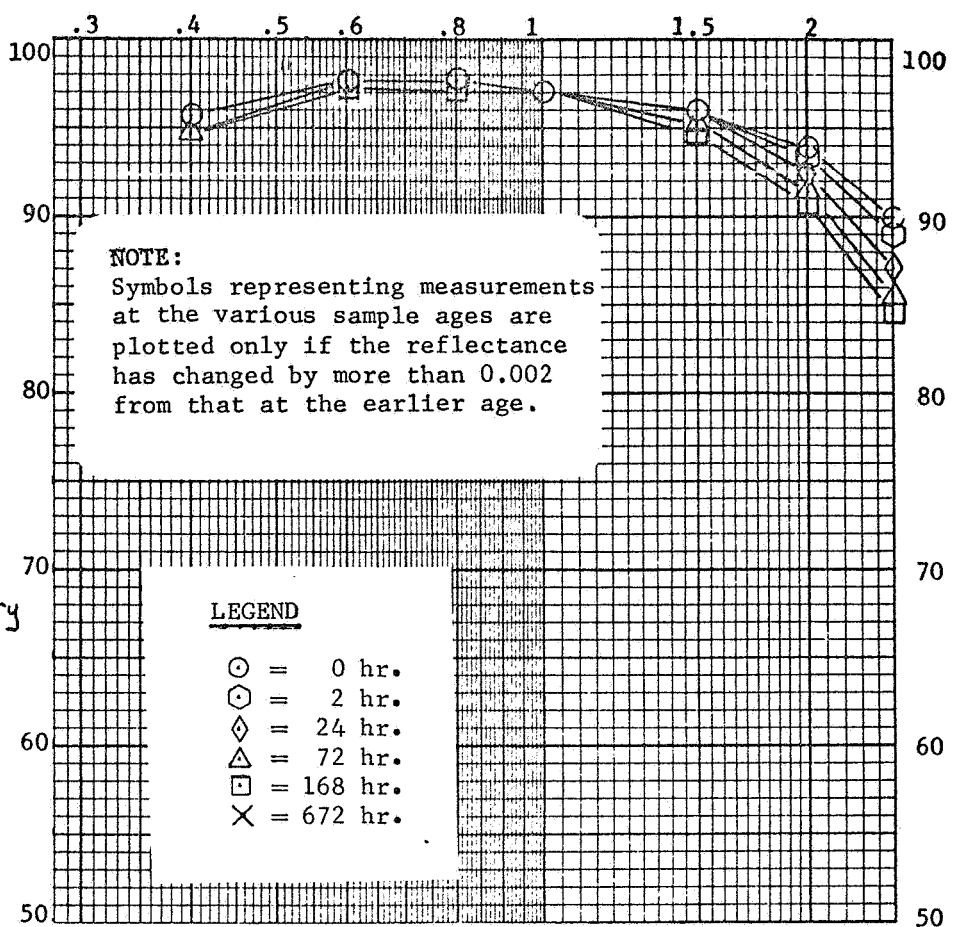AZIMUTHAL, φ = Arbitrary

MEASUREMENT

INSTRUMENTS

FIGURE A4
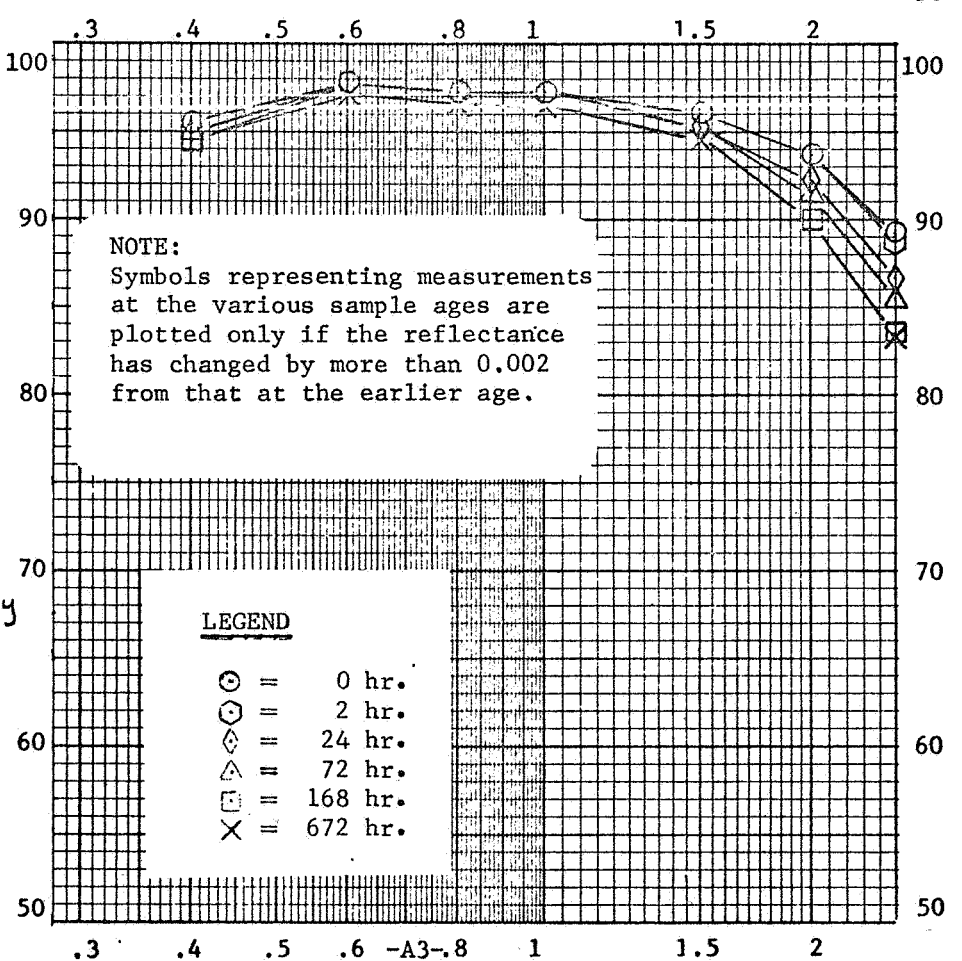
WAVELENGTH (MICRONS)

NOTE:
Symbols representing measurements
at the various sample ages are
plotted only if the reflectance
has changed by more than 0.002
from that at the earlier age.

LEGEND

⊙ = 0 hr.
⬡ = 2 hr.
◇ = 24 hr.
△ = 72 hr.
⊡ = 168 hr.
✕ = 672 hr.

SPECTRAL DIRECTIONAL REFLECTANCE

CUSTOMER CODE NO.:

TRW DESIGNATION:

S/N 577-68

MATERIAL:

Smoked MgO, 2mm
Thick-no electro-
static field.

ANGLES:

POLAR, $\theta = 10°$

AZIMUTHAL, $\phi = $ Arbitrary

MEASUREMENTS

INSTRUMENTS

FIGURE A5

WAVELENGTH (MICRONS)

NOTE:
Symbols representing measurements
at the various sample ages are
plotted only if the reflectance
has changed by more than 0.002
from that at the earlier age.

LEGEND

⊙	=	0 hr.
⬡	=	2 hr.
◇	=	24 hr.
△	=	72 hr.
□	=	168 hr.
✕	=	672 hr.

SPECTRAL DIRECTIONAL REFLECTANCE
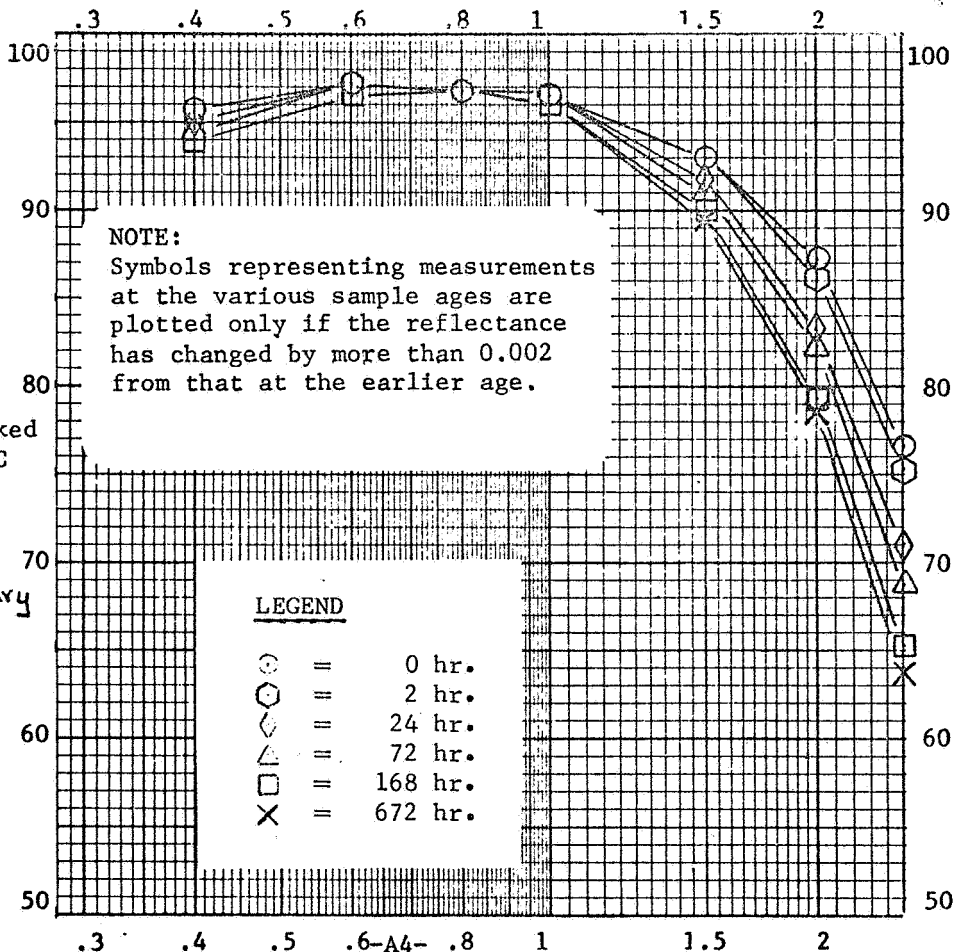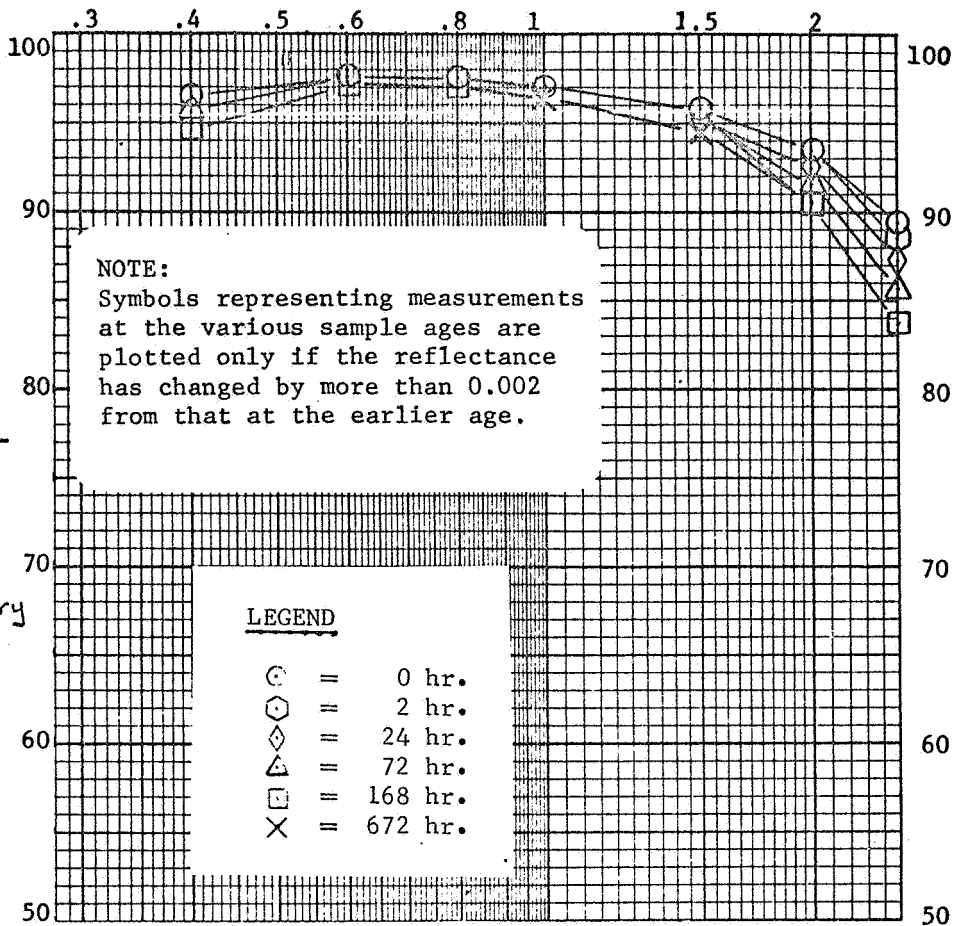
CUSTOMER CODE NO.:

TRW DESIGNATION:

S/N 578-68

MATERIAL

Pressed MgO, 2mm
thick, powder baked
18 hours at 290°C
before pressing.

ANGLES:

POLAR, $\theta = 10°$

AZIMUTHAL, $\phi = $ Arbitrary

MEASUREMENT

INSTRUMENTS

FIGURE A6

WAVELENGTH (MICRONS)

NOTE:
Symbols representing measurements
at the various sample ages are
plotted only if the reflectance
has changed by more than 0.002
from that at the earlier age.

LEGEND

⊙	=	0 hr.
◯	=	2 hr.
◇	=	24 hr.
△	=.	72 hr.
□	=	168 hr.
✕	=	672 hr.

SPECTRAL DIRECTIONAL REFLECTANCE

-A4-

CUSTOMER CODE NO.:

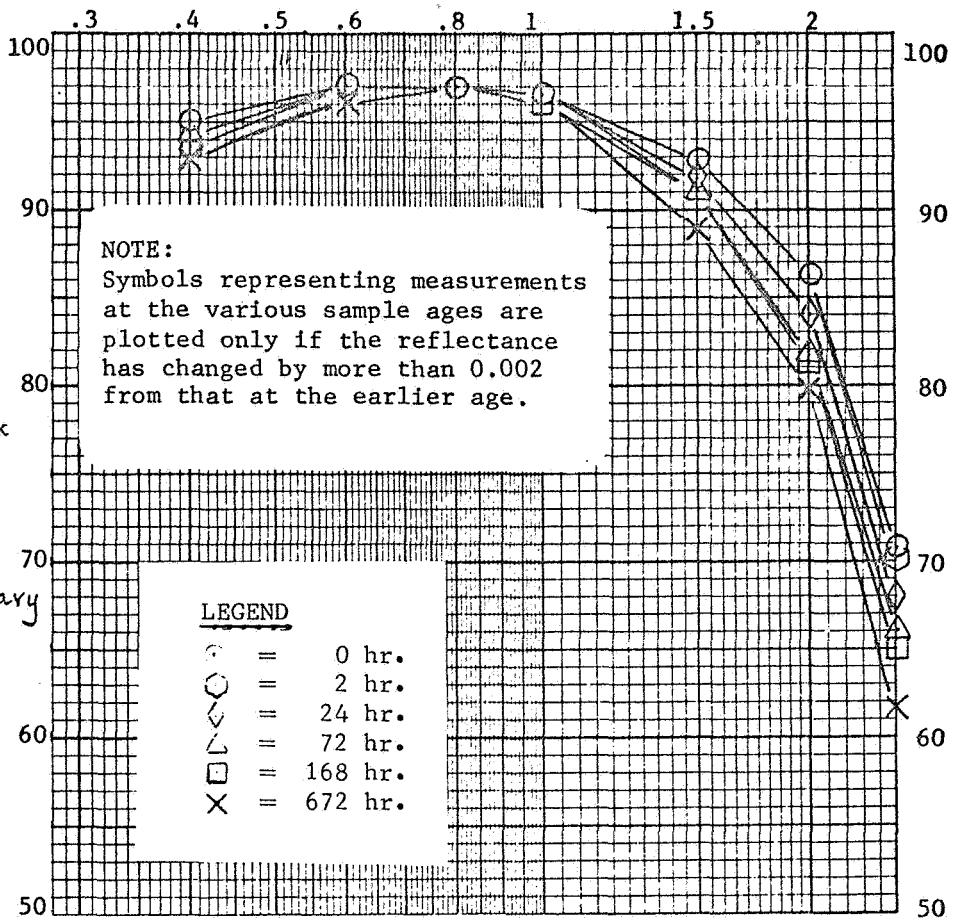TRW DESIGNATION:
     S/N 579-68

MATERIAL:
     Pressed MgO
     Powder, 3mm thick
     (432 g/cm^2)

ANGLES:

POLAR, θ = 10°

AZIMUTHAL, ϕ = Arbitrary

MEASUREMENTS

INSTRUMENTS

FIGURE A7

NOTE:
Symbols representing measurements at the various sample ages are plotted only if the reflectance has changed by more than 0.002 from that at the earlier age.

LEGEND

☉ = 0 hr.
○ = 2 hr.
◇ = 24 hr.
△ = 72 hr.
□ = 168 hr.
✕ = 672 hr.

SPECTRAL DIRECTIONAL REFLECTANCE

WAVELENGTH (MICRONS)

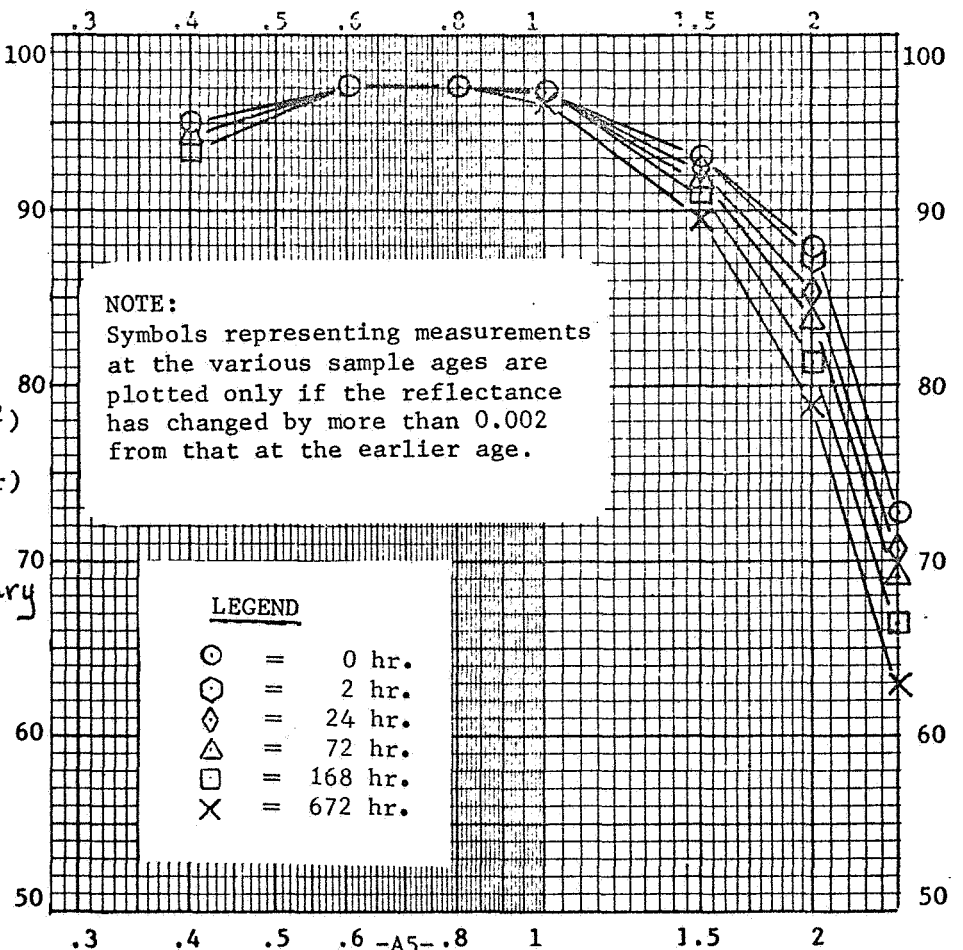CUSTOMER CODE NO.:

TRW DESIGNATION:
     S/N 580-68

MATERIAL
     Pressed MgO Powder,
     4mm thick (432 g/cm^2)
     (used powder as re-
     ceived from supplier)
ANGLES:

POLAR, θ = 10°

AZIMUTHAL, ϕ = Arbitrary

MEASUREMENT

INSTRUMENTS

FIGURE A8

NOTE:
Symbols representing measurements at the various sample ages are plotted only if the reflectance has changed by more than 0.002 from that at the earlier age.

LEGEND

☉ = 0 hr.
○ = 2 hr.
◇ = 24 hr.
△ = 72 hr.
□ = 168 hr.
✕ = 672 hr.

SPECTRAL DIRECTIONAL REFLECTANCE

WAVELENGTH (MICRONS)

-A5-

CUSTOMER CODE NO.:

TRW DESIGNATION:
   S/N 581-68

MATERIAL:
   Pressed MgO Powder,
   4mm thick (432 g/cm^2)

ANGLES:
POLAR, $\theta = 10°$
AZIMUTHAL, $\phi = $ Arbitrary

MEASUREMENTS
INSTRUMENTS

FIGURE A9

WAVELENGTH (MICRONS)

NOTE:
Stored in Dessicator in Nitrogen
atmosphere except for 1 hour
exposure to air.

LEGEND

⊙ = 0 hr.
✕ = 672 hr.

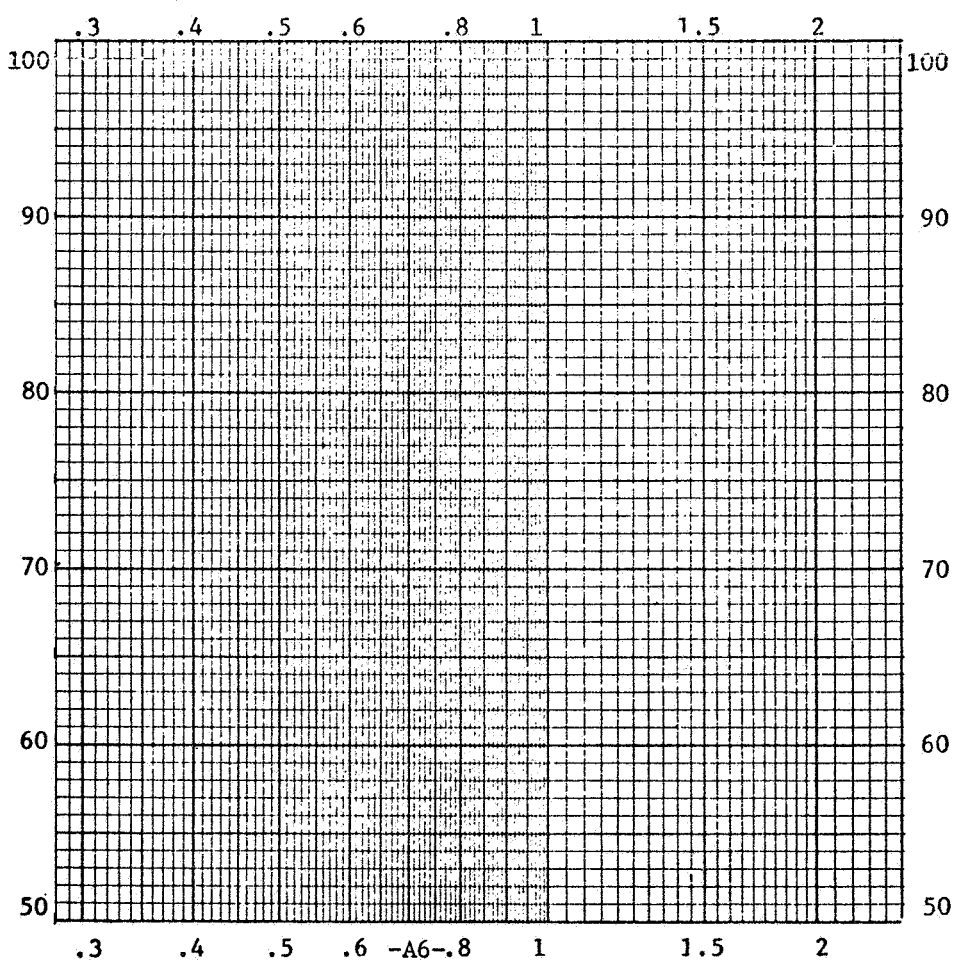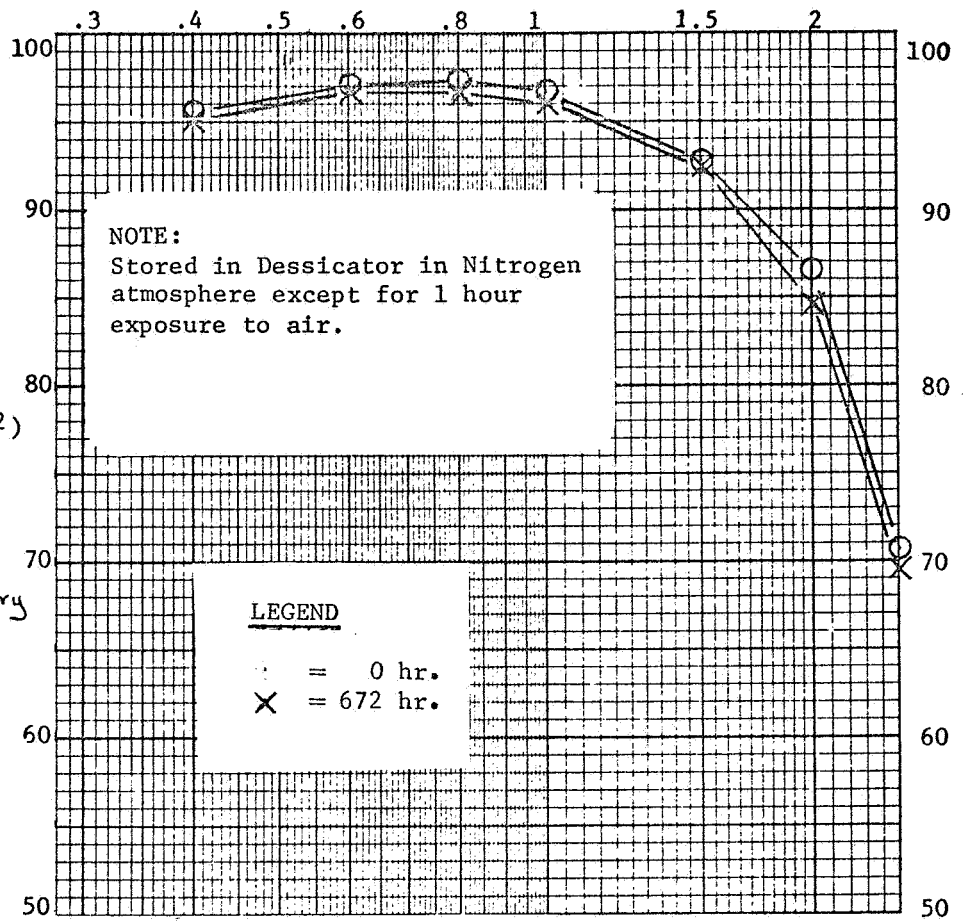SPECTRAL DIRECTIONAL REFLECTANCE

CUSTOMER CODE NO.:

TRW DESIGNATION:

MATERIAL

ANGLES:
POLAR, θ
AZIMUTHAL, ϕ

MEASUREMENT
INSTRUMENTS

FIGURE A10

WAVELENGTH (MICRONS)

SPECTRAL DIRECTIONAL REFLECTANCE

-A6-

109

TABLE A-1

TABULATION OF CORRECTED VALUES OF SPECTRAL DIRECTIONAL REFLECTANCE

Sample 570-68 – Smoked MgO – 1 mm thick – 170 hours old

Polar Angle θ	0°		10°		30°		40°		50°		75°	
Polarization Relative to Plane of Incidence	‖	⊥	‖	⊥	‖	⊥	‖	⊥	‖	⊥	‖	⊥
Wavelength (Microns)												
.40	.941	.945	.939	.942	.946	.946	.950	.950	.957	.955	.973	.972
(average)	.943		.940		.946		.950		.956		.972	
.60	.988	.991	.987	.990	.984	.981	.982	.984	.983	.983	.985	.988
(average)	.990		.988		.982		.983		.983		.986	
.80	.987	.987	.985	.985	.981	.978	.982	.983	.983	.982	.987	.988
(average)	.987		.985		.980		.982		.982		.988	
1.00	.978	.979	.976	.977	.978	.979	.975	.980	.974	.981	.979	.989
(average)	.978		.976		.978		.978		.978		.984	
1.50	.957	.953	.949	.947	.954	.953	.957	.959	.969	.963	.971	.973
(average)	.955		.948		.954		.958		.966		.972	
2.00	.912	.911	.907	.906	.913	.917	.918	.921	.924	.926	.942	.943
(average)	.912		.906		.915		.920		.925		.942	
2.50	.842	.838	.828	.827	.837	.835	.840	.843	.852	.856	.881	.879
(average)	.840		.828		.836		.842		.854		.880	

TABLE A-2

TABULATION OF CORRECTED VALUES OF SPECTRAL DIRECTIONAL REFLECTANCE

Sample 571-68 – Smoked MgO – 2 mm thick – 186 hours old

Polar Angle θ	0°		10°		30°		40°		50°		75°	
Polarization Relative to Plane of Incidence	‖	⊥	‖	⊥	‖	⊥	‖	⊥	‖	⊥	‖	⊥
Wavelength (Microns)												
.40	.944	.948	.943	.946	.952	.951	.956	.953	.961	.959	.973	.973
(average)	.946		.944		.952		.954		.960		.973	
.60	.993	.998	.988	.989	.987	.988	.988	.989	.988	.989	.988	.991
(average)	.966		.988		.988		.988		.988		.990	
.80	.988	.990	.984	.983	.987	.986	.987	.988	.990	.992	.988	.988
(average)	.989		.984		.986		.988		.991		.988	
1.00	.985	.984	.976	.984	.981	.989	.982	.989	.981	.981	.987	.983
(average)	.984		.980		.985		.983		.981		.985	
1.50	.965	.961	.955	.959	.964	.969	.968	.974	.967	.973	.977	.983
(average)	.963		.957		.966		.971		.965		.980	
2.00	.929	.931	.924	.927	.927	.937	.935	.944	.939	.946	.952	.963
(average)	.931		.926		.932		.940		.942		.958	
2.50	.870	.868	.862	.860	.867	.867	.870	.873	.883	.886	.901	.904
(average)	.869		.861		.867		.872		.884		.904	

TABLE A-3

TABULATION OF CORRECTED VALUES OF SPECTRAL DIRECTIONAL REFLECTANCE

Sample 572-68 – Electrostatically Smoked MgO – 3 mm thick
172 hours old

Polar Angle θ	0°		10°		30°		40°		50°		75°	
Polarization Relative to Plane of Incidence	‖	⊥	‖	⊥	‖	⊥	‖	⊥	‖	⊥	‖	⊥
Wavelength (Microns)												
.40	.932	.931	.931	.935	.938	.940	.937	.940	.943	.945	.963	.957
(average)	.932		.933		.939		.938		.944		.960	
.60	.977	.978	.977	.979	.978	.983	.980	.987	.978	.987	.982	.986
(average)	.978		.978		.980		.984		.984		.984	
.80	.974	.975	.974	.977	.977	.981	.980	.981	.983	.983	.983	.981
(average)	.974		.976		.978		.980		.983		.982	
1.00	.975	.976	.973	.977	.979	.981	.978	.983	.979	.985	.981	.984
(average)	.976		.975		.980		.980		.982		.982	
1.50	.962	.964	.961	.964	.967	.969	.968	.970	.969	.971	.971	.976
(average)	.963		.962		.968		.969		.970		.974	
2.00	.926	.934	.928	.933	.932	.937	.935	.940	.939	.944	.952	.958
(average)	.930		.930		.934		.938		.942		.955	
2.50	.867	.866	.866	.865	.871	.872	.874	.877	.885	.886	.901	.907
(average)	.866		.866		.872		.876		.886		.904	

TABLE A-4

TABULATION OF CORRECTED VALUES OF SPECTRAL DIRECTIONAL REFLECTANCE

Sample 576-68 – Smoked MgO – 4 mm thick – 175 hours old

Polar Angle θ	0°		10°		30°		40°		50°		75°	
Polarizarion Relative to Plane of Incidence	‖	⊥	‖	⊥	‖	⊥	‖	⊥	‖	⊥	‖	⊥
Wavelength (Microns)												
.40	.931	.937	.931	.936	.937	.939	.938	.940	.946	.948	.960	.967
(average)	.934		.934		.938		.939		.947		.961	
.60	.982	.980	.981	.980	.982	.984	.985	.985	.985	.986	.983	.987
(average)	.981		.980		.983		.985		.986		.985	
.80	.975	.979	.973	.976	.980	.981	.980	.980	.981	.980	.985	.983
(average)	.977		.974		.981		.980		.980		.984	
1.00	.975	.979	.973	.976	.976	.981	.976	.981	.981	.985	.980	.982
(average)	.977		.974		.978		.978		.983		.984	
1.50	.957	.959	.954	.960	.961	.966	.961	.972	.964	.976	.973	.983
(average)	.958		.957		.964		.966		.970		.978	
2.00	.924	.927	.918	.925	.926	.930	.931	.933	.934	.937	.944	.958
(average)	.926		.922		.928		.932		.936		.951	
2.50	.860	.856	.854	.853	.855	.858	.858	.861	.868	.874	.891	.897
(average)	.858		.854		.856		.860		.871		.894	

TABLE A5

TABULATION OF CORRECTED VALUES OF SPECTRAL DIRECTIONAL REFLECTANCE

Sample 577-68 – Smoked MgO – 2 mm thick – No Electro-static Field – 240 hours old

Polar Angle θ	0°		10°		30°		40°		50°		75°	
Polarization Relative to Plane of Incidence	∥	⊥	∥	⊥	∥	⊥	∥	⊥	∥	⊥	∥	⊥
Wavelength (Microns)												
.40	.930	.929	.932	.930	.933	.934	.937	.938	.942	.945	.965	.962
(average)	.930		.931		.934		.938		.944		.964	
.60	.979	.980	.982	.979	.986	.985	.987	.984	.988	.987	.992	.990
(average)	.980		.980		.986		.986		.988		.991	
.80	.978	.977	.976	.975	.982	.980	.980	.980	.990	.984	.990	.987
(average)	.978		.976		.981		.980		.987		.988	
1.00	.976	.981	.976	.981	.984	.989	.983	.991	.984	.990	.986	.993
(average)	.978		.978		.986		.987		.987		.990	
1.50	.960	.967	.959	.965	.965	.968	.965	.969	.973	.975	.981	.983
(average)	.964		.962		.966		.967		.974		.982	
2.00	.924	.935	.925	.932	.931	.937	.935	.943	.940	.948	.956	.963
(average)	.930		.928		.934		.939		.944		.960	
2.50	.857	.856	.855	.855	.857	.861	.860	.863	.874	.871	.896	.902
(average)	.856		.855		.859		.862		.872		.899	

TABLE A6

TABULATION OF CORRECTED VALUES OF SPECTRAL DIRECTIONAL REFLECTANCE

Sample 579-68 – Pressed MgO Powder – 3 mm thick 174 hours old

Polar Angle θ	0°		10°		30°		40°		50°		75°	
Polarization Relative to Plane of Incidence	∥	⊥	∥	⊥	∥	⊥	∥	⊥	∥	⊥	∥	⊥
Wavelength (Microns)												
.40	.919	.923	.919	.924	.926	.931	.928	.933	.939	.939	.958	.959
(average)	.921		.922		.928		.930		.939		.958	
.60	.974	.975	.975	.975	.977	.978	.977	.978	.080	.979	.977	.981
(average)	.974		.975		.978		.978		.979		.979	
.80	.971	.971	.969	.970	.976	.976	.974	.978	.978	.982	.980	.984
(average)	.971		.970		.976		.976		.980		.982	
1.00	.907	.971	.970	.969	.974	.976	.975	.976	.975	.978	.978	.983
(average)	.970		.970		.975		.976		.976		.980	
1.50	.916	.916	.915	.914	.921	.922	.925	.926	.930	.930	.946	.946
(average)	.916		.914		.922		.926		.930		.946	
2.00	.828	.832	.829	.833	.835	.840	.842	.847	.849	.855	.877	.882
(average)	.830		.831		.838		.844		.852		.880	
2.50	.659	.666	.657	.663	.672	.671	.681	.684	.700	.703	.748	.755
(average)	.662		.660		.672		.682		.702		.752	

TABLE A7

TABULATION OF CORRECTED VALUES OF SPECTRAL DIRECTIONAL REFLECTANCE

Sample 580-70 – Pressed MgO Powder – 4mm thick – 171 hours old

Polar Angle θ	0°		10°		30°		40°		50°		75°	
Polarization Relative to Plane of Incidence	∥	⊥	∥	⊥	∥	⊥	∥	⊥	∥	⊥	∥	⊥
Wavelength (Microns)												
.40	.930	.931	.929	.932	.930	.937	.933	.935	.941	.945	.955	.957
(average)	.930		.930		.934		.934		.943		.956	
.60	.984	.983	.980	.982	.982	.985	.983	.986	.983	.985	.982	.986
(average)	.984		.981		.984		.984		.984		.984	
.80	.991	.985	.984	.982	.984	.990	.984	.988	.984	.985	.988	.986
(average)	.988		.983		.987		.986		.984		.987	
1.00	.975	.982	.974	.980	.978	.988	.975	.986	.984	.988	.986	.989
(average)	.978		.977		.983		.980		.986		.988	
1.50	.922	.923	.919	.921	.926	.928	.932	.934	.937	.936	.951	.953
(average)	.922		.920		.927		.933		.936		.952	
2.00	.826	.827	.821	.831	.837	.843	.845	.852	.855	.860	.882	.888
(average)	.826		.826		.840		.848		.858		.885	
2.50	.676	.679	.669	.676	.689	.692	.696	.699	.714	.725	.757	.773
(average)	.678		.672		.690		.698		.720		.765	

113

CUSTOMER CODE NO.:

TRW DESIGNATION:

S/N 570-68

MATERIAL:
Smoked MgO, 1mm thick
Electrostatic field
used ∼ 170 hours old

ANGLES:

POLAR, θ

AZIMUTHAL, φ

MEASUREMENTS

INSTRUMENTS

FIGURE A10

WAVELENGTH (MICRONS)

SPECTRAL DIRECTIONAL REFLECTANCE

- Polar Angle, ⊖, = 0°
- Polar Angle, ⊗, = 40°
- Polar Angle, ⊖, = 75°

CUSTOMER CODE NO.:

TRW DESIGNATION:
S/N 571-68

MATERIAL
Smoked MgO, 2mm thick
Electrostatic field
used, ∼186 hours old

ANGLES:

POLAR, θ

AZIMUTHAL, φ

MEASUREMENT

INSTRUMENTS

FIGURE A11

WAVELENGTH (MICRONS)
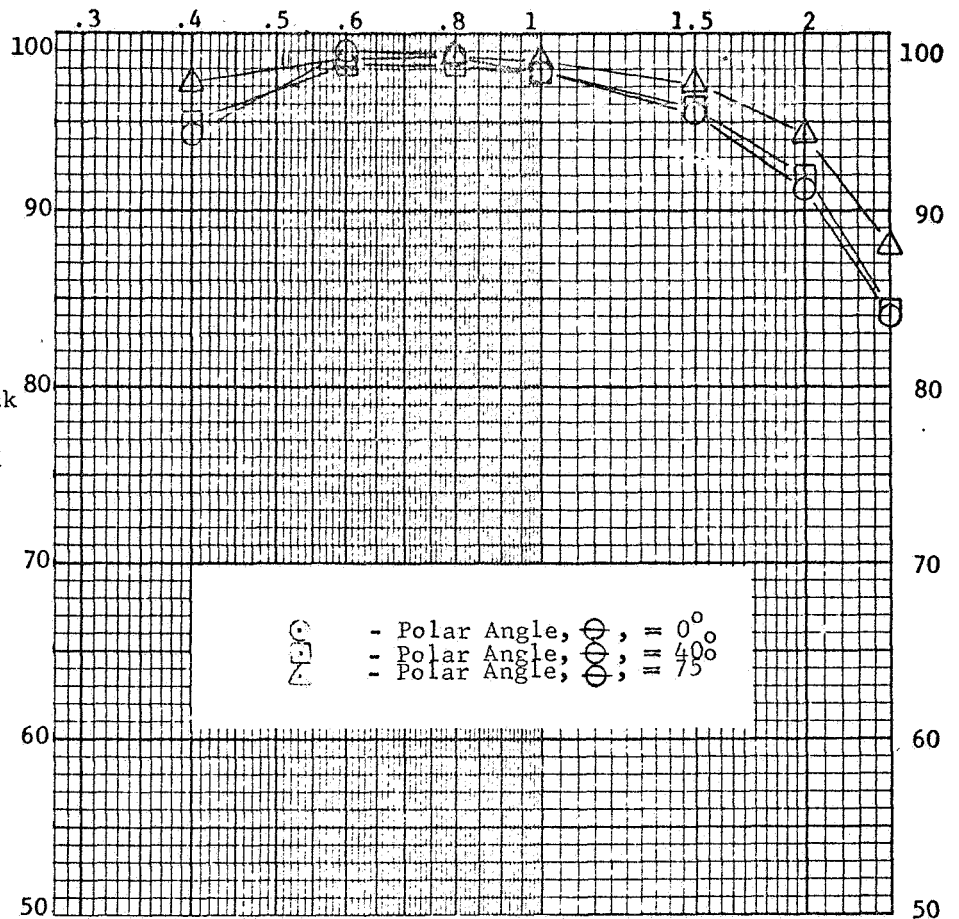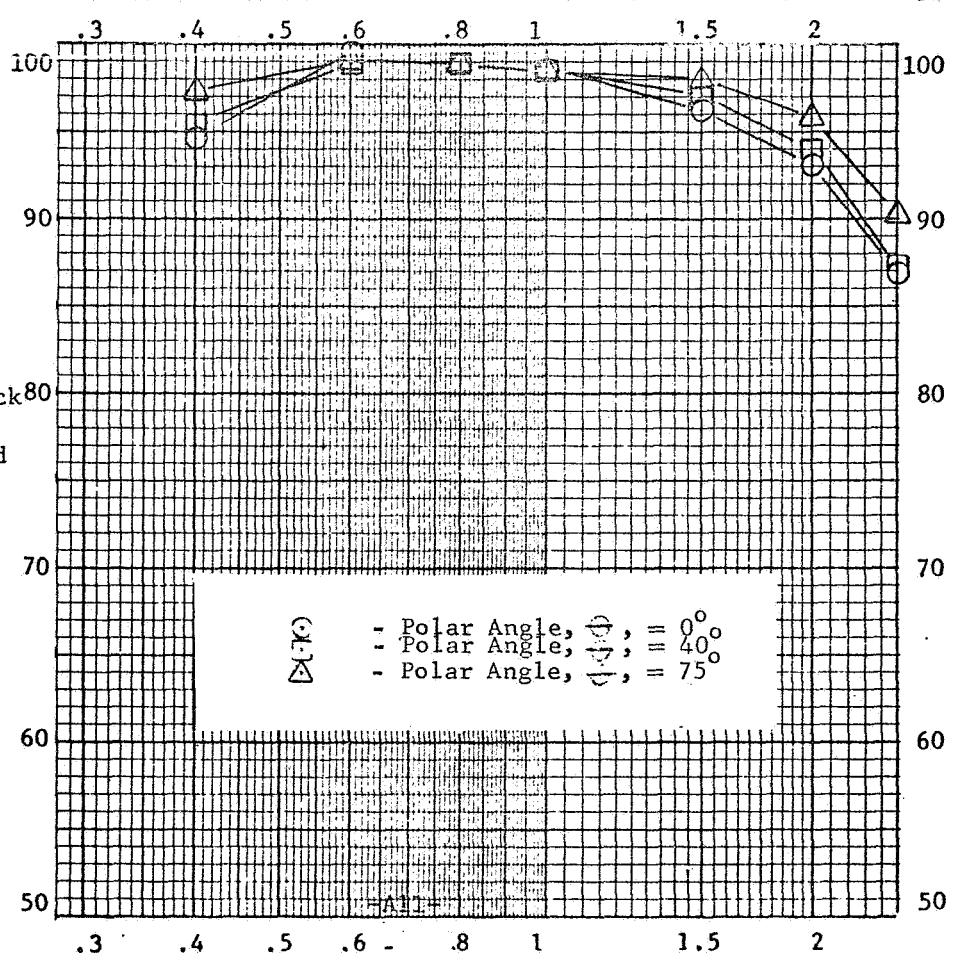
SPECTRAL DIRECTIONAL REFLECTANCE

- Polar Angle, ⊖, = 0°
- Polar Angle, ⊖, = 40°
- Polar Angle, ⊖, = 75°

114

CUSTOMER CODE NO.:

TRW DESIGNATION:
  S/N 572-68

MATERIAL:
  Smoked MgO, 3mm thick
  Electrostatically
  Applied, ~ 172 hours old

ANGLES:

POLAR, θ

AZIMUTHAL, φ

MEASUREMENTS

INSTRUMENTS

    ⊙ - Polar Angle, ⟵, = 0°
    ⊡ - Polar Angle, ⟵, = 40°
    △ - Polar Angle, ⟵, = 75°

FIGURE A12

WAVELENGTH (MICRONS)

SPECTRAL DIRECTIONAL REFLECTANCE

CUSTOMER CODE NO.:

TRW DESIGNATION:
  S/N 576-68

MATERIAL
  Smoked MgO, 4mm thick
  Electrostatic field
  used, ~ 175 hours old

ANGLES:

POLAR, θ

AZIMUTHAL, φ

MEASUREMENT

INSTRUMENTS

FIGURE A13
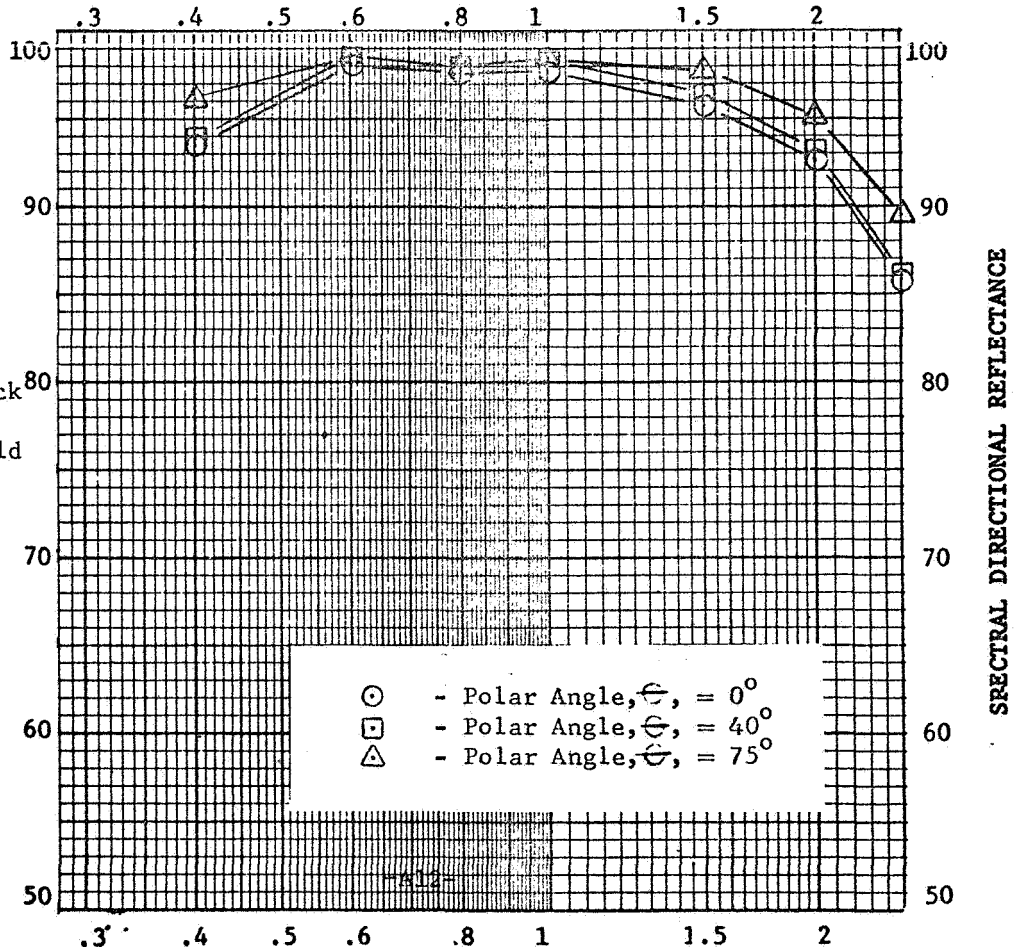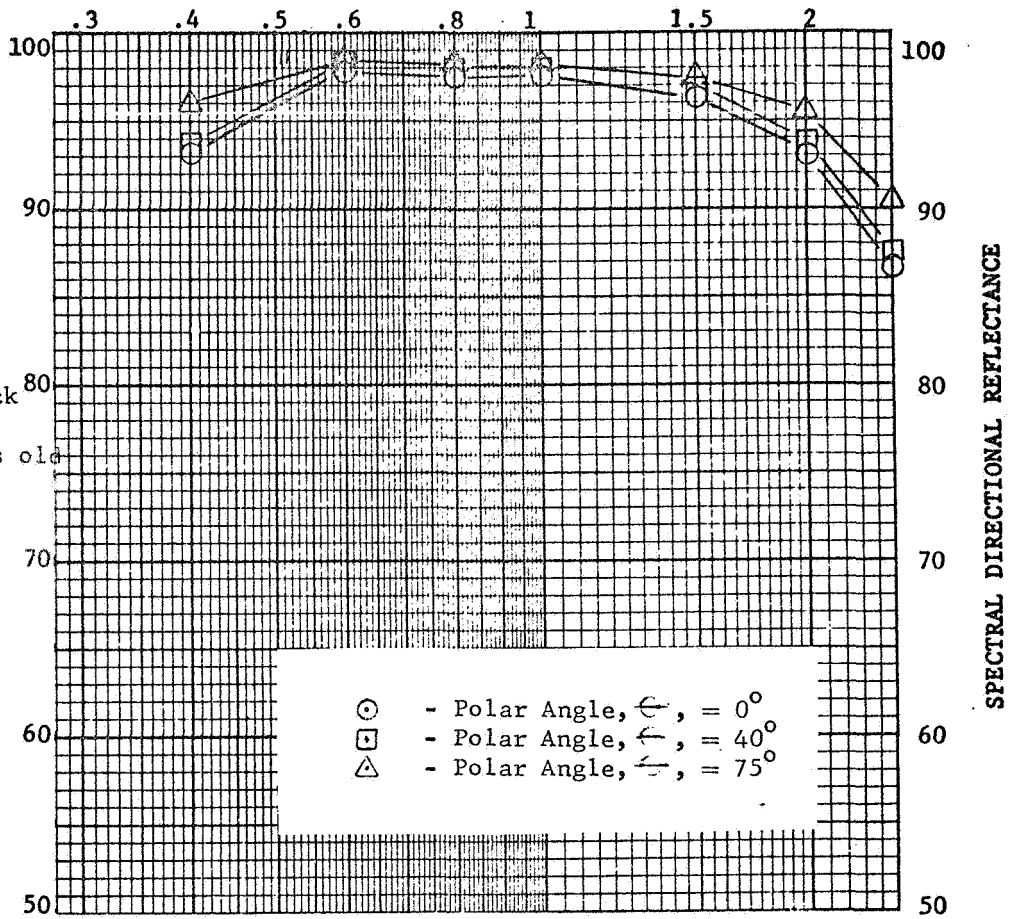
    ⊙ - Polar Angle, ⟵, = 0°
    ⊡ - Polar Angle, ⟵, = 40°
    △ - Polar Angle, ⟵, = 75°

WAVELENGTH (MICRONS)

SPECTRAL DIRECTIONAL REFLECTANCE

CUSTOMER CODE NO.:

TRW DESIGNATION:
S/N 577-68

MATERIAL:
Smoked MgO, 2 mm thick
No electrostatic field,
$\sim$ 240 hours old

ANGLES:

POLAR, θ

AZIMUTHAL, ϕ

MEASUREMENTS

INSTRUMENTS

FIGURE A14

WAVELENGTH (MICRONS)

SPECTRAL DIRECTIONAL REFLECTANCE

○ — Polar Angle, θ, = 0°
□ — Polar Angle, θ, = 40°
△ — Polar Angle, θ, = 75°

CUSTOMER CODE NO.:

TRW DESIGNATION:
S/N 579-68

MATERIAL
Pressed MgO Powder,
3 mm thick, $\sim$ 174
hours old

ANGLES:

POLAR, θ

AZIMUTHAL, ϕ

MEASUREMENT

INSTRUMENTS

FIGURE A15

WAVELENGTH (MICRONS)
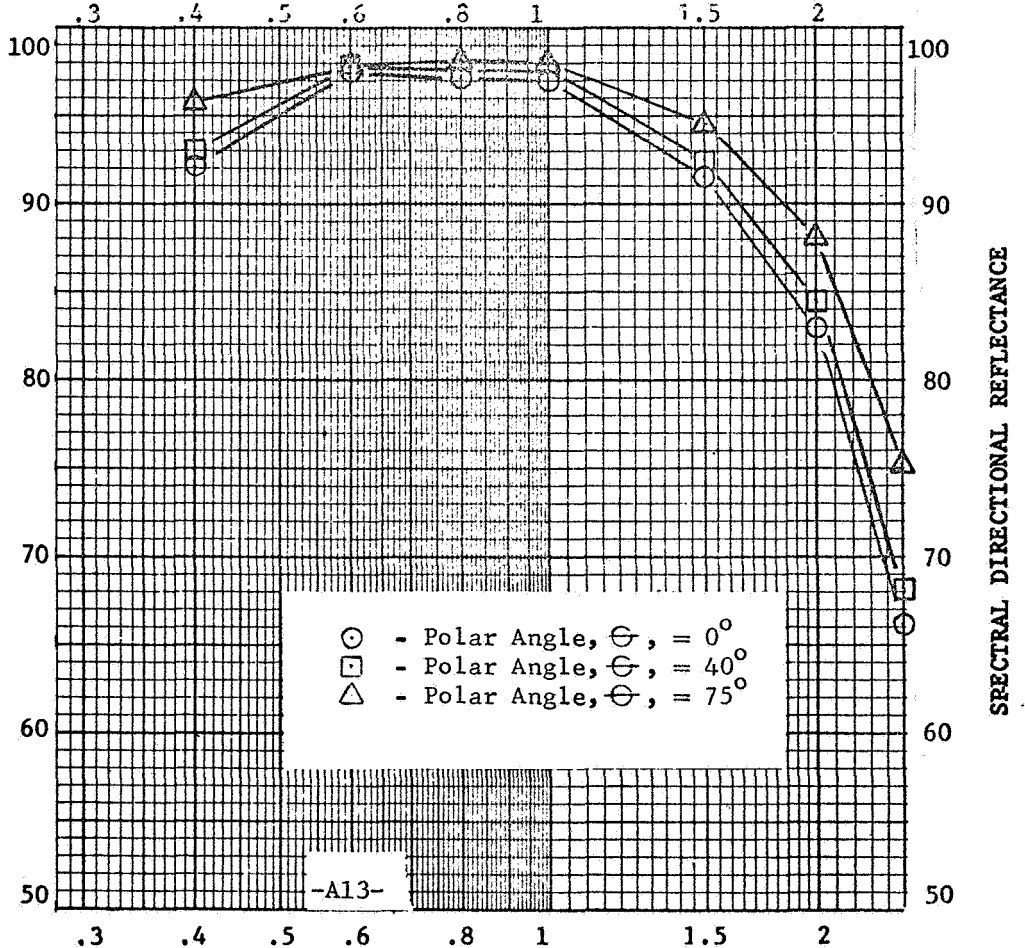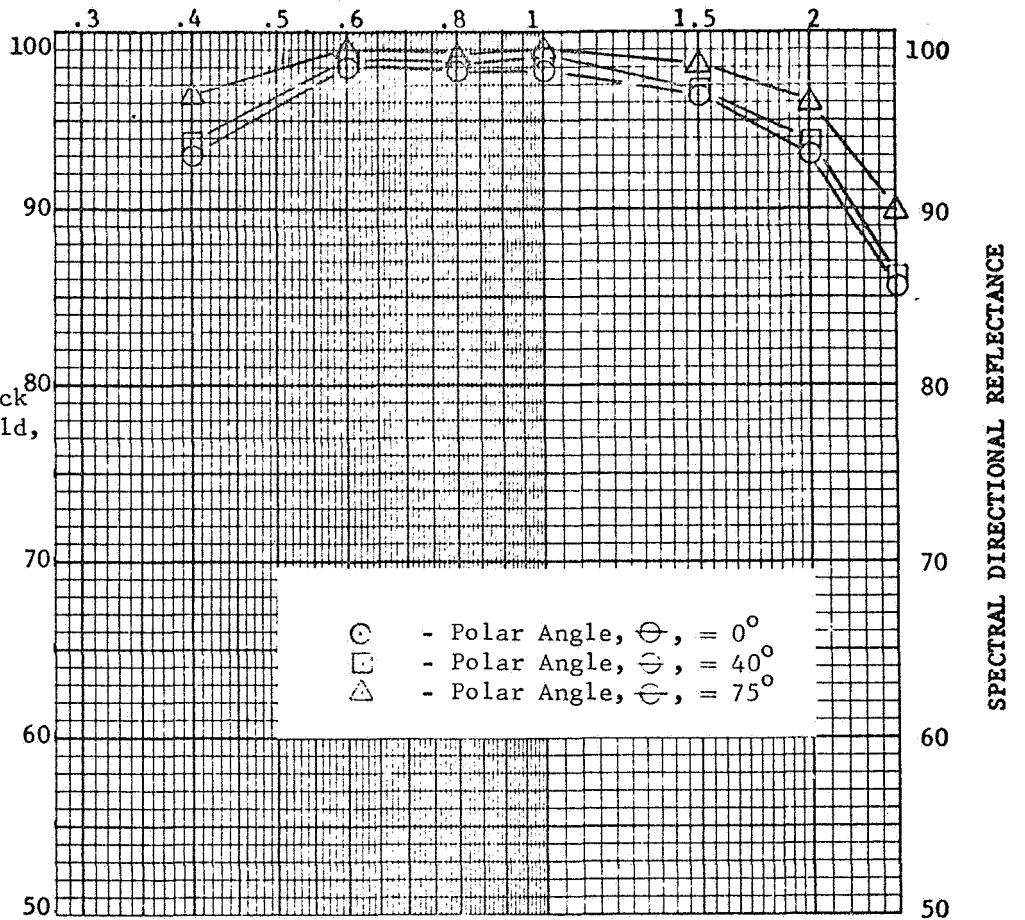
SPECTRAL DIRECTIONAL REFLECTANCE

⊙ — Polar Angle, θ, = 0°
□ — Polar Angle, θ, = 40°
△ — Polar Angle, θ, = 75°

CUSTOMER CODE NO.:

'TRW DESIGNATION:
  S/N 580-68

MATERIAL:
  Pressed MgO Powder,
  4 mm thick, ~ 171
  hours old.

ANGLES:

POLAR, θ

AZIMUTHAL, φ

MEASUREMENTS

INSTRUMENTS

  FIGURE A16
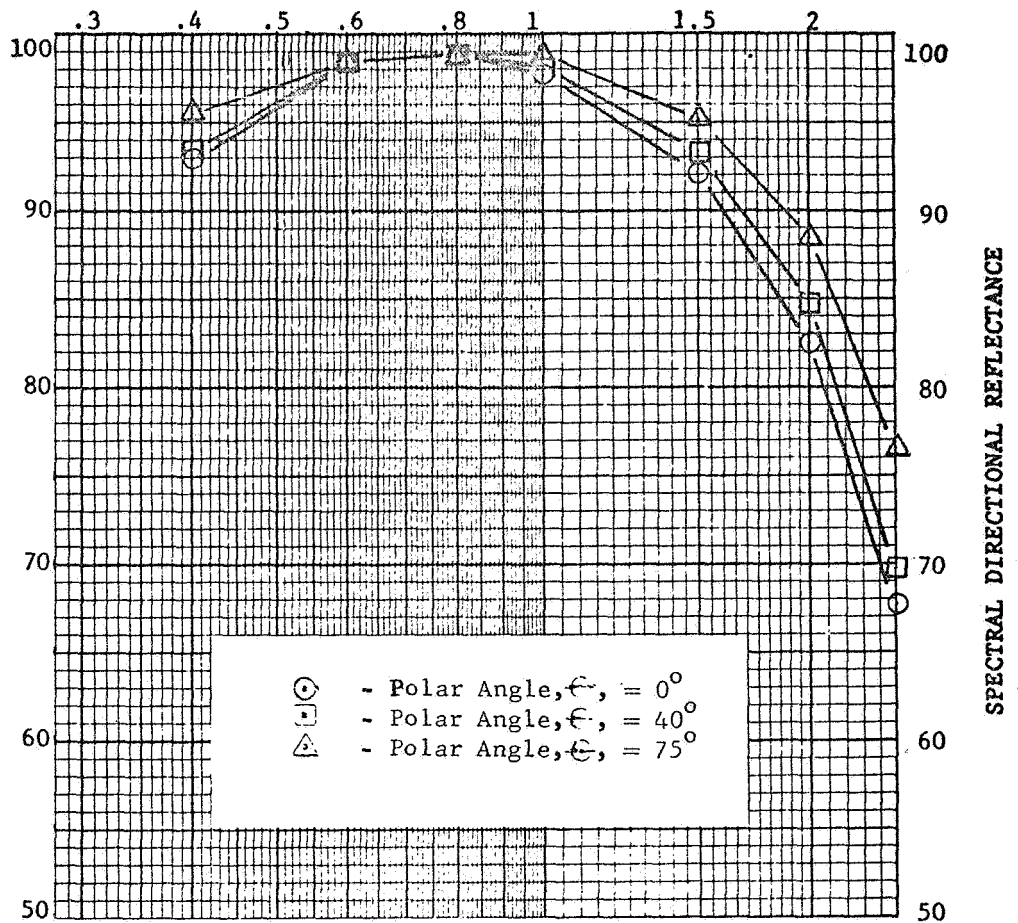
WAVELENGTH (MICRONS)

⊙ - Polar Angle, θ, = 0°
▣ - Polar Angle, θ, = 40°
△ - Polar Angle, θ, = 75°

SPECTRAL DIRECTIONAL REFLECTANCE

CUSTOMER CODE NO.:

TRW DESIGNATION:

MATERIAL

ANGLES:

POLAR, θ

AZIMUTHAL, φ

MEASUREMENT

INSTRUMENTS

  FIGURE A17

WAVELENGTH (MICRONS)

SPECTRAL DIRECTIONAL REFLECTANCE

-A14-
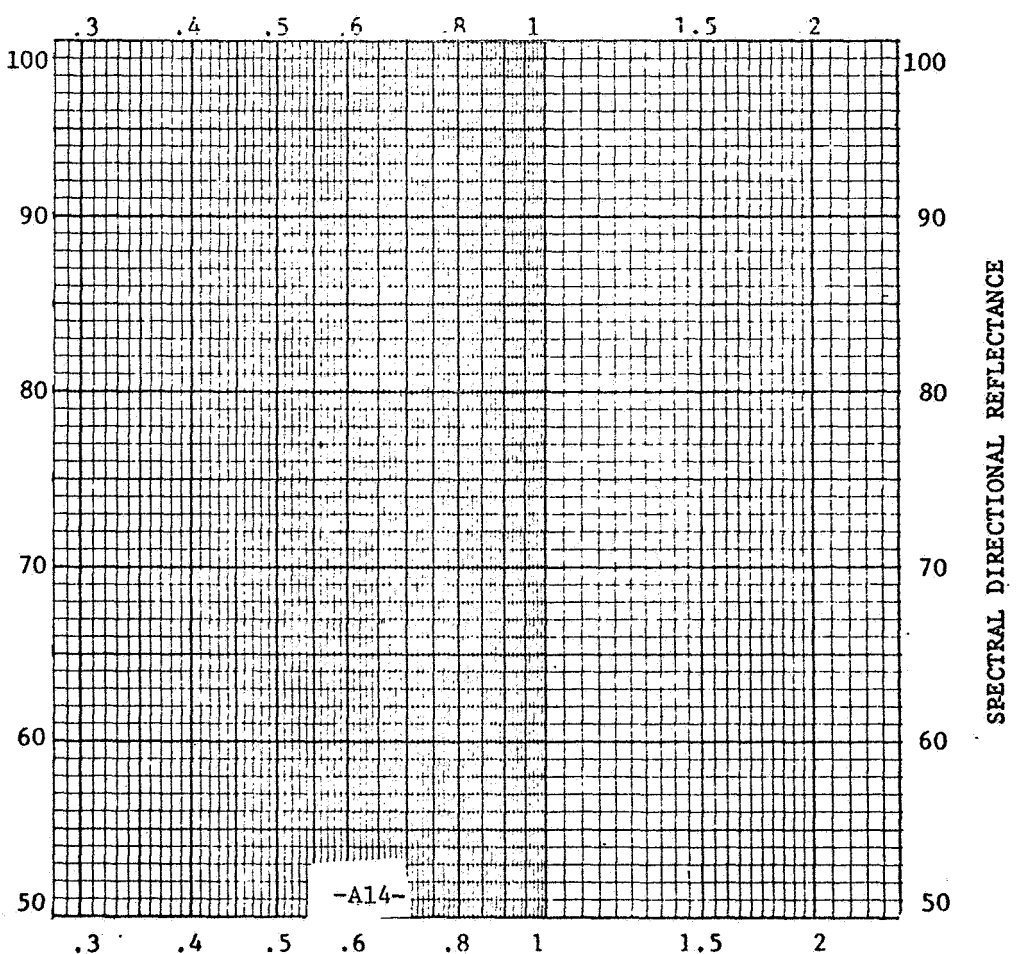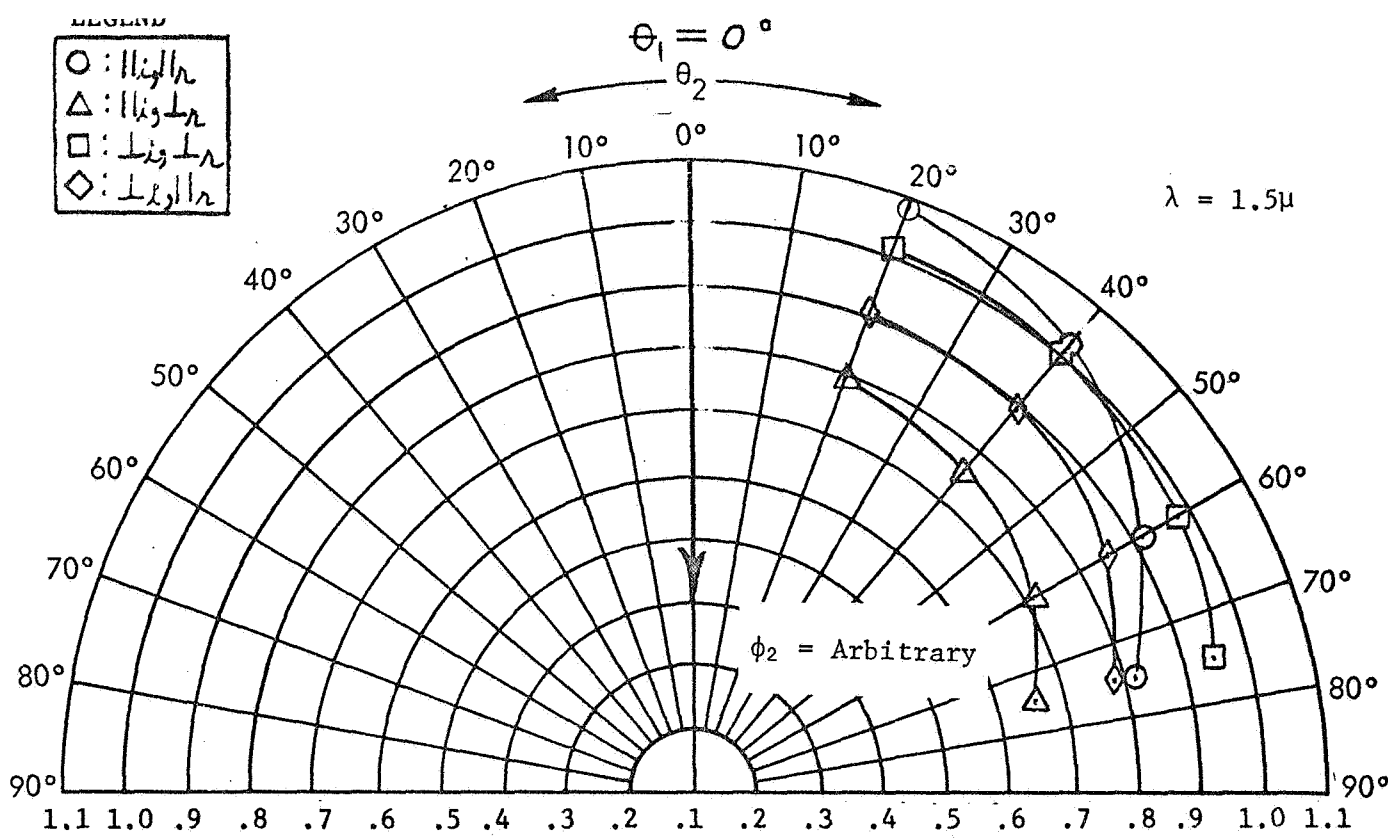
FIGURE A17   RELATIVE BIDIRECTIONAL REFLECTANCE OF MgO SMOKE, ELECTROSTATICALLY DEPOSITED, 3mm THICK, SAMPLE 572-68
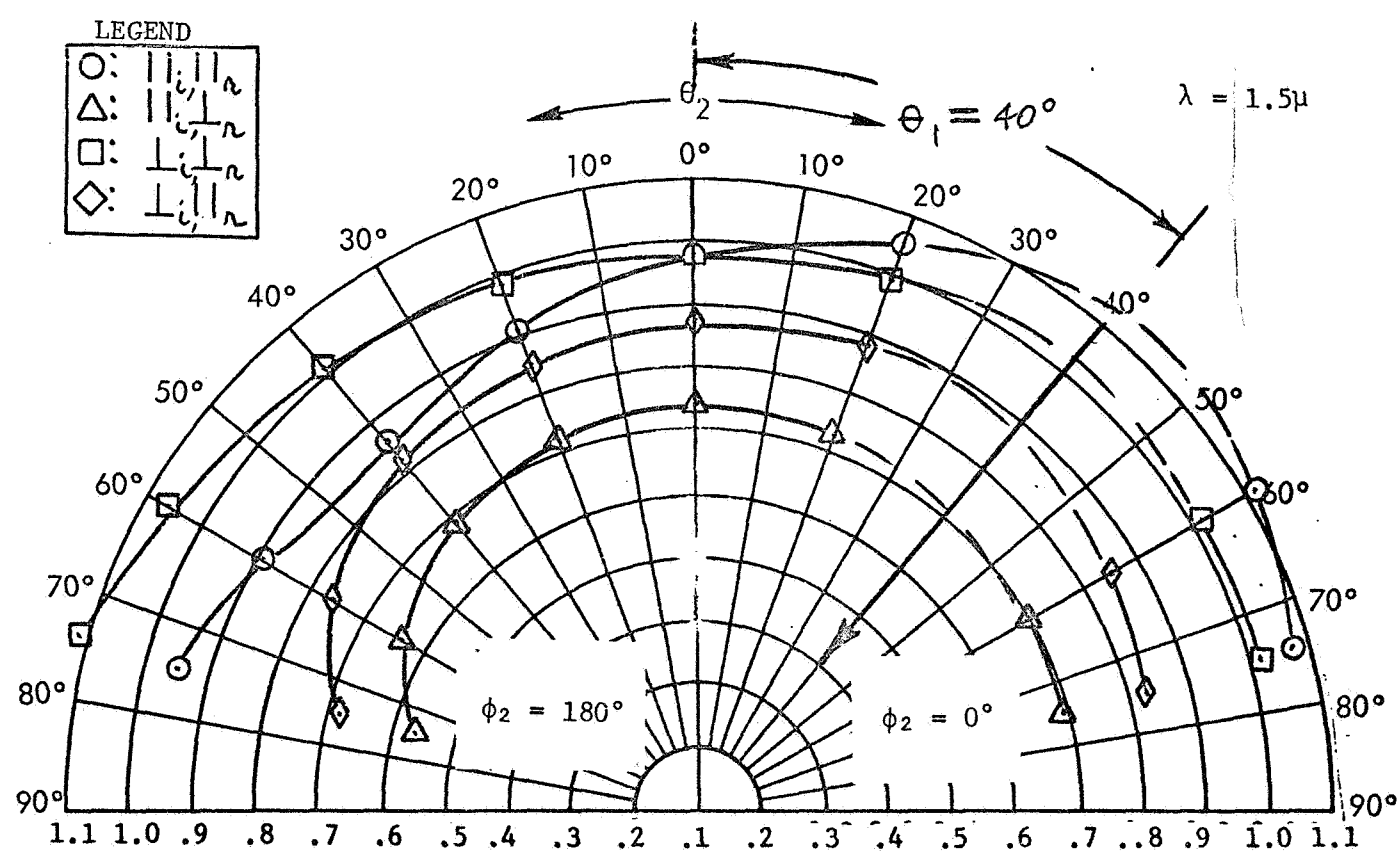
FIGURE A18   RELATIVE BIDIRECTIONAL REFLECTANCE OF MgO SMOKE, ELECTROSTATICALLY DEPOSITED, 3mm THICK, SAMPLE 572-68
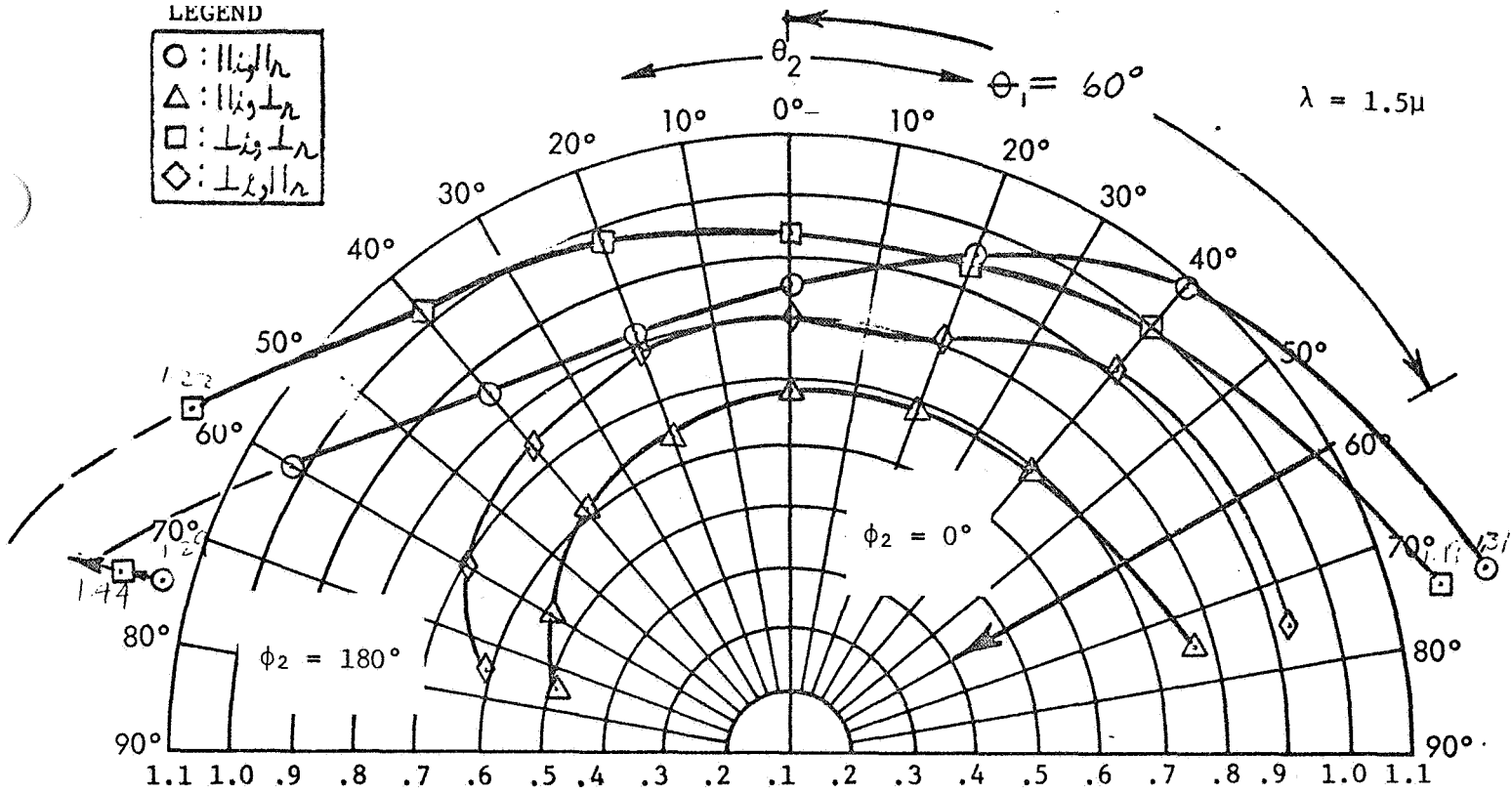
FIGURE A19   RELATIVE BIDIRECTIONAL REFLECTANCE OF MgO SMOKE, ELECTROSTATICALLY
DEPOSITED, 3mm THICK, SAMPLE 572-68
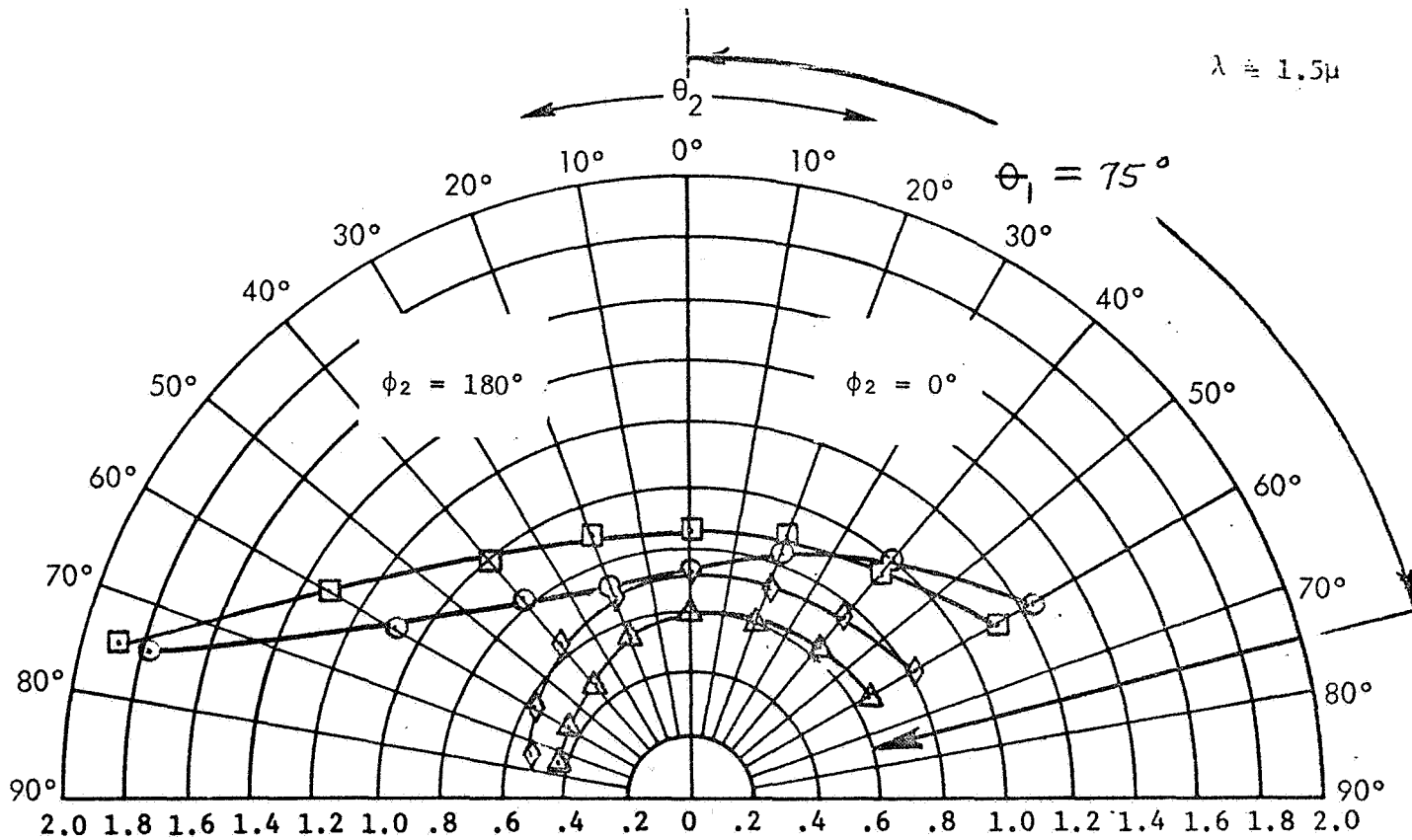
FIGURE A20   RELATIVE BIDIRECTIONAL REFLECTANCE OF MgO SMOKE, ELECTROSTATICALLY
DEPOSITED, 3mm THICK, SAMPLE 572-68
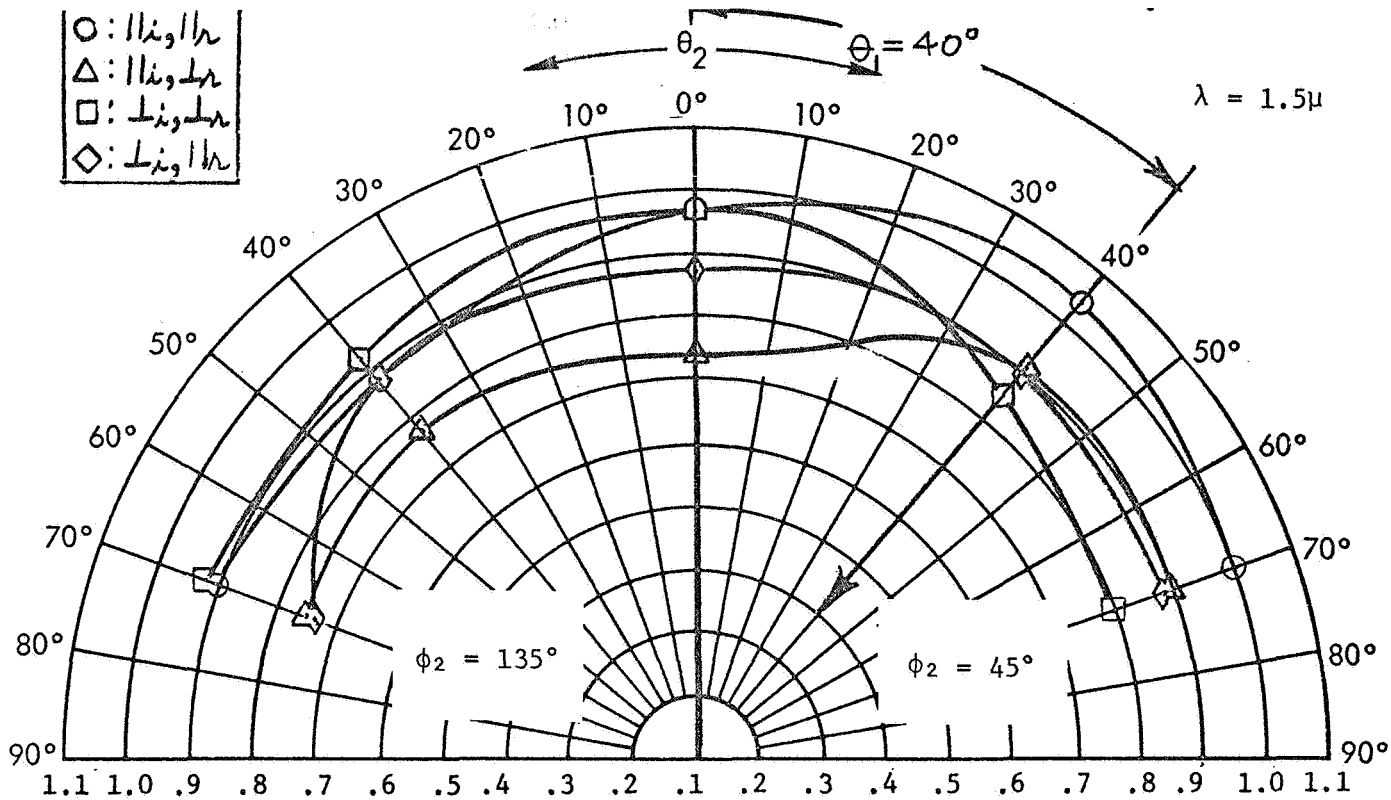
FIGURE A21   RELATIVE BIDIRECTIONAL REFLECTANCE OF MgO SMOKE, ELECTROSTATICALLY
DEPOSITED, 3mm THICK, SAMPLE 572-68
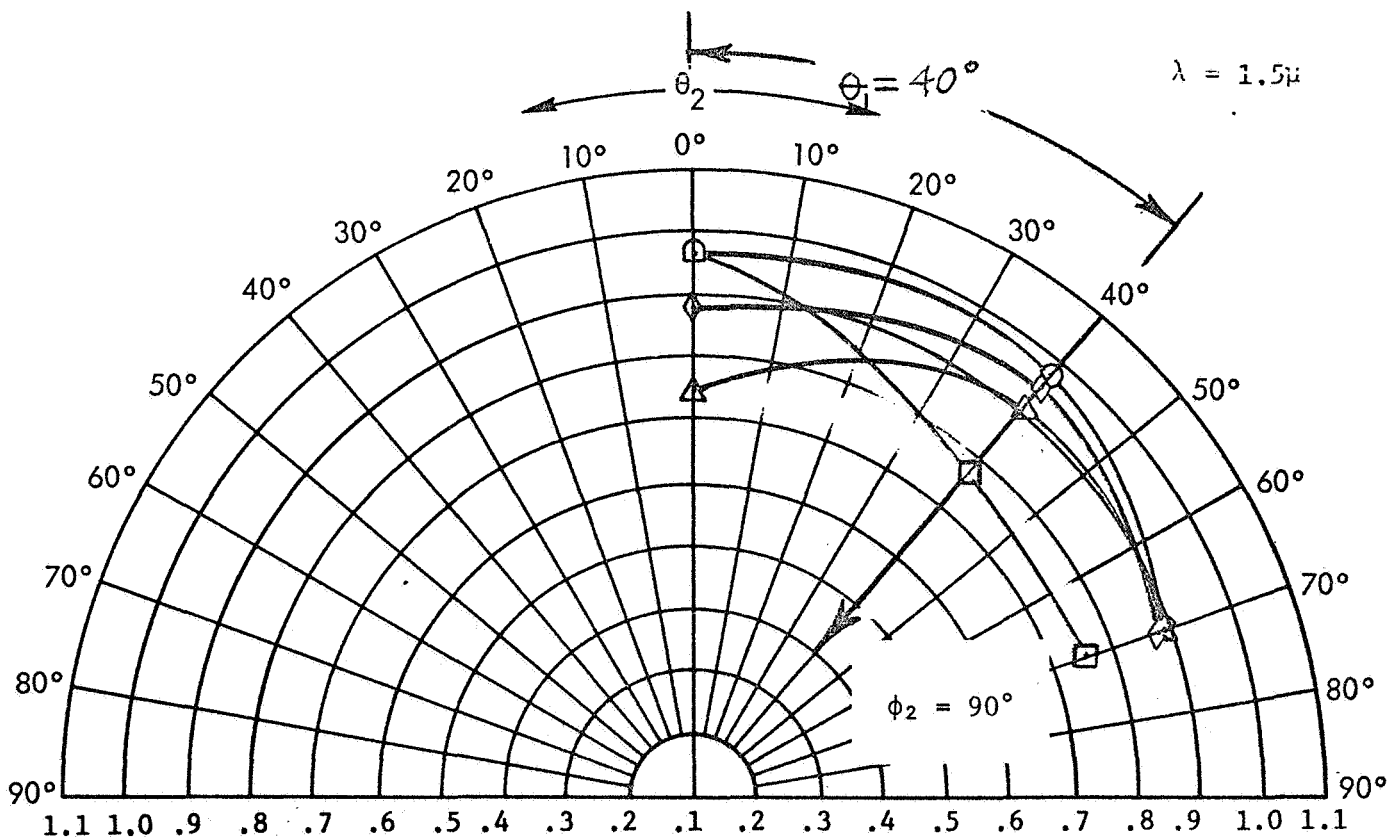
FIGURE A22:   RELATIVE BIDIRECTIONAL REFLECTANCE OF MgO SMOKE, ELECTROSTATICALLY
DEPOSITED, 3mm THICK, SAMPLE 572-68
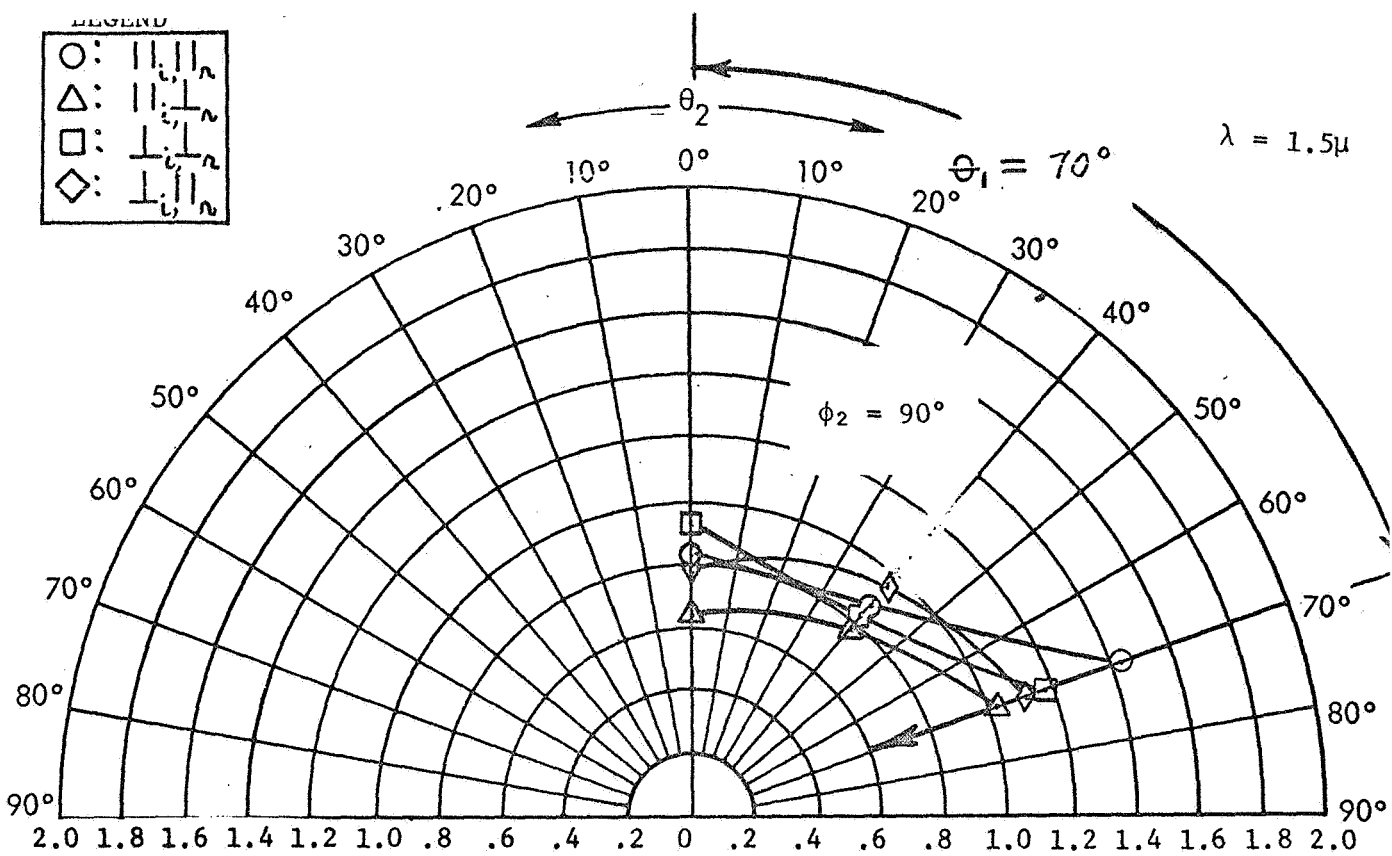
FIGURE A23: RELATIVE BIDIRECTIONAL REFLECTANCE OF MgO SMOKE, ELECTROSTATICALLY DEPOSITED, 3mm THICK, SAMPLE 572-68
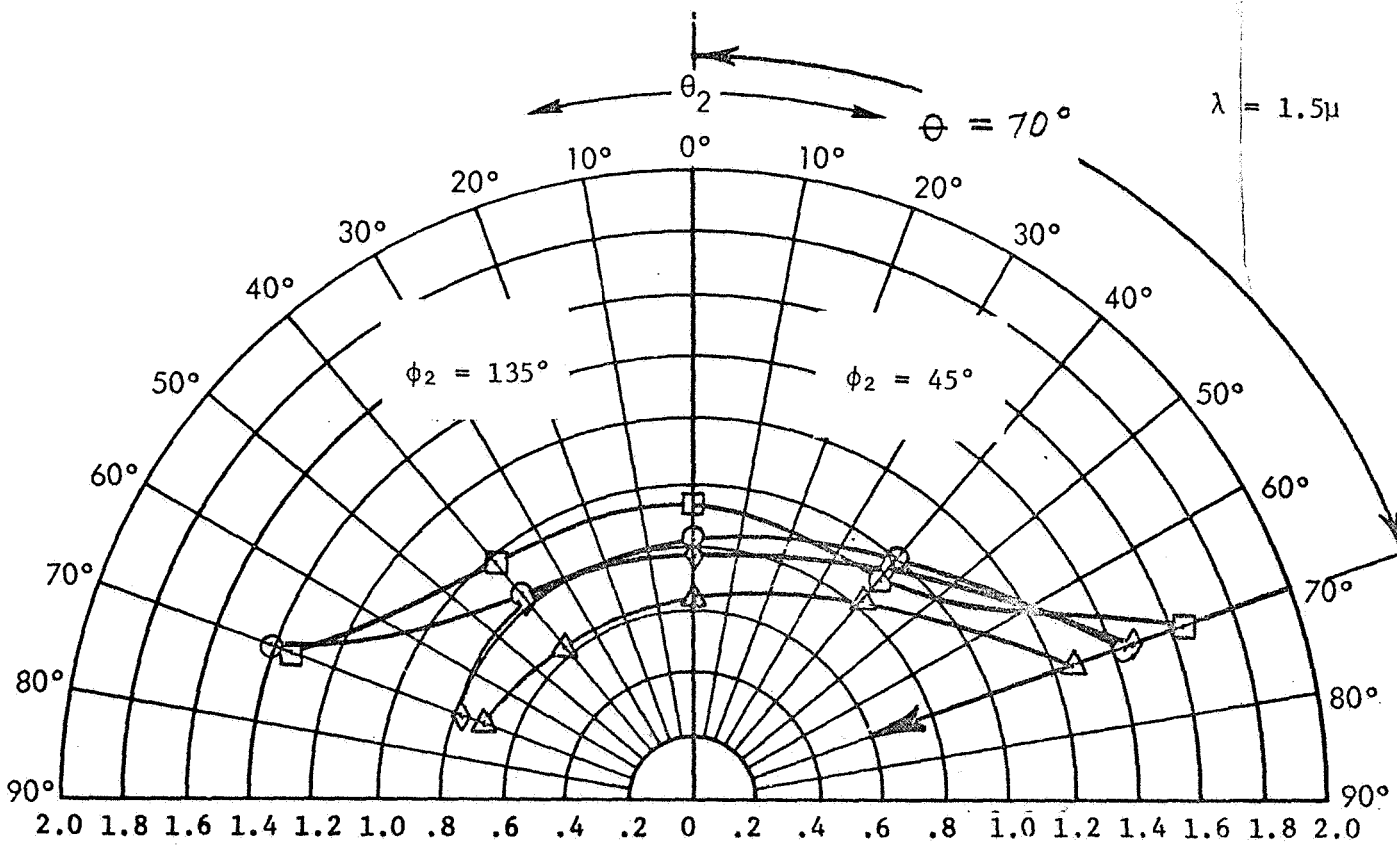
FIGURE A24: RELATIVE BIDIRECTIONAL REFLECTANCE OF MgO SMOKE, ELECTROSTATICALLY DEPOSITED, 3mm THICK, SAMPLE 572-68
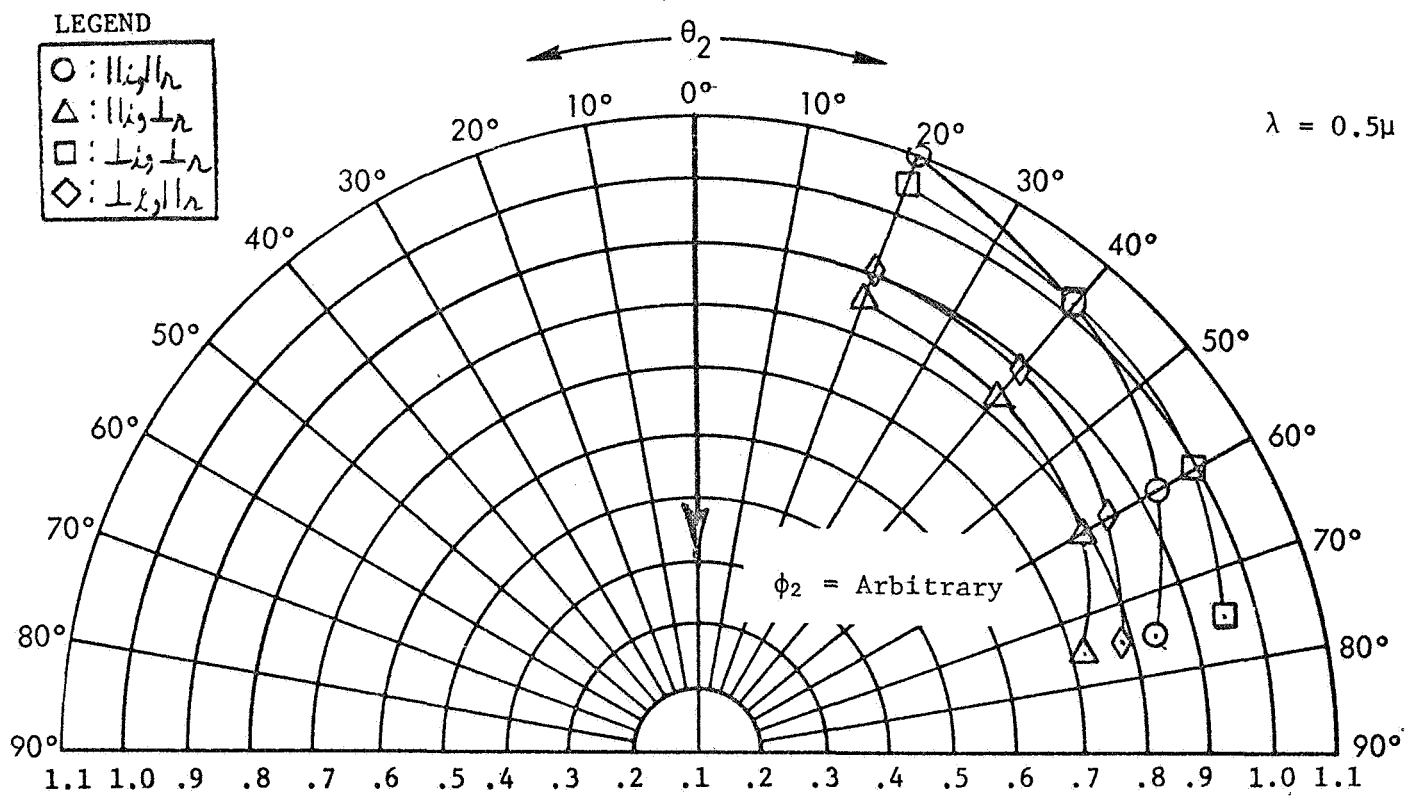
FIGURE A25: RELATIVE BIDIRECTIONAL REFLECTANCE OF MgO PRESSED POWDER, 4mm THICK, SAMPLE 580-68
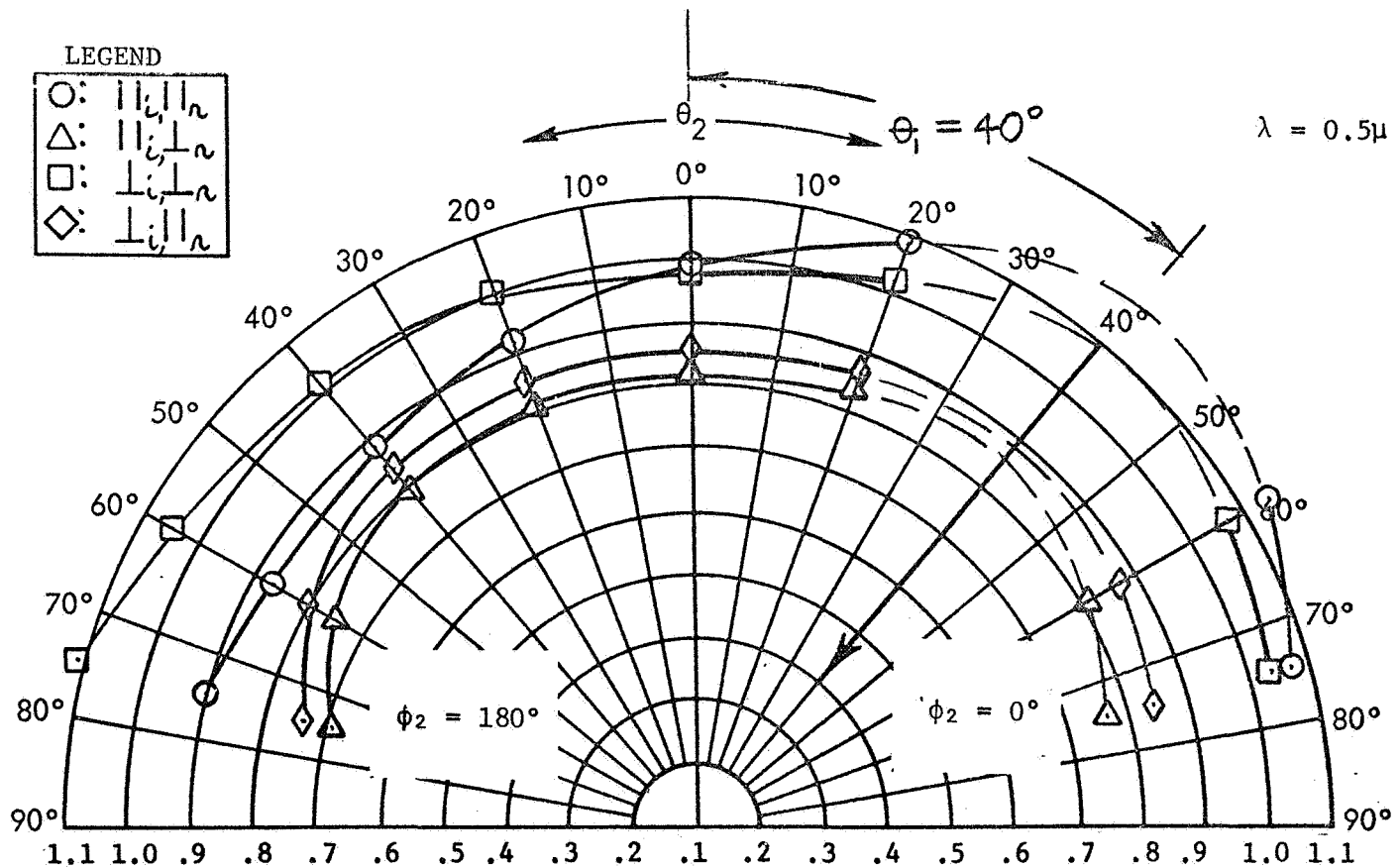
FIGURE A26: RELATIVE BIDIRECTIONAL REFLECTANCE OF MgO PRESSED POWDER, 4mm THICK, SAMPLE 580-68
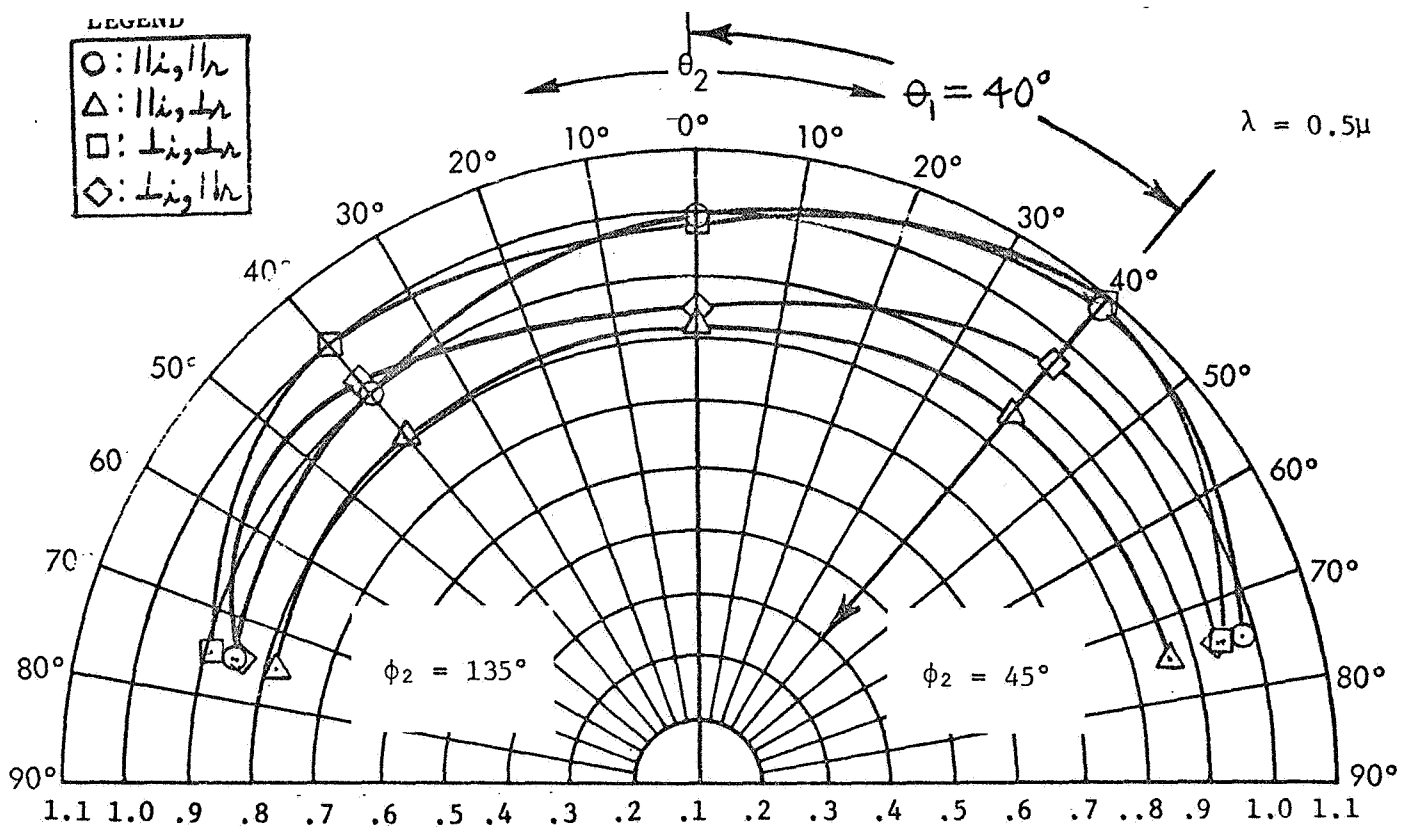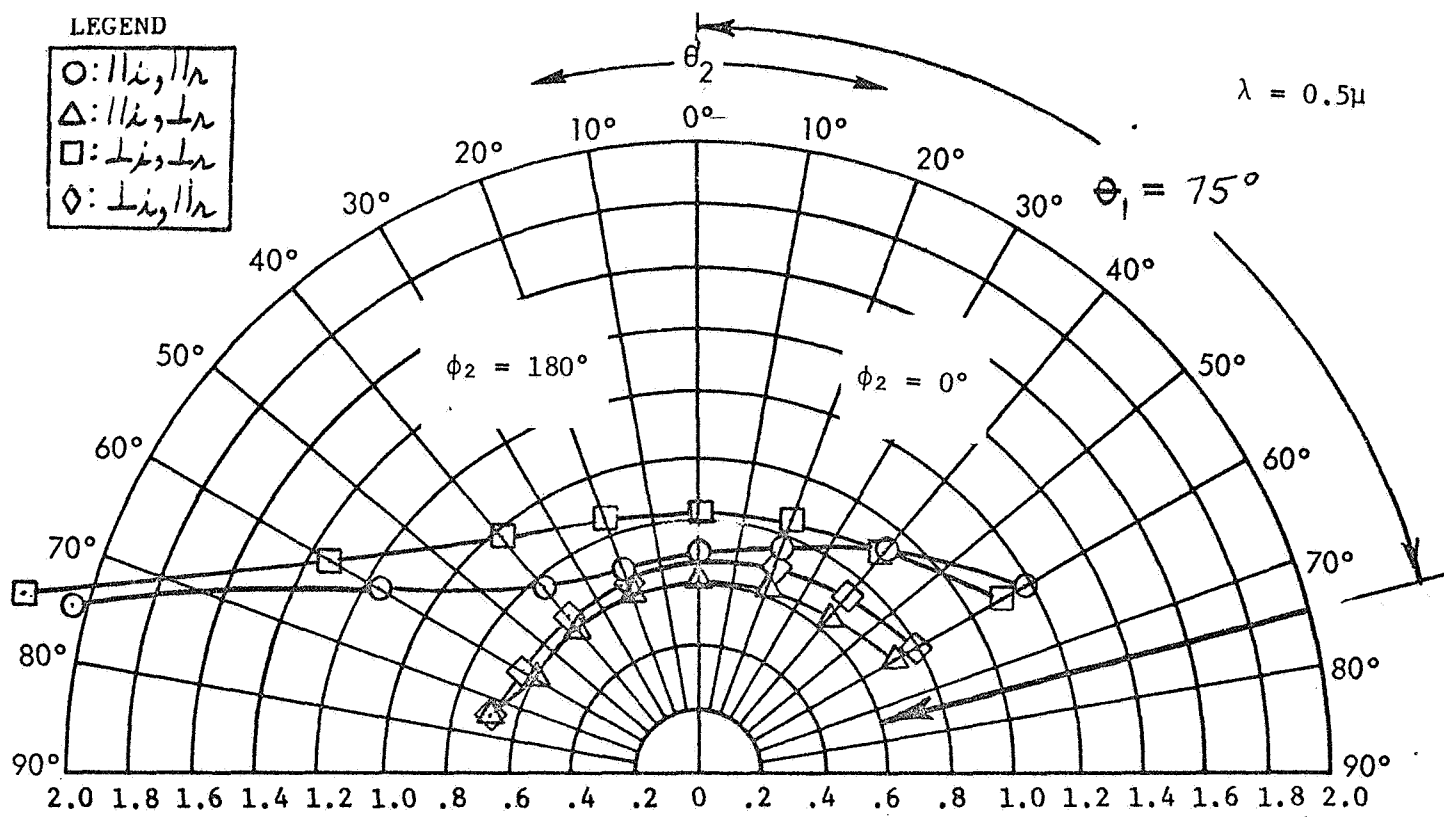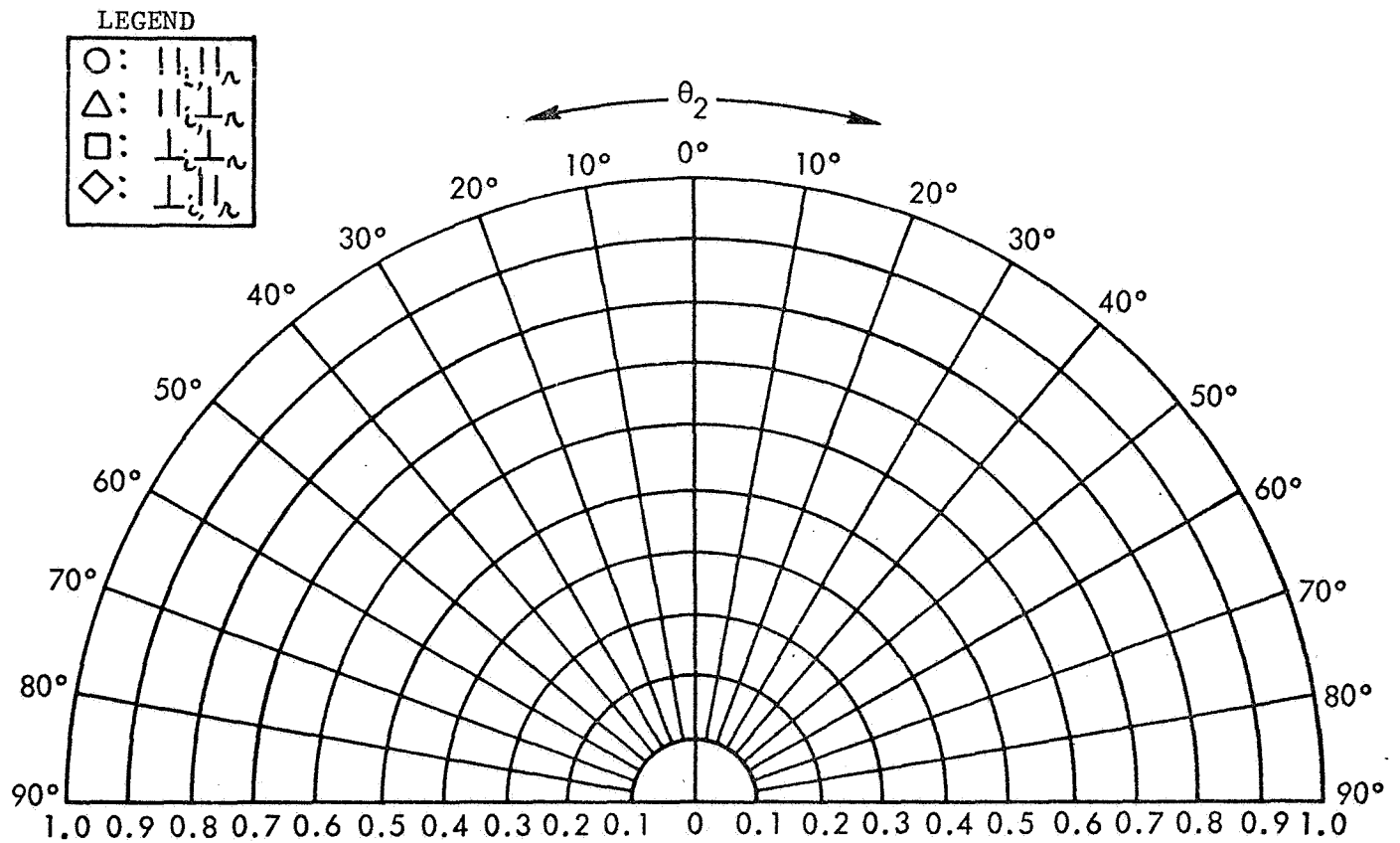
FIGURE A27: RELATIVE BIDIRECTIONAL REFLECTANCE OF MgO PRESSED POWDER, 4mm THICK, SAMPLE 580-68
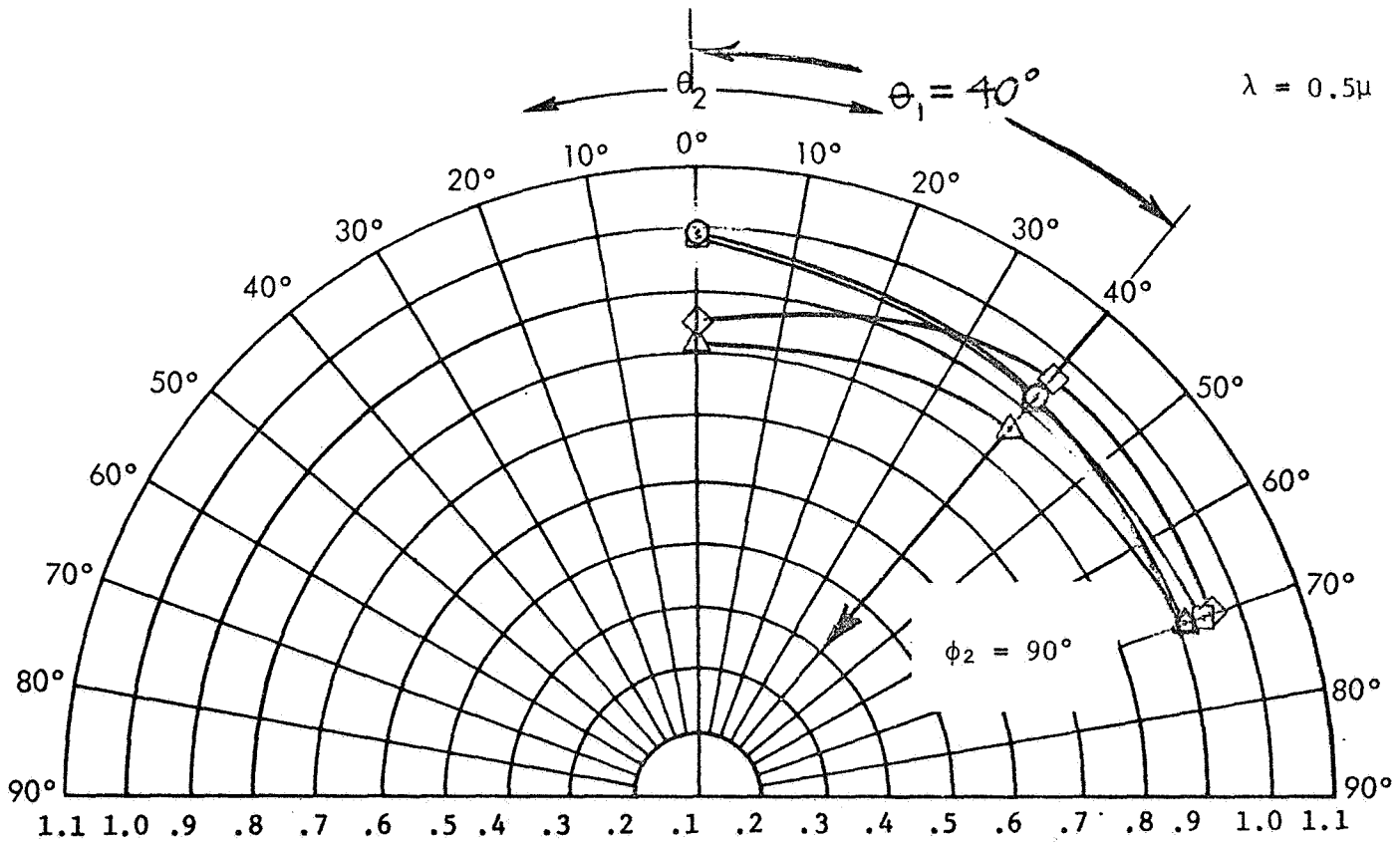
FIGURE A28: RELATIVE BIDIRECTIONAL REFLECTANCE OF MgO PRESSED POWDER, 4mm THICK, SAMPLE 580-68
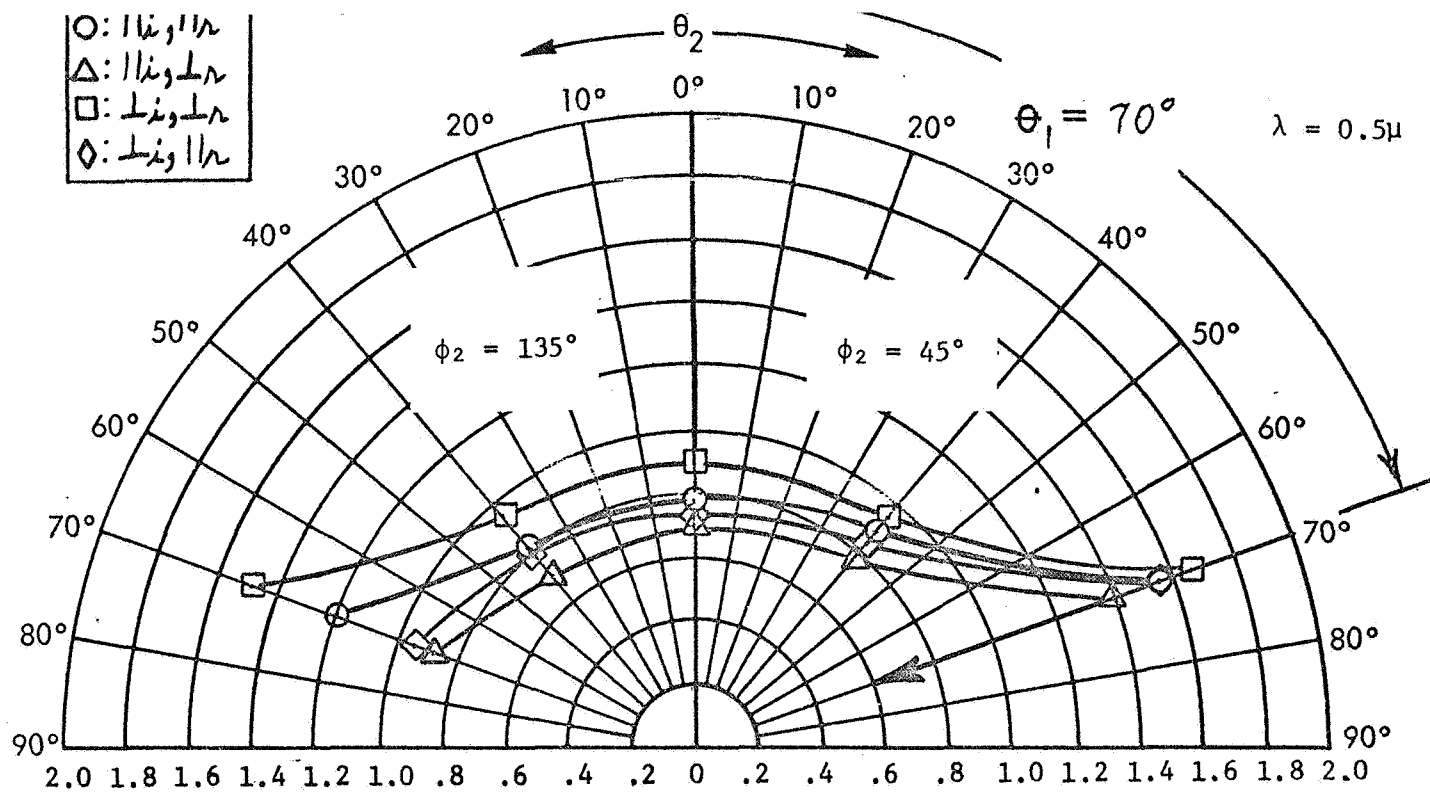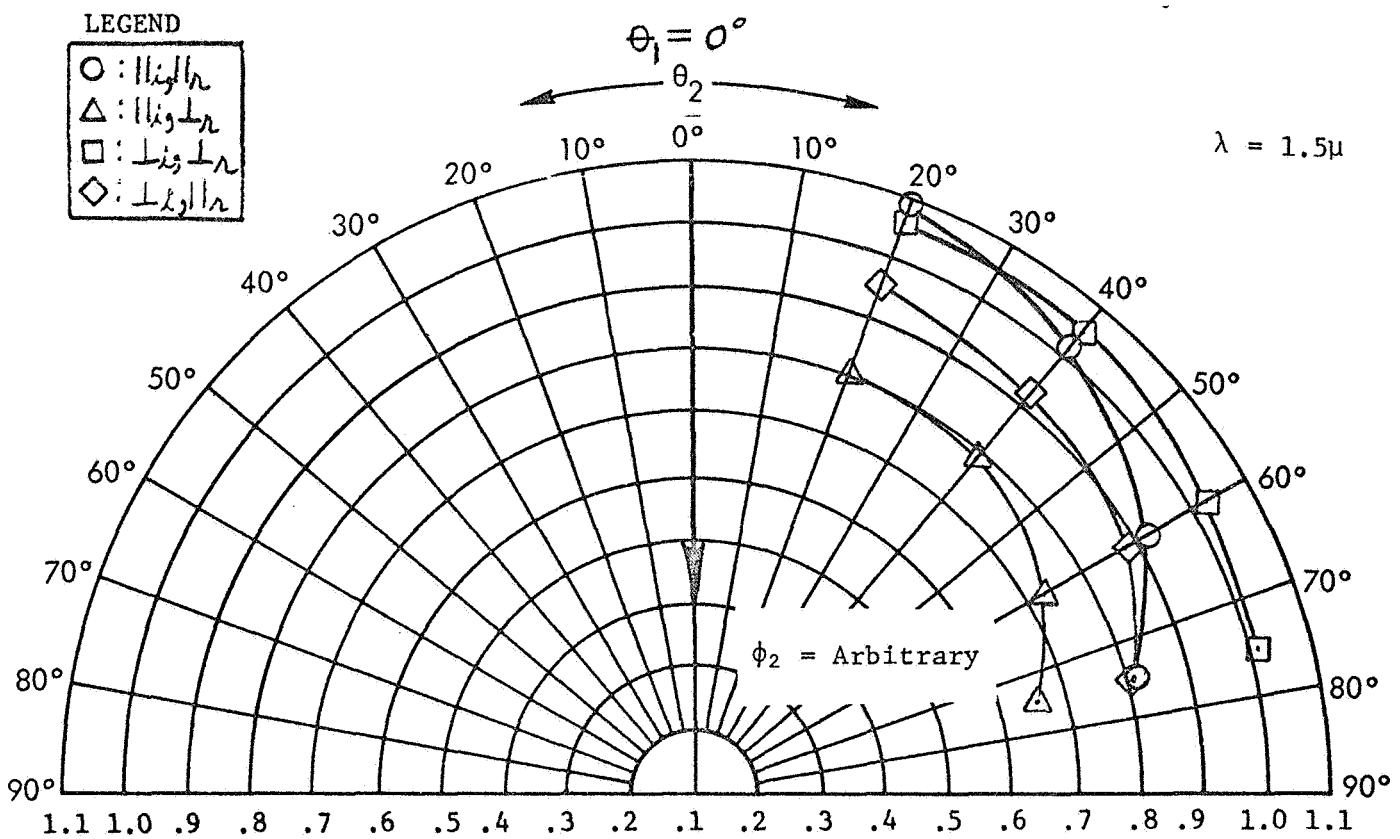
FIGURE A29: RELATIVE BIDIRECTIONAL REFLECTANCE OF MgO PRESSED POWDER, 4mm THICK, SAMPLE 580-68
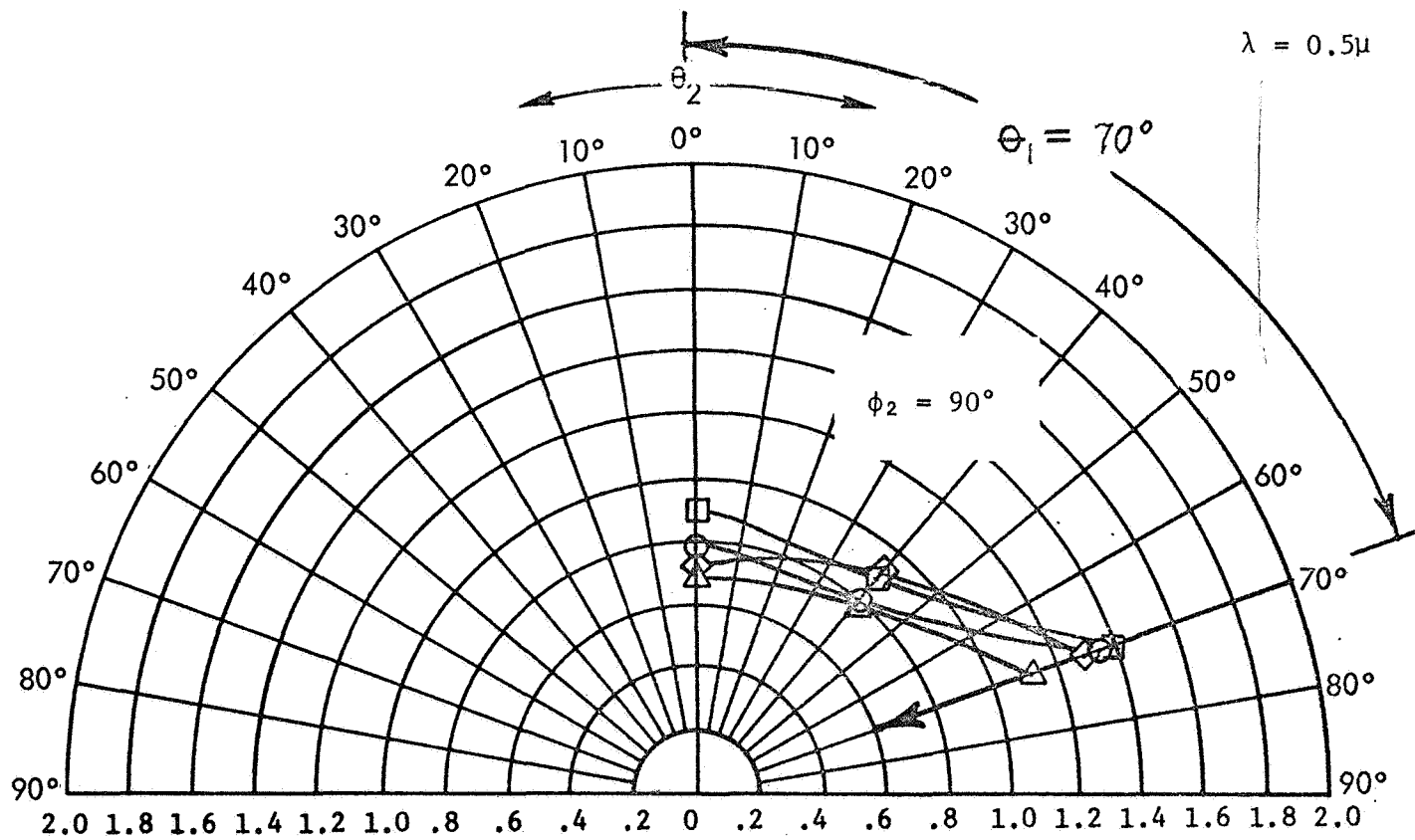
FIGURE A30: RELATIVE BIDIRECTIONAL REFLECTANCE OF MgO PRESSED POWDER, 4mm THICK, SAMPLE 580-68
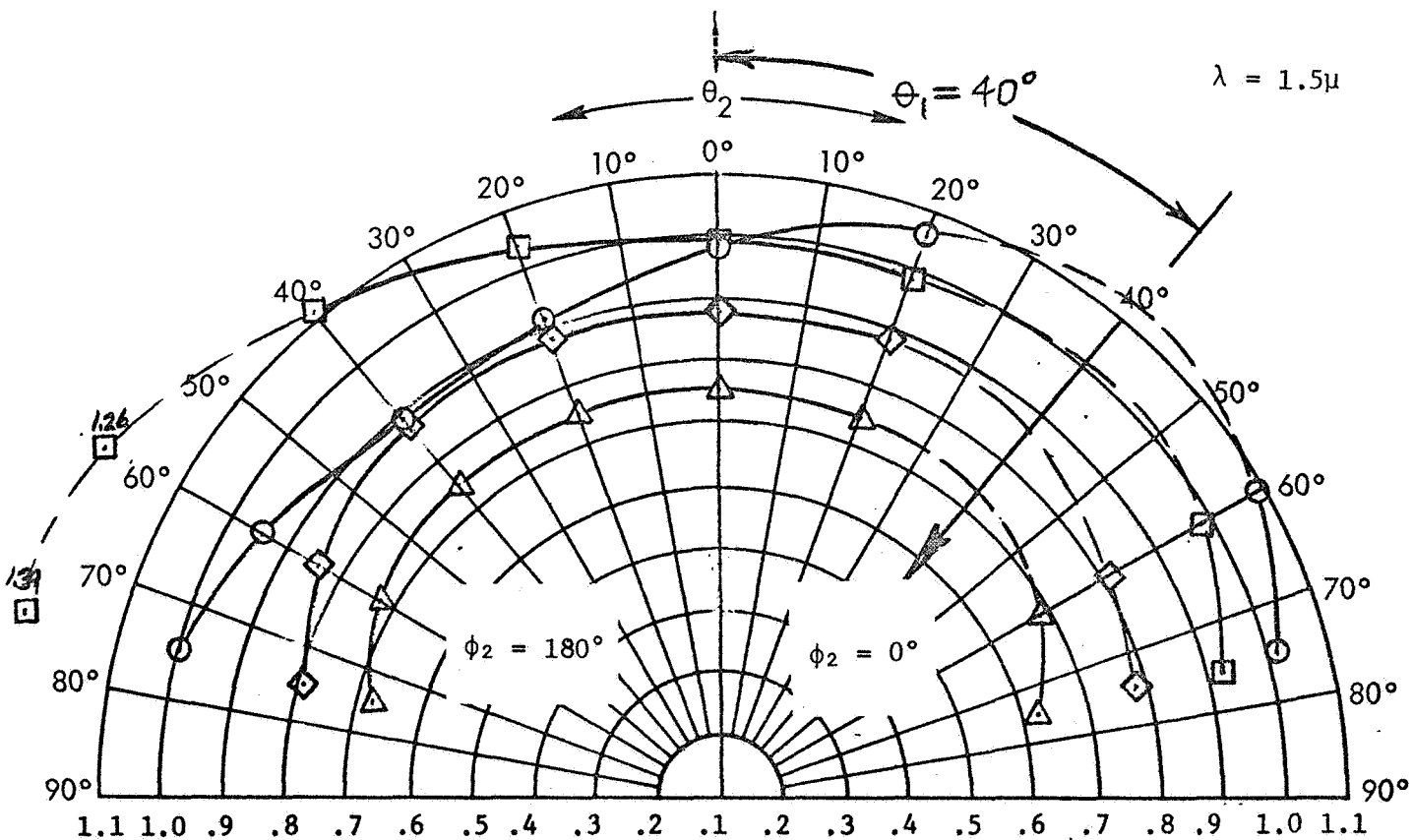
FIGURE A31: RELATIVE BIDIRECTIONAL REFLECTANCE OF MgO PRESSED POWDER, 4mm THICK, SAMPLE 580-68

125

FIGURE A32: RELATIVE BIDIRECTIONAL REFLECTANCE OF MgO PRESSED POWDER, 4mm THICK, SAMPLE 580-68

FIGURE A33: RELATIVE BIDIRECTIONAL REFLECTANCE OF MgO PRESSED POWDER, 4mm THICK, SAMPLE 580-68
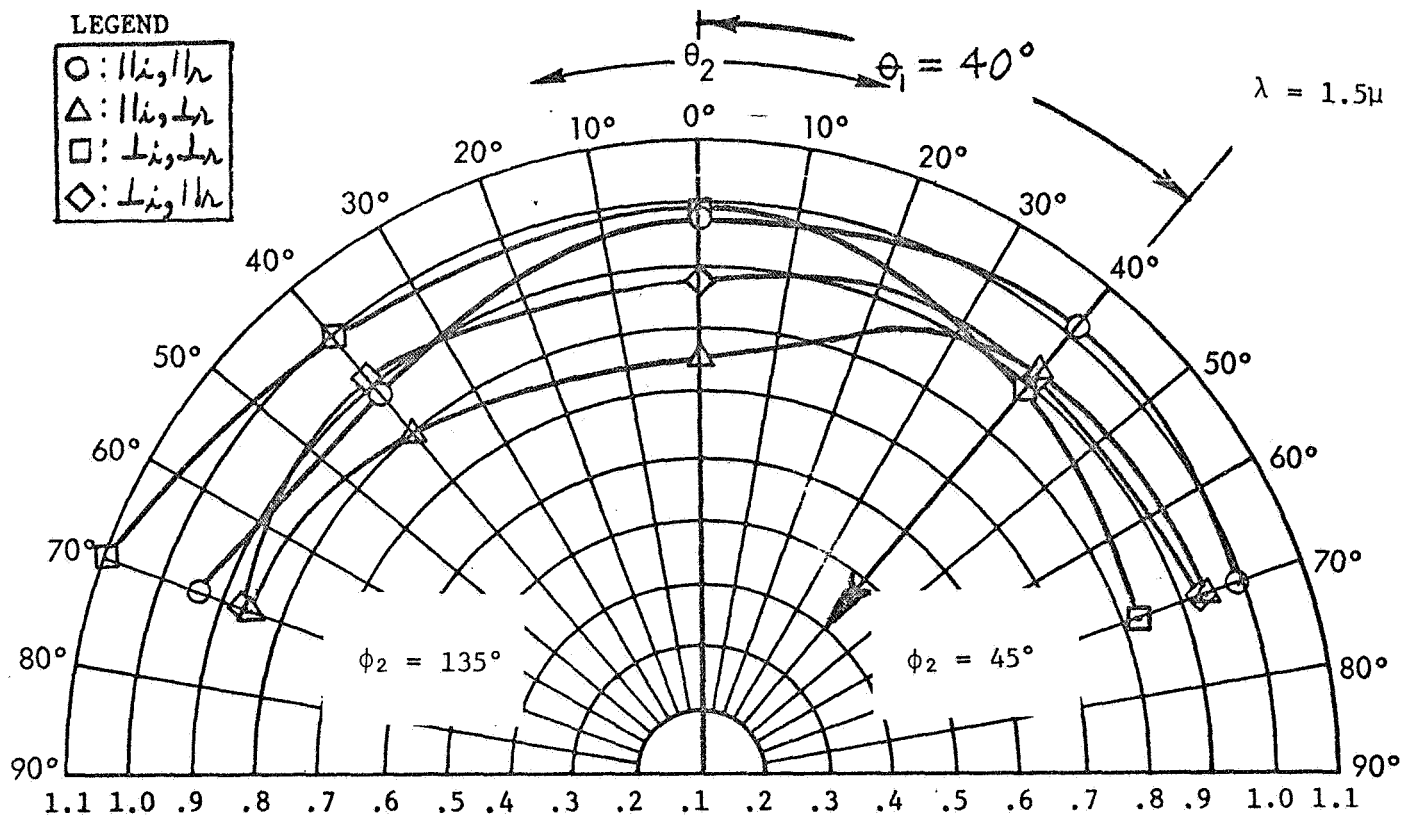
FIGURE A34: RELATIVE BIDIRECTIONAL REFLECTANCE OF MgO PRESSED POWDER, 4mm THICK, SAMPLE 580-68
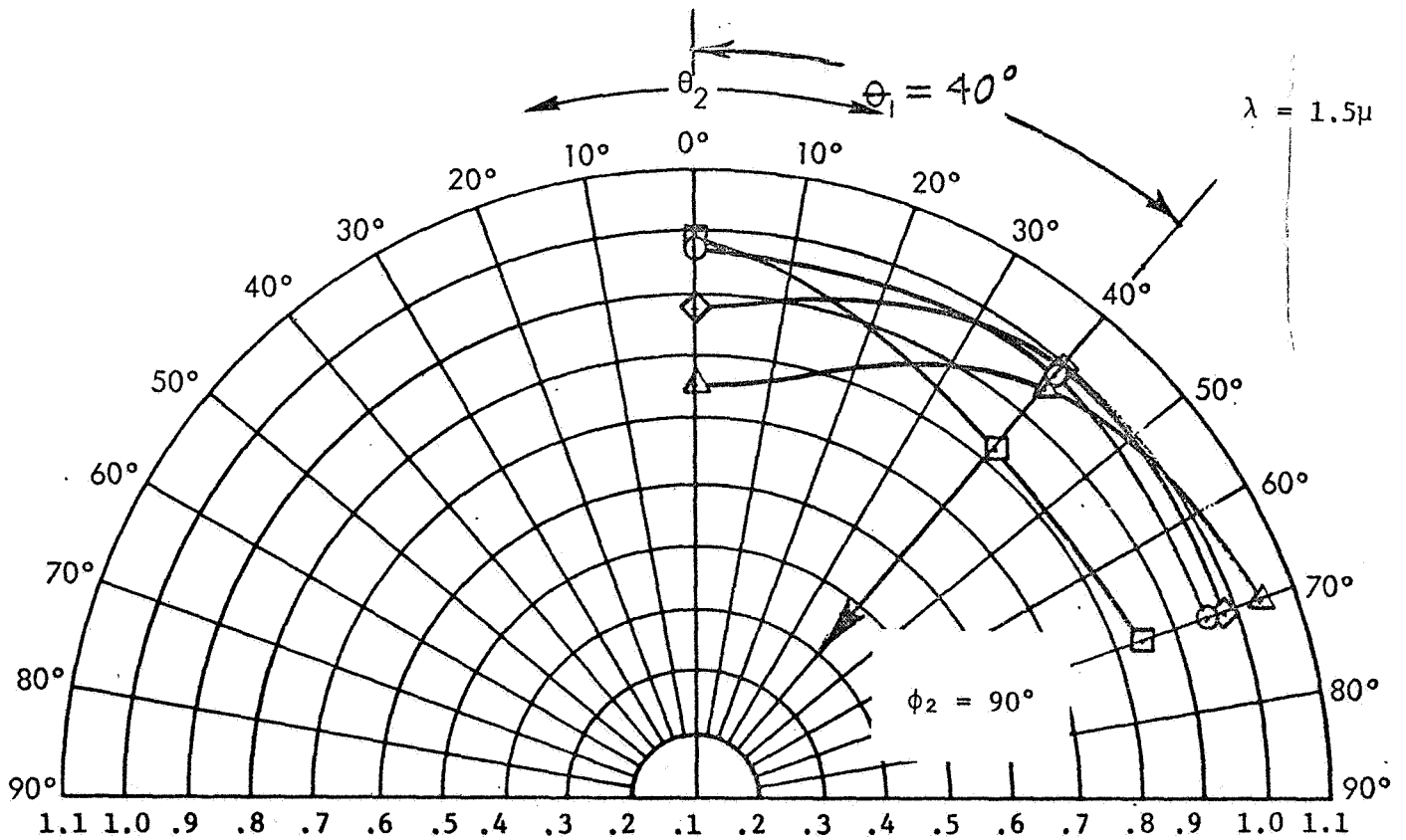

FIGURE A35: RELATIVE BIDIRECTIONAL REFLECTANCE OF MgO PRESSED POWDER, 4mm THICK, SAMPLE 580-68
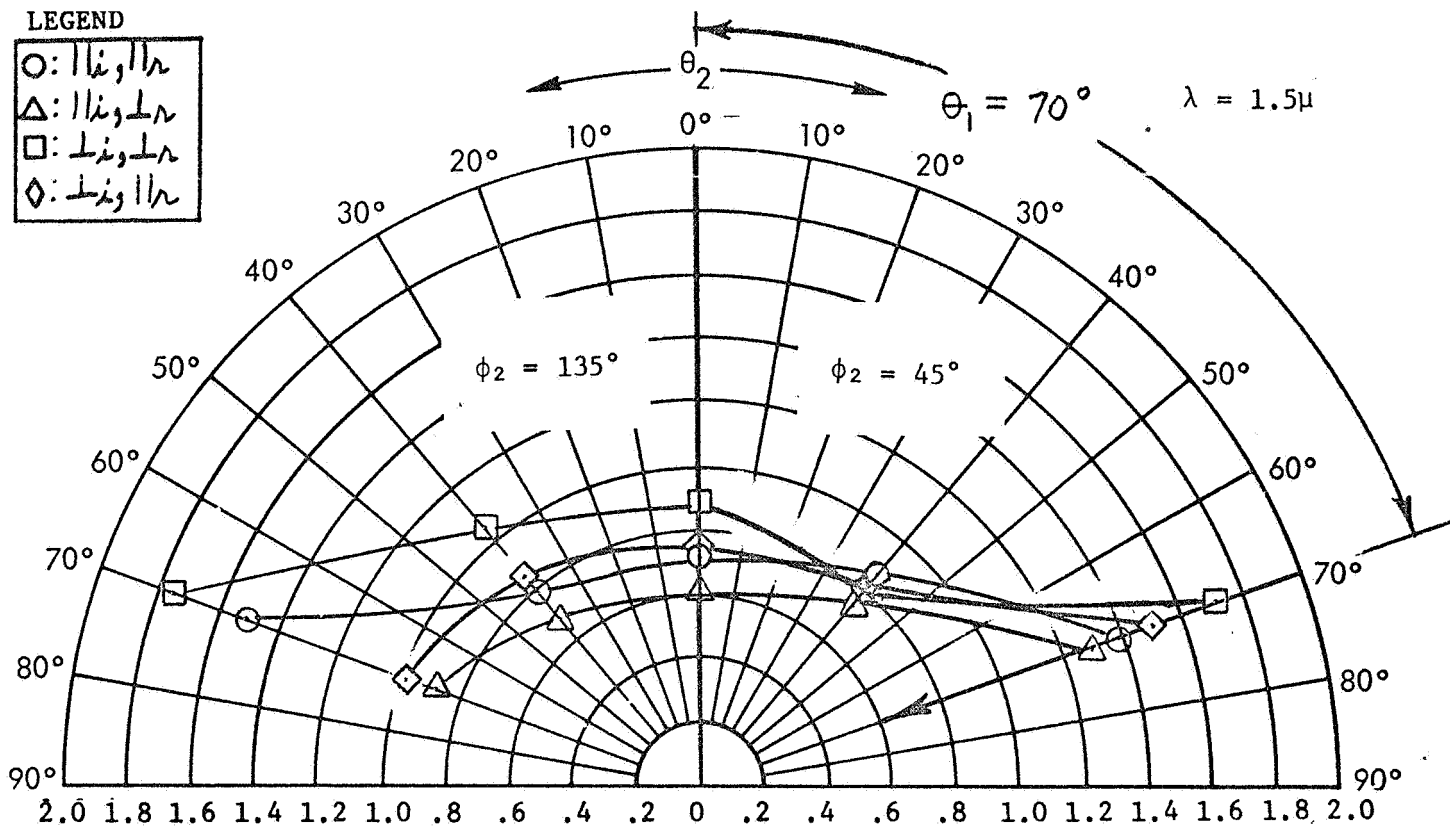
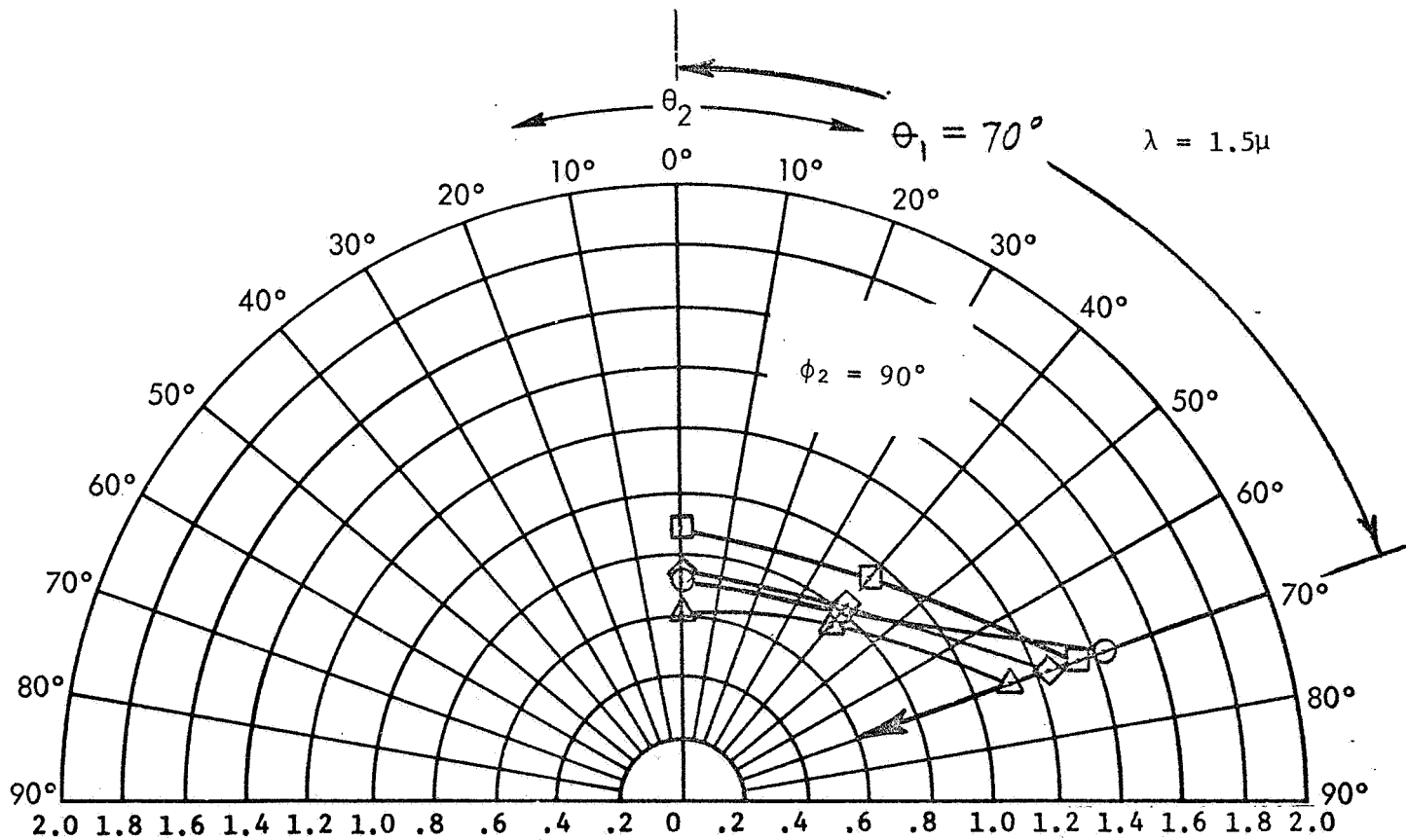FIGURE A36: RELATIVE BIDIRECTIONAL REFLECTANCE OF MgO PRESSED POWDER, 4mm THICK, SAMPLE 580-68

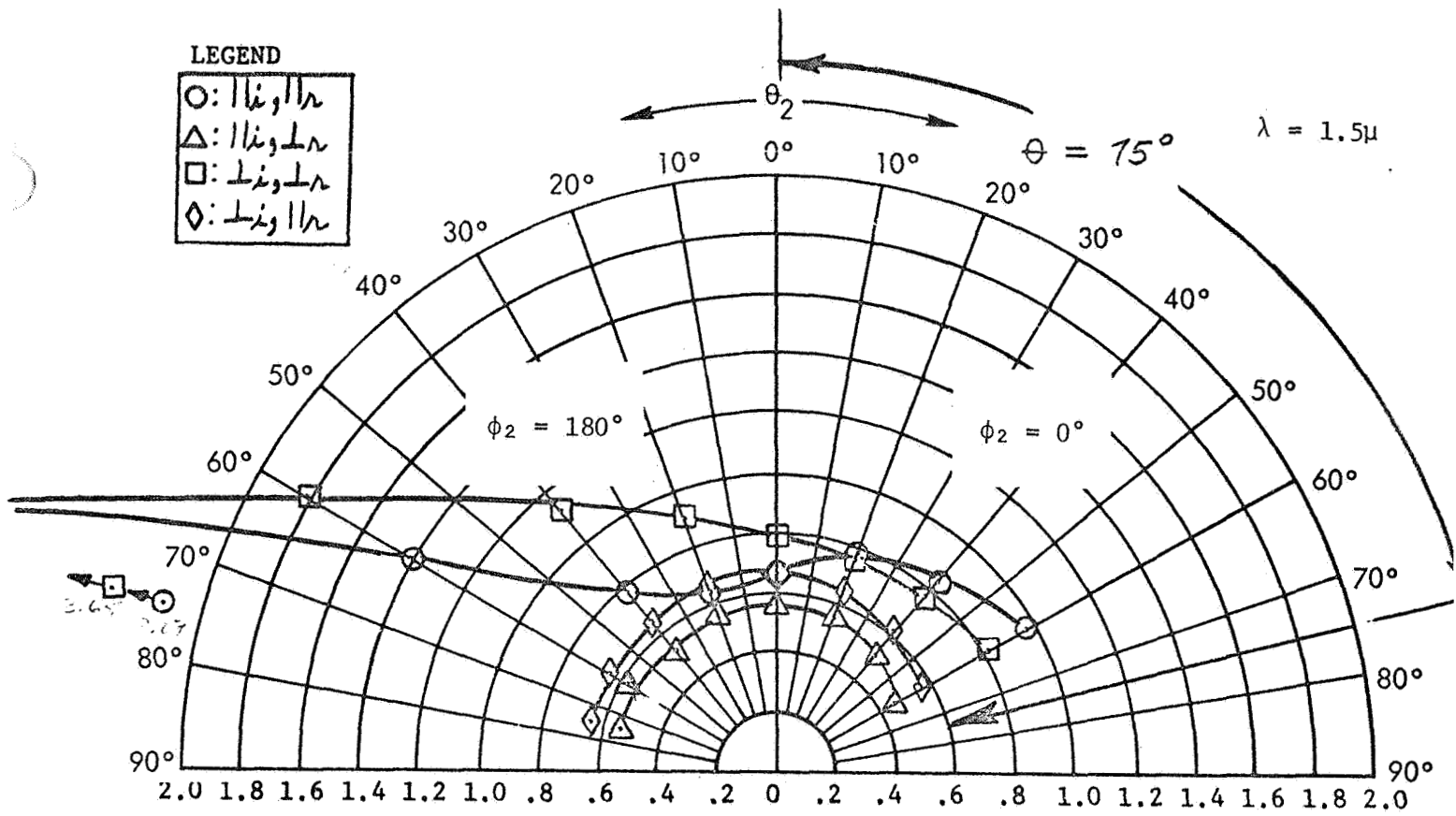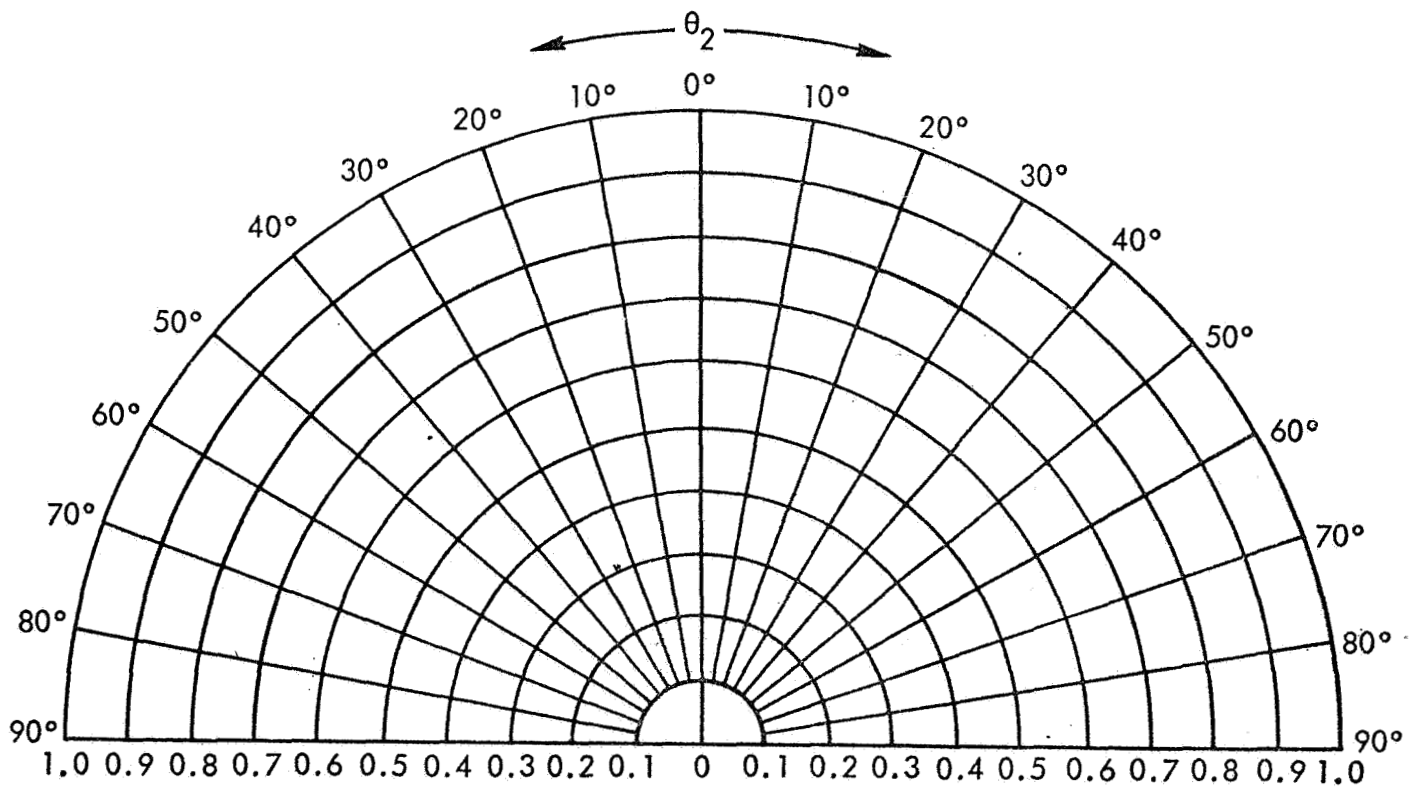FIGURE A37: RELATIVE BIDIRECTIONAL REFLECTANCE OF MgO PRESSED POWDER, 4mm THICK, SAMPLE 580-68

FIGURE A38: RELATIVE BIDIRECTIONAL REFLECTANCE OF MgO PRESSED POWDER, 4mm THICK, SAMPLE 580-68

129

DETAILED COMMENTS ON THE BIDIRECTIONAL REFLECTANCE OF MAGNESIUM OXIDE SURFACES

Plane of Reflectance is the same as the Plane of Incidence ($\phi_2 = 0, 180°$)

θ_1	SAMPLE	λ	FIGURE	
0°				
	572-68 (smoked)	0.5	1-28	Fairly diffuse, $\rho_B(20°) - \rho_B(75°) \simeq 15\%$; reflectance decreases for $\theta_2 > 50°$, same applies for each polarization; $\rho_B(\perp,\perp)$ is slightly higher than $\rho_B(\parallel,\parallel)$ except for $\theta_2 < 40°$ where $\rho_B(\perp,\perp) \simeq \rho_B(\parallel,\parallel)$; more depolarization for $\perp$ incidence.
		1.5	A17	Similar to $\rho_B(0.5\mu)$ except considerably less depolarized and $\rho_B(\perp,\perp)$ is more diffuse than $\rho_B(\parallel,\parallel)$; $\rho_B(20°)-\rho_B(75°) \simeq 25\%$
	580-68 (pressed)	0.5	A25	Similar to smoked MgO at same conditions except depolarization is less for $\perp$ incidence.
		1.5	A32	Similar to smoked MgO at same conditions except $\rho_B(\perp,\perp)$ is more diffuse.
40°				
	(smoked)	0.5	1-29	$\rho_B(\perp,\perp)$ and $\rho_B(\parallel,\parallel)$ are fairly diffuse for $\phi_2 = 180°$ with $\rho_B(\perp,\perp)$ larger than $\rho_B(\parallel,\parallel)$ by $\simeq 10\%$. In backward direction ($\phi_2 = 0°$), $\rho_B(\parallel,\parallel) > \rho_B(\perp,\perp)$ slightly, and back reflectance > forward reflectance: $10\% >$ for $\rho_B(\perp,\perp)$ and $20°>$for $\rho_B(\parallel,\parallel)$. $\rho_B(\perp,\parallel)$ and $\rho_B(\parallel,\perp)$ decrease rapidly with θ_2 for $\phi_2 = 180°$; thus, depolarization is less for forward angles, especially high forward angles. Depolarization is more complete for $\rho_B(\perp,\perp)$ at the backward angle.
		1.5	A18	Depolarization is less complete than for $\lambda = 0.5\mu$. Difference between $\rho_B(\perp,\perp)$ and $\rho_B(\parallel,\parallel)$ is greater.
	(pressed)	0.5	A26	The differences between $\rho_B(\parallel,\parallel)$ and $\rho_B(\perp,\perp)$ are greater than for smoked MgO, especially in forward direction. $\rho_B(\perp,\parallel)$ and $\rho_B(\parallel,\perp)$ are nearly equal and fairly cosine. Depolarization, in general, is less complete than for smoked MgO.
		1.5	A33	Quite similar to smoked Mgo at same conditions except higher reflectance in forward direction.
60°				
	(smoked)	0.5	1-30	$\rho_B(\perp,\perp)$ and $\rho_B(\parallel,\parallel)$ increase rapidly with increasing θ_2, from $\theta_2 > 20°$ both in backward and forward direction. $\rho_B(\perp,\parallel)$ and $\rho_B(\parallel,\perp)$ increase with θ_2 in forward direction ($\phi_2 = 180°$). $\rho_B(\parallel,\parallel) - \rho_B(\parallel,\perp)$ is about twice the value of $\rho_B(\perp,\perp) - \rho_B(\perp,\parallel)$ in the backward direction. ρ_B is much less diffuse for $\theta_1 = 60°$ than for $\theta_1 = 0°$ or $40°$ for all polarizations of incident and reflected energy.

13°

θ_1	SAMPLE	λ	FIGURE

$\rho_B(\perp,\perp) > \rho_B(\|,\|)$ in forward direction and $\rho_B(\perp,\perp) < \rho_B(\|,\|)$ in backward direction. At high angles in forward direction, the reflected beam is very polarized regardless of polarization of incident beam.

1.5 A19 — $\rho_B(\|,\|)$ and $\rho_B(\perp,\perp)$ increase rapidly with increasing θ_2 in forward direction. Same characteristics as for $\lambda = 0.5$ except more energy scattered in the forward plane and decreased back-reflectance.

NOTE: No $\theta_1 = 60°$ data was taken for pressed MgO.

75°

(smoked) 0.5 1-31 — $\rho_B(\perp,\perp)$ and $\rho_B(\|,\|)$ are nearly equal. $\rho_B(\|,\perp)$ and $\rho_B(\perp,\|)$ are nearly equal and almost diffuse in forward direction and increase with θ_2 in backward direction. The ρ_B's at the various polarization conditions are in the same relative order as for $\theta_1 = 60°$ in backward and forward directions. The backward reflectance is larger than the forward reflectance up to at least $\theta_2 = 60°$.

1.5 A20 — Depolarization is less complete than at $\lambda = 0.5$ and forward scattering is greater.

(pressed) 0.5 A31 — Similar to smoked MgO except forward scattering is larger. Back scattering is about the same.

1.5 A38 — $\rho_B(\perp,\|)$ and $\rho_B(\|,\perp)$ are fairly diffuse. $\rho_B(\perp,\perp)$ is much larger than $\rho_B(\|,\|)$ in the forward direction. Very much forward scattering of $\rho_B(\perp,\perp)$ and $\rho_B(\|,\|)$.

Plane of Reflectance is out of the Plane of Incidence ($\phi_2 \neq 0°$, $180°$)

θ_1	SAMPLE	λ	FIGURE	ϕ_2

40°

(smoked) 0.5 1-32 45°&135° — Fairly diffuse except for $\theta_2 \geq 70°$, where depolarization decreases. $\rho_B(\perp,\perp)$ and $\rho_B(\|,\|)$ are about the same. $\rho_B(\perp,\|) > \rho_B(\|,\perp)$ by about 10%. ρ_B values are generally larger in $\phi_2 = 45°$ plane than in $\phi_2 = 135°$ plane. "Over-depolarization" [$\rho_B(\perp,\|) > \rho_B(\perp,\perp)$] occurs for $\theta_2 \geq 60°$ in the $\phi_2 = 45°$ plane.

1-33 90° — $\rho_B(\perp,\|)$ and $\rho_B(\|,\perp)$ are about the same as for $\phi_2 = 45°$, $135°$ but $\rho_B(\perp,\perp)$ and $\rho_B(\|,\|)$ are smaller. "Over-depolarization" occurs for $\perp$ incidence at $\phi_2 \geq 15°$.

θ_1	SAMPLE	λ	FIGURE	ϕ_2	
		1.5	A21	45°&135°	Fairly diffuse. For ∥ incidence, depolarization is less complete than for ⊥ incidence. ρ_B values for ∥ incidence are higher in $\phi_2 = 45°$ plane than in 135° plane. "Over-depolarization" occurs for incidence at $\phi_2 = 45°$ and $\theta_2 > 30°$.
			A22	90°	Similar to ρ_B at $\lambda = 0.5\mu$ and same conditions. "Over-depolarization" for $\theta_2 > 20°$.
		0.5	A27	45°&135°	Fairly diffuse. Relatively more energy is reflected in $\phi_2 = 45°$ plane than in $\phi_2 = 135°$ plane. Depolarization is much less complete than for smoked MgO at same conditions.
			A28	90°	$\rho_B(\perp,\perp)$ and $\rho_B(\|,\|)$ are very nearly equal and quite diffuse. Depolarization is fairly complete.
		1.5	A34	45°&135°	"Over-depolarization" for incidence in $\phi_2 = 45°$ plane at $\phi_2 > 30°$. Generally more energy is reflected in the $\phi_2 = 135°$ plane than for smoked MgO at same conditions.
			A35	90°	"Over-depolarization" for incidence at $\phi_2 > 15°$ and for ∥ incidence at $\theta_2 > 45°$. Otherwise, similar to ρ_B of smoked MgO at same conditions.
70°					
	(smoked)	0.5	1-34	45°&135°	Very non-diffuse with increasing ρ_B at high values of θ_2 in both $\phi_2 = 45°$ and $\phi_2 = 135°$ planes. Depolarization almost complete for ⊥ incidence in $\phi_2 = 45°$ plane. ρ_B for ⊥ incidence > ρ_B for ∥ incidence.
			1-35	90°	Generally, "over-depolarization" for ⊥ incidence. Very incomplete depolarization for ∥ incidence. ρ_B increases with θ_2. $\rho_B(\|,\|) > \rho_B(\perp,\perp)$ slightly for $\theta_2 = 70°$.
		1.5	A24	45°&135°	$\rho_B(\perp,\|)$ and $\rho_B(\|,\perp)$ are fairly diffuse in $\phi_2 = 135°$ plane but not in $\phi_2 = 45°$ plane where reflectance increases with ϕ_2. $\rho_B(\perp,\perp)$ and $\rho_B(\|,\|)$ always increase with θ_2. $\rho_B(\perp,\perp)$ and $\rho_B(\|,\|)$ exchange places regarding relative magnitude in both planes. $\rho_B(\perp,\perp)$ is generally higher, however.
			A23	90°	"Over-depolarization" for ⊥ incidence for $\theta_2 > 15°$. $\rho_B(\|,\|) > \rho_B(\perp,\perp)$ by ≈ 25% at $\theta_2 = 70°$.

-A29-

132

(pressed) 0.5   A29   45°&135°   Generally same as for smoked MgO at same condi-
                                   tions except larger values of ρ_B.

                A30   90°   Generally same as for smoked MgO at same conditions
                                   except larger values of ρ_B. Nearly complete
                                   depolarization for $\perp$ incidence.

        1.5   A36   45°&135°   Generally similar as for smoked MgO at same con-
                                   ditions except considerable larger (25%) in
                                   $\phi_2 = 135°$ plane.

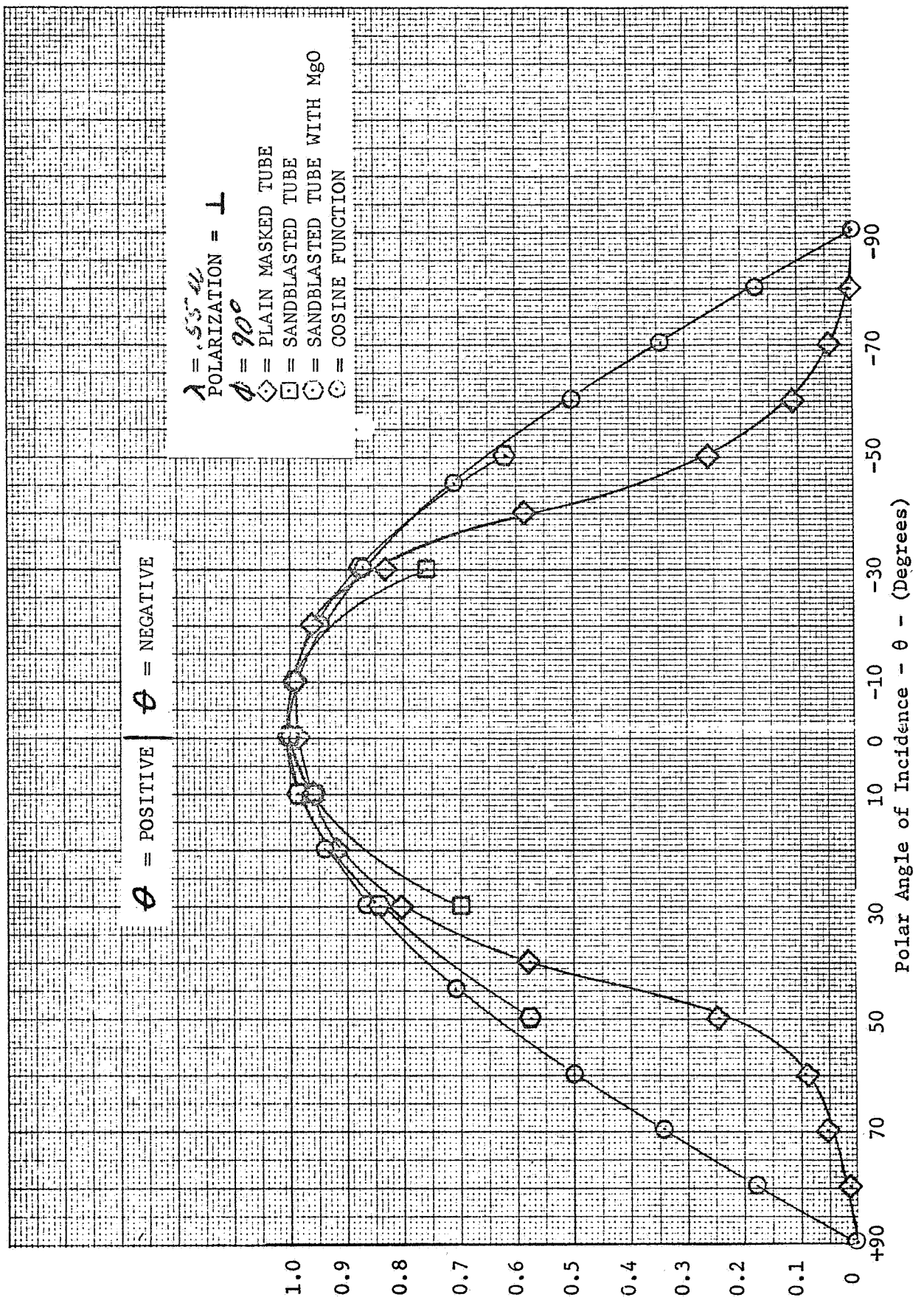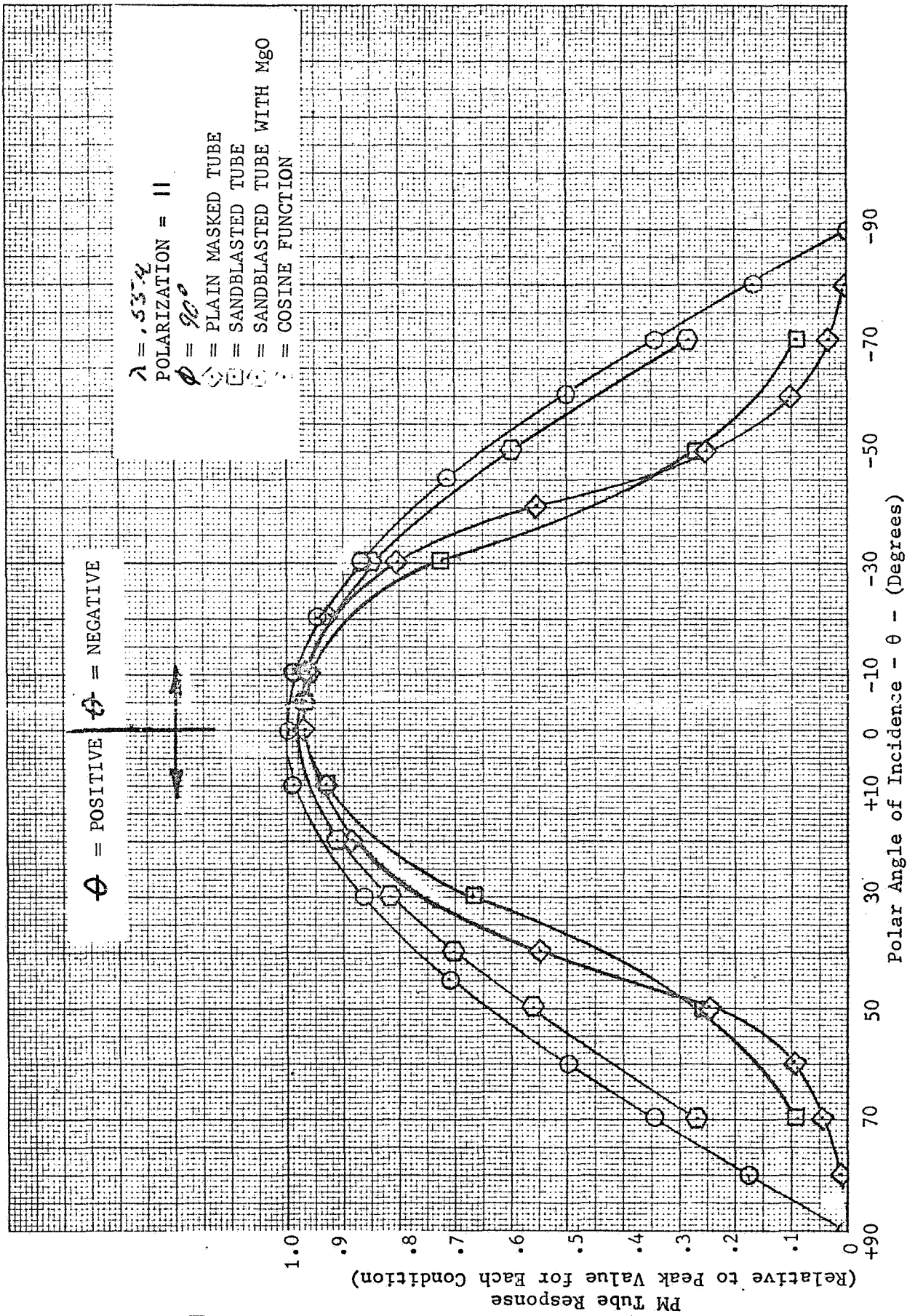   A37   90°   Less diffuse than smoked MgO at same conditions.
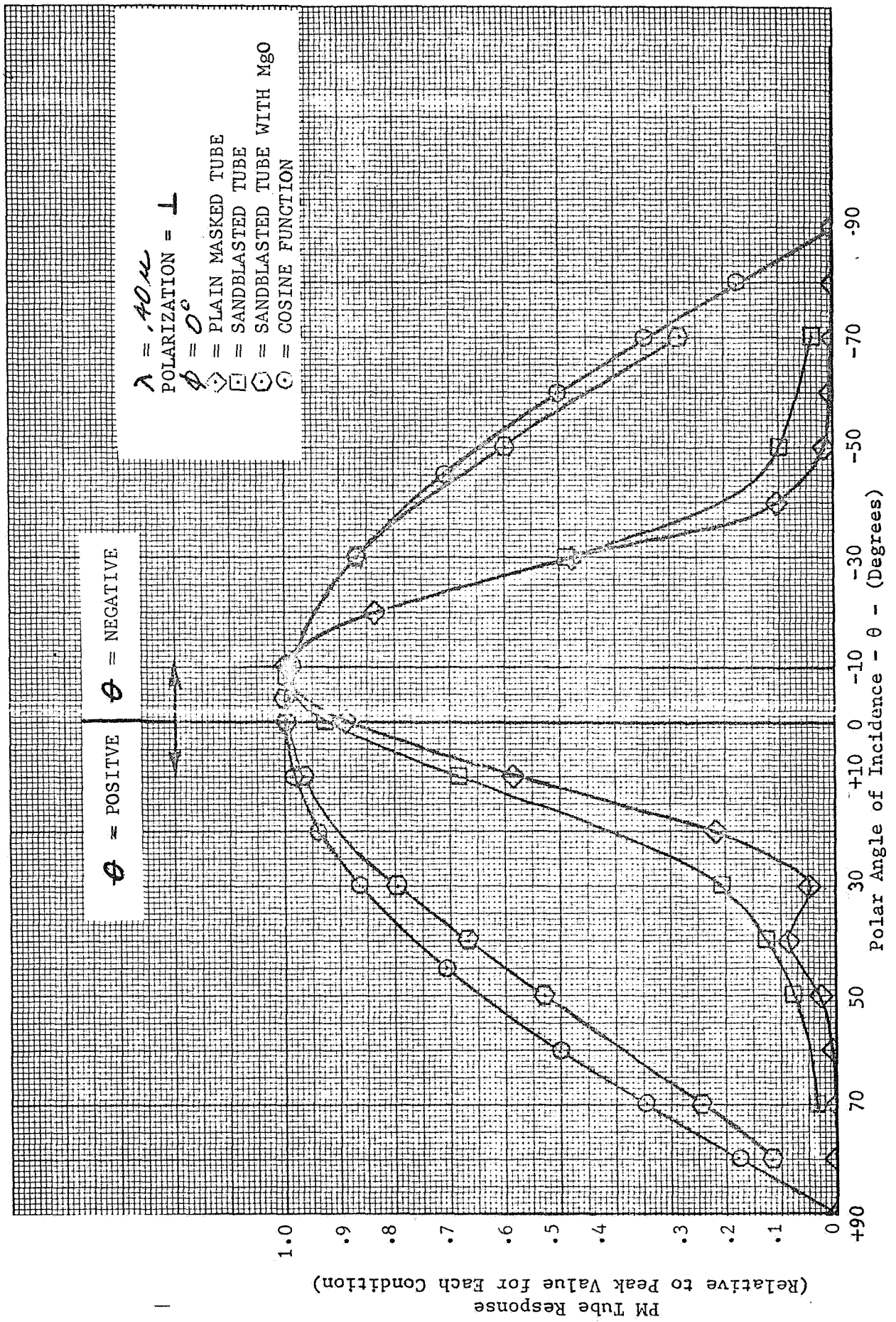
133

FIGURE A39

Polar Angle of Incidence – θ – (Degrees)

$\lambda = .55 \mu$
POLARIZATION = $\perp$
$\phi = 90°$

◇ = PLAIN MASKED TUBE
□ = SANDBLASTED TUBE
⬡ = SANDBLASTED TUBE WITH MgO
◯ = COSINE FUNCTION

θ = POSITIVE | θ = NEGATIVE

FIGURE A40

λ = .53 μ
POLARIZATION = ‖
φ = 90°

○ = PLAIN MASKED TUBE
□ = SANDBLASTED TUBE
◇ = SANDBLASTED TUBE WITH MgO
⬡ = COSINE FUNCTION

θ = POSITIVE | θ = NEGATIVE

Polar Angle of Incidence – θ – (Degrees)

PM Tube Response
(Relative to Peak Value for Each Condition)

FIGURE A41

Polar Angle of Incidence – θ – (Degrees)

PM Tube Response
(Relative to Peak Value for Each Condition)

$\lambda = .40\mu$
POLARIZATION = $\perp$
$\emptyset = 0°$
$\emptyset \diamondsuit$ = PLAIN MASKED TUBE
$\square$ = SANDBLASTED TUBE
$\bigcirc$ = SANDBLASTED TUBE WITH MgO
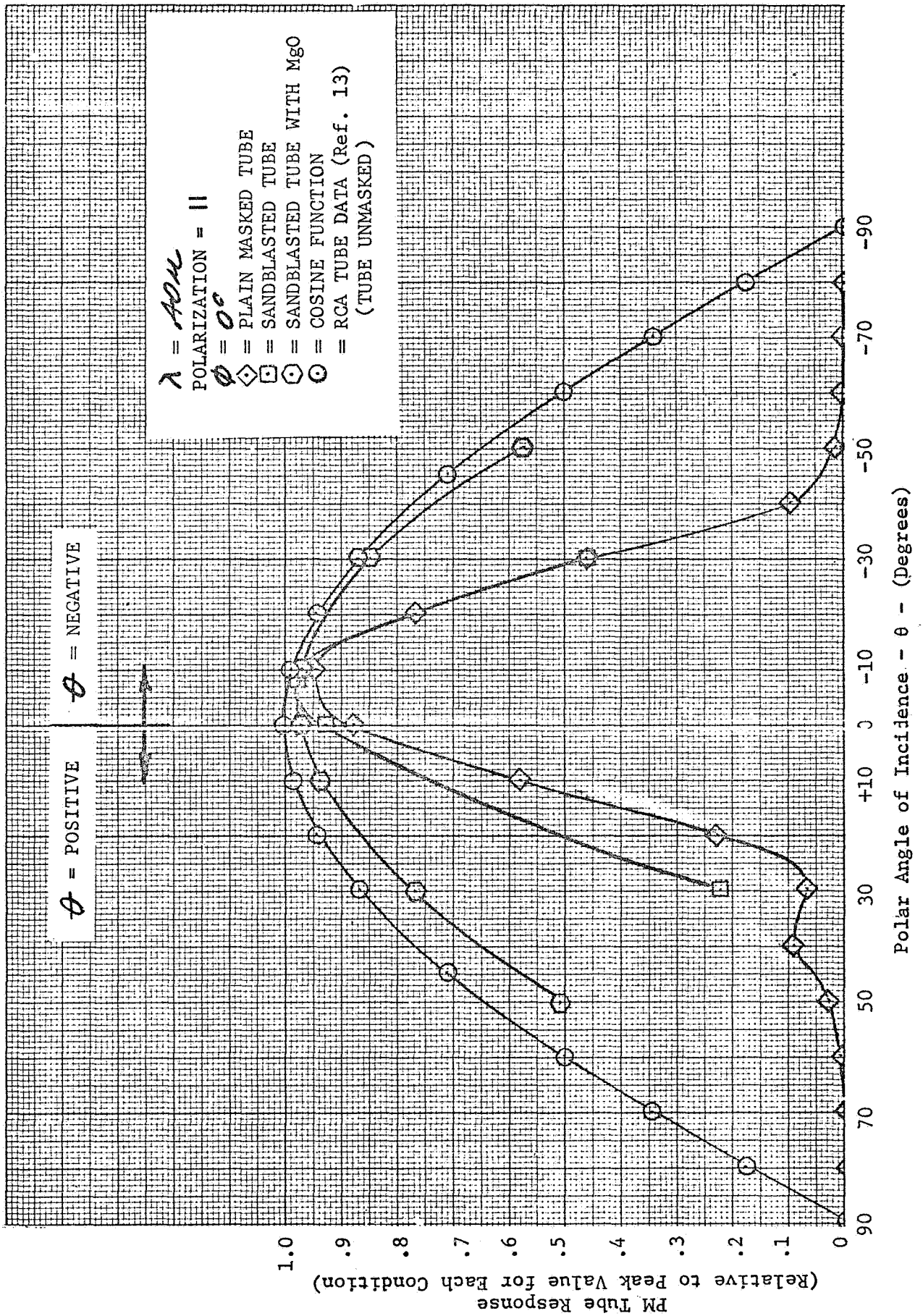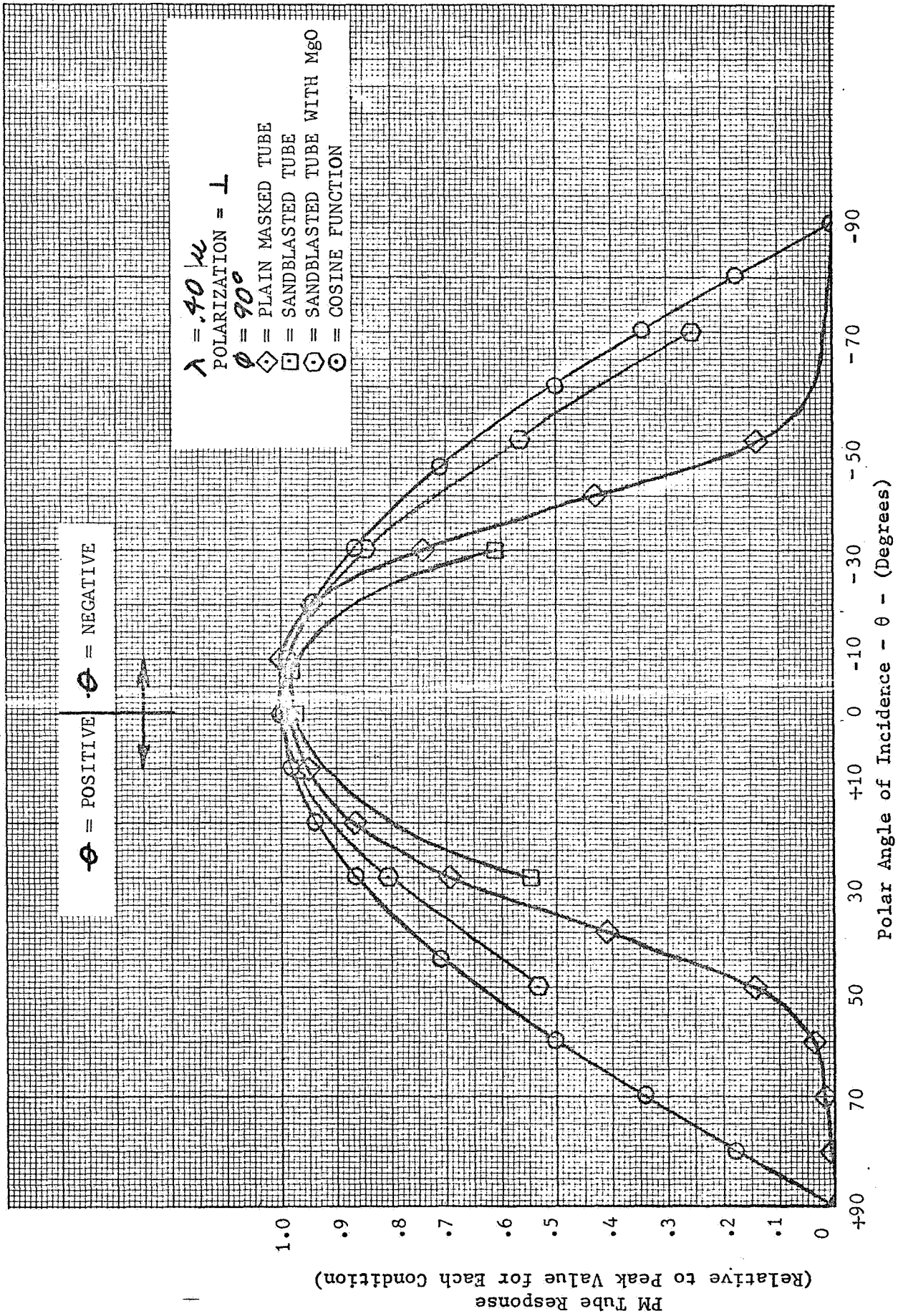$\odot$ = COSINE FUNCTION

θ = POSITIVE | θ = NEGATIVE

13

FIGURE A42

FIGURE A43

FIGURE A44